SPINNING DYNAMICS AND PERFORMANCES OF MODIFIED RING SPUN YARNS

RONG YIN

Ph.D

The Hong Kong Polytechnic University

2018

The Hong Kong Polytechnic University

Institute of Textiles and Clothing

Spinning Dynamics and Performances of Modified Ring Spun Yarns

Rong YIN

A thesis submitted in partial fulfilment of the requirements for the degree of Doctor of Philosophy

Jun 2017

Certificate of Originality

I hereby declare that this thesis is my own work and that, to the best of my knowledge and belief, it reproduces no material previously published or written, nor material that has been accepted for the award of any other degree or diploma, except where due acknowledgement has been made in the text.

_____ (Signature)

Rong YIN (Name of student)

Abstract

Spinning is a fundamental method to produce long strands from staple raw fibers of cotton, wool, flax, or other material. Twisting is a vital process to determine the staple yarn structure and performances like strength (tenacity), elongation, evenness and hairiness. Till now, ring spinning continues to predominate in yarn manufacturing industry due to its high yarn quality and flexibility in materials and yarn counts. With the increasing demand of novel features or improving qualities, many modifications have been developed, such as Compact, Siro and Solo. In recent years, a novel spinning technology, named Nu-Torque, has been developed by introducing a false-twisting unit into the conventional ring frame for producing low twist and soft handle single yarns. The modified cotton yarns and fabrics have significant advantages in terms of soft handle, higher yarn strength at lower twist factor, lower residual torque and low knitted fabric spirality after washing and tumble-dry cycles. Among over ten mills using the technology, 10 to 40% increment in production rate has been achieved for cotton ring yarns with various versions of the technology. In addition, a significant average energy saving of 337Kwh/ton was reported by a mill producing Ne 30 and 1100 Kwh/ton for another mill for spinning Ne 80 yarns.

Although the low twist and soft handle single yarns have been achieved, several urgent issues relating to spinning dynamics and yarn performances need to be addressed. Firstly, twist generation and propagation are of particular interest because they answer several key questions including the amount of false-twist generated by the false-twister, false-twisting efficiency and blockage rate, as well as the relationships between false-twisting efficiency and system parameters. The false-twisting unit employed in this study is single friction-belt with circular cross-section. It has been identified that the moving belt generates the false-twists into yarn, meanwhile traps the upward propagation of the real twist as well as congests the downward propagation of the false twists. In this study, a steady-state model of yarn dynamics in the modified ring spinning system has been proposed, which deals with two important phenomena simultaneously, that is, twist generation and twist propagation. The model was validated by experiments and a good agreement has been demonstrated. For the first time, influences of several parameters

on the twisting process have been revealed in terms of false-twisting efficiency, propagation coefficients of twist trapping and congestion. Based on the proposed model, a systematic simulation has been carried out to evaluate effects of system parameters on the false-twisting efficiency as well as propagation coefficients. In order to minimize the number of experiments, response surface methodology involving a central composite design in three factors of twist multiplier, speed ratio and wrap angle was successfully employed for the study and analysis. The significant terms of the models were studied and it reveals that the speed ratio and wrap angle are statistically significant for the responses of twist efficiency, propagation coefficients of twist trapping and congestion. And more importantly, linear relationships are found among the three responses.

Secondly, Stability is the basic requirement for any practical applications. Unstable twist generation and propagation arising from the vibration of the false-twister, forced variation of the electric motor as well as electric interference or malfunction may results in poor spinnability as well as uneven features or imperfections of the resultant yarns, such as strength deterioration, diameter irregularity and wrapping fibers along yarn length. On the other hand, for a stable process or product, it should permit a certain tolerance for the system variation or error. However, little work has been found in the literature thus remains elusive. In this study, twist stability and robustness is concerned and their relations to the belt spatial position and properties are elaborated. Based on twist kinematics, a transient model has been proposed to study twist variations during yarn formation process. Three idealized cases that cause twist variations are investigated, namely step function, rectangular function and periodic function changes in false twist. Even though several assumptions have been proposed to make the analysis manageable, the findings have provided a clear clue of the significant twist levels that can generate in the zones of the machine. It has been verified by the experiments that the resultant yarn properties within 30% periodic change in false twist demonstrated no obvious difference in properties when compared to the yarn without variation. From model simulation, it has been found that twist variations in different zones are different and the effect on final yarns is limited. It is also suggested by the model that zone length has a significant influence on the twist redistributions. Besides, reducing the twist efficiency and the twist blockage rate leads to decreasing twist variation and balancing time in three zones. In particular, belt oscillation has little influence on twist variations and

wool-like fiber is easier to cause large twist variations in spinning process than that of cotton-like fiber at the same condition.

Thirdly, in previous study, our group has found severe deterioration of yarn neps for production of high count yarns. The blackboard evenness also proves that the produced yarns have one grade worse than that of control yarns. Although optimizations have been carried out to adjust the spinning parameters in order to control the yarn evenness, the results are less satisfied. So far, the mechanism behind the fact has not been fully explored yet. In order to solve the severe deterioration of yarn neps in the modified system, in this study systematic investigation of Ne 40 cotton yarns has been carried out. The study includes three aspects, namely belt spatial positions, system parameters, and friction surface of the belt. Belt spatial installation position is an important issue with special interest for mill applications. It is not only restricted by the space of different spinning machines, but also affects the stability and quality of the yarns. As a key component, the belt friction surface may have large influences on false-twisting process, and determine the final yarn performances. Moreover, the belt friction surface and their interplay with yarn properties have been investigated systematically. Based on the preliminary analysis of belt friction surface and geometry, potential influencing factors were identified, and the fractional factorial methodology was employed to find out the statistically significant factors on yarn tenacity, evenness and hairiness. According to the experimental results, twist factor, speed ratio and wrap angle were confirmed as the significant parameters on yarn properties in terms of tenacity, evenness, neps (+140%), and hairiness, therefore, these three parameters were selected for further study using response surface methodology to find the optimal value for yarn production. The second-order equations were obtained to examine and estimate the relationships between the factors and responses, and the overlaid contour plot was employed to find the optimal results. The optimized yarn with 11.1% twist reduction apparently outweighed the conventional yarn in hairiness and has slight improvements in yarn evenness and thick places (+50%); whereas the neps (+140%) of the optimized yarn is still 50% worse than that of the corresponding ring yarn. In order to overcome the occurrence of neps, the mechanism of neps generation has been studied and promising solutions to alleviate or diminish such yarn imperfections have also been put out. Neps generated in this system are mainly caused by rearrangement of the yarn surface fiber along its axis. The yarn neps can be successfully suppressed by either shortening interactive path or arranging the

fibers in a completely parallel and close position before untwisting is imparted, which have been verified by the experiments. It has also been found from the experiments that the belt hardness is independent of the occurrence of neps (+140%) and the belt with rough surface morphology even deteriorates the situation. With the combination of compact device and belt-type false-twister, the wrap angle can be further enlarged by introducing a rotatable guide installed between the front roller and the belt to enhance the yarn tenacity and the twist factor can be further decreased from 3.2 to 2.8 to achieve a low residual torque and soft handle feeling yarns.

Finally, this study explores the surface characteristics and properties of knitted fabrics produced by the modified yarns and compares with the fabrics made from the conventional ring yarns. For preparing fabric samples, quantities of the Ne 40 modified yarns as well as conventional yarns were spun, respectively. Then, the prepared cop yarns were wound on the cone before knitting. After that, three single yarns were fed into the gauge of flat knitting machine and the interlock structure was adopted to avoid the fabric spirality. Properties and performances of the knitted fabrics were evaluated and compared, including fabric weight, thickness, loop length, bursting strength, air permeability, thermal property, pilling resistance, etc. The knitted fabrics made from the modified yarns show a 6.28% higher in bulkiness than that of the conventional yarns, resulting to a better capacity of thermal insulation and warmer feeling. Moreover, these two fabrics show similar bursting strength and same pilling grade.

Publications Arising from the Thesis

Journals Papers:

1. Y. Guo, J. Feng, **R. Yin**, X. G. Wang, M. van der Sluijs, X. M. Tao, Investigation and Evaluation on Fine Upland Cotton Blend Yarns Made by the Modified Ring Spinning System, *Textile Research Journal*, **85**(13): 1355-1366 (2015).

2. **R. Yin**, X. M. Tao, & B. G. Xu, Mathematical Modeling of Yarn Dynamics in a Generalized Twisting System, *Scientific Reports*, **6**: 24432 (2016).

3. **R. Yin**, X. M. Tao, & B. G. Xu, Variation of False-twisting on Spinning Process Stability and Resultant Yarn Properties in a Modified Ring Spinning Frame, accepted by *Textile Research Journal*.

4. **R. Yin**, X. M. Tao, & B. G. Xu, Effects of Friction Surface of False-twister on Modified Ring Spun Yarns, submitted to *Textile Research Journal*.

Conferences Papers:

1. **R. Yin**, B. G. Xu, & X. M. Tao, The Effect of Free Oscillations of Friction-belt False-twister on Dynamical Twist Distribution in a Modified Ring Spinning System, *Cross-straits Conference on Textiles 2014*, Hong Kong, China, December, 318-322 (2014).

2. **R. Yin**, X. M. Tao, & B. G. Xu, Twisting Robustness in the Ring Spinning System with Single Friction-belt False-twister, *The Fiber Society's Spring 2017 Conference*, Aachen, Germany, May, 91 (2017).

3. **R. Yin**, X. M. Tao, & B. G. Xu, Yarn Dynamics on a Moving Belt in the Ring Spinning System, *14th Asian Textile Conference*, Hong Kong, China, June, 157-159 (2017).

Patents:

1. X. M. Tao & **R. Yin**, Method and Apparatus for Industrially Producing Staple Yarns, submitted.

Acknowledgements

Firstly, I would like to express my deepest appreciation to my chief supervisor Prof. Xiao-ming TAO for her expert guidance, excellent suggestions and firm supports throughout this study. The breadth and depth of her knowledge, spanning from chemistry to physics, from textiles to mechanics, amazed me ever since the start of this study. Her passion for scientific discovery and enthusiasm to scientific knowledge have set a perfect example for the rest of my academic life. It is my life-long fortune to be supervised by her.

I would also like to convey my deep gratitude to my co-supervisor Dr. Bin-gang XU for his valuable advices, critical comments and consistent supports during my PhD study.

I appreciate the great help from our brilliant group members: Dr. Jie FENG for his valuable suggestions on experimental issues, Dr. Ying GUO for her management of the related project, Dr. Sheng-yan LI for her helpful and interesting discussions on spinning triangle, Dr. Xin-xin HUANG for her assistance in high-speed photography, Dr. Tao HUA for his discussions on the yarn and fabric properties.

My sincere thanks are also given to Mr. Wai-man CHU, Mr Cheuk-wai LAU in spinning workshop, Dr. Su LIU and Dr. Jinyun ZHOU in knitting workshop, and Ms. M.N. SUN in physical lab for their technical support and help.

I am indebted to my colleagues in Prof. Tao's group, with whom I have great pleasure to study and live: Dr. Bo ZHU, Dr. Zhi-feng ZHANG, Dr. Wei ZHENG, Dr. Lin SHU, Dr. Wei-jing YI, Dr. Qiao LI, Dr. Fei WANG, Dr. Song CHEN, Dr. Ze-guang Pei, Dr. Bao YANG, Dr. Wei ZENG, Mr. Shi-rui LIU, Mr. Ze-hua PENG, Mr. Ke CHEN, Mr. Xi WANG, Ms. Ying LI, Ms. Li-juan LIANG, Ms. Shu-ping LIN, Ms. Su LIU, Ms. Ying XIONG, Ms, Yu-heng ZHANG, Mr. Zi-heng ZHANG, Mr. Jian-liang GONG, Ms. Li-sha ZHANG, Ms. Yu-fei Xiang, et al.

Finally, I would like to express my special appreciations to my parents, my wife, and my children. Without their love and encouragement, this thesis would never be done.

Table of Contents

Certificate of Originality I
Abstract II
Publications Arising from the Thesis VI
Acknowledgements VII
Table of Contents VIII
List of Figures XIII
List of Tables XVII
Chapter I Introduction 1
1.1 Research Background 1
1.2 Aims and Objectives 3
1.3 Research Methodology 4
1.4 Significance and Values 5
1.5 Structure of the Thesis 6
Chapter II Literature Review 8
2.1 Spun Yarn Technologies 8
2.1.1 Conventional Method 8
2.1.2 Unconventional Methods 9
2.1.2.1 Rotor spinning 9
2.1.2.2 Friction spinning 11
2.1.2.3 Air jet spinning 12
2.1.2.4 Vortex spinning 13
2.1.3 Modified Ring Spinning Methods 14
2.1.3.1 Siro-spun spinning 14
2.1.3.2 Solo-spun spinning 15
2.1.3.3 Compact spinning 16
2.1.3.4 Other ring-based methods 17
2.2 Nu-Torque Technology 18
2.2.1 The origins of Nu-Torque 18
2.2.2 False-twisting Principles and Units 21
2.2.3 Analysis to the Yarn Structures and Performances 24
2.3 Yarn Twist Analysis 26
2.3.1 Twist Modeling 27

2.3.2 Yarn Twist Measurement....30
2.4 Yarn Tension Analysis....35
2.4.1 Yarn Tension Modeling....35
2.4.2 Yarn Tension Measurement....37
2.5 Optimization of Yarn Properties....38
2.6 Problem Statement....39
2.7 Summary....41

Chapter III Yarn Dynamics in the Ring Spinning System with Single Friction-belt False-twister....43
3.1 Theoretical Modeling....43
3.1.1 Definitions....43
3.1.2 Equations of Motion....46
3.1.2.1 Assumptions....46
3.1.2.2 Coordinate systems....47
3.1.2.3 Force balance....48
3.1.2.4 Moment balance....50
3.1.2.5 Calculating the coefficients of twist efficiency and twist blockage....50
3.1.2.6 Boundary equations....51
3.1.2.7 Dimensionless equations....52
3.1.3 Method of Numerical Solution....53
3.2 Experimental setup....55
3.2.1 Measurement of Yarn Tension....55
3.2.2 Measurement of Yarn Twist and Deviation Angle....56
3.3 Results and discussion....59
3.3.1 Verification of Model....59
3.3.2 Error Analysis....60
3.3.3 Distributions of Tension, Deviation Angle and Twist....61
3.3.4 Twist Efficiency, Propagation and Blockage....64
3.3.5 Torsional Rigidity....68
3.4 Systematically Investigation of the Twisting Process via Response Surface Methodology....68
3.4.1 Experimental Design....69
3.4.2 Results and Discussions....72
3.4.2.1 Analysis of variance (ANOVA)....72

3.4.2.2 Reduced regression models 74
3.4.2.3 Model validation 75
3.4.2.4 Effect of control variables on the responses 77
3.4.2.5 Relationships among three responses 78
3.5 Summary 80

Chapter IV Yarn Kinematics in the Ring Spinning System with Single Friction-belt False-twister 82
4.1 Theoretical Modeling 82
4.1.1 Assumptions 82
4.1.2 Twist Distributions in the Steady-state 83
4.1.3 Twist Redistributions in the Transient-state 85
4.1.3.1 Step function variation 85
4.1.3.2 Rectangular function variation 88
4.1.3.3 Sinusoidal function variation 94
4.2 Experimental Setup 97
4.2.1 Measurement of Belt Speed 97
4.3 Results and Discussions 98
4.3.1Verification of Model 98
4.3.2 Yarn Properties and Final Twist 100
4.4 Simulations 101
4.4.1 Step Function Variation 102
4.4.2 Rectangular Function Variation 104
4.4.3 Sinusoidal Function Variation 108
4.5 Summary 110

Chapter V Study of Yarn Properties in the Ring Spinning System with Single Friction-belt False-twister 112
5.1 Belt Position 112
5.1.1 Single Belt 112
5.1.2 Double Belt 118
5.2 Belt Friction Surface and Geometry 125
5.1.1 Measurement of Coefficient of Friction 127
5.1.2 Measurement of Yarn Twist in High-twisted Zone 129
5.2 Most Influencing Factors on the Yarn Properties 130
5.2.1 Material Preparation 130

5.2.2 Yarn Measurement 131
5.2.3 Experimental Design 132
5.2.4 Results and Discussion 133
5.3 Parameter Optimization 138
5.3.1 Experimental Design 138
5.3.2 Results and Discussion 140
5.3.2.1 Measured yarn performance 140
5.3.2.2 Fitted equations 141
5.3.2.3 Model validation 142
5.3.2.4 Effects of control variables on the responses 143
5.3.2.4 Optimization of yarn properties 148
5.4 Further Investigation on Yarn Neps 151
5.4.1 The occurrence of neps during spinning 151
5.4.2 Improving yarn neps by shortening yarn path on the belt 154
5.4.3 Improving yarn neps by increasing belt hardness and surface roughness 155
5.4.4 Improving yarn neps by controlling fibers in the spinning triangle 155
5.5 Summary 158

Chapter VI Performances of Knitted Fabrics Made from the Modified and Conventional Yarns 160
6.1 Experimental 160
6.1.1 Yarn Preparation 160
6.1.2 Fabric Preparation 161
6.1.3 Testing Method 161
6.2 Results and Discussions 162
6.2.1 Yarn Properties 162
6.2.2 Fabric Properties 163
6.3 Summary 167

Chapter VII Conclusions and Future Work 168
7.1 Conclusions 168
7.1.1 Yarn Dynamic Model 168
7.1.2 Yarn Kinematic Model 169
7.1.3 Investigation of Yarn Properties 169

7.1.4 Evaluation of knitted Fabrics 171
7.2 Limitations and Future Work 171
Appendices 173
Appendix A: Jacobian matrix *A(x)* 173
Appendix B: Flow diagram of calculating the three coefficients 174
Appendix C: Parameter optimization in double-belt system 175
References 186

List of Figures

Figure 1-1 A schematic diagram of Nu-Torque technology 2

Figure 2-1 A schematic view of ring spinning process 9
Figure 2-2 A schematic view of rotor spinning process [2] 10
Figure 2-3 A schematic view of friction spinning process [2] 11
Figure 2-4 A schematic diagram of air-jet spinning process [56] 13
Figure 2-5 A schematic diagram of vortex spinning [60] 14
Figure 2-6 Spinning triangle of Siro-spun process [70] 15
Figure 2-7 Solo-spun spinning attachment [73] 16
Figure 2-8 A schematic view of compact spinning process [30] 17
Figure 2-9 Influence of twist on yarn strength [102] 19
Figure 2-10 Seam displacement on a knitted sweater (left) and 'Snakes' on a denim (right) 20
Figure 2-11 A schematic diagram of the modified ring spinning process 21
Figure 2-12 Formation and release of twist on static and running yarn [103] 22
Figure 2-13 Spinning triangles of 58 tex Nu-Toruqe yarn (left) and normal ring yarn (right) [104] 23
Figure 2-14 Magnetic spindle (left) and friction-belt (right) false-twisters 23
Figure 2-15Ne 20 Nu-Torque yarn with 440 tpm (left) and 20 Ne normal ring yarn with 634 tpm (right) 24
Figure 2-16 3D configurations of a fiber in a ring yarn (a) and a Nu-Toruqe yarn (b) with 29.53 tex and 440 turns/m [106] 25
Figure 2-17 Typical cross-sectional images of Tencel yarn (20Ne, α_e =2.5) under undeformed state: ring Tencel yarn (left) and Nu-torque tencel yarn (right) [108] 26
Figure 2-18 Nu-Torque products in the market 26
Figure 2-19 Twisting of a yarn element 27
Figure 2-20 Force acting on a yarn element 29
Figure 2-21 Hand-held yarn Tensiometer (left) and general purpose online tension sensors (right) 37
Figure 2-22 Technical roadmap 41

Figure 3-1 A novel twisting system.....46
Figure 3-2 Modeling analysis of a yarn segment. (a) A yarn segment in the moving coordinate system. (b) Forces acting on a yarn element. (c) Analysis on yarn motion. 48
Figure 3-3 Geometrical boundary condition.....52
Figure 3- 4 Calibration of yarn tension.....56
Figure 3- 5 Measured yarn tension 56
Figure 3- 6 A high-speed photography system 57
Figure 3- 7 Determination of yarn twist from image 58
Figure 3- 8 Calibration of yarn twist.....58
Figure 3- 9 Yarn dynamic performances on the moving belt. (a) Tension distributions for three cases. (b) Distributions of deviation angle for three cases. (c) Twist distributions for three cases.....63
Figure 3- 10 Twist efficiency and coefficients of twist trapping and congestion by univariate experiment. (a) Different twist levels. (b) Different tension levels. (c) Different speed ratio. (d) Different wrap angle.....67
Figure 3-11 Calculated torsional rigidities for different cases.....68
Figure 3-12 Normal probability plots of residuals for responses.....76
Figure 3-13 Response surface plots for (a) twist efficiency, (b) twist trapping, and (c) twist congestion.....78
Figure 3-14 Linear relationships among three responses.....80

Figure 4-1 A schematic diagram of the novel twisting system 84
Figure 4-2 Twist blockage in twisting zone: (a) twist trapping in region BC (b) twist congestion in region BC.....85
Figure 4-3 Calibration of the speed sensor 98
Figure 4-4 Sinusoidal variation of the false twist and comparison of experimental data against predicted data in OA zone.....100
Figure 4-5 Twist variations in the three zones after a step change in false twist.....102
Figure 4-6 Effects of system parameters on $\overline{\Delta T_1}$ and $\overline{B_{T1}}$ 103
Figure 4-7 Effects of system parameters on $\overline{\Delta T_3}$ and $\overline{B_{T3}}$ 104
Figure 4-8 Twist changes in the three zones after a small rectangular change in false twist of duration $\overline{\Delta t}$ 105

Figure 4-9 Effects of system parameters on $\overline{\Delta T_1}$ and $\overline{B_{T1}}$ 106
Figure 4-10 Effects of system parameters on $\overline{\Delta T_3}$ and $\overline{B_{T3}}$ 107
Figure 4-11 Twist changes in three zones by sinusoidal variation in false twist 109
Figure 4-12 Effects of $\overline{f}$, $\overline{l_1}$ and belt properties on the amplitude of $\overline{\mathbf{T_1}}$ and $\overline{\mathbf{T_3}}$ 110

Figure 5- 1 Schematic view of belt position in a ring spinning frame.....114
Figure 5- 2 Calculated wrap angles $\angle AO_1B_0$ (up) and $\angle AO_1B_1$ (down).....115
Figure 5- 3 Calculated maximum variations of the wrap angle.....116
Figure 5- 4 Calculated yarn guide friction angles $\angle B_0G_0X_0$ (up) and $\angle B_1G_1X_0$ (down) 117
Figure 5- 5 The feasible region and wrap angle in Cartesian coordinate system 118
Figure 5-6 Schematic view of belts position in a ring spinning frame 120
Figure 5-7 Calculated wrap angles of the upper belt $\angle AO_1B$ (a) and lower belt $\angle CO_2D_0$ (b) and $\angle CO_2D_1$ (c) 122
Figure 5-8 Calculated maximum variation angle of the lower belt 123
Figure 5-9 Calculated friction angle of the guide $\angle D_0G_0X_0$ (a) and $\angle D_1G_1X_0$ (b).123
Figure 5-10 Calculated total wrap angle in the feasible region 124
Figure 5-11 The effect of *L* on the maximum wrap angle of the two belts.....125
Figure 5-12 Calculated total wrap angle at *L*=90 mm 125
Figure 5- 13 Schematic view of the designed device for measuring the coefficient of friction.....127
Figure 5- 14 Yarn twists in high-twisted zone for different belts.....130
Figure 5-15 Significance of four selected parameters on yarn performance 135
Figure 5-16 Main effect of yarn performance.....138
Figure 5-17 Effects of three factors on yarn mean tenacity 144
Figure 5-18 Effects of three factors on yarn evenness.....145
Figure 5-19 Effects of three factors on thin places (-40%).....145
Figure 5-20 Effects of three factors on thick places (+50%) 146
Figure 5-21 Effects of three factors on neps (+140%).....147
Figure 5-22 Effects of three factors on hairiness (S3) 148
Figure 5-23 Overlaid contour plot of yarn performances 149
Figure 5-24 Scanned images of blackboard evenness.....151
Figure 5-25 Movements of the yarn and belt in the system.....153

Figure 5-26 Transverse movement of the yarn on the belt.....153
Figure 5-27 Enlarging wrap angle by introducing a rotatable guide.....157
Figure 5-28 The rotatable guide (left) and its dimension (right) 157

Figure 6-1 Blackboard evenness of C-3.6C and C-3.2S cone yarns.....163
Figure 6-2 Bursting strength of knitted fabrics (t-test *p*-value: 0.85) 165
Figure 6-3 Air permeability of knitted fabrics (t-test *p*-value: 0.30).....165
Figure 6-4 Thermal conductivity of knitted fabrics (t-test *p*-value: 0.00) 166
Figure 6-5 Q-Max of knitted fabrics (t-test *p*-value: 0.01) 166
Figure 6-6 ICI pilling grade of knitted fabrics (t-test *p*-value: 1.00) 167

List of Tables

Table 2-1Comparison of various spun yarn technologies 17
Table 2-2 Comparison of various twist measurement methods 34

Table 3-1 Parameters for case study 59
Table 3-2 Results of simulated values and experimental observations 60
Table 3-3 Parameters of different univariate experiment 64
Table 3-4 Coded and actual level for each variables of the CCD 69
Table 3-5 Coded and actual levels in experimental design by CCD method 71
Table 3-6 Analysis of variance for responses 73
Table 3-7 Analysis of the reduced regression model 74
Table 3-8 Model verifications for 9 cases 76

Table 4-1 System parameters 98
Table 4-2 Measured properties of conventional yarns and yarns with and without belt speed variations 101

Table 5-1 Belt specifications 128
Table 5-2 Measured coefficients of friction 128
Table 5-3 Fiber and roving specifications 130
Table 5-4 Yarn tests and standards 131
Table 5-5 Fractional factorial design 132
Table 5-6 Experimental design expressed in natural variables 132
Table 5-7 Yarn properties of fractional factorial experiments 133
Table 5-8 Analysis of variance for responses 136
Table 5-9 Coded and actual level for each variables of the CCD 139
Table 5-10 Actual levels in experimental design by CCD method 139
Table 5-11 Measured yarn performance of RSM experiments 140
Table 5-12 Fitted equations of Ne 40 yarns in coded values 142
Table 5-13 Model verifications for 9 cases 142
Table 5-14 The optimized parameters for Ne 40 cotton yarn 149
Table 5-15 Properties of the optimized and conventional yarns 150

Table 5-16 Blackboard evenness of the optimized and conventional yarns 151
Table 5-17 Yarn properties affected by belt diameter 154
Table 5-18 Yarn properties affected by belt surface hardness and roughness.....155
Table 5-19 Yarn properties produced by the combination of Nu-Toruqe and Compact 157

Table 6-1 Yarn spinning parameters.....160
Table 6-2 Knitting parameters.....161
Table 6-3 Fabric testing standards and apparatus 162
Table 6-4 Properties of the cone yarns.....162
Table 6-5 Blackboard evenness of the Ne 40 cone yarns.....163
Table 6-6 Fabric specifications 164

Chapter I Introduction

1.1 Research Background

Spinning is a fundamental method to impart strength and make continuous yarns by twisting short or staple fibers [1]. The yarns are then woven or knitted into fabrics for apparel and home-textile applications, where cotton, wool or man-made synthetic fibers are used [2]. With an output of 41,021,976 tons produced from all fibers and world cotton consumption of 23,633,845 tons in 2012[3], spun yarns show the dramatic swell of global textiles and apparel industry in the past decades. Among all the spinning technologies, ring spinning has become the most dominating method since it was invented in the 19th century. According to the latest statistics by International Textile Manufacturers Federation[3], the total number of ring spindles in the world was an astounding 244,863,631 in 2012, and the total number of open-end rotors was 8,322,831, adding much smaller number of other spinning methods such as jet spinning, vortex spinning, etc.

Twisting is a vital process because it determines the staple yarn structure and yarn performances like strength (tenacity), elongation, evenness and hairiness, by manipulating a bundle of separated short fibers and assembling them into a consolidated yarn. In most textile manufacturing processes, the number of twist in yarn varies along its length because of the positive twisting torque generated by twisting element or twist blockage by contacting the surface of a machine part. Much valuable work has been carried out to investigate the twisting processes in ring spinning [4], rotor spinning [5-7], friction spinning [8], self-twist spinning [9], air-jet spinning [10], etc. Meanwhile, the twist blockage caused by yarn guide [11] and tension meter [12, 13] in spinning and weaving/knitting machine has been widely explored. However, few studied the situation in which twisting generation and twist blockage coexist on one machine part.

Currently, a novel twisting technology, named Nu-Torque, has been developed for producing low twist and soft handle singles yarns by introducing one or two friction-belts [14], which are incorporated in conventional ring spinning machine as false-twisting elements, and at the same time blocks the propagation of twist from the spindle and the false-twisting element, as shown in Figure 1-1. Due to the

incorporating of the false-twister, twist distributions in the yarn spinning zone are altered. In the upstream of the false-twister, a high twist level is achieved by combined twist coming from the false-twister and twist propagation through the false-twister from the traveler, which modifies the geometry of spinning triangle and greatly influences the distribution of fiber tension forces and fiber arrangements in a yarn, resulting in modified yarn structure and properties; while in the downstream of the false-twister, a low twist yarn is obtained by 10-40% traveler twist reduction without notable yarn ends down, which results in a low residue torque and soft handle style [15, 16].

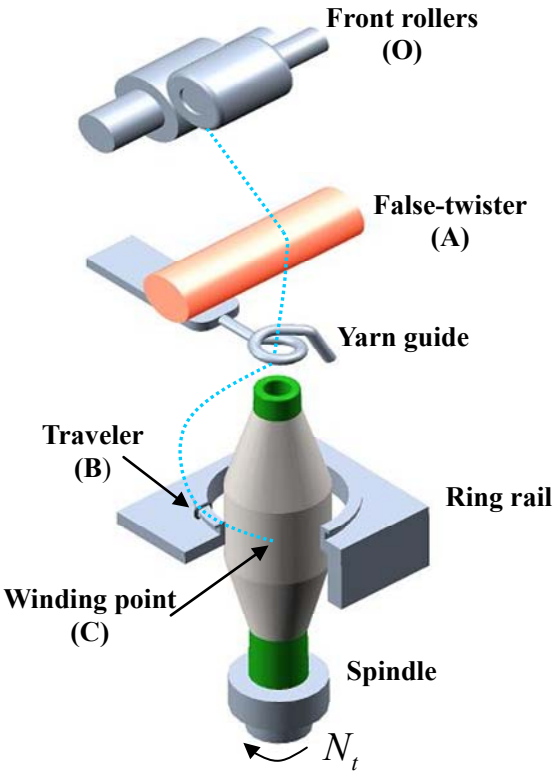

Figure 1-1 A schematic diagram of Nu-Torque technology

Structural analysis revealed that most internal fibers of the modified cotton ring yarns have much lower inclination angles and some fibers have the inclination angle of alternating orientation, thus yielding a reduced yarn torque. Besides, the modified cotton yarns have a densely packed zone which is located in somewhere half way from the centre to the surface of the yarn, thus the low twisted yarn can still hold itself with a comparable tenacity and show good pilling property. Comparative studies [15, 17, 18] have proved that the modified cotton yarns and fabrics have evident merits in terms of soft handle, higher yarn strength at lower twist factor, lower

residual torque and low knitted fabric spirality after washing and tumble-dry cycles. Among over ten mills using the technology, 10 to 40% increment in production rate has been achieved for cotton ring yarns with various versions of the technology. In addition, a significant average energy saving of 337KWh/ton was reported by a mill producing Ne 30 and 1100 Kwh/ton for another mill for spinning Ne 80 yarns.

Although the previous work [19, 20 21-23] have revealed the spinning triangle, internal structure as well as unique properties of the resultant yarns and fabrics, foundation mechanisms of the false-twisting process, stability of false-twister subject to external perturbation, as well as effects of belt spatial and friction surface on the false-twisting process and yarn properties remain research gaps. The twist generation and propagation play a critical role in forming unique structure and performance of the resultant yarns. It is therefore of great importance to understand the relations among twisting process, system parameters as well as the yarn properties. Moreover, as a twisting element, the belt geometric structure, and friction surface may affect on twisting process and surface appearance of resultant yarns. In addition, stability of the twisting process may be influenced by vibrations of the belt since the twist element belongs to a kind of elastomer, which contributes to variation of the false twist. Therefore, the proposed research will also study effects of false-twisting variations on the twisting process as well as resultant yarn properties.

1.2 Aims and Objectives

The proposed project is concerned with a systematic investigation on experiment, modeling, and analysis of yarn dynamics in a novel twisting system, with single friction-belt false-twister introduced in the conventional ring spinning frame, for producing low twist yarns with the following specific objectives:

(1) to understand the novel twisting phenomenon through establishing a steady-state model of yarn dynamics on a moving belt and to systematically study effects of system parameters on yarn tension and twist distributions in the twisting process, which determine the yarn internal structure and physical properties;

(2) to study system stability and robustness by building up a transient model of yarn twist perturbed by variations of the false twist and check yarn properties affected by such variation;

(3) to solve excessive yarn neps by widely exploring effects of belt friction

surface and spatial position and quantitatively examining relationships between system parameters and physical properties of resultant yarns;

(4) to evaluate and compare properties of knitted fabrics produced by the conventional and modified yarns such as fabric weight, thickness, loop length, bursting strength, air permeability, thermal property, pilling resistance, etc.

1.3 Research Methodology

After reviewing the relevant literatures, the research methodology is declared for the systematic investigation on the novel twisting system including machine modification, spinning parameters, and yarn evaluation.

(1) A steady-state model of yarn dynamics on a moving belt

In this study, a steady-state model has been proposed to study yarn dynamics on a moving belt. The novel twisting system has been investigated by incorporating both twisting generation as well as twist blockage. Dynamic equations of moving yarn have been established and solved numerically by Newton-Raphson method. The simulation results were validated by the measurement system using high-speed photography and tension sensor. Influences of various system parameters in terms of twist factor, traveler weight, speed ratio and wrap angle on twisting efficiency of moving belt, propagation coefficients of twist trapping and congestion were examined;

(2) A transient model of yarn twist kinematics

In order to assess stability of yarn twist affected by variations of false twist in a modified ring spinning frame as well as to comprehend effects of system parameters on twist redistributions, a theoretical model has been proposed based on twist kinematics. Three idealized cases that cause twist variations in spinning process have been studied, namely step change, rectangular change and sinusoidal variation in false twist. With the developed model, essential system parameters were numerically examined and their quantitative relationships were analyzed. Moreover, a control and measuring system were built up for online control movement of false-twister and measure instant yarn twist. Comparisons were made between theoretical calculations and experimental observations. More important, yarn properties affected by twist variations were assessed.

(3)Exploration of friction-belt on yarn properties

Since the friction-belt has been employed as a false-twister and directly contacts

with yarns, it is of great importance to understand effects of belt friction surface and spatial position on the system parameters as well as resultant yarn properties in the modified ring spinning system. Belt with different diameter, hardness, coefficient of friction and roughness were explored, and their effects on yarn properties were examined. Moreover, the belt spatial position in the ring spinning system was introduced and their relations with belt wrap angle were numerically calculated. In order to systematic evaluation of yarn properties produced in the ring spinning system with single friction-belt false-twister, a systematic optimization has been conducted to fully examine the quantitative relationships between various system parameters and yarn properties (Ne 40 cotton yarn). First, based on the preliminary analysis of belt friction surface and spatial position, the underlying factors were identified. The fractional factorial methodology has been employed to investigate the significance of each factors on the yarn properties. Then, response surface methodology (RSM) involving a central composite design (CCD) in three factors of twist multiplier, speed ratio and wrap angle has been employed for the study and analysis. The obtained quadratic regression models has been validated by normal probability analysis and another nine randomly selected experiments. The significant terms of the models were studied and relationships among the responses were discussed.

(4) Investigation of fabric properties made from the modified yarns

For preparing fabric samples, quantities of Ne 40 modified yarns as well as conventional yarns were spun, respectively. Then, the prepared cop yarns were wound on the cone before knitting. After that, three single yarns were fed into the gauge of flat knitting machine and the interlock structure was adopted to avoid the fabric spirality. Properties and performances of the knitted fabrics were evaluated and compared, including fabric weight, thickness, loop length, bursting strength, air permeability, thermal property, pilling resistance, etc.

1.4 Significance and Values

The project generates at least three original and innovative outcomes. A steady-state model and a transient model have been proposed. These two models give rise to a better comprehending of the mechanisms of false-twister adopted in a ring spinning frame and provide method of calculating the practical levels of twist

control required to reduce certain remarkable yarn faults.

Moreover, the modified ring spinning technology is further developed for production of higher quality yarns, compared with conventional ring yarns spun with the same fiber count. With superior handle and other excellent properties of yarns and fabrics, the project helps staple fibers to be better applied.

Another long term significance of the project is that it provides new insight to the yarn twisting system. Specifically, the treatment of the false-twister in current work uses the moving belt, which can be replaced by other types of twisters for practical applications. Secondly, the work is based on the ring spinning frame, which can be further extended to other twisting frames like rotor, friction, air-jet, etc. Thirdly, the outcomes and findings in the current work also provide references for applications in the fields of smart textiles for functional activities.

1.5 Structure of the Thesis

The thesis is composed of seven chapters. Chapter I introduces the research background, aims and objectives, research methodology and significance and values. The outline of the thesis is given.

Chapter II presents an extensive review on the spun technologies, including the conventional, unconventional and modified ring-based methods, and their resultant yarn structures and properties. Moreover, methods of theoretical modeling and experimental measurement of yarn tension and twist are retrospected. In addition, optimization methods of yarn properties are covered. Finally, the research gaps and problems are stated and summarized.

Chapter III proposes a theoretical model of yarn dynamics on single friction-belt false-twister in a modified ring spinning system. Equations of yarn motion are established and the boundary value problems are numerically solved by Newton-Raphson method. The simulation results are validated by experiments and a good agreement has been demonstrated. Influences of several parameters on the twisting process have been revealed in terms of twist efficiency of the moving friction-belt, propagation coefficients of twist trapping and congestion. Based on the proposed model, the twisting process of yarn dynamics on a moving belt is systematically examined using response surface methodology. The significant terms are identified and relations among the responses of twist efficiency, propagation

coefficients of twist trapping and congestion are investigated.

Chapter IV reports on effects of variation of false twist on process stability and resultant yarn quality in a modified ring spinning frame. Based on twist kinematics, a transient model is proposed. Three idealized cases that cause twist variations in spinning process are investigated, namely step function, rectangular function and periodic function changes in false twist. The simulation results are validated by experiments and a good agreement has been demonstrated. With the developed model, essential system parameters are numerically examined and their quantitative relationships are studied. The practical implications are discussed.

Chapter V systematically studies the properties of Ne 40 cotton yarn produced by the modified ring spinning system. Based on the analysis of belt friction surface and geometry, potential influencing factors are identified, and the fractional factorial methodology is employed to find out the statistically significant factors on yarn tenacity, evenness and hairiness. Then, these factors are further explored using response surface methodology. The second order equations are obtained to examine and estimate the relationships between the factors and responses. Finally, the yarn with optimized parameters is spun and compared with the conventional yarn.

Chapter VI explores and compares the surface characteristics, physical properties of the knitted fabrics made from the conventional and modified yarns, including fabric weight, thickness, loop length, bursting strength, air permeability, thermal property, pilling resistance, etc.

Chapter VII provides a general conclusions of the present study as well as limitations and suggestions for the future work.

Chapter II Literature Review

This chapter presents an extensive review on the spun technologies, including the conventional, unconventional and modified ring-based methods, and their resultant yarn structures and properties. Moreover, research methods of theoretical modeling and experimental measurement of yarn tension and twist, optimization of yarn properties are covered. The purpose of this review is to develop a complete understanding of the previous research in this area, and identify issues for further investigations.

2.1 Spun Yarn Technologies

2.1.1 Conventional Method

Among all spinning technologies commonly in use, ring spinning is the most predominant one for staple fiber production because of the high quality of its resultant yarn and wide range in terms of the applicability of raw materials and yarn count it can manufacture [24, 25]. Three steps are completed by this machine simultaneously and continuously, they are drawing out fiber strand to the required count, inserting twist to the yarn by means of a rotating traveler as well as winding the yarn onto a bobbin.

As displayed in Figure 2-1, the yarn package is firmly sit on a spindle driven by a motor and the traveler is held by the ring which is installed around the spindle. After delivering from the front rollers, the drafted fiber strands are twisted in to a yarn, and then led to the yarn package. The traveler cooperates with the spindle so as to wind the twisted yarn on a cop driven by the spindle. Actually, the rotation speed of spindle is slightly higher than that of the traveler, and the difference between them is the yarn delivery speed. The ring moves up and down during the spinning process, which decides the profile of yarn package.

Ring spun yarns produce high quality and are flexible in processing various materials and yarn count. The yarn is comparatively compact and the majority fibers in the ring yarn have a concentric helix structure [26, 27]. The fiber is uniformly arranged along the radial direction of the yarn, without wrapper or hooked fibers. The concentric conical structure of minority fibers in a yarn is the result of intensive

fiber migration, which in turn is determined by the geometric dimension of the spinning triangle [28, 29].

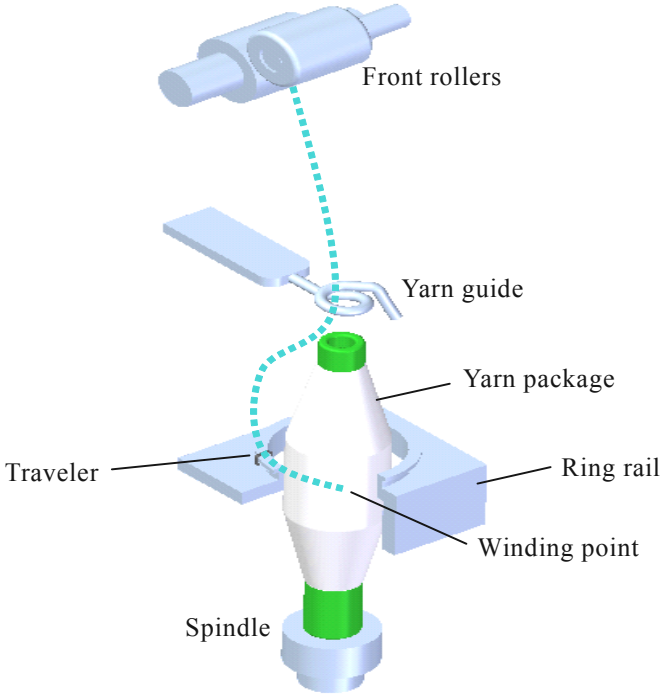

Figure 2-1 A schematic view of ring spinning process

However, ring spinning method is relatively expensive due to its low production efficiency and the additional processes (roving and winding) involved [30, 31]. A large number of unconventional spinning methods have been developed to improve productivity and shorten spinning procedures, like rotor, air-jet , vortex and friction spinning.

2.1.2 Unconventional Methods

2.1.2.1 Rotor spinning

Rotor spinning is an effective and significant spinning method by separating twisting and winding in the yarn production process [24, 25]. The success of rotor spinning is attributed to a substantial improvement in productivity, and the possibility of full automation of the spinning process [32]. Currently, the production rate of rotor spinning has exceeded 200 m/min, and can produce yarn count up to Ne 60 in the textile mill (e.g. Rieter ComfoRo® rotor system). Rotor spinning offers not

only high productivity but also superiority in yarn hairiness, evenness and abrasion in comparison with ring yarns [33].

As shown in Figure 2-2, fibers are provided to the rotor system in the form of sliver, which is fed by the feed roller and plate. Fibers and trash are separated and the latter is removed by trash extraction. The silver fibers on the opening roller are drafted under a high ratio and the fibers are then flowed down the transport channel into the rotor. The rotor has partial vacuum, therefore the separated fibers are further attenuated by the air steam in the transport channel. Fibers are condensed in the groove of the rotor due to the air drag and centrifugal forces generated by the rotation of the rotor. At the same time, the tail end is twisted with each revolution of the rotor to form a rotor spun yarn. The yarn is then taken up by a pair of rollers to form yarn package.

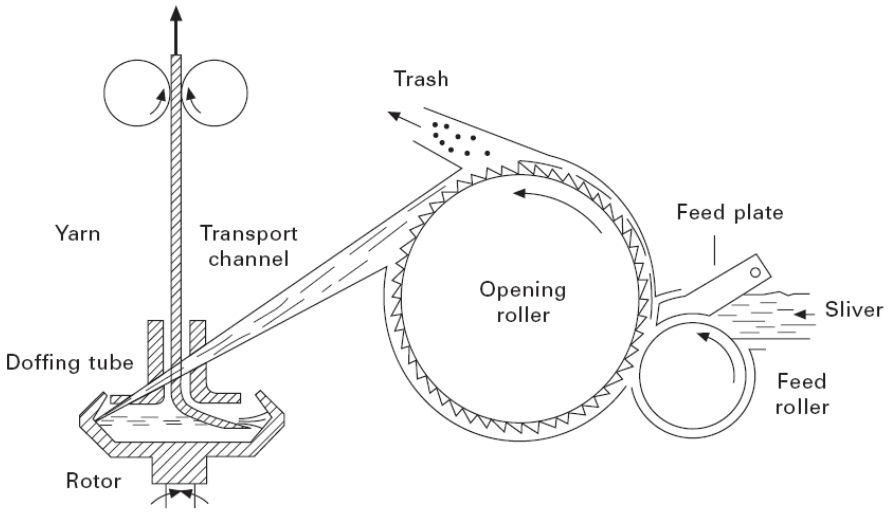

Figure 2-2 A schematic view of rotor spinning process [2]

Rotor spun yarns exhibit unique structure and properties [34]. The core fibers are densely packed and the sheath fibers are loosely packed, while the wrapper fibers are wrapped around the outside of the yarn at a very large inclination to the yarn axis [35, 36]. Fiber migration in rotor yarn are very local and tied only to the fibers of adjacent layers with lots of hooks and looped fibers [37]. Rotor spun yarns are weaker than ring spun yarn because of high numbers of disoriented folded fibers, low level of fiber migration, less packing and presence of wrapper fibers [38]. Rotor spun yarn also shows higher abrasion resistance and more extensible, but limitations on harsh

handle and finer count [39, 40].

2.1.2.2 Friction spinning

The significant merit for friction spinning system is low spinning tension and high production speed up to 500 m/min can be achievable [25, 41]. It can produce yarn count up to 40Ne in the textile industry (e.g. DREF-5 System). This system stands unique in producing multi-component yarns from a wide range of different fibers, when compared to other spinning methods [42].

As depicted in Figure 2-3, the friction spinning system is composed of the following operations: feeding a sliver of fibers into the inlet rollers, separating the sliver into individual fibers by carding drum, reassembling and twisting the fibers to form the yarn by spinning drums, finally winding the yarn onto a bobbin to form a yarn package [43]. The fibers are twisted by rotating perforated cylinder, in close proximity with each other and driven in the same direction.

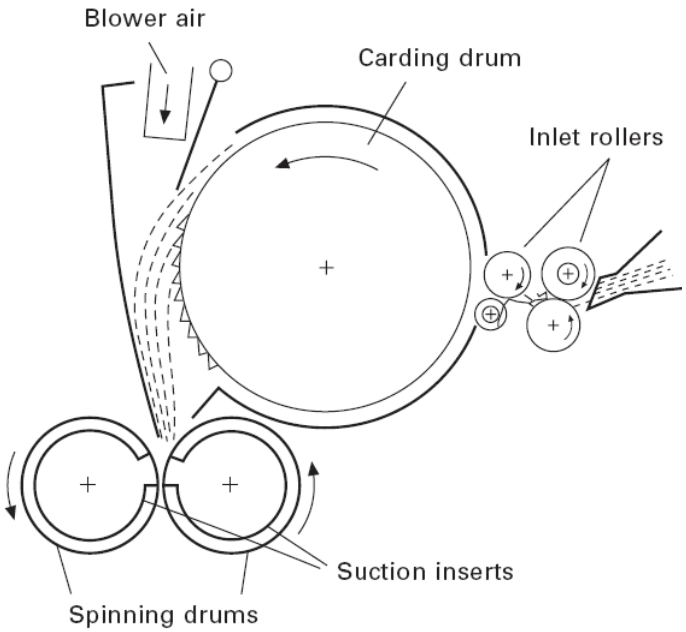

Figure 2-3 A schematic view of friction spinning process [2]

The internal structure of a friction spun yarn is featured by its inferior fiber helix angle, buckled and folded fiber configurations, and loose packing of the fibers in the cross-section, associated with low tension during yarn production [44, 45]. In the friction spinning system, a fiber is not fed to the yarn tail at the same position along

the tail length, which results in that some parts of a fiber appear at the yarn surface and other parts closer to the yarn centre [46-49]. The fiber-strength translation efficiency is very low in friction spun yarns and the minimum number of fibers needed in friction spun yarns is higher than in other spinning methods [50].

With respect to yarn properties, friction spun yarns show lower tenacity than ring and rotor spun yarns, and the magnitude of difference depends on the raw material, spinning conditions, and machine versions used [51]. Besides, friction spun yarns are also inferior in terms of unevenness, imperfections, strength variability, and hairiness. The mass irregularity of air jet, ring, and wrap spun yarns is similar, but friction spun yarns have a higher irregularity, although lower than that of rotor spun yarns [52]. The imperfections are also less in friction spun yarns than in rotor spun yarns but were higher than those in ring and air jet spun yarns. Further, friction spun yarns are more hairy and susceptible to stripping back and thus abrading easily. For hairiness longer than 3 mm, friction spun yarns are more hairy than ring spun yarns, while rotor spun yarns demonstrate the lowest value in both aspects [53, 54].

2.1.2.3 Air jet spinning

Air jet spinning has become a promising technology for producing staple fiber yarns with high productivity [2]. And its productivity is independent of yarn counts and the amount of twist in the yarn [55]. Murata Vortex Spinner (MVS) is one famous air jet machine which can produce finer yarns up to Ne 60.

As demonstrated in Figure 2-4, Murata Jet Spinner (MJS) is composed of passing an attenuated fiber strand through two pneumatic nozzles situated between the front rollers of the three-line drafting system and the delivery rollers. Sliver is fed into the machine and further drafted to the final yarn count, meanwhile yarn is twisted by means of swirl flow of high pressured air. Finally, the delivery rollers take up the yarn and transport it to a bobbin for winding. During the spinning process, some fibers at the edges of the ribbon are not fully twisted by the first nozzle, thus they obtain less twist than those fibers in the main bundle. When the yarn is untwisted by the second nozzle, the edge fibers are untwisted to a greater degree than their original twist. Therefore they are subjected to give a real twist in the direction reverse to that of the upstream twist. The main fibers in the yarn are untwisted into parallel fibers, forming the core while edge fibers are wrapped around the core

forming the wrapper fiber layer. The purpose of the second nozzle is to increase the fiber-fiber interaction thus given better yarn strength. The air flow in the second nozzle tends to untwist the core of the yarn to give the straight parallel arrangement of the fibers. Simultaneously the edge fibers, due to their less preliminary twists, are untwisted and then wrapped in the reverse direction around the core. Unlike the wrapper fibers in the rotor yarn, the surface fibers of the air jet yarn are helical in nature.

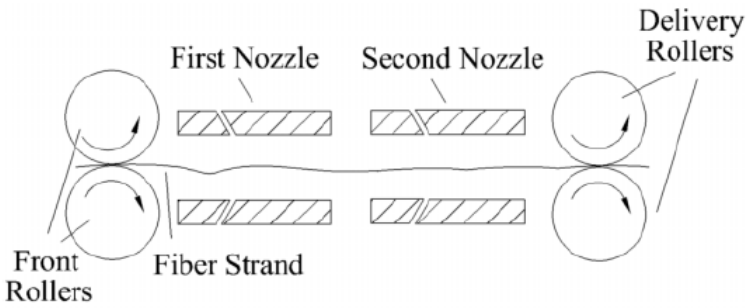

Figure 2-4 A schematic diagram of air-jet spinning process [56]

The air jet yarns have a special fasciated structure, which comprise an untwisted core of parallel fibers, accounting for 85-95% of the yarn mass, and a surface wrapping of fibers [57]. The wrap fibers decide the compactness and the strength of the yarn, which force radial pressure over the core fibers and prevent their slippage during deformation [58]. Even so, the tensile strength of air jet yarns is lower than that of rotor and ring yarns. The untwisted core fibers have very low snarling tendency and the lack of twist in the air jet yarn core contributes to the low pilling property. Also it has been identified that with the increase of the number of the core fibers, the proportion of the protruding fibers is reduced, thus leading to lower yarn hairiness. The typical properties revealed by the air jet yarns have weaker tensile strength, low snarling and pilling tendency, as well as high stiffness and high shrinkage.

2.1.2.4 Vortex spinning

Vortex spinning is a refinement of air-jet spinning.[59] In vortex spinning, the twisting system has only one nozzle and the second nozzle is replaced by a hollow spindle which can be stationary or rotatory.[56] High pressure and high speed air is

injected into the nozzle chamber, and swirling airflow is then formed inside the nozzle chamber. It can be seen from Figure 2-5 that with the high-speed swirling airflow, the fibers is rotated and helical wrapped. In this way, twists are imparted into the yarn, and the resultant yarn is delivered out of the nozzle and wound onto a bobbin.

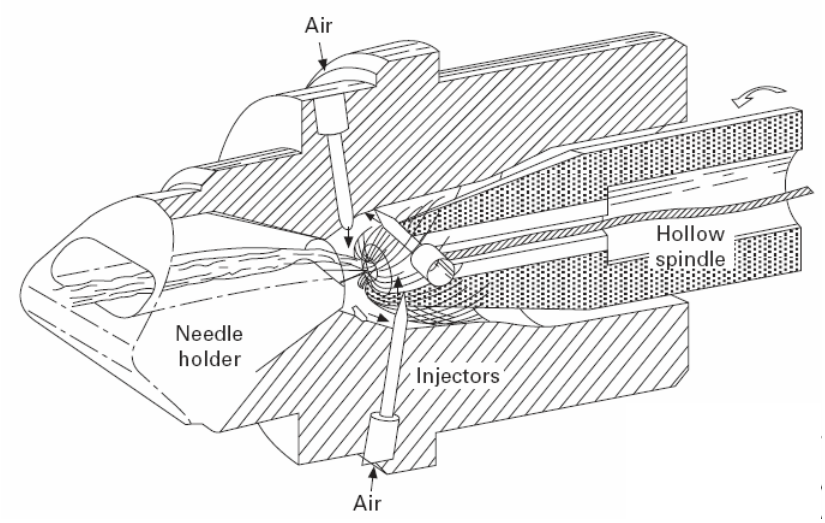

Figure 2-5 A schematic diagram of vortex spinning [60]

Like rotor spinning, vortex spinning is a cost-saving method to produce yarns since its high productivity as well as less production stages. Moreover, vortex yarns are more even, but weaker and have a harsher feeling than ring spun yarns.

2.1.3 Modified Ring Spinning Methods

2.1.3.1 Siro-spun spinning

Siro-spun spinning introduced the outcome of self-twist technology to the ring spinning, and combined spinning and doubling in one step [61-65]. As demonstrated in Figure 2-6, two rovings are fed in parallel into the drafting system, which are separated by two roving guides and attenuated separately. The twist is inserted as for a normal single yarn by means of ring and traveler. Two roving strands are combined after passing the front rollers, with certain twist produced in the individual strands right up to the nip line. After passing the front rollers, the two strands are combined to produce a two fold-like yarn. Although Siro-spun spinning was originally proposed for long staple fibers, it has become widely used in the short staple

spinning process [66, 67]. The main advantage of Siro-spun spinning is cost-saving, allowing a two fold-like yarn to be spun in one operation. Compared with conventional ring yarns, the Siro-spun yarns have smoother surface, higher tenacity, less hairiness and better frictional properties [68, 69] .

Figure 2-6 Spinning triangle of Siro-spun process [70]

2.1.3.2 Solo-spun spinning

Since singles worsted yarns are easily broken during weaving, it is necessary to produce two-fold, or ply yarns that can survive the tension. Solo-spun spinning is, therefore, invented to manufacture a singles yarn that can be successfully woven [71].

As shown in Figure 2-7, the Solo-spun spinning uses a easy, cheap, clip-on attachment to ring spinning machines that produces stable, single-ply worsted yarns [72]. The attachment is composed of an additional small roller clipped onto the spinning frame which is slotted with the lands and slots alternating around the circumference driven by the bottom roller. The function is to separate the roving strand into several sub-strands that are continually being altered, in order to enhance the fiber-trapping. The sub-strands converge at varied angles and rates to obtain a subtly entangled structure with locally differing twist levels.

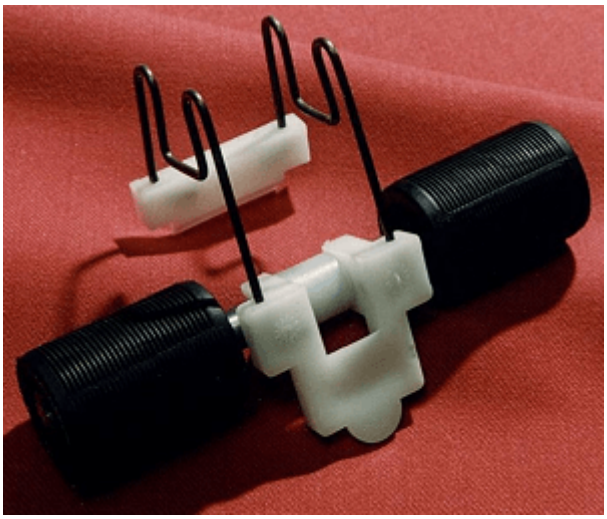

Figure 2-7 Solo-spun spinning attachment [73]

Solo-spun spinning improves yarn properties without the necessity of feeding two rovings as well as the extra components to handle them. It greatly reduces yarn hairiness and enhances fiber security so that a Solo-spun yarn can be weaved without sizing [74, 75]. The weaving performance of a Solo-spun yarn is better than that of a matched two-fold yarn using the same material, although the yarn evenness is slightly worse [76].

2.1.3.3 Compact spinning

Compact spinning has been recognised as a revolution in ring spinning, which is claimed to provide superior quality and better raw material utilisation [77]. Compact spinning modifies the spinning triangle with some additional attachments [78]. As shown in Figure 2-8, the concept of compact spinning is to minimize the width of fiber strand and a great reduction of the spinning triangle, realized via pneumatic or mechanical condensing system [30]. Ceramic thickening funnel condensing (Rotorcraft RoCoS) belongs to mechanical compact spinning pattern. Pneumatic pattern includes perforated drum condensing (Rieter ComforSpin Com4, K42 K46), lattice apron condensing (Suessen Elite Compact), and perforated apron condensing (Zinser Impact FX).

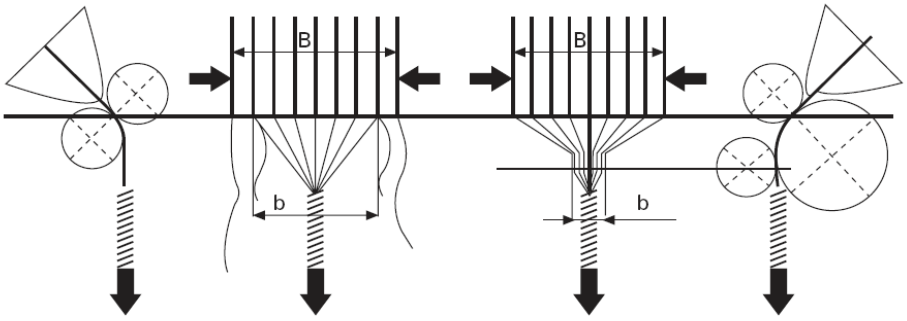

Figure 2-8 A schematic view of compact spinning process [30]

The low hairiness, high strength, and sound evenness are typical merits of compact yarns [78, 79]. Another advantage of compact spinning is to reduce twist level by 10-15% while keeping the same yarn strength as the ring spun yarn [80]. This results in increased productivity and decreased energy consumption. Compact spinning also provide chances for great cost-savings in the downstream processes [81-84].

2.1.3.4 Other ring-based methods

In the recent years, many new ring-based spinning technologies have been proposed to improve the yarn properties or spinnability such as embeddable and locatable spinning [85-88], jet-ring spinning [89-91] , jet-siro spinning [92-95] ,ring spinning with a diagonal path [96, 97], contact surface spinning [98], siro-solo spinning [99, 100], etc. However, most of them are still lab-based studies, which have not been commercialized due to some constraints of the specification or operation for mass production.

To sum up. rotor, air-jet, vortex and friction spinning can improve production efficiency and shorten spinning procedures, but in terms of yarn property and applicability of raw materials, ring spinning is still the major technology. New ring-based technologies like Compact, Siro-spun and Solo-spun can improve yarn properties by controlling the distribution of fibers in spinning triangle. However, all these technologies cannot significantly reduce the residual torque in singles yarns, not to mention the fabric performance, like seam displacement, spirality, distortion, etc. Various spinning technologies are summarised in Table 2-1.

Table 2-1Comparison of various spun yarn technologies

Type	Specific method	Advantages	Disadvantages
Conventional	Ring	●high quality ●flexible for materials ●flexible for counts	●low efficiency ●high residual torque ●high hairiness
Unconventional	Rotor Air-jet Vortex Friction	●high efficiency ●increased bulkiness	●Low strength ●Worse evenness ●count limitations ●material limitations
Ring-based	Siro-spun	●high strength ●low hairiness ●good evenness	●high residual torque ●low efficiency
	Solo-spun	●low hairiness ●good fiber security	●worse evenness ●low efficiency
	Compact	●low hairiness ●high strength ●good evenness	●high residual torque ●low efficiency
	Nu-Torque	●low hairiness ●low residual torque ●low twist ●improved efficiency	●worse evenness ●wrap structure

2.2 Nu-Torque Technology

2.2.1 The origins of Nu-Torque

Fundamental study of yarn structural mechanics has led to the invention and commercialization of a major breakthrough technology in staple yarn production. In conventional staple yarns, fibers are held together by the fiber-to-fiber friction that is derived from the pressure generated by the coaxial fiber helices. During the yarn production process, twisting increases fiber coherence and imparts strength to a staple yarn. The initially straight fibers are deformed into helices with mechanical

energy stored in the form of residual torque in the staple yarn. At low twist levels, the yarn fails due to fiber slippage; at high twist, the fiber slippage is largely stopped by high fiber-to-fiber interaction and thus the yarn failure mechanism is dominated by fiber breakage. Moreover, high twist decreases the conversion of fiber strength into the yarn strength because of fiber obliquity with regard to the yarn axis. Thus the maximum yarn tenacity is usually arrived at an in-between twist level. [101] Hearle *et al.* [1] expressed the above relationship by the following simplified equation

$$\frac{yarn\ strength}{fibre\ strength} = \cos^2\alpha(1-\frac{k}{\sin\alpha}) \qquad (2\text{-}1)$$

where α is the yarn surface twist angle, and *k* is a "slip factor" that decreases with increasing fiber length, fineness and fiber friction, and also with increasing fiber entanglement. The yarn twist and strength relationship is shown schematically in Figure 2-9.

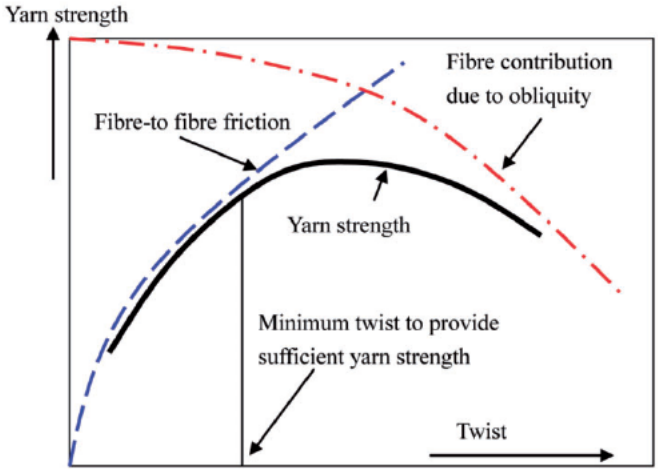

Figure 2-9 Influence of twist on yarn strength [102]

Yarn residual torque is the most prominent factor causing yarns to spiral, distorting single jersey knitted fabrics, resulting in surface unevenness of denim fabric after stone-wash finishing, as displayed in Figure 2-10. On the other hand, there is no residual torque in the yarns if they were not subject to twisting during the process. The lower the yarn twist, the higher the productivity and the lower the residual torque. However, lowering yarn twist inversely decreases yarn strength, even making the yarn not workable at all. It is a classic paradox in structural mechanics of ring spun yarns.

Figure 2-10 Seam displacement on a knitted sweater (left) and 'Snakes' on a denim (right)

From the advent of the ring spinning technology some 200 years ago, it has been widely accepted that it is not possible for a singles ring yarn to have low twist, low residual torque and high strength at the same time. To date, conventional ring spinning techniques cannot significantly reduce yarn residual torque by reducing twist while maintaining high yarn strength. Consequently, further yarn setting procedures are required in downstream processing, such as steaming, plying, and even chemical treatments. However, these treatments causes increase in energy consumption, discharges of waste gas, wastewater and chemicals, as well as fiber damage.

Since 1995, a major breakthrough in yarn spinning technology, namely the Nu-Torque technology has been achieved. It provides the means to produce low twist and low torque singles ring yarn in a single step on a ring spinning frame by modifying the yarn structure. Compared to the conventional spinning method, the main principle of Nu-Torque technology is to install false-twisting devices between the front rollers and the yarn guide in a traditional ring spinning machine, as shown in Figure 2-11. In this way, when fibers pass through the nip point of the front rollers, the twist in the spinning triangle raises to a maximum value. The extreme tension variation enlarges fiber migration. In the downstream zone of the false twister, the reverse twists are immediately introduced until the final twist remaining is that of the original low twist yarn. At last, the extra twist introduced by the false twister is removed. This technology yields novel yarns with unique structure and exciting properties, such as low torque, reduced twist and relatively higher strength.

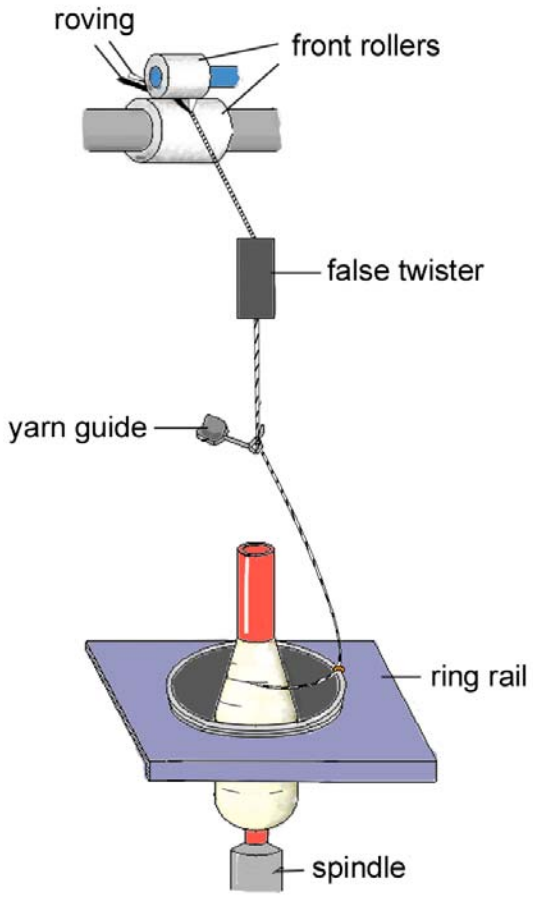

Figure 2-11 A schematic diagram of the modified ring spinning process

2.2.2 False-twisting Principles and Units

The mechanism of false-twisting is to twist a moving yarn and then continuously released on exiting the twist unit, as demonstrated in Figure 2-12 . For a static situation, with no axial yarn feed, an equal and opposite twist is formed in the upstream and downstream of the twist unit, respectively. When the yarn is fed in an axial direction through the twist unit, the twist inserted to the upstream yarn is offset by an equal and opposite twist downstream of the unit. As a result, the yarn remains zero twist downstream of the false-twister.

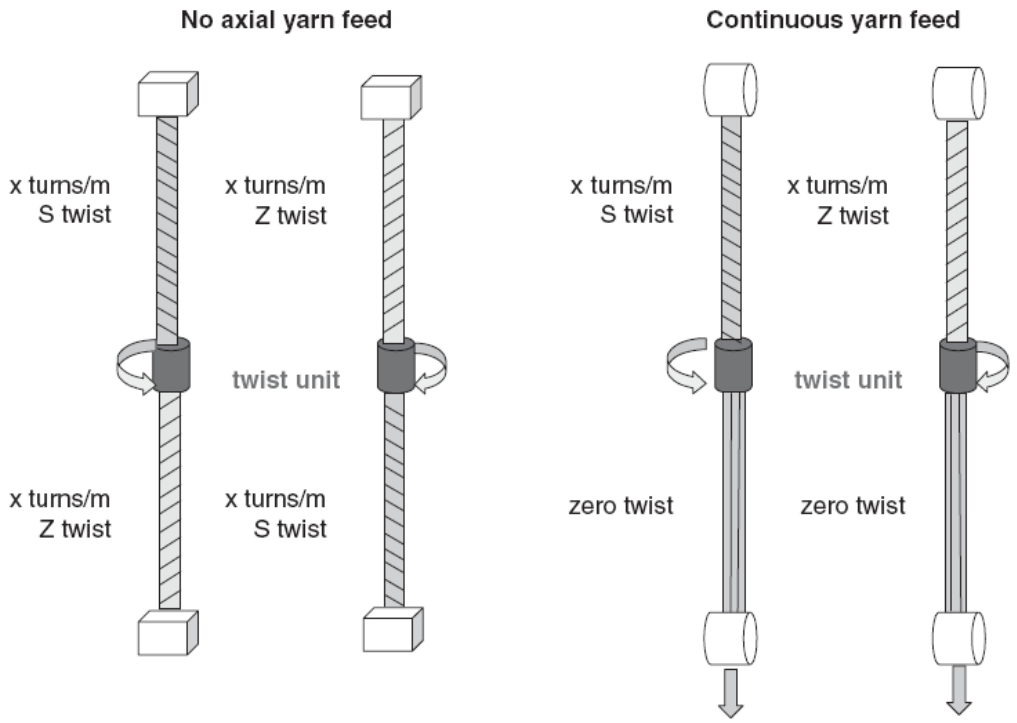

Figure 2-12 Formation and release of twist on static and running yarn [103]

The function of the false-twister is to impart false twists to yarns, change the fiber tension and its distribution in the spinning triangle, combined with the untwisting at the exit of false-twisting zones, to alter the arrangement of fibers and balance their residual torque in the yarn. Specifically, the height of the spinning triangle is greatly shortened because of the high twist level, as shown in Figure 2-13. Moreover, the high twist increases the tension forces of edge fibers in the spinning triangle, meanwhile it buckles the middle fibers, forming a split structure. As a result, the extreme tension variation enlarges fiber migration and fiber-to-fiber interaction are greatly enhanced, resulting in a particular yarn structure. A theoretical model based on the energy method indicates that the split structure in the spinning triangle increases the tension variation and finally obtains a low residual torque yarn. [19-21] In addition, the high twist decreases the chance of yarn ends down in the spinning triangle. After the twist unit, the yarn tension is high, which helps to hold the particular structure in the untwisting process and ensure the yarn quality in the low twist spinning.[15, 16]

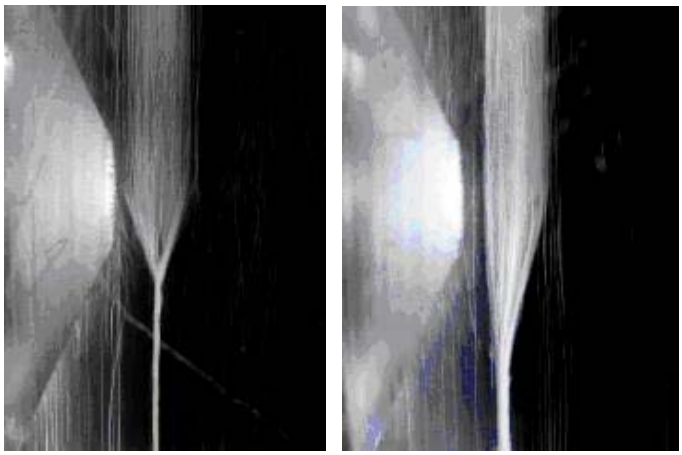

Figure 2-13 Spinning triangles of 58 tex Nu-Toruqe yarn (left) and normal ring yarn (right) [104]

In the early design, the twist insertion unit adopted was the magnetic spindle, which comprises a rotating pin around which the yarn is looped, as shown in Figure 2-14. The housing for the pin is fitted with a fine tube at entry and exit, and the external surfaces of these tubes are driven by frictional contact on rotating drive surfaces, which are held against the drive surfaces by a magnetic force. The exact twist imparted to the yarn is determined by

$$false\ twist\ \ (tpm) = \frac{rotational\ \ speed\ \ of\ \ \ pin\ \ (rpm)}{yarn\ \ delivery\ \ speed\ \ (m/min)} \qquad (2\text{-}2)$$

An important parameter, D/Y ratio, is defined as the ratio of the pin rational speed to the ring spindle speed, and it has a linear relationship with the false twist.

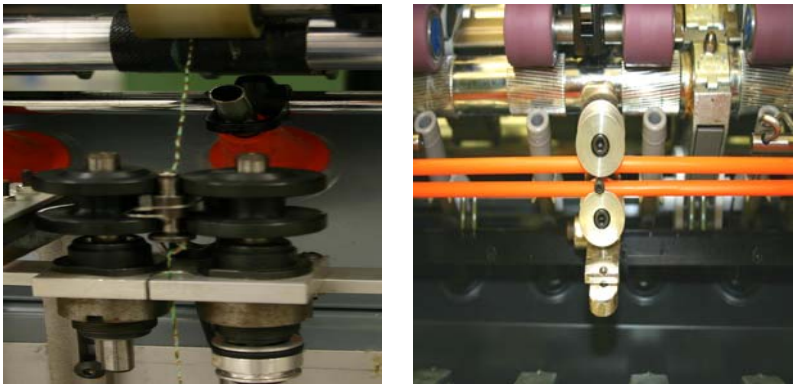

Figure 2-14 Magnetic spindle (left) and friction-belt (right) false-twisters

The advantages of magnetic spindle are small and reliable, high twist levels achievable, and accurately control the amount of false twist. It is, however,

expensive, high noise emission, time-consuming to thread the pin and high yarn tension after the spindle which limits the production of finer count yarns. Recently, a new type of false-twister, namely the friction-belt type twist unit, has been developed and employed for finer modified yarns, as shown in Figure 2-14. Here, the yarn is twisted by frictional contact with the surface of a moving belt. One or two friction-belts can be used to impart false twist to the yarn, depending on the requirement of false-twisting levels. A critical parameter, speed ratio defined as the ratio of moving belt speed to yarn delivery speed, is introduced to quantify the false twist. However, unlike the magnetic pin type, the false twist is not linear to the speed ratio in friction-belt type. More importantly, the twist generation and propagation process in the friction-belt type system is not clear so far. Therefore, in this project, it is important to address the twisting process in a modified ring spinning system with friction-belt false-twister.

2.2.3 Analysis to the Yarn Structures and Performances

In terms of surface appearance, most fibers in the normal ring yarn have almost the same helix angle in relation to the yarn axis, and many long protruding fibers outside the yarn body. In contrast, some fibers are wrapped on the surface of Nu-torque yarn in a reserve orientation and hold the yarn body tightly. Those reversely wrapped fibers make contribution to the yarn hairiness and strength, as displayed in Figure 2-15.

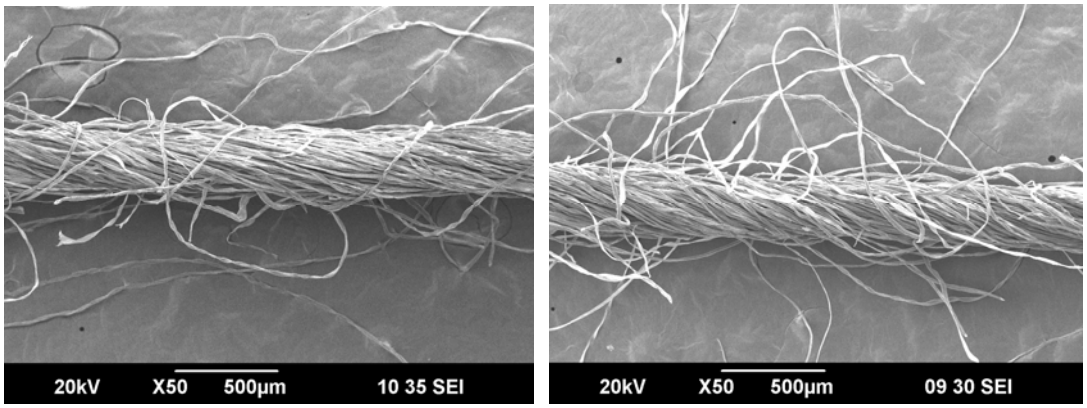

Figure 2-15Ne 20 Nu-Torque yarn with 440 tpm (left) and 20 Ne normal ring yarn with 634 tpm (right)

A great number of experiments indicate the majority of fibers in the Nu-Torque

yarns exhibit a figure of deformed non-concentric conical helixes with the axis of helix changing substantially in space. On the contrary, the majority fibers in conventional yarns follow two forms, they are, concentric helix and concentric conical helix, in which the helical axis accords with the yarn axis, as illustrated in Figure 2-16. [105]

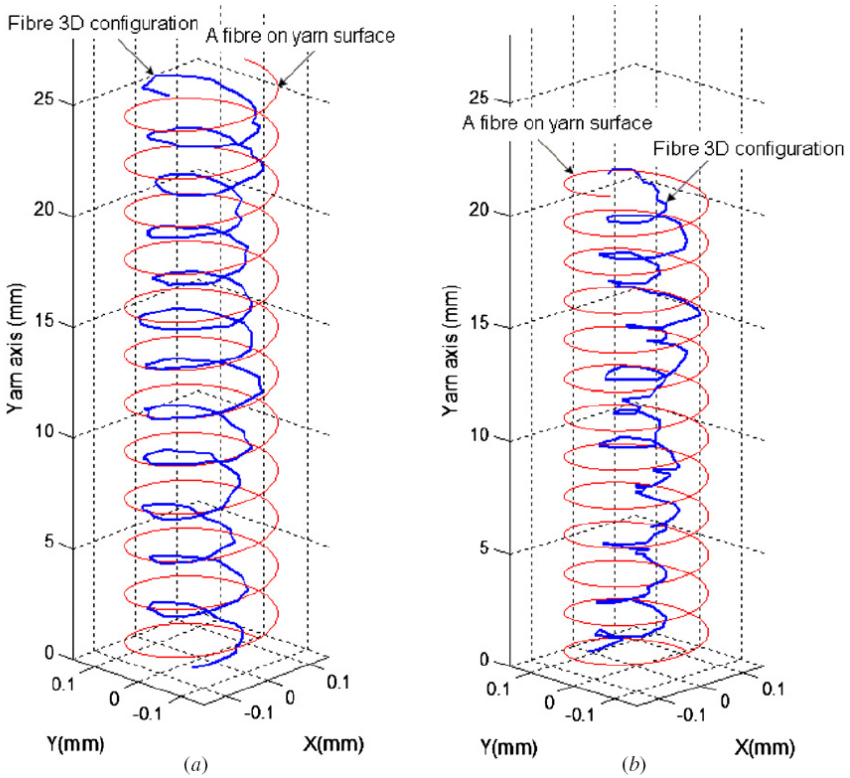

Figure 2-16 3D configurations of a fiber in a ring yarn (a) and a Nu-Toruqe yarn (b) with 29.53 tex and 440 turns/m [106]

It can be found in Figure 2-17 that the majority fibers in the low torque yarn have a tendency to be arranged near yarn center, and vary their radial positions frequently with slightly larger migration amplitude. Such internal characteristics facilitate the increment of frictional force between fibers and then substantially enhance the interaction between fibers, thus improve the yarn strength, decreasing the occurrence of fiber slippage during rupture process. Moreover, some fiber segments in the Nu-Torque yarns exist local reversion of helix orientation in a random style. Since there exist some fiber segments with negative orientation direction, the mean helix angle of individual fibers in the Nu-Torque yarn is lower than that of the conventional yarns. The existence of those local reversion fiber

segments helps to balance the residual torque in yarns. [107]

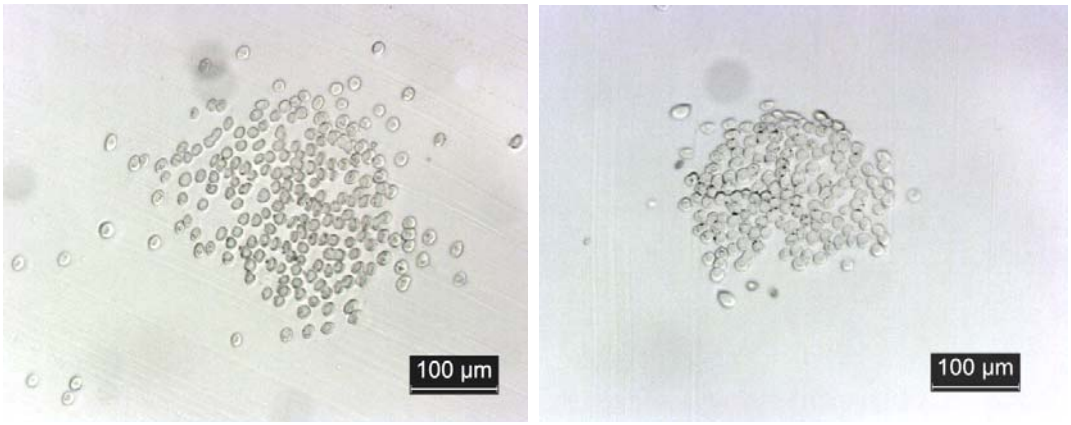

Figure 2-17 Typical cross-sectional images of Tencel yarn (20Ne, α_e =2.5) under undeformed state: ring Tencel yarn (left) and Nu-torque tencel yarn (right) [108]

A wide variety of Nu-Torque products have been developed with unique features and high added-values. Yarns exhibit extra-low twist and residual torque but high strength.[18, 23] Knitted fabrics have low spirality after washing and possess unique cashmere-like soft handle.[109-111] Woven fabrics have better tearing strength and abrasion resistance.[104, 112] Towels have a full handle and high level of water absorption. Apparel possess smooth and clean surface. Additionally, fabrics can be dyed easily using smaller amount of dyes. Products include cotton sweaters, T shirts, jeans, flannel clothing and towels, as shown in Figure 2-18 . Resultant yarns, fabrics and apparels of famous brands are popular in US, Europe, Japan and China.

Figure 2-18 Nu-Torque products in the market

2.3 Yarn Twist Analysis

Twist is defined as the number of turns in a unit length of yarn, which is employed to impart coherence and tensile integrity on the spun yarn in conventional

staple fiber spinning systems. Among the list of yarn quality factors, twist ranks second next to yarn count in terms of significance due to impact of final yarn property [24]. It is important not only because the degree of twist in the final yarn influences yarn characteristics like strength, handle and hairiness, but also because it determines the spun yarn structure by manipulating a bundle of separated short fibres and assembling them into a consolidated yarn. The twist variation in a yarn has been widely accepted for prime cause for 'Barre defects' on fabrics due to different dye absorption levels of high and low twisted segments.

2.3.1 Twist Modeling

Kinematics is a concept that describes the geometry motion without consideration of the causes of motion [113]. A generalized partial differential formula was deduced to describe a twisting process in air-jet spinning system [10]

$$\frac{\partial T}{\partial t}+\frac{\partial (vT)}{\partial l}=\frac{\partial n}{\partial l} \tag{2-3}$$

where T represents the yarn twist per unit length, l means the unit length of the yarn, v be the linear speed of the yarn, n is the yarn rotational speed, t denotes time interval, as shown in Figure 2-19.

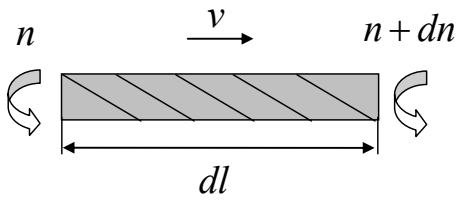

Figure 2-19 Twisting of a yarn element

Later, the same kinematic twisting equation was proposed based on the theory of twist flow Q, [114] which is defined as

$$Q=\frac{Tdx}{dt}=Tv \tag{2-4}$$

The increment of twist flow in the yarn element at a time dt roots in the sum of the relative rotation between two ends and the twist input to the unit length dx, which is equal to the increment of twist in dx during the time interval dt

$$\frac{\partial (Tdx)}{\partial t}dt=(\frac{\partial n}{\partial l}-\frac{\partial Q}{\partial l})dxdt \tag{2-5}$$

Since l is independent of t, and $Q = Tv$, obtaining

$$\frac{\partial T}{\partial t} = \frac{\partial n}{\partial l} - \frac{\partial Q}{\partial l} \tag{2-6}$$

The twisting Equation 2-6 can be further simplified for steady-state conditions,

$$\lim_{t\to\infty} \frac{\partial T}{\partial t} = \frac{\partial n}{\partial l} - \frac{\partial Q}{\partial l} \tag{2-7}$$

In practice,

$$T = \frac{n}{v} \tag{2-8}$$

Equation 2-8 expresses the fact that the twist at one point is equal to the ratio of thread rotational speed to the delivery speed at the same position in a steady-state.

When n and Q are independent of l, a first order ordinary differential equation governing the twist of yarn is derived as

$$\frac{\partial T}{\partial t} = \frac{n - Q}{l} \tag{2-9}$$

Although the kinematic model is simple and straightforward, it is of great importance to link the yarn twist to the machine setting, a crucial parameter determining the production quality, and provides a method to assess the twisting stability in different processing zones. However, it did not receive much attention by previous scholars; the only notable work was conducted by Denton [115-117], who analyzed the twist variation in a false-twist-texturing machine by using the Equation 2-9. It was found that the change of false twisting rate for a short time can affect the yarn twist variation along its threadline for a considerable distance and the variation in false twist is augmented in the downstream of the texturing process.

For friction-belt false-twister, the instant false twist can not be exactly controlled due to the substantial and frequent change of yarn-belt contact modes between sliding and rolling, thus the yarn waggles forward and backward over the belt non-periodically. Moreover, the oscillation of elastic friction-belt, the variation of friction-belt speed, and the irregular yarn surface also contribute to the false-twisting change, resulting in uneven features of the spun yarns, such as yarn strength variation, diameter irregularity and wrapping fibers along yarn length. In this project, kinematic model will be adopted to investigate the yarn twist distributions subject to these external perturbations, and examine the resultant yarn properties affected by them.

Kinetics is concerned with the relationship between the motion of bodies and its causes, namely force and torques, which is derived from kinematics by the adoption of the concept of mass. From Newton's 2nd law, the moment equilibrium for a yarn element can be deduced as

$$\frac{D(2\pi n)}{Dt} Idl = \frac{\partial M}{\partial l} dl + mdl \tag{2-10}$$

where $\frac{D}{Dt}$ is the substantive derivative, I is the moment inertia, M is the yarn torsional moment, and mdl is the external twisting moment, as shown in Figure 2-20.

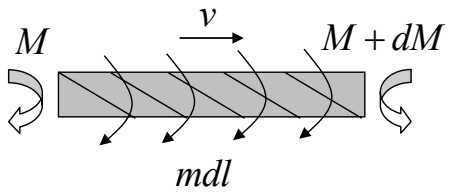

Figure 2-20 Force acting on a yarn element

Since yarn rotational speed n is a function of t and l, the angular acceleration term in the left side of the Equation 2-10 can be deduced as

$$\frac{D(2\pi n)}{Dt} = 2\pi(\frac{\partial n}{\partial t} + v\frac{\partial n}{\partial l}) \tag{2-11}$$

Moreover, the yarn torsional moment M is also related to the twist, tension and other factors, but in practice a linear relationship between moment and twist is assumed for simplification; that is

$$M = KT \tag{2-12}$$

Therefore, the kinetic equation of twisting is given by

$$2\pi I(\frac{\partial n}{\partial t} + v\frac{\partial n}{\partial l}) = K\frac{\partial T}{\partial l} + m \tag{2-13}$$

The twisting Equation 2-13 can be further simplified for steady-state conditions,

$$\lim_{t\to\infty} 2\pi I(\frac{\partial n}{\partial t} + v\frac{\partial n}{\partial l}) = K\frac{\partial T}{\partial l} + m \tag{2-14}$$

In practice,

$$\frac{\partial T}{\partial l} = \frac{m}{2\pi I v^2 - K} \tag{2-15}$$

Much valuable work has been carried out from researchers in textiles and apparel to investigate the spinning process based on kinetics, including ring spinning [118], and

rotor spinning [5, 6]. Apparently, it is necessary to develop a theoretical model for the dynamic performance of the yarn motion on a friction-belt false-twister. Yarn tension and twist distributions over the belt can be numerically examined, so as to have a better understanding on the yarn dynamic behavior in the modified ring spinning system.

Twist propagation is the same mechanics in nature as that of torsional wave for a thin rod with a circular cross-section. The twist propagation equation can be derived by combining the kinematic equation and kinetic Equation [114]. After rearrangement, one can obtained the twist wave equation as

$$\frac{\partial^2 T}{\partial t^2} + 2v\frac{\partial^2 T}{\partial t \partial l} + (v^2 - v_0^2)\frac{\partial^2 T}{\partial l^2} = \frac{\partial m}{\partial l} \tag{2-16}$$

where v_0 is the propagation velocity of yarn twist, which can be expressed by

$$v_0 = \sqrt{\frac{K}{2\pi I}} \tag{2-17}$$

The solution of propagation equation can be constructed by the superposition of two spreading waves in converse direction: one wave in positive direction at a higher propagation speed $v_0 + v$, another in the reverse direction at a lower propagation speed $v_0 - v$. The twist propagation speed is important in investigation of twist distribution, especially for high-speed spinning system, and the twist wave equation can be applied on any particular system. In the ring spinning process, the yarn delivery speed is two-order of magnitude lower than the twist propagation speed, therefore, the twist propagation speed is less significant in the present study.

2.3.2 Yarn Twist Measurement

Traditionally, there exist two standard testing methods for yarn twist measurement. One method (ASTM D1423-02) for yarn twist measurement is realized by direct counting that a yarn sample with a specified testing length is manually untwisted by rotating one end at the reverse direction of yarn twist with a required pretension until it is possible to insert a needle between the individual fibers at the one end and to traverse it across another end, and the number of turns required to remove the twist is reported in turns per unit length of the twisted yarn. This method is fundamental and common in industry for measuring ply and coarser yarns, but it is

time consuming and cannot ensure fibers entirely parallel and straightforward for measuring single yarns [119].

Another measurement method is accomplished by removing all the twists from a certain length of a yarn clamped on a twist tester with a required pretension and then by retwisting in the reverse direction until the twisted yarn contracts to its initial length with original tension (ASTM D1422-99). Although untwist-retwist method is simple, easy procedure and short test time, it is a destructive method and cannot be performed on-line. This method is based on the assumption that the amount of twist put in is equal to the twist that has been removed. However, this is not necessarily the case; inherent of which is the possibility of the fibers slipping along the yarn axis as the yarn is being untwisted, which results in uncontrolled elongation of the test length. The consequence is that the opposite twist added is larger than that of the initial twist [120, 121].

In order to overcome the drawbacks mentioned above, novel approaches have been proposed for yarn twist measurement. Yarn twist can be evaluated indirectly by testing the orientation angle of the fiber and the yarn diameter using the following equation,

$$T = \frac{\tan(\theta)}{\pi d} \tag{2-18}$$

where T is the yarn twist, θ is the fiber helix angle, and d is the yarn diameter.

The fibers used for the estimation can either be surface fibers or tracer fibers. Surface fibers are laid along the twisting curves on the surface of a yarn, whereas tracer fibers are an extremely small proportion of dyed fibers adopted and blended with unstained fibers before yarn spinning, devised by Morton and Yen [122] in 1952. Compared to the position of surface fibers, the majority tracer fibers are randomly arranged inside the yarn body with similar statistical features as other fibers. For displaying the position of trace fibers, the yarn sample is required to be immersed in a specific solvent with the same refractive index of the unstained fibers to optically dissolve these fibers. Different from the yarn containing tracer fibers, no such treatment is needed in the image acquisition of yarn surface fibers.

Vas et al [123] developed a special image processing system for measuring yarn diameter and twist angle. A CCD video camera with a resolution of 760 x 576 pixels was fastened on a microscope and directly connected to the computer through an image acquisition card. The yarn diameter was evaluated by calculating the transition

curves of the gray density, and then averaged by INFL method (the distance of the two inflexion points of the transition curve) and PERC method (the distance of points by given percentages of the maximum density value) with same weight. In the measurement of local twist angel on the surface of the yarn, 5x5 top hat filter was adopted to detect the dominant gradient angle. Cybulska [124] identified the helix angle of surface fibers via image processing method to estimate the yarn twist. After the segmentation and filtering process of a yarn image, the twisting lines formed by individual fibers on the yarn surface can be estimated for the surface helical angle and yarn twist. Huang and Liu [125] derived the trigonometric relationship between the measured rectangular components of the chain-coded curves by tracing the path of individual fibers and the twist angle of a yarn was statistically calculated from all the estimated trigonometric relationships. Based on a similar principle, Basu et al [126] analyzed the diameter and twist of rotor spun cotton yarns by calculating the average values with 200 readings using Image-Pro-Plus 4.0 software. Jia [127] also measured the yarn twist by computing the mean angle of yarn surface fibers. In his method, a yarn image was first transformed into a binary one and then converted by using the 2D Fourier transform to determine accurate data on helix angle. Linear regression method was adopted to process the grey levels of the resultant Fourier spectrum image. Ozkaya [128] proposed a hybrid method using frequency domain filtering together with the spatial analysis of the yarn surface, providing superior results in terms of accuracy, and found that the diameter measured from the back-lit yarn images is much more accurate than those obtained from front-lit image. More recently, a non-destructive, indirect method for calculating the yarn twist based on light scattering and diffraction was proposed by Pei and Tao [129]. The surface twist angle was measured by determining the direction of the line with the highest intensity on the backward light scattering pattern and the yarn diameter was measured by using the small-angle far-field diffraction pattern of the yarn body. This method can obtain short-term variations of twist and has potential to measure on-line yarn twist and its distribution.

Although the measuring principle is plausible, the accuracy cannot be ensured partly because there is no generally accepted definition of yarn diameter which distinguishes the yarn hairiness from the yarn body and partly because the randomly oriented fibers protruding on yarn surface may affect the veracity of yarn helix angle. Also the error may blow up by combining two variables together.

In the digital acquisition of tracer fibers for appraisalling the structural properties

of spun yarns , a CCD camera coupled with a magnifying glass could be introduced to obtain the images of a yarn when it is moving through a container filled with an appropriate immersion liquid. A plane mirror with 45 degree to the observation direction was placed beneath the yarn so that the yarn could be viewed simultaneously from two perpendicular directions. Since the unstained fibers which came into being the bulk of the yarn are optically dissolved, the path of the dyed tracer fibers could be identified. After the acquisition of yarn images, yarn twist was derived either by measuring fiber helix angle and diameter or directly by calculating the length of one turn of twist. For the latter, Fourier transform was commonly introduced to calculate the frequency (turns/mm) of fiber path, which is a feasible way to obtain the mean twist for a long segment of yarn as well as twist variation in a short term. Except for the fiber helix angle, yarn diameter and twist level of the spun yarn, the fiber geometry could also be used for the estimation of other yarn structural properties, such as fiber radial position, and other migration characteristics. This method is more effective in determining yarn twist level, but the limitation is that the preparation, procedure and post processing of twist measurement are really complicated and time-consuming.

Another technique for twist measurement of spun and ply yarns was implemented based on the eccentric shape of yarn cross-sections.[130] An elliptic yarn cross-section instead of circular was approximated to represent an irregular close-packed polygonal outline. A high resolution line-scan camera was built to capture the yarn diameter at 6 angles with 30 degree apart. On account of symmetry, 12 data were obtained for each yarn cross-section. Then yarn eccentricity, major and minor axes and orientation of the major axis were determined either by arithmetic or geometric fitting. Then, yarn twist was investigated based on the feature that the direction of the major axis rotated cyclically with the yarn twist. In order to overcome the difficulty that twist is irregularly distributed and concentrated in the thin places of the yarn, a sine function was introduced to fit the mean eccentricity value.

The aforementioned methods are suitable for the twist measurement of spun yarns, whereas they are helpless in dealing with on-line measurement of instant twist during the spinning process. A non-contact monitor system for dynamic tension and twist measurement has been proposed.[131] One sensor was installed on the front roller to detect its rotational speed, while another sensor was fixed on the ring rail to acquire the rotational speed of the traveler. The computer collected the data from the two sensors and calculated the instant twist by the following equation,

$$T = \frac{N}{\pi n d} \tag{2-19}$$

where N is the rotational speed of the traveler, n is the rotational speed of the front roller, and d is the diameter of the front roller.

By using the similar principle, a device was developed to measure the rotational speed of the spindle.[132] An optical sensor was introduced right above the yarn guide to detect the balloon movement. For each revolution, the light beam was interrupted by the ballooning yarn twice and signal was gathered by receiver at the opposite side of the balloon. Therefore, the spindle speed and its variation could be obtained. However, this approach can not provide the information of the yarn twist distributions along the threadline since the yarn twist propagates from the traveler to the spinning zone, which is altered by hysteresis and blockage during the spinning process.

A more straightforward and reliable method for online measurement has been recognized by many researchers [22, 133], which uses a high speed camera to acquire the images of black-white yarn during the spinning process. One black and unstained rovings with the similar count are fed into the back rollers simultaneously. As a result of twisting, the bundle of straight and parallel fibers is laid along the helix curve on the yarn surface, and yarn twist could be directly read by the interval of black and white fiber bundles. Table 2-2 summaries the aforementioned methods in terms of their merits and shortcomings.

Table 2-2 Comparison of various twist measurement methods

Sources	Specific method	Advantages	Disadvantages
ASTM D1423-02	direct counting	simple and direct	time-consuming, destructive and offline
ASTM D1422-99	untwist-retwist	simple, easy procedure and short test time	offline, destructive and long-segment measurement
Morton and Yen [122]	tracer fiber helix and yarn diameter	non-contact and effective	offline, complicated and time-consuming
Vas et al [123],	surface fiber helix	non-destructive,	offline and no

Cybulska [124], Huang and Liu [125], Basu *et al* [126], Jia [127], Ozkaya [128], Pei and Tao [134]	and yarn diameter	non-contact and short-segment measurement	consensus on diameter measurement
Jasper *et al* [130]	eccentric shape of yarn cross-sections	non-contact and short-segment measurement	offline, complicated and time-consuming
Mei *et al* [131], Vuyst [132]	spindle speed and front roller speed	non-contact and online	restrict to ring spinning and long-segment measurement
Tang *et al* [133], Feng *et al* [22]	black and white yarn using high speed photography	online, effective and high resolutions	expensive

2.4 Yarn Tension Analysis

In the ring spinning process, yarn tension plays an important role on the yarn formation and resultant yarn quality. Tension is prevented to exceed the strength of the yarn at any instant; on the other hand, the tension at which the yarn is formed affects its structure and properties. At a macro level, power consumption in the spinning process is proportional to the yarn tension, it is, therefore, important to balance the tension level to minimize the power consumption while maximizing the yarn quality.[4]

2.4.1 Yarn Tension Modeling

The earliest research paper regarding to the theory of ring spinning, which is the theory of the yarn dynamics between the yarn guide and the wound point, can be traced back to 1881 [135]. In order to derive the analytic approximations, the equations of motions and boundary conditions were simplified and some significant terms such as air-drag were neglected, which in turn produced results of little practical value. An account of this history and the state of theory up to 1965 can be found in [136], and

the formulas of motion for the yarn and the traveler were derived. The significance of the air-drag and the acceleration components in the governing formulas was comprehended and in the 1950s some limited numerical results of these formulas were received. Up-to-date advances in computer science since 1965 has raised a renewed attention to this problem. An integrated approach to yarn dynamics of the ring spinning process was initiated by Batra et al [137, 138]. However, the adoption of the traveler formula to construct a full set of boundary conditions for the governing formulas had not been entirely developed until Fraser [4], who completed the theory for steady-state balloons and simulated the balloon dynamic response.

In the aforementioned papers, the yarn is assumed to be perfectly flexible, inextensible, uniform cross-section and density, and only tension forces acting in the yarn. In the following study, accounts are taken of yarn elasticity, yarn non-uniformity, variations in yarn delivery speed, yarn bending and torsional rigidity, and the effect of a control ring. The influence of yarn elasticity on balloon shape and tension in over-end unwinding [139] and ring spinning balloon [140] was investigated. It was shown that the effect was very small for typical unwinding tensions and in the case of the tensions encountered in ring spinning. The effect of yarn non-uniformity on the stability of the ring spinning balloon [141, 142] indicated that even a slub that in practice would be considered quite small could have a significant effect on the stability of the yarn balloon. The analysis of the stability of balloon shapes subjected to small velocity perturbations [143] revealed some of the rich bifurcation behaviors shown by the solutions of the equations subject to boundary conditions of ring spinning and two-for-one twister. The yarn modeling [118] based on rod theory [144] proved that the bending and torsional stiffness of the yarn in typical ring spinning process had a negligible effect and the yarn path in the ring spinning balloon could be obtained independently of the twist. The effect of a control ring on the ring spinning balloon was studied [145] and it was found that the control ring lowered the yarn tension in the balloons, and extended the stable region of parameter space.

In addition, a great number of studies related to other spinning methods such as rotor spinning [6, 7, 146-148], friction spinning [149, 150] and vortex spinning [56, 151], have been carried out.

2.4.2 Yarn Tension Measurement

The current state of the art yarn tension meters, whether mechanical or electrical, employ a three-pulley system, as shown in Figure 2-21. It is worked by the theory that when a yarn is passed over a sensing head, it tends to displace the head from its original position due to certain amount of tension present in the yarn. This displacement alters the output of the circuit in the form of voltage, either because of variation in resistance, in the case of strain gauges, or because of variation in capacitance, in the case of capacitive transducers, or because of variation in the strength of the magnetic field, in the case of Hall sensors. In the case of a strain gauges, a half or full Wheatstone bridge is constructed and the resistance of the gauge alters due to bending or compression of the gauge, caused due to external force applied on it. In the case of Hall sensors, a voltage is generated transversely to the current flow direction in an electric conductor, if a magnetic field is applied perpendicularly to the conductor. [152] The merits of electronic yarn tension meters are their ability to measure yarn tension over a wider range, very precise at high velocities, easy to collect data from the sensor, connectivity to PCs, and good frequency response.

Figure 2-21 Hand-held yarn Tensiometer (left) and general purpose online tension sensors (right)

Recently, the non-contact yarn tension measurement has raised increasing attention by researchers [153, 154]. The yarn tension is obtained by comparing the yarn strain measured by a CCD camera with the stress-strain curve of the yarn produced. The strain of the yarn is calculated by

$$\varepsilon = \frac{d_1 - d_0}{d_0} \tag{2-20}$$

where d_1 is the measured yarn diameter under tension, d_0 is the yarn diameter without tension.

And the yarn tension can be calculated as follow

$$T = EA\varepsilon \tag{2-21}$$

Where E is Young's modulus of the yarn, and A is the cross-sectional area of the yarn.

This method provides new idea for online measuring yarn tension, especially for the places that the contact tension meter can not measure such as ballooning zone and winding zone, however, the accuracy of the method still needs improving.

2.5 Optimization of Yarn Properties

As we known, fiber properties, spinning methods, as well as spinning parameters have large impinges on the resultant yarn properties, such as tenacity, elongation, evenness, and hairiness. When the fiber properties and spinning method are ensured, optimization methodology can be employed to study the relationships between yarn properties and spinning parameters, and the optimum yarn properties can be obtained with proper setting of spinning parameters. In general, optimization methods can be divided into arithmetic methods [155], such as Johnson method, Palmer method and Gupta method, numerical methods [156] such as linear programming, dynamic programming and nonlinear programming, and estimation methods [157] such as Least Squares and Point Estimation. In particular, the response surface methodology [23, 158, 159] based on Least Squares technology has been widely employed in the experiment design, and Box-Behnken and Central Composite designs are often adopted.

Before parameter optimization, the Fractional Factorial Methodology (FFM) can be used to determine which system parameters may have significant impinges on yarn properties. For Nu-Torque system, the parameters include spindle speed, yarn twist, traveler weight, speed ratio, and wrap angle, which are selected as potentially influential input variables. Based on the analysis results, the statistically significant factors affecting yarn tenacity, evenness, hairiness and snarling are chosen for further investigation. Then with the help of Response Surface Design (RSM), second-order polynomial response surface models are set-up to predict and explain

the relationship between yarn properties and the variables. Further, the optimization scheme was then designed by using Central Composite Design (CCD). For low-count cotton yarns [104, 110], it was found that the speed ratio and twist factor had significant effects on yarn tenacity and wet snarling, while for high-count yarns [112], the speed ratio and traveler weight had marked influences on tenacity and hairiness.

2.6 Problem Statement

Driven by the excessive market demand for producing superior yarns with high-added value, it is necessary to further exploit this technique to finer count yarns. The technical dilemma lies in that severe yarn imperfections, especially for yarn neps (+140%), are generated, attributed to rearrangement of surface fibers along yarn axis due to the frictional force between the false-twisting unit and modified yarns. Although some attempts have been made to extend this technology to finer modified yarns (Ne 60-80) and significant merits in tenacity and hairiness were discovered as compared to conventional yarns, worse yarn imperfections were observed. Another problem lies in the maneuverability for practical application. Piecing yarn for double-belt system is much more time-consuming and difficult than single-belt system. If the yarn breaks and wraps onto the belt, the adjacent yarns along the belt movement direction will be easily broken. Therefore, it draws high demand for the tender and factory management.

Due to the yarn imperfections and poor maneuverability caused by the double-belt false-twister, in the current work single-belt false-twister is adopted to explain or solve the aforementioned problems by the following viewpoints, as shown in Figure 2-22.

(1) As a false-twisting element, belt friction surface may have large influence on the false-twisting process, and determine the final yarn performances. Besides wrap angle and speed ratio, belt material, hardness, and coefficient of friction also contribute to the false-twisting efficiency. In this work, the belt friction surface and their interplay with yarn properties will be investigated systematically. The importance of each parameter on the false-twisting efficiency and yarn properties will be studied.

(2) Tension and twist distributions in the spinning process are important to make better understanding the novel spinning method. In the twisting zone, high

twist changes the shape and fiber tension distributions in the spinning triangle, forming a particular tight structure, while in the untwisting zone, the twist are greatly reduced on the belt and final structure is formed. The deep comprehension of tension and twist distributions make us easier to find a way to solve the worse evenness encountering in the double-belt system.

(3) Twist generation and propagation are of particular interest in this study because they answer several basic questions. The number of twist is generated by the false-twister and its twist efficiency remain veiled, and the proportion of the real twist and false twist in the spinning triangle is another basic question to be answered. In case of double-belt system, the twist generation and propagation become much more complicated, and we can make better understanding the twist distributions in each zones.

(4) Belt spatial position is another important question of special interest for practical applications. It is not only restricted by the space of different spinning machines, but also affects the stability and quality of the yarn. Stability is the basic requirement for any practical applications. For a stable process or product, it permits certain tolerance for system variation or error. In the present study, the twist stability and robustness will be concerned and their relations to the belt position and properties will be elaborated.

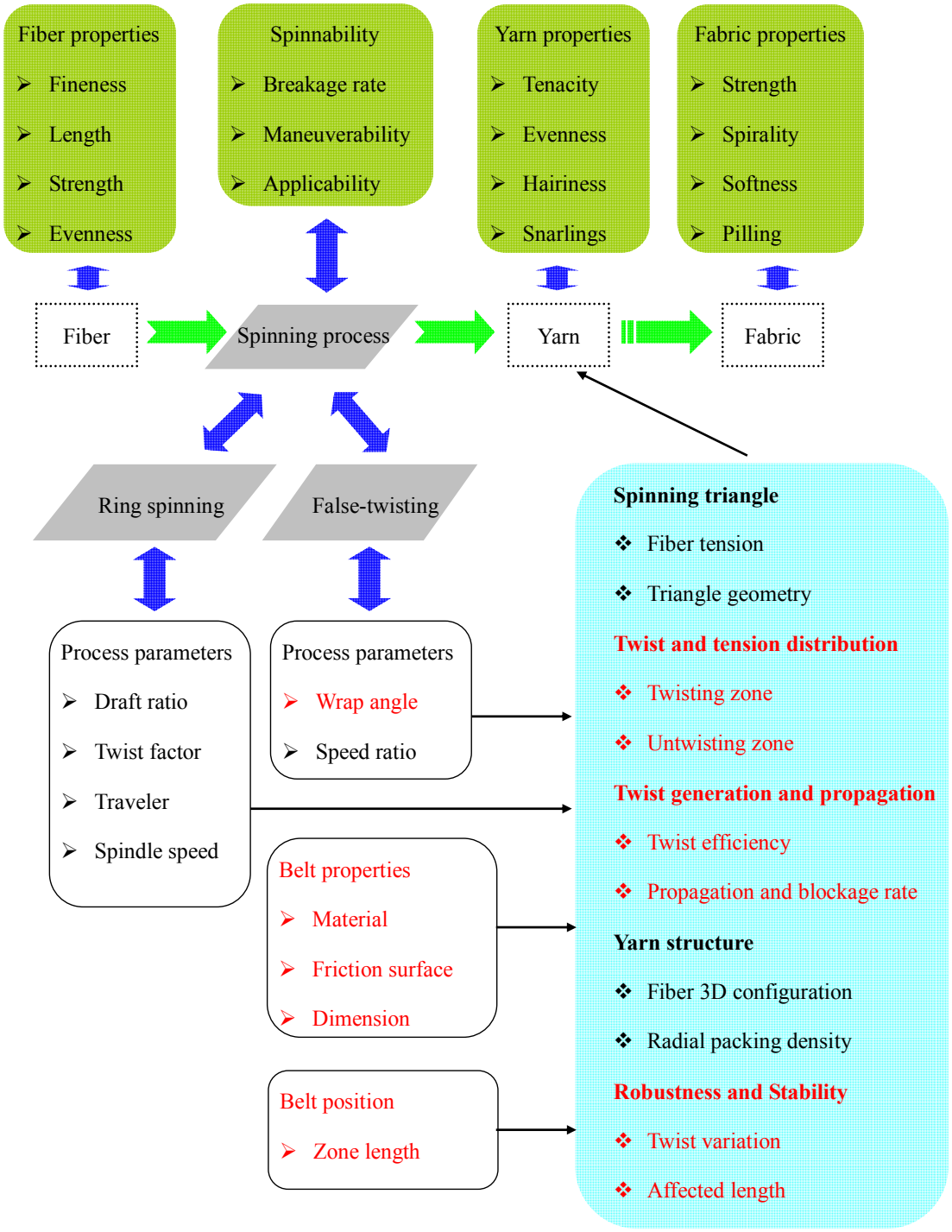

Figure 2-22 Technical roadmap

2.7 Summary

In this chapter, prior work on the spun yarn technologies and their developments has been broadly reviewed. Yarn characteristics and performances made by various spinning system, including ring spinning, unconventional spinning systems, and

ring-based systems have been retrospected.

Moreover, the newly developed spinning technique, Nu-Torque, has been introduced in terms of its origins, false-twisting principles, false-twisting units, yarn structures and performances. In particular, Nu-Torque technology not only increases yarn productivity, but also improves yarn properties in some respects.

In order to facilitate the theoretical and experimental studies conducted in the present study, literatures related to yarn twist and tension theories as well as their measurement methods have been reviewed. In this project, twist kinematics and twist kinetics will be adopted to investigate the yarn dynamic performances in the modified ring spinning process. Literature review on yarn twist and tension measurements reveals that using a high speed camera to acquire the images of black-white, and employing contact three-pulley tensiometer are probably the most suitable and effective methods for online twist and tension measurements.

Further, optimization methods used in previous research have been introduced, and it can be concluded that the FFM and RSM are probably the most suitable and effective methods for yarn property optimization.

Finally, current problems of Nu-Torque technology have been stated and summarized. Foundation mechanisms of the false-twisting process, effects of belt spatial and friction surface on the false-twisting process and yarn properties, and stability of false-twister subject to external perturbations remain research gaps to be explored.

Chapter III Yarn Dynamics in the Ring Spinning System with Single Friction-belt False-twister

Twisting is an important process to form a continuous yarn from short fibers and to determine the structure and properties of the resultant yarn. In this chapter, we proposes a new theoretical model of yarn dynamics in a modified ring spinning system, which deals with two important phenomena simultaneously, that is, twist generation and twist propagation. Equations of yarn motion are established and the boundary value problems are numerically solved by Newton-Raphson method. The simulation results are validated by experiments and a good agreement has been demonstrated for the ring spinning system with a single friction-belt as the twisting element. For the first time, influences of several parameters on the twisting process have been revealed in terms of twist efficiency of the moving friction-belt, propagation coefficients of twist trapping and congestion. Moreover, we systematically examine the twisting process of yarn motion on a moving belt based on the proposed model. Response surface methodology (RSM) involving a central composite design (CCD) in three factors of twist multiplier, speed ratio and wrap angle is successfully employed for the study and analysis. The reduced regression models are validated by normal probability analysis and another nine randomly selected experiments. The significant terms of the models are studied and it reveals that the speed ratio and wrap angle are statistically significant for the responses of twist efficiency, propagation coefficients of twist trapping and congestion. And more importantly, linear relationships are found among the three responses. The results are of particular interest to make better comprehending of the function and role played by the belt in the ring spinning system.

3.1 Theoretical Modeling

3.1.1 Definitions

As shown in Figure 3-1, the modified ring spinning system is composed of delivery rollers at point A, a translationally moving belt, which contacts with the yarn in zone BC and a twister at point D. Hence, there are two twisters in the system: one is the real-twister at point D; another is the false-twister which generates the torque by

the frictional moment at zone BC. During the spinning process, the yarn moves at a constant velocity *v*, but its twist level is altered in different zones. The bifurcations or instabilities of twisted yarn, as twisted elastic rod, under specific conditions [160, 161] are unlikely to occur in our study. Torsional bifurcations are prohibited to happen because the levels of tension and twist are controlled below the critical value. Thus the twisting process is stable.

In order to describe the processes of this twisting system, three concepts are introduced to describe the roles played by friction, correspondingly, three coefficients are defined. The first concept is the twisting efficiency of the moving belt. At the contacting area of the yarn surface and the belt, the frictional moment forces the yarn to rotate along its axis. If there is no slippage or jumping of the yarn on the moving belt, then the yarn's tangential velocity and the moving velocity of the belt at the contacting point should be the same. In this situation, the twist efficiency of the belt is unity. Normally the twist efficiency is a value close to but below the unity. To determine it, let R_0 be the radius of the yarn, $n_c = T_c v$ be the rotational speed of the yarn, T_c be the total twist generated by the moving belt, v be the delivery speed of the yarn, and v_b be the moving speed of the belt, the twist efficiency of the moving belt is expressed as

$$\lambda = \frac{2\pi R_0 T_c v}{v_b} \tag{3-1}$$

The second effect is the twist trapping in the up-ward propagation of the real twist inserted by D. Without the existence of the belt, the yarn twist generated by the real-twister at point D can be freely propagated into zone AB. Due to the introduction of the moving belt, a certain proportion of this twist is blocked because of the frictional moment generated in zone BC. To quantify this effect, let T_t be the total twist lost in zone BC, and T_{CD} be the twist in zone CD, then the propagation coefficient of twist trapping is defined as

$$k = 1 - \frac{T_t}{T_{CD}} \tag{3-2}$$

The last effect of friction is the twist congestion, which occurs in the downward propagation of twist in zone AB. The downward travelling yarn has a twist thus a tendency to untwist in zone BC. It is subject to another frictional moment, as a result, the rotating trend of the yarn is reduced, which blocks the yarn twist propagating into

zone CD. The result is that the yarn twist is increased in zone AB. Let T_h be the total twist increment in zone AB, then the propagation coefficient of the twist congestion is defined as

$$\eta = \frac{T_c}{T_c + T_h} \tag{3-3}$$

From the kinematic point of view, the twist in zone AB in Figure 3-2 can be expressed as

$$T_{AB} = kT_{\mathrm{CD}} + \frac{\lambda T_{BC}}{\eta} \tag{3-4}$$

where $T_{BC} = \frac{v_b}{2\pi R_0 v}$ is the theoretical twist generated by the moving belt, and all three coefficients range from 0 to 1.

The similarities of the twist trapping and twist congestion of the false-twister are: 1) Both are caused by friction. 2) They block the twist propagation. 3) They will not change the final yarn twist. The difference between the two is that in trapping, the tangential component of the frictional force reduces twist to the yarn; while in congestion, the tangential component of the friction force adds twist to the yarn. Thus, the functions of the friction force are to simultaneously insert twist in zone AB, congest the generated twist downwards, and trap the twist generated by the twister D upwards. In the steady state, there is no twist-gain from the moving belt in zone CD because the frictional moment generates identical number of twists in each of the two zones, but in opposite directions. Therefore, when the yarn moves, the two parts offset each other, resulting in zero twist-gain in zone CD.

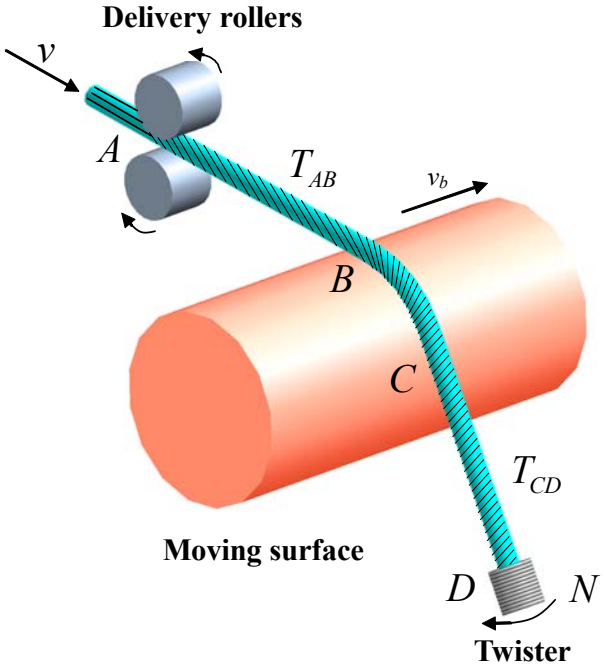

Figure 3-1 A novel twisting system

3.1.2 Equations of Motion

3.1.2.1 Assumptions

Several assumptions are made in the analysis: 1) The yarn is assumed to be inextensible since twisting of yarn is the dominating phenomenon, the deformation in the yarn axial direction is small thus can be ignored; 2) The yarn is assumed to have small bending moment during the process. This assumption is made based on the fact that yarn twist used in this study is at least one order of magnitude higher than that of the yarn bending curvature, although the bending and torsional stiffness of the yarn are of the same order. [144, 162] The resultant torque is much higher than the moment generated by bending against the moving belt, therefore, it is reasonable to omit the bending effect; 3) A uniform yarn is assumed with a single linear density and cross-sectional area and remains circular on the belt; 4) The weight of yarn is relatively small when compared with other forces thus can be neglected; 5) The moving belt has much greater rigidities thus can be regarded as non-deformable; 6) The moving belt is smooth with a constant curvature radius; 7) A linear relationship between the yarn twist and torque is assumed according to previous experimental results reported [163, 164]; 8) The model is built in a steady state, thus time-dependent

terms in the equations are ignored; 9) The study deals with stable twisting processes where no mechanical instability or bifurcation occurs.

3.1.2.2 Coordinate systems

Considering an arbitrary point **Q** of the yarn, which at time *t* is at a distance *s* measured along the yarn from the initial contacting point **A (***s=0***)**, as shown in Figure 3-2a. For the convenience of analysis, a fixed cylindrical coordinate system is selected with base vectors $\mathbf{e_r}$, $\mathbf{e_\psi}$, $\mathbf{e_z}$. The origin of coordinate **O** coincides with the centre of the initial contacting surface, and the z axis of the system is in line with the central axis of the rigid belt with its positive direction towards the moving direction. Let r_0, ψ, z be the cylindrical coordinates corresponding to the coordinate frame and $\mathbf{R}(s,t) = r_0\mathbf{e}_r + z\mathbf{e}_z$ be the position vector of Q relative to the origin O.

In order to simplify the derivation, a moving coordinate frame with its base unit vectors $\mathbf{e}_\tau$, $\mathbf{e}_h$, $\mathbf{e}_v$ is introduced. In Figure 3-2b, π is the plane tangent to the moving belt at point Q. The unit vectors $\mathbf{e}_\tau$ and $\mathbf{e}_h$ are that in the direction of yarn motion and that normal to the tangent plane π, respectively, and $\mathbf{e}_v$ is expressed as $\mathbf{e}_v = \mathbf{e}_h \times \mathbf{e}_\tau$. θ is the angle formed between $\mathbf{e}_\tau$ and $\mathbf{e}_\psi$. In this analysis, we define that θ is positive when $\mathbf{e}_\psi$ is at the right side of $\mathbf{e}_\tau$, negative when $\mathbf{e}_\psi$ is at the left side of $\mathbf{e}_\tau$.

In a cylindrical coordinate system (r_0, ψ, z), $\mathbf{e}_\tau$, $\mathbf{e}_h$, $\mathbf{e}_v$ can be written as

$$\mathbf{e}_\tau = \frac{d\mathbf{R}}{ds} = r_0 \frac{d\psi}{ds}\mathbf{e}_\psi + \frac{dz}{ds}\mathbf{e}_z \tag{3-5}$$

$$\mathbf{e}_h = \mathbf{e}_r \tag{3-6}$$

$$\mathbf{e}_v = \mathbf{e}_h \times \mathbf{e}_\tau = -\frac{dz}{ds}\mathbf{e}_\psi + r_0 \frac{d\psi}{ds}\mathbf{e}_z \tag{3-7}$$

Also, the second derivative of **R** with respective to *s* can be expressed in the same manner as

$$\frac{d^2\mathbf{R}}{ds^2} = -r_0\left(\frac{d\psi}{ds}\right)^2 \mathbf{e}_r + r_0 \frac{d^2\psi}{ds^2}\mathbf{e}_\psi + \frac{d^2z}{ds^2}\mathbf{e}_z \tag{3-8}$$

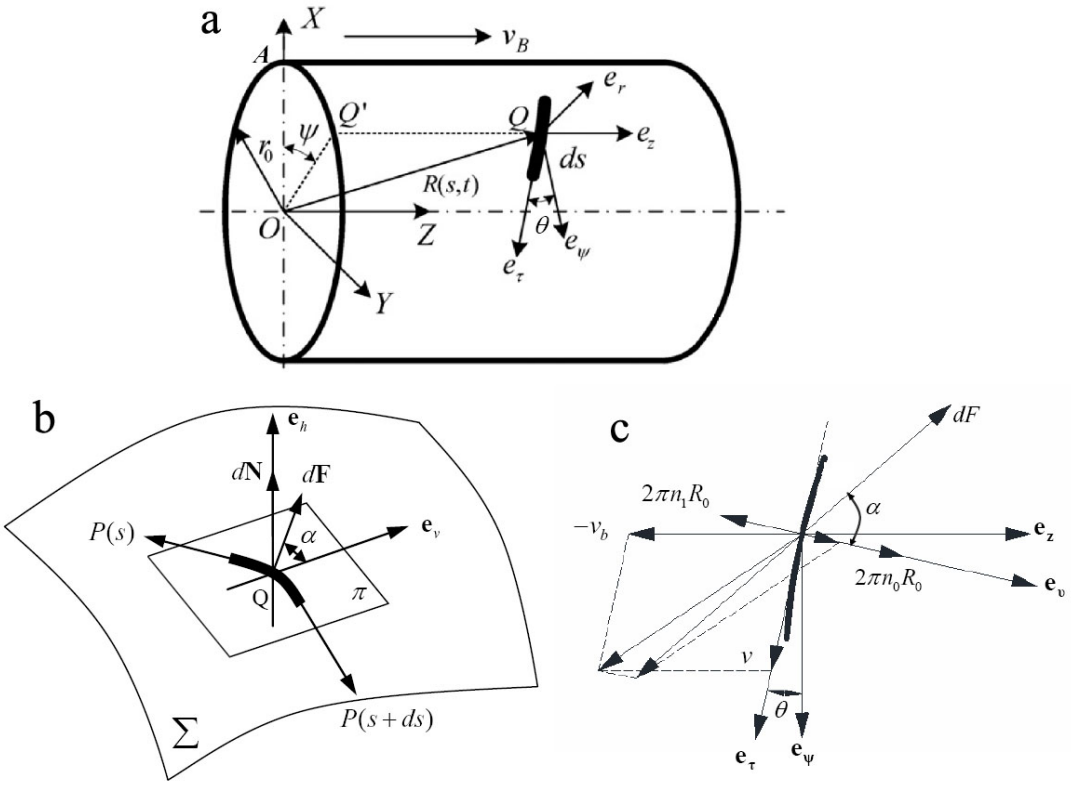

Figure 3-2 Modeling analysis of a yarn segment. (a) A yarn segment in the moving coordinate system. (b) Forces acting on a yarn element. (c) Analysis on yarn motion.

3.1.2.3 Force balance

If $\mathbf{P}(s,t)$ is the tension in the yarn at **Q**, $\mathbf{N}(s,t)$ is the normal reaction force, and $\mathbf{F}(s,t)$ is the friction force, then the full vector form of the time-dependent equation of motion for yarn at **Q** is [165]

$$m\Delta^2\mathbf{R} = \frac{\partial}{\partial s}\left(|\mathbf{P}|\frac{\partial \mathbf{R}}{\partial s}\right) + \mathbf{F} + \mathbf{N} \tag{3-9}$$

where m is the linear density of the yarn. The differential operator $\triangle$ is given by $\Delta = \frac{\partial}{\partial t} + v\frac{\partial}{\partial s}$, where v is the constant delivery speed of the yarn. In the steady state, the solution of Equation (3-9) is independent of time, and the operator reduces to $\Delta = v\frac{d}{ds}$. Therefore, Equation (3-9) can be rewritten as

$$mv^2\frac{d^2\mathbf{R}}{ds^2} = \frac{d|\mathbf{P}|}{ds}\frac{d\mathbf{R}}{ds} + |\mathbf{P}|\frac{d^2\mathbf{R}}{ds^2} + \mathbf{F} + \mathbf{N} \tag{3-10}$$

The unit normal reaction force **N,** in the moving coordinate system, can be expressed as

$$\mathbf{N} = |\mathbf{N}|\mathbf{e}_h \tag{3-11}$$

The friction force acting on the yarn as it slides over the belt follows the Coulomb friction law

$$\mathbf{F} = \mu|\mathbf{N}|(\cos\alpha\mathbf{e}_v - \sin\alpha\mathbf{e}_\tau) \tag{3-12}$$

where μ is the friction coefficient between the yarn and belt surface, α is the friction angle between the direction of friction force and the unit vector $\mathbf{e}_v$.

The yarn speed on the belt is composed of three components: yarn rotational speed around its own axis $2\pi R_0(n_1 - n_0)\mathbf{e}_v$, yarn delivery speed $v\mathbf{e}_\tau$, and moving speed of belt $v_b\mathbf{e}_z$, as shown in Figure 3-2c, where n_0 is the rotational speed of the yarn generated by the twister, and n_1 is the rotational speed of the yarn generated by the moving belt. Thus, the angle α can be derived as

$$\alpha = arc\tan\frac{v_b\sin\theta + v}{v_b\cos\theta + 2\pi R_0(n_1 - n_0)} \tag{3-13}$$

The inextensible condition gives

$$\frac{d\mathbf{R}}{ds}\cdot\frac{d\mathbf{R}}{ds} = 1 \tag{3-14}$$

Therefore, the following equation can be obtained

$$\frac{d^2\mathbf{R}}{ds^2}\cdot\frac{d\mathbf{R}}{ds} = 0 \tag{3-15}$$

The scalar formulas of Equation (3-10) in the moving coordinate system can be rewritten after some rearrangement as follows,

$$\begin{cases} \dfrac{d|\mathbf{P}|}{ds} - \mu|\mathbf{N}|\sin\alpha = 0 \\ -r_0\left(\dfrac{d\psi}{ds}\right)^2\left(|\mathbf{P}| - mv^2\right) + |\mathbf{N}| = 0 \\ r_0\left(|\mathbf{P}| - mv^2\right)\left(\dfrac{d^2\psi}{ds^2}\dfrac{dz}{ds} - \dfrac{d^2z}{ds^2}\dfrac{d\psi}{ds}\right) + \mu|\mathbf{N}|\cos\alpha = 0 \end{cases} \tag{3-16}$$

According to the analysis of differential geometry in Figure 3-2a, one can obtain

$$\sin\theta = \frac{dz}{ds} \text{ and } \cos\theta = r_0\frac{d\psi}{ds} \tag{3-17}$$

And the following equations can be derived

$$\frac{d^2z}{ds^2} = \cos\theta\frac{d\theta}{ds} \text{ and } \frac{d^2\psi}{ds^2} = -\frac{1}{r_0}\sin\theta\frac{d\theta}{ds} \tag{3-18}$$

Substituting Equations (3-17) and (3-18) into Equation (3-16), eliminating the unit normal reaction force **N**, the two independent first-order differential equations are obtained

$$\begin{cases} \dfrac{d|\mathbf{P}|}{d\psi} - \mu\cos\theta\sin\alpha\left(|\mathbf{P}| - mv^2\right) = 0 \\ \dfrac{d\theta}{d\psi} - \mu\cos\theta\cos\alpha = 0 \end{cases} \tag{3-19}$$

3.1.2.4 Moment balance

As shown in Figure 3-2b, the moment equilibrium for a yarn element can be derived as

$$2\pi IDnds = \frac{\partial M}{\partial s}ds + m_f ds \tag{3-20}$$

where I is the moment of inertia per unit length of yarn, n is the rotational speed of yarn around its own axis, M is the yarn torque, m_f is the external moment and in the case of the friction moment, $m_f = \mu|\mathbf{N}|\cos\alpha R_0$, in which R_0 is the radius of yarn.

In the steady state, Equation (3-20) becomes

$$2\pi Iv\frac{dn}{ds} = \frac{dM}{ds} + m_f \tag{3-21}$$

Since a linear relationship is assumed between the twist and torque ($M=KT$), together with the twist flow equilibrium ($\frac{dn}{ds} = v\frac{dT}{ds}$), Equation (3-21) can be further expressed as

$$\left(2\pi Iv^2 - K\right)\frac{dT}{ds} = m_f \tag{3-22}$$

Substituting Equation (3-17) into Equation (3-22), the following equation can be obtained.

$$\left(2\pi Iv^2 - K\right)\frac{dT}{d\psi} = \mu R_0|\mathbf{P}|\cos\alpha\cos\theta \tag{3-23}$$

3.1.2.5 Calculating the coefficients of twist efficiency and twist blockage

Substituting and rearrangement of Equations (3-13) and (3-23) yield:

$$\frac{dT}{d\psi} = H\left(\cos\theta v_b + 2\pi R_0 n_1 - 2\pi R_0 n_0\right) \tag{3-24}$$

where $H = \dfrac{\mu R_0}{2\pi I v^2 - K} \dfrac{|\mathbf{P}|\cos\theta}{\sqrt{(v_b \sin\theta + v)^2 + [v_b \cos\theta + 2\pi R_0 (n_1 - n_0)]^2}}$.

Equation (3-24) shows that yarn twist variation is depended on three factors: the first factor contains the velocity component of the moving rigid belt, the second and third factors contain the rotational speeds of the yarn generated by the false-twister and real-twister, respectively.

Integrating Equation (3-24) into the following

$$T_{AB} - T_{CD} = \int_0^{\varphi} H\cos\theta v_b d\psi + \int_0^{\varphi} 2\pi H R_0 n_1 d\psi - \int_0^{\varphi} 2\pi H R_0 n_0 d\psi = T_c + T_h - T_t \tag{3-25}$$

Replacing T_c, T_h and T_t into Equations (3-1 to 3-3), and the three key coefficients are given by

$$\lambda = \frac{2\pi R_0 v}{v_b} \int_0^{\varphi} H v_b \cos\theta d\psi \tag{3-26}$$

$$k = 1 - \frac{\int_0^{\varphi} 2\pi H R_0 n_0 d\psi}{T_{CD}} \tag{3-27}$$

$$\eta = \frac{1}{1 + \int_0^{\varphi} \dfrac{2\pi R_0 n_1}{v_b \cos\theta} d\psi} \tag{3-28}$$

3.1.2.6 Boundary equations

This system is composed of three first-order differential Equations (3-18 and 3-22). In addition, the rotational speed n_1 and the torsional rigidity *K* are two unknown constant values. Therefore, totally five boundary conditions are needed to make this problem solvable.

One boundary equation can be derived based on the geometrical condition, as shown in Figure 3-3. The delivery rollers at the point A and the twister at the point D are in the same plane that parallels to the XOY plane. The length of line AB and CD are at least one order of magnitude higher than that of curve BC. Therefore, the deviation angles for line AB and CD follow,

$$\frac{\sin\theta_{AB}}{\sin\theta_{CD}} = -\frac{l_{CD}}{l_{AB}} \tag{3-29}$$

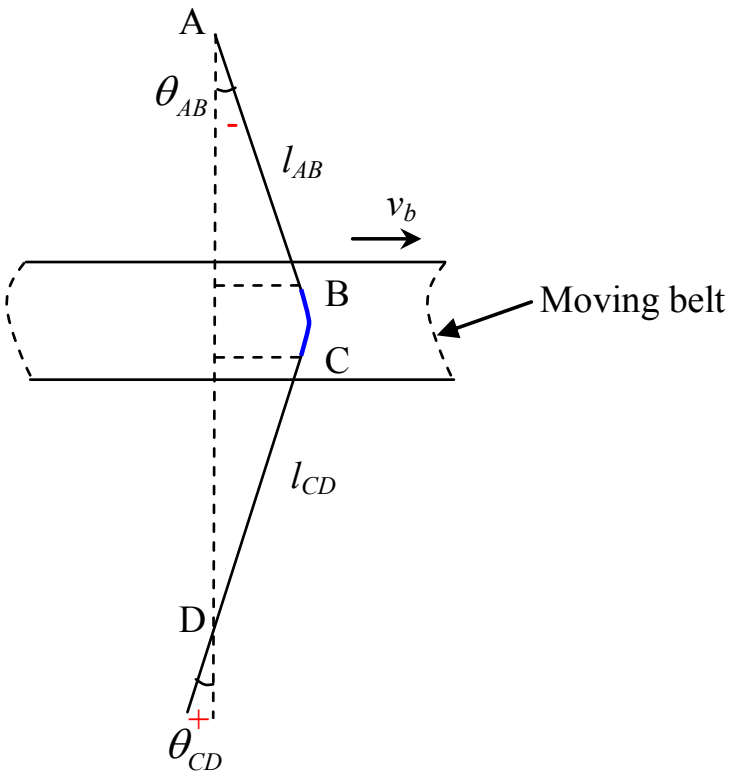

Figure 3-3 Geometrical boundary condition

Another boundary equation is directly obtained from the kinematic formula. Multiplying delivery speed v in Equation (3-1) and replacing n_1 by $\lambda T_{BC} v$, and rearranging the equation lead to

$$n_1 = (T_{AB} - kT_{CD})\eta v \tag{3-30}$$

The other three boundary values are $|\mathbf{P}|_{\mathrm{AB}}$, T_{AB} and T_{CD}, which were obtained from the measurements using the high-speed camera and tension meter systems.

3.1.2.7 Dimensionless equations

The convenient scales for the dimensionless analysis are belt radius r_0 for length, yarn delivery speed v for speed, yarn tension $|\mathbf{P}|_{\mathrm{AB}}$ for force per unit length, yarn twist T_{CD} for twist. All variables are normalized in a dimensionless form as follows

$$
\begin{aligned}
&\overline{\mathbf{R}} = \mathbf{R}T_{CD} = r_0 T_{CD}\mathbf{e}_r + zT_{CD}\mathbf{e}_z = \overline{r}_0\mathbf{e}_r + \overline{z}\mathbf{e}_z \\
&\overline{s} = sT_{CD}, \overline{R}_0 = R_0 T_{CD}, \overline{l}_{AB} = l_{AB}T_{CD}, \overline{l}_{CD} = l_{CD}T_{CD} \\
&\overline{v}_b = \frac{v_b}{v}, \overline{n}_0 = \frac{n_0}{T_{CD}v}, \overline{n}_1 = \frac{n_1}{T_{CD}v} \\
&\overline{T}_{AB} = \frac{T_{AB}}{T_{CD}}, \overline{T}_{CD} = 1, \overline{T} = \frac{T}{T_{CD}} \\
&\overline{|\mathbf{P}|}_{AB} = 1, \overline{|\mathbf{P}|}_{CD} = \frac{\overline{|\mathbf{P}|}_{CD}}{|\mathbf{P}|_{AB}}, \overline{|\mathbf{P}|} = \frac{|\mathbf{P}|}{P_{\mathrm{AB}}}, \overline{N} = \frac{N}{P_{AB}}, \overline{m} = \frac{mv^2}{P_{AB}} \\
&\overline{K} = \frac{KT_{CD}^2}{P_{AB}}, \overline{I} = \frac{Iv^2T_{CD}^2}{P_{AB}}
\end{aligned}
\tag{3-31}
$$

Since $\overline{m}$ and $\overline{I}$ are small terms in the equations, they can be omitted without losing the accuracy of the solutions. The dimensionless equations of force equilibrium and twist distribution become

$$
\begin{cases}
\dfrac{d\overline{|\mathbf{P}|}}{d\psi} - \mu\cos\theta\sin\alpha\overline{|\mathbf{P}|} = 0 \\
\dfrac{d\theta}{d\psi} - \mu\cos\theta\cos\alpha = 0 \\
\overline{K}\dfrac{d\overline{T}}{d\psi} = \mu\overline{R}_0\overline{|\mathbf{P}|}\cos\alpha\cos\theta
\end{cases}
\tag{3-32}
$$

where $\alpha = arc\tan\dfrac{\overline{v}_b\sin\theta + 1}{\overline{v}_b\cos\theta + 2\pi\overline{R}_0(\overline{n}_1 - \overline{n}_0)}$.

The dimensionless forms of the boundary conditions are

$$
\frac{\sin\theta_{AB}}{\sin\theta_{CD}} = -\frac{\overline{l}_{CD}}{\overline{l}_{AB}},\ \overline{n}_1 = (\overline{T}_{AB} - k)\eta,\ \overline{|\mathbf{P}|}_{\mathrm{AB}},\ \overline{T}_{\mathrm{AB}} \text{ and } \overline{T}_{\mathrm{CD}} = 1 \tag{3-33}
$$

3.1.3 Method of Numerical Solution

The finite difference method for the numerical solution was applied to solve the equations presented in this project with Matlab. The transformed Equation (3-32) were integrated numerically over the domain $0 \le \psi \le \varphi$. First, the wrap angle φ was divided into *n* small segments, and each segment had an equal degree φ / n. Then, the variables $\overline{|\mathbf{P}|}$, θ, $\overline{T}$ were discretized as follows,

$$\begin{cases} \overline{|\mathbf{P}|}_i : \overline{|\mathbf{P}|}_1, \overline{|\mathbf{P}|}_2 ..... \overline{|\mathbf{P}|}_{n-1}, \overline{|\mathbf{P}|}_n \\ \theta_i : \theta_1, \theta_2 ..... \theta_{n-1}, \theta_n \\ \overline{T}_i : \overline{T}_1, \overline{T}_2 ..... \overline{T}_{n-1}, \overline{T}_n \end{cases} \tag{3-34}$$

and replacing the derivatives with respect to ψ by central difference operators,

$$\begin{cases} \dfrac{d\overline{|\mathbf{P}|}_i}{d\psi} = \dfrac{\overline{|\mathbf{P}|}_{i+1} - \overline{|\mathbf{P}|}_i}{\varphi / n} \\ \dfrac{d\theta_i}{d\psi} = \dfrac{\theta_{i+1} - \theta_i}{\varphi / n} \\ \dfrac{d\overline{T}_i}{d\psi_i} = \dfrac{\overline{T}_{i+1} - \overline{T}_i}{\varphi / n} \end{cases} \tag{3-35}$$

Therefore, the differential equations were simplified to algebraic equations as follows,

$$\begin{cases} F_{1,i} = \overline{|\mathbf{P}|}_{i+1} - \overline{|\mathbf{P}|}_i - \dfrac{\varphi}{n}\mu \sin\alpha_i \cos\theta_i \left(\overline{|\mathbf{P}|}_i - \bar{m}\right) = 0 \\ F_{2,i} = \theta_{i+1} - \theta_i - \dfrac{\varphi}{n}\mu \cos\alpha_i \cos\theta_i = 0 \qquad ,i = 1,2,...,n-1 \\ F_{3,i} = \overline{T}_{i+1} - \overline{T}_i + \dfrac{\varphi}{n} \dfrac{\mu \cos\alpha_i \cos\theta_i \overline{R}_0 \overline{|\mathbf{P}|}_i}{2\pi\overline{I} - \overline{K}} = 0 \end{cases} \tag{3-36}$$

The boundary conditions were also transformed below,

$$\begin{aligned} f_1 &= \overline{|\mathbf{P}|}_{AB} \\ f_2 &= \frac{\sin\theta_{AB}}{\sin\theta_{CD}} + \frac{\overline{l}_{CD}}{\overline{l}_{AB}} = 0 \\ f_3 &= \overline{T}_{AB} \\ f_4 &= \overline{T}_{CD} \\ f_5 &= \overline{n}_1 - (\overline{T}_{AB} - k\overline{T}_{CD})\eta = 0 \end{aligned} \tag{3-37}$$

The solutions were found by the following scheme: First, initialize the known parameters and input the three boundary values from the experimental measurement. Next, create trial matrix $\mathbf{X}_0$ which was composed of unknown variables $\overline{|\mathbf{P}|}_i$, θ_i, $\overline{T}_i$, and unknown constant value *K*. Then, create trial values for λ, k, η, thus, $\overline{n}_1$ was calculated using Equation (3-30). After that, Jacobian matrix *A(x)* was generated, as shown in Appendix A, and iterated by the Newton-Raphson scheme until the norm of the functions was smaller than $1e^{-5}$. If the results of two adjacent iteration for $\overline{n}_1$ was larger than $1e^{-5}$, use the new $\overline{n}_1$ as trial values for iteration. Finally, the three

unknown variables and two unknown constant values were obtained, and λ, k, η were computed. The flow chart of calculating the above three coefficients can be found in Appendix B.

3.2 Experimental setup

The experiments were conducted on a ring spinning frame (Zinser 351) by installing a moving belt with diameter of 6mm between the front rollers and the yarn guide. A cotton yarn with linear density of Ne 32 and diameter of 0.16 mm was adopted for the measurement. The measurement system was composed of two parts. One was for online acquisition of yarn tension, which included a strain gauge sensor (Honigmann tension meter 125.12, 100cN maximum range, 0.1cN precision, 15^{o} measuring angle), A/D converter (ZTIC USB-7660, digital I/O, USB form factor, 48 channels analog input, 12 bits size, 50KHz maximum clock rate, 0-10V voltage range, 5MΩ input impedance) and computer software (NI Labview 7.5). The second part was for continual and automatic image acquisition, storage and analysis of yarn instant twist including a high-speed camera (Phantom MIRO 4, CMOS sensor, 800 x 600 pixels, over 1200 fps at full resolution, 22 μm pixel size, 12-bit depth), which was connected to a personal computer installed with camera control software and Nikon micro lens (AF Micro-Nikkor 60 mm f/2.8D). Using the system, all data were acquired under the above mentioned conditions, ensuring repeatability. In addition, the frictional coefficient of the yarn and the belt was measured on the Shirley friction meter. In the following analysis, tension $|\mathbf{P}|_{AB}$, twist T_{AB}, and T_{CD} were measured as the boundary conditions to solve the theoretical model, while tension $|\mathbf{P}|_{CD}$, deviation angle θ_{AB} and θ_{CD} were measured to verify the accuracy of the theoretical model.

3.2.1 Measurement of Yarn Tension

Before online measurement of yarn tension, the strain sensor must be calibrated by corresponding material to be measured. According to the instruction provided by the manufacture, 50cm of measured material was threaded into the sensor mounted with a stand and sensor clamping device with a suitable calibration weight, and then moved the measured material slowly and smoothly, at a speed approximates 0.5 m/s.

The process was repeated thrice and the results were recorded. In the calibration process, yarn tensions with various dead weights were tested by the tension meter and the results were shown in Figure 3-4. The measuring value covers all the operational range in the experiment. As displayed in Figure 3-4, the measured data are very close to the real weight and the results can be expressed by the linear regression formula as

$$Y=1.001X-0.081 \tag{3-38}$$

The correlation coefficient is 0.999.

For online tension measurement, the sampling frequency was 1000Hz and 3000 data was gathered for each measurement, as shown in Figure 3-5.

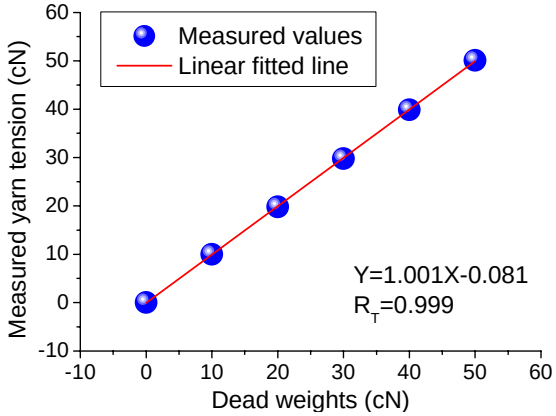

Figure 3- 4 Calibration of yarn tension

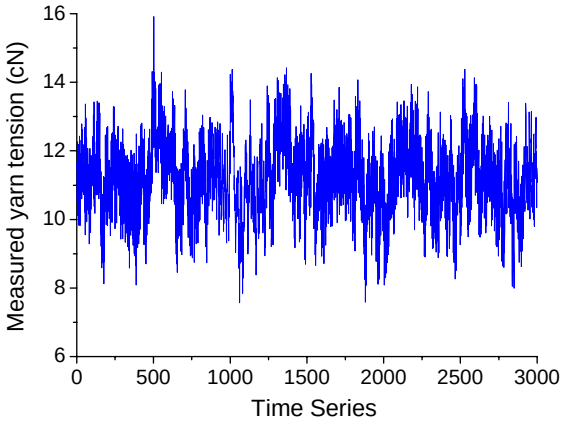

Figure 3- 5 Measured yarn tension

3.2.2 Measurement of Yarn Twist and Deviation Angle

As shown in Figure 3-6, high-speed photography technique was applied to capture images of yarn twist, and the system is composed of a high-speed camera, a

light source and tripod frames. The tripod frame of the high-speed camera was used to locate the direction of camera lens perpendicular to the yarn profile, which ensures the precision of the measurement. The light was used for providing sufficient illumination during the shooting process.

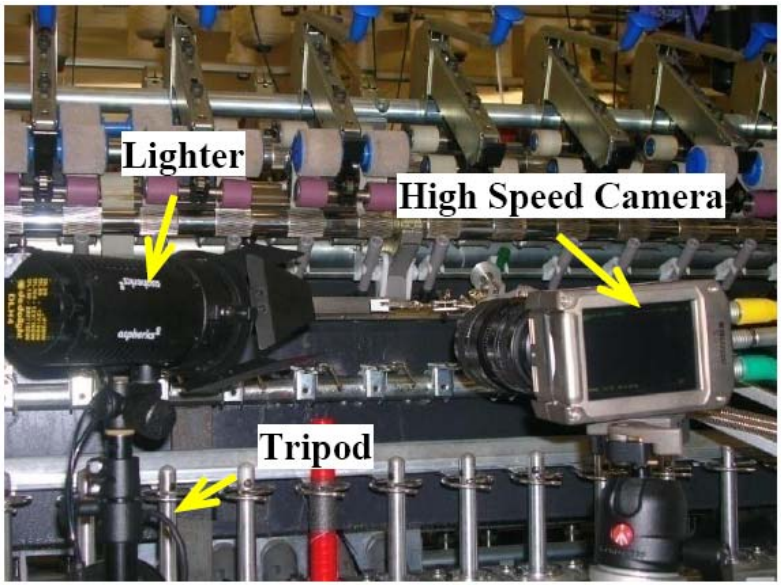

Figure 3- 6 A high-speed photography system

In order to obtain the twist from images, a black-white yarn was adopted, which used one black and unstained cotton rovings with the similar count feeding into the back rollers simultaneously. As a result of twisting, the bundle of straight and parallel fibers was laid along the helix curve on the yarn surface, and yarn twist could be directly read by the interval of black and white fiber bundles. And a scale paper of 1 mm x 1 mm size was put beneath the yarn to calculate the real length of one twist turn, as shown in Figure 3-7. The yarn twist can be derived by $T=1/h$, where T represents the number of twist turns per unit length, h is the length of one turn of twist. Sixty images were used for the computation of yarn twist at each boundary. And for each image, three readings were extracted, generating 180 raw data.

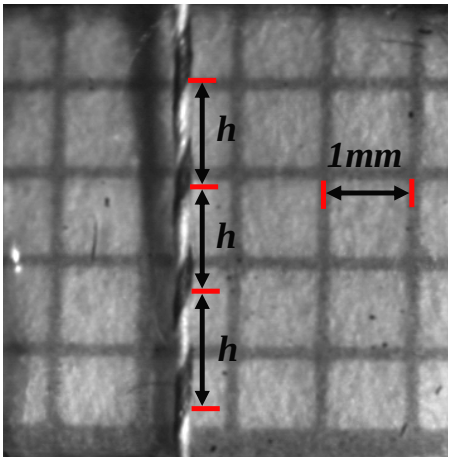

Figure 3- 7 Determination of yarn twist from image

Before measurement of the twist, the high-speed camera system was calibrated. Six twist levels were used for calibration and images of the twist were captured under a resolution of 512 × 512 pixels with a sampling frequency of 1000 frames per second. The measured values were compared with the results by using standard testing method ASTM D1423-02. As shown in Figure 3-8, twist measured by the high-speed photography method is approximately linear against the benchmark results by the standard method, which implies that the high-speed photography method can provide adequate accuracy and reliability for twist measurement. The relationship can be expressed by the linear regression equation as

$$Y=0.915X+9.018 \tag{3-39}$$

The correlation coefficient is 0.999.

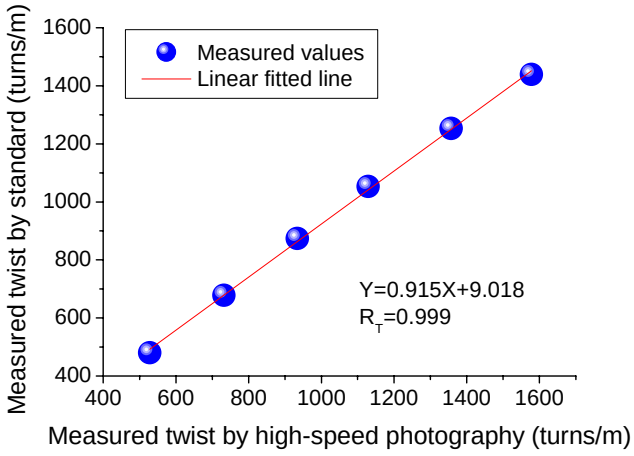

Figure 3- 8 Calibration of yarn twist

By using the same principle, the deviation angle at two boundaries can be measured by the high-speed photography method. One hundred images were used for the calculation of deviation angle at each boundary.

According to the aforementioned calibration results, it can be summarized that the proposed measurement system is suitable for measuring yarn twist and tension with excellent veracity and repeatability.

3.3 Results and discussion

3.3.1 Verification of Model

The dynamic model was verified before further investigation. Three cases with different operational parameters were studied, as shown in Table 3-1. After numerical simulation, the results of $|\mathbf{P}|_{AB}$, θ_{AB} and θ_{CD} were theoretically obtained and then compared with experimental measurements for verification.

The moving belt was installed at the middle of the delivery rollers and the twister. Ne 32 black-white yarn was used for the experiments. The radius of the yarn was 0.08mm, and the frictional coefficient of the yarn and moving belt was 0.81. Based on the parameters given in Table 3-1, simulation results of distributions of yarn twist, tension and deviation angle on the moving belt for the three cases were obtained.

Table 3-2 lists the simulated and measurement values of yarn tension and deviation angle. In all three cases, the difference between simulated values and experimental observations is smaller than 10%, which implies that the simulated figures match well with the measurement values and the theoretical model can predict a relatively accurate value of the problem. Additionally, the variation of tension measurement is smaller than 10%, while that for the measured twist and deviation angle are as large as 15.97% and 15.87% in case 2 and case 3, respectively. The large variations of yarn twist and deviation angle are mainly caused by the relative motion of the yarn on the moving belt.

Table 3-1 Parameters for case study

Case	v (m/s)	φ (^{o})	T_{CD} (turns/m) [CV%]	$\lvert\mathbf{P}\rvert_{CD}$ (cN) [CV%]	$\overline{T}_{AB}$ [CV%]	R_0 (mm)	$\overline{v}_b$	μ	$\frac{\overline{l}_{AB}}{\overline{l}_{CD}}$
1	0.24	50	656	14.30	1.57	0.08	2	0.81	1

			[15.97]	[8.32]	[14.47]				
2	0.27	50	556 [13.49]	13.62 [9.81]	1.26 [12.96]	0.08	1	0.81	1
3	0.27	70	549 [15.10]	15.08 [7.43]	2.08 [13.13]	0.08	2	0.81	1

Table 3-2 Results of simulated values and experimental observations

Case	$\lvert\mathbf{P}\rvert_{AB}$			θ_{AB}			θ_{CD}		
	M [CV%]	S	E (%)	M [CV%]	S	E (%)	M [CV%]	S	E (%)
1	10.33 [8.58]	10.35	0.19	-15.65 [11.67]	-17.15	9.58	16.23 [12.43]	17.15	5.67
2	8.62 [7.94]	7.95	7.77	-11.32 [8.76]	-12.42	9.72	11.86 [15.87]	12.42	4.51
3	9.58 [9.32]	9.91	3.44	-22.73 [11.68]	-23.77	4.58	-22.42 [11.32]	23.77	6.02

Note that M, S and E represent the measured value, simulated value, and error, respectively.

3.3.2 Error Analysis

The error caused by the assumption should be analysized and evaluated. Assumption 1 is inextensible yarn. The measured Young's modulus in axial direction is 288.46cN/tex, and the maximum tension in this study is 20cN, therefore the calculated maximum strain is 0.47%. Therefore, it is reasonable to assume an inextensible yarn.

Assumption 2 is small bending moment to be neglected. According to Love [144], the expressions of curvature and twist are: the curvature $\kappa = \frac{d\theta}{ds} = \frac{1}{\rho}$. The radius of curvature of yarn in this paper equals to the radius of columnar surface plus the yarn radius as follow $\rho = r + R_0 = 3\times10^{-3} + 0.08\times10^{-3} = 3.08\times10^{-3}$ m, $\kappa = \frac{1}{\rho} = 324.68 m^{-1}$ and the twist $\tau = \frac{d\phi}{ds}$. In our work, the mean value of yarn twist on the moving surface is larger than 650 turns/m, that is 4083.95m^{-1}. Therefore, the twist is one order of magnitude larger than that of the yarn curvature. It is reasonable to neglect the bending moment without much loss of precision of the model.

Assumption 3 is an uniform yarn. Fraser[142] has studied the effect of yarn non-uniformity on the stability of the ring-spinning balloon, and found even a quite modest slub can have a very significant effect on the stability of free ring-spinning balloon. In practice concentrated slubs that add a yarn as much as 400% additional

mass into the yarn are not uncommon. Therefore, the uneven features may have some effects on the simulated results.

The weight of yarn is neglected in Assumption 4. The yarn count for the study is 18.45tex, and the maximum yarn inactive path is less than 5mm, therefore the weight of yarn is less than 9.23×10^{-5} cN, six order of magnitude less than yarn tension, thus can be neglected.

Assumption 5 is a non-deformable belt. The Young's modulus of belt is 50Mpa, the Normal force is less than 28.28 cN, and the contacting area is less than $0.64 mm^2$, thus maximum strain of belt calculated is 0.707%, thus can be neglected.

Assumption 6 is a smooth belt with a constant curvature radius This is a good assumption, since the error of belt diameter is smaller than 0.2%.

A linear relationship between the yarn twist and torque is assumed in Assumption 7. According to the mechanics of material, $\frac{M}{GI_p} = \frac{d\varphi}{dx} = 2\pi T$. Therefore, $M = 2\pi GI_p T = KT$, since $2\pi GI_p$ is a constant parameter.

The model is built in a steady state, thus time-dependent terms in the equations are ignored in Assumption 8. Since the measurement is averaged, the simulated values should be close to the experiment values.

Assumption 9 is a stable twisting process. Since the twist level is not to high and yarn tension is not too low, therefore mechanical instability or bifurcation is not happened in this system.

3.3.3 Distributions of Tension, Deviation Angle and Twist

Figure 3-9a displays the simulated results of distributions of yarn tension on the moving belt against the wrap angle for three cases. Generally, the yarn tension increases linearly with the increase of wrap angle, and the tension values are raised by 38.72%, 71.58%, and 54.28% for three cases, respectively. Case 1 and 2 show that the ratio of tension in our system does not follow Euler's equation, which is only related to frictional coefficient and wrap angle by $P_2 / P_1 = e^{\mu\theta}$. In other word, tension changes in this kind of twisting system should use the treatment expressed in the first formula of Equation (3-32).

Figure 3-9b plots the distributions of deviation angle against the wrap angle for

the three cases. Since the length of line AB is the same as that of line CD, the deviation angle of line AB has the identical absolute value of that of line CD. Moreover, at the middle of wrap angle, 25^{o} for case 1 and 2, and 35^{o} for case 3, the deviation angles in all the cases are larger than zero, which means the yarn curves on the moving belt are not strictly antisymmetric.

Figure 3-9c depicts the distributions of twist against the wrap angle for the three cases. For all cases, the twist decreases greatly as the wrap angle increases, therefore the yarn undergoes an untwisting process on the moving belt. In case 1 and 2, the twists are reduced by 36.43% and 20.79%, respectively, while in case 3, a higher level of reductions of 51.93% is recorded. This reduction in case 3 may be caused by the increased wrap angle, which increases the contact friction between the yarn and the moving belt.

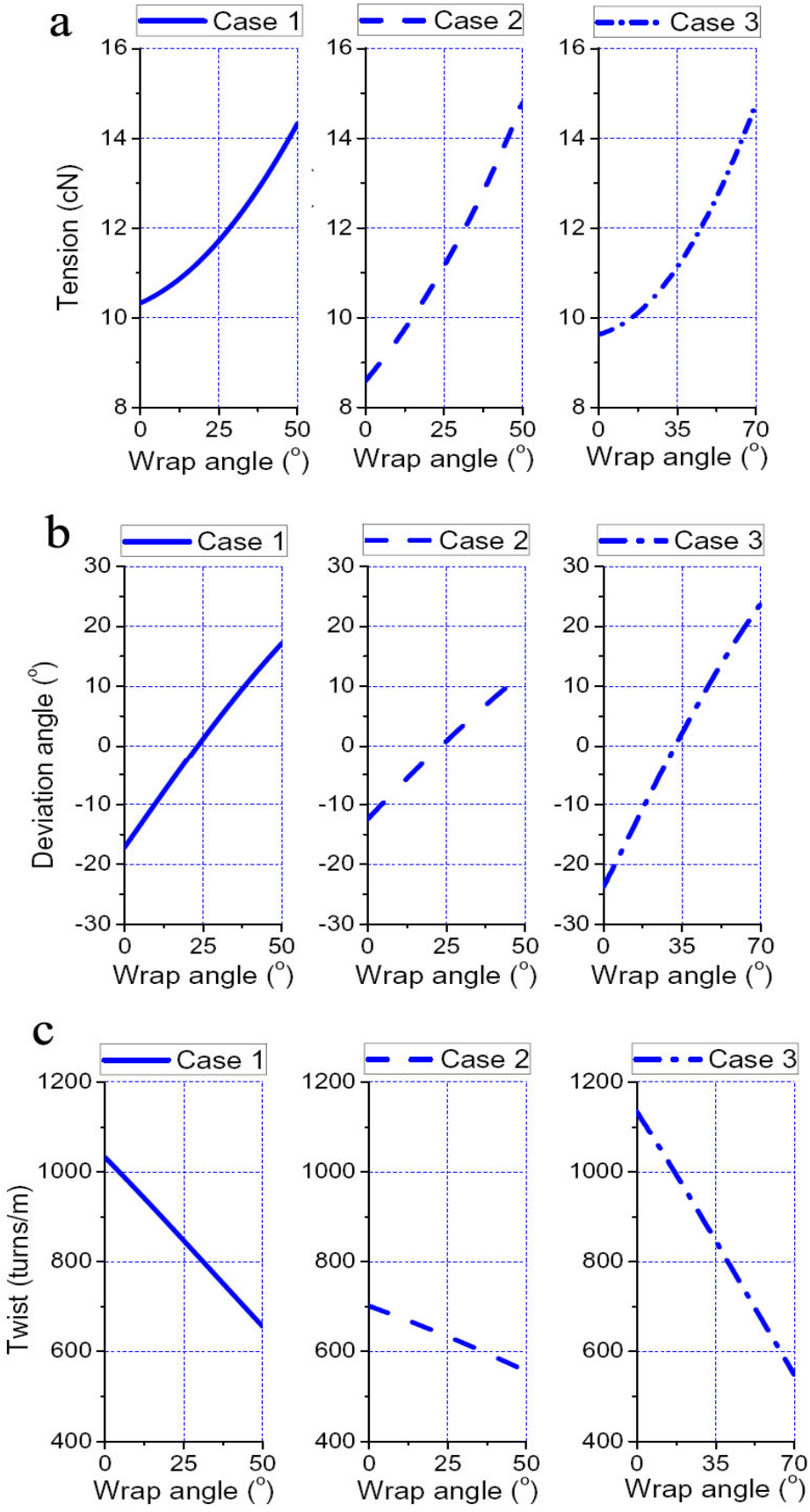

Figure 3- 9 Yarn dynamic performances on the moving belt. (a) Tension

distributions for three cases. (b) Distributions of deviation angle for three cases. (c) Twist distributions for three cases.

3.3.4 Twist Efficiency, Propagation and Blockage

From Equations (3-26 to 3-28), twist efficiency, coefficients of twist congestion and trapping can be calculated. The relationships between the twisting coefficients and four influencing factors, that is, yarn twist, tension, speed ratio, and wrap angle, were revealed.

The effect of yarn twist

Five twist levels of 458, 563, 656, 794 and 901 turns/m at the twister D were used. The other parameters are listed in Table 3-3. It was noted that the delivery speed of the yarn varied with the different twist levels because of the machine setting. Moreover, due to the effect of twist contraction, the tension $|\mathbf{P}|_{CD}$ slightly increases with the increment of twist level.

Table 3-3 Parameters of different univariate experiment

No.	v (m/s)	φ (^{o})	T_{CD} (turns/m) [CV%]	$\|\mathbf{P}\|_{CD}$ (cN) [CV%]	$\overline{T}_{AB}$	$\overline{v}_b$
1-1	0.33	50	458 [17.92]	14.12 [7.55]	1.91 [15.70]	2.0
1-2	0.27		563 [18.23]	14.21 [8.32]	1.67 [14.57]	
1-3	0.24		656 [15.97]	14.30 [7.47]	1.57 [14.47]	
1-4	0.21		794 [14.72]	15.14 [8.36]	1.43 [14.91]	
1-5	0.18		901 [14.55]	16.52 [8.44]	1.35 [14.22]	
2-1	0.27	50	561 [14.56]	19.80 [8.22]	2.06 [15.41]	2.0
2-2			568 [16.15]	16.22 [8.24]	1.83 [15.32]	
2-3			563 [18.23]	14.27 [9.26]	1.67 [14.57]	
2-4			578 [16.40]	13.28 [9.62]	1.59 [16.54]	
2-5			543 [15.89]	12.72 [8.22]	1.60 [13.67]	
3-1	0.27	50	556 [13.49]	13.62 [8.92]	1.26 [12.96]	1.0
3-2			566	13.98	1.51	1.5

			[15.17]	[8.42]	[14.70]	
3-3			563 [18.23]	14.22 [8.08]	1.67 [14.57]	2.0
3-4			570 [16.02]	14.62 [8.27]	1.75 [12.02]	2.5
3-5			552 [17.26]	14.82 [9.12]	1.85 [14.07]	3.0
4-1	0.27	30	534 [15.14]	14.33 [8.80]	1.39 [15.43]	2.0
4-2		50	563 [18.23]	14.29 [8.45]	1.67 [14.57]	
4-3		70	549 [15.10]	15.11 [9.34]	2.08 [13.13]	
4-4		90	562 [15.44]	16.24 [8.23]	2.35 [15.11]	

Figure 3-10a plots the twist efficiency, coefficients of twist trapping and congestion against twist levels. The twist efficiency of the moving belt shows a mild descending trend from 10.66% to 9.25% when the yarn twist doubles, while the trapping and congestion coefficients maintain around 0.9 for various twist level. It is evident that the twist efficiency and the propagation coefficients are not affected by the change of yarn twist. In addition, the low twist efficiency and high propagation coefficients are caused by the relative motion of the yarn and the moving belt. In most circumstances, the yarn slips on the moving belt, therefore the level of twist blockage is low and the propagation is high.

The effect of yarn tension

Five different tension levels ranging from 19.80 to 12.72 cN at zone CD were used with other parameters listed in Table 3-3. The number of twist in zone CD was set at 560 turns/m as compared with a 3% difference of the measured twist.

Figure 3-10b displays the twist efficiency, propagation coefficients of twist trapping and congestion with regard to various tension levels. It implies that the yarn tension has a large impact on the twist efficiency. The twist efficiency was increased greatly from 8.70% to 14.95% when the tension level rises from 12.72 to 19.80 cN. Besides, the propagation coefficients of twist trapping and congestion decrease with the increase of the tension. A high yarn tension results in a high normal force acting on the moving belt, thus achieves a high twist efficiency and low propagation coefficients.

The effect of speed ratio

Five different speed ratios from 1 to 3 were studied with other parameters for the experiment listed in Table 3-3. With the increase of speed ratio, the yarn tension also slightly increases. This is because the deviation angle θ_{CD} is also increased when adopting a higher speed ratio, thus the frictional angle of the yarn and yarn guide is raised, resulting in a higher yarn tension in zone CD.

As shown in Figure 3-10c, when the speed ratio increases from 1 to 3, the number of twist in zone AB rises continuously by 45%. Nevertheless, the twist efficiency does not show the same trends. With the increasing of speed ratio, the twist efficiency of the moving belt goes up at first, and then reaches the maximum values at the speed ratio of 1.5. then decreases with further increasing of the speed ratio. On the contrary, the propagation coefficients of twist trapping and congestion exhibit a reverse trend, reaching the bottom values at the speed ratio of 1.5.

The effect of wrap angle

Figure 3-10d illustrates near linear relationships can be obtained between the three coefficients and the wrap angle. The twist efficiency is increased by 3.21 times as the wrap angle triples. By contrast, the propagation coefficients decrease from 0.91 and 0.92 to 0.81 and 0.84, respectively. It can be concluded that the twist trapping and congestion have the same trends with the change of system parameters, which means the moving belt blocks the both-side twist propagation with a similar amount. Moreover, the twist efficiency displays a reverse trend compared to that of propagation of twist trapping and congestion.

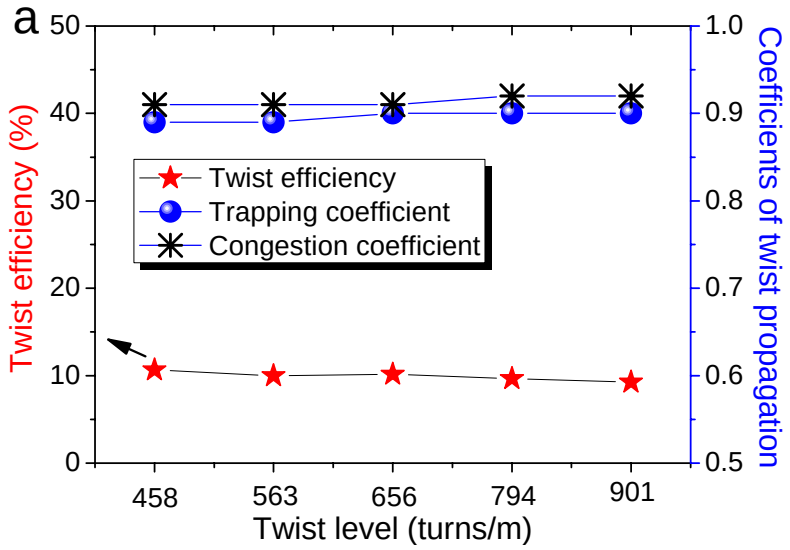

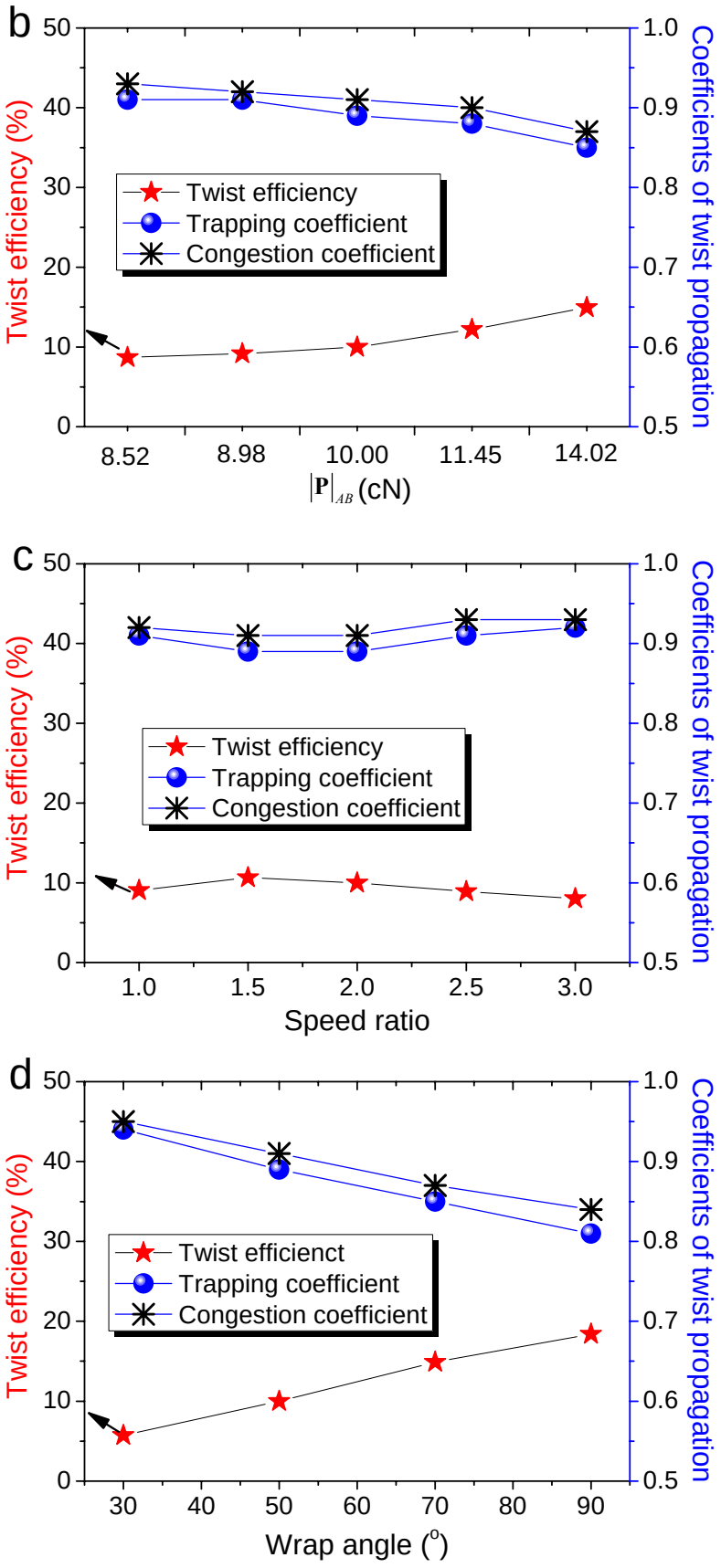

Figure 3- 10 Twist efficiency and coefficients of twist trapping and congestion by univariate experiment. (a) Different twist levels. (b) Different tension levels. (c)

Different speed ratio. (d) Different wrap angle.

3.3.5 Torsional Rigidity

Yarn torsional rigidity is the ratio of the applied torque and angle of twist, which is influenced by yarn geometry, tension, and processing history, etc. Figure 3-11 displays the calculated torsional rigidities for different cases, showing significant variations. In case 2-1, the torsional rigidity reaches as high as 2.70 x 10^{-8} Nm^2 due to the high tension value, and in other cases, the value ranges from 1.3 to 2.0 x 10^{-8} Nm^2. Therefore, the torsional rigidity can not be set as a constant known value for simulation because it changes with the system parameters.

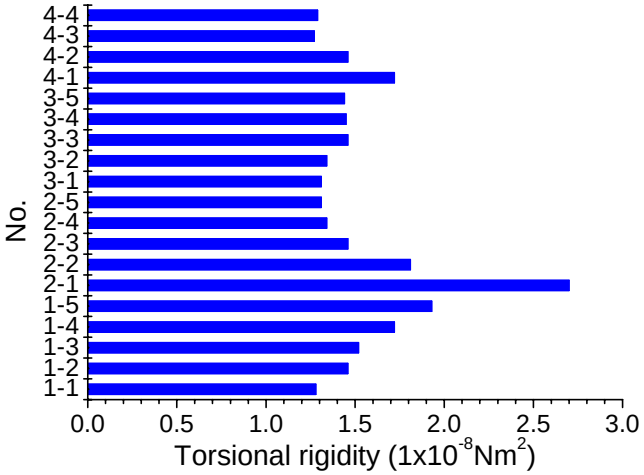

Figure 3-11 Calculated torsional rigidities for different cases

3.4 Systematically Investigation of the Twisting Process via Response Surface Methodology

Based on the proposed model, a systematic simulation has been carried out to evaluate effects of system parameters on the false-twisting efficiency as well as propagation coefficients. In order to minimize the number of experiments, response surface methodology involving a central composite design in three factors of twist multiplier, speed ratio and wrap angle was successfully employed for the study and analysis. The significant terms of the models were studied and relationships among three responses were investigated.

3.4.1 Experimental Design

Design of experiment (DOE) is a systematic and rigorous approach for the collection and analysis of the data with a limited expenditure to ensure a valid, defensible, and supportable engineering conclusions [166]. In statistics, response surface methodology (RSM) uses a sequence of designed experiments to exam the relationships between several input parameters and one or more response variables [167]. In order to reduce the number of experiments needed, a central composite design (CCD) was employed for deriving a quadratic polynomial model for the response variable [168]. Three important variables, twist factor (X_1), speed ratio (X_2), and wrap angle (X_3) were chosen as the independent variables and twist efficiency (Y_1), propagation coefficients of twist trapping (Y_2) and congestion (Y_3) were the dependent response variables. The range and levels of the independent variables investigated were previously chosen according to the results of single factor tests, as listed in Table 3-4. Although yarn tension may have a large impact on the three responses, it was not considered here for further investigation not only because its value can not be arbitrarily changed at such a wide range as in the single factor tests for industry production, but also the fact that it is not a continuously adjustable parameter for the experiment. The independent variables were tested in an orthogonal 2^3 CCD with six center points and six star points. Each of the independent variables was conducted at five different levels as per CCD in three variables with a total of 20 experiments [23]. The plan of CCD in coded levels of three independent variables is shown in Table 3-5. The statistical significance level (p value) was set at 0.05. The coded and actual values of the design were generated in a randomized run order using Minitab 16 software. Based on the RSM, quadratic polynomial regression equations are developed to fit the experimental data, as show in the following equation,

$$Y = C_0 + \sum_{i=1}^{K} C_i X_i + \sum_{j=1}^{K} C_{ii} X_i^2 + \sum_{i=1}^{K-1} \sum_{j=2}^{K} C_{ij} X_i X_j + \varepsilon \ (i < j) \tag{3-40}$$

where Y is the response, C_0 is constant, C_i, C_{ii} and C_{ij} are regression coefficients and X_i are the coded factors, ε is the error and K is the number of independent variables.

Table 3-4 Coded and actual level for each variables of the CCD

Variables	Code	Variation levels				
		-1.682	-1	0	+1	+1.682
Twist factor	X_1	2.51	2.91	3.50	4.09	4.49
Speed ratio	X_2	1.01	1.41	2.00	2.59	2.99

Wrap angle (^{o})	X_3	30.00	42.16	60.00	77.84	90.00

Table 3-5 Coded and actual levels in experimental design by CCD method

Run order	Coded levels			Independent variables			Responses		
	X_1	X_2	X_3	Twist factor	Speed ratio	Wrap angle	Twist efficiency (Y_1)	Trapping coefficient (Y_2)	Congestion coefficient (Y_3)
1	0	-1.682	0	3.50	1.01	60.00	0.126	0.873	0.892
2	-1	-1	+1	2.91	1.41	77.84	0.166	0.829	0.860
3	0	0	0	3.50	2.00	60.00	0.124	0.874	0.895
4	-1	+1	-1	2.91	2.59	42.16	0.073	0.926	0.939
5	0	+1.682	0	3.50	2.99	60.00	0.098	0.900	0.916
6	+1	-1	+1	4.09	1.41	77.84	0.143	0.853	0.877
7	+1.682	0	0	4.49	2.00	60.00	0.130	0.867	0.889
8	+1	+1	-1	4.09	2.59	42.16	0.070	0.929	0.941
9	0	0	-1.682	3.50	2.00	30.00	0.043	0.956	0.966
10	-1.682	0	0	2.51	2.00	60.00	0.152	0.844	0.872
11	0	0	0	3.50	2.00	60.00	0.133	0.864	0.887
12	0	0	0	3.50	2.00	60.00	0.131	0.866	0.889
13	+1	-1	-1	4.09	1.41	42.16	0.103	0.896	0.912
14	0	0	+1.682	3.50	2.00	90.00	0.171	0.821	0.854
15	0	0	0	3.50	2.00	60.00	0.131	0.866	0.889
16	0	0	0	3.50	2.00	60.00	0.144	0.853	0.878
17	-1	-1	-1	2.91	1.41	42.16	0.101	0.898	0.915
18	-1	+1	+1	2.91	2.59	77.84	0.124	0.870	0.893
19	+1	+1	+1	4.09	2.59	77.84	0.109	0.886	0.905
20	0	0	0	3.50	2.00	60.00	0.107	0.890	0.908

3.4.2 Results and Discussions

3.4.2.1 Analysis of variance (ANOVA)

ANOVA is a statistical technique to analyze the differences among group means and their associated procedures, which is accomplished by subdividing the total variation in a dataset into component parts allied with sources of variation for testing hypotheses on the variables of the model [169, 170]. Precision of a parameter estimation depends on the degree of freedom (DF), which equals to the number of experiments subtract the number of additional parameters estimated for that calculation [171]. Followed by Fisher's statistical test (*F* test), ANOVA was employed to study the importance of each independent variable [172]. *F* value is calculated by the regression mean square divided by the real error mean, which implies the influence of each controlled parameter on the model [173, 174]. The ANOVA data in Table 3-6 lists *F* value for twist efficiency, propagation coefficient of twist trapping and congestion as 10.36, 11.16 and 11.33 respectively, suggesting that the regression equation is highly significant. Generally, the large Fisher value denotes that the variation in the responses can be interpreted by the model . The associated *p* value is an important parameter to estimate if *F* value is large enough to display statistical significance [175, 176]. The *p* values is the index of the significance of the test, whose value below 0.05 indicates that the model and the associated terms are statistically significant at 95% confidence level [177-179]. The significance of each coefficient is also determined by the *F* and *p* values [180, 181]. ANOVA indicated that the highest significant level was shown by the wrap angle (X_3), followed by the speed ratio (X_2) and lastly, the quadratic wrap angle (X_3*X_3), while the interaction terms (X_1*X_2, X_1*X_3, X_2*X_3), the linear and quadratic twist factors (X_1, X_1*X_1) were less significant.

Table 3-6 also shows multiple correlation coefficient (R^2) and adjusted R^2. The R^2 implies the variation of the response in the model [182]. The higher the R^2, the better the model fits the data. The values of R^2 were calculated to be 90.31%, 90.95% and 91.07% for twist efficiency, propagation coefficients of twist trapping and congestion, respectively, implying that the experimental data was well-fitted. The adjusted R^2 explains the number of predictors in the model and is useful for comparing models with different numbers of predictors [183]. The high value of adjusted R^2 supports a high correlation between the experimental and the predicted data [170]. In this study, the

values of adjusted R^2 for twist efficiency, propagation coefficients of twist trapping and congestion were 81.59%, 82.80% and 83.03%, respectively, which means the regression models were statistically significant. The lack-of-fit *p* value of the model for twist efficiency, propagation coefficients of twist trapping and congestion were 0.334, 0.332 and 0.312, respectively, which were higher than 0.05, indicating that the models fitted all of the design points well.

Table 3-6 Analysis of variance for responses

Term	DF	Seq. SS	Adj. MS	*F*	*p*
Twist efficiency					
Regression	9	0.017579	0.001953	10.36	0.001
X_1	1	0.000423	0.000423	2.24	0.165
X_2	1	0.002481	0.002481	13.16	0.005
X_3	1	0.012325	0.012325	65.35	0.000
X_1*X_1	1	0.000106	0.000106	0.56	0.471
X_2*X_2	1	0.000819	0.000819	4.34	0.064
X_3*X_3	1	0.001249	0.001249	6.62	0.028
X_1*X_2	1	0.000001	0.000001	0.01	0.940
X_1*X_3	1	0.000171	0.000171	0.91	0.363
X_2*X_3	1	0.000028	0.000028	0.15	0.707
Residual error	10	0.001886	0.000189		
Lack-of-fit	5	0.001131	0.000226	1.50	0.334
Pure error	5	0.000755	0.000151		
Total	19	0.019465			
R^2=90.31%	R^2(adj.)=81.59%				
Trapping coefficient					
Regression	9	0.019255	0.002139	11.16	0.000
X_1	1	0.000465	0.000465	2.43	0.150
X_2	1	0.002383	0.002383	12.44	0.005
X_3	1	0.014050	0.014050	73.32	0.000
X_1*X_1	1	0.000122	0.000122	0.64	0.444
X_2*X_2	1	0.000934	0.000934	4.88	0.052
X_3*X_3	1	0.001106	0.001106	5.77	0.037
X_1*X_2	1	0.000001	0.000001	0.01	0.940
X_1*X_3	1	0.000190	0.000190	0.99	0.343
X_2*X_3	1	0.000021	0.000021	0.11	0.747
Residual error	10	0.001916	0.000192		
Lack-of-fit	5	0.001152	0.000230	1.51	0.332
Pure error	5	0.000765	0.000153		
Total	19	0.021171			
R^2=90.95%	R^2(adj.)=82.80%				
Congestion coefficient					
Regression	9	0.013140	0.001460	11.33	0.000
X_1	1	0.000234	0.000234	1.82	0.207
X_2	1	0.001745	0.001745	13.54	0.004
X_3	1	0.009509	0.009509	73.79	0.000
X_1*X_1	1	0.000077	0.000077	0.60	0.458

X_2*X_2	1	0.000519	0.000519	4.02	0.073
X_3*X_3	1	0.000950	0.000950	7.37	0.022
X_1*X_2	1	0.000000	0.000000	0.00	1.000
X_1*X_3	1	0.000113	0.000113	0.87	0.372
X_2*X_3	1	0.000008	0.000008	0.06	0.808
Residual error	10	0.001289	0.000129		
Lack-of-fit	5	0.000791	0.000158	1.59	0.312
Pure error	5	0.000498	0.000100		
Total	19	0.014429			
R^2=91.07%	R^2(adj.)=83.03%				

Seq. SS: sequential sum of squares, Adj. MS: adjusted mean squares

3.4.2.2 Reduced regression models

Since there were some insignificant terms existing in the regression models, it was necessary to simply them by eliminating insignificant terms. Decreasing the number of terms can make the model manageable, meanwhile increase the precision of the predictors. By examining the *F* and *p* values of each coefficient, it was found that all terms containing twist factor (X_1) over the range of 2.51 to 4.49 has little impact on the responses, thus should be removed from the models. Moreover, the interaction terms should also be removed as they are not significant for the models. The significant terms for the models were wrap angle (X_3), speed ratio (X_2) and quadratic wrap angle (X_3*X_3). The quadratic wrap angle (X_2*X_2) was reserved as it is significant at 10% level. Therefore, these four terms were employed to reconstruct the regression formulas. The results of simplified model and ANOVA are listed in Table 3-7, from which we can concluded that the reduced model was superior to the complete quadratic equations because the reduced models have higher *F* values and lower *p* values than those of previous ones. Moreover, all the four terms were statistically significant for the three responses and the adjusted R^2 were better than the previous ones, implying that the reduced regression models were significant and adequate to depict the actual relationship between the responses and inputs.

Table 3-7 Analysis of the reduced regression model

Term	DF	Seq. SS	Adj. MS	*F*	*p*
Twist efficiency					
Regression	4	0.016850	0.004212	24.16	0.000
X_2	1	0.002481	0.002481	14.23	0.002
X_3	1	0.012325	0.012325	70.69	0.000
X_2*X_2	1	0.000888	0.000888	5.09	0.039
X_3*X_3	1	0.001335	0.001335	7.66	0.014

Residual error	15	0.002615	0.000174		
Lack-of-fit	4	0.000994	0.000248	1.69	0.223
Pure error	11	0.001621	0.000147		
Total	19	0.019465			
R^2=86.56%	R^2(adj.)=82.98%				
Trapping coefficient					
Regression	4	0.018455	0.004614	25.49	0.000
X_2	1	0.002383	0.002383	13.16	0.002
X_3	1	0.014050	0.014050	77.61	0.000
X_2*X_2	1	0.001012	0.001012	5.59	0.032
X_3*X_3	1	0.001191	0.001191	6.58	0.022
Residual error	15	0.002716	0.000181		
Lack-of-fit	4	0.000997	0.000249	1.60	0.244
Pure error	11	0.001719	0.000156		
Total	19	0.021171			
R^2=87.17%	R^2(adj.)=83.75%				
Congestion coefficient					
Regression	4	0.012708	0.003177	27.70	0.000
X_2	1	0.001745	0.001745	15.21	0.001
X_3	1	0.009509	0.009509	82.90	0.000
X_2*X_2	1	0.000565	0.000565	4.92	0.042
X_3*X_3	1	0.001015	0.001015	8.85	0.009
Residual error	15	0.001720	0.000115		
Lack-of-fit	4	0.000690	0.000172	1.84	0.192
Pure error	11	0.001031	0.000094		
Total	19	0.014429			
R^2=88.08%	R^2(adj.)=84.90%				

3.4.2.3 Model validation

It is necessary to check the regression model to guarantee that adequate prediction to the actual data is obtained [134]. Diagnostic plots such as normal probability plots shown in Figure 3-12 enable to judge the normal distribution of the residuals. The residual is the error between the experimental data and the simulated value by the theoretical model. A small residual value represents a high accuracy of the prediction by the model. In Figure 4-18, the data points on the figure were close to the straight line, implying that the data was normally distributed.

The regression models were also investigated by nine sets of randomly selected data . As shown in Table 3-8, the estimated results generally agreed well with the experimental data, particularly for trapping and congestion coefficients. Errors between the estimated and experimental values for three responses were generally less than 10%. All the above results implied that the reduced regression equations provided sufficient accuracy for predicting the responses. Based on the analysis above, the

reduced regression models were capable of estimating and explaining the actual relationships between twist efficiency, propagation coefficients and the various system parameters of twist factor, speed ratio and wrap angle.

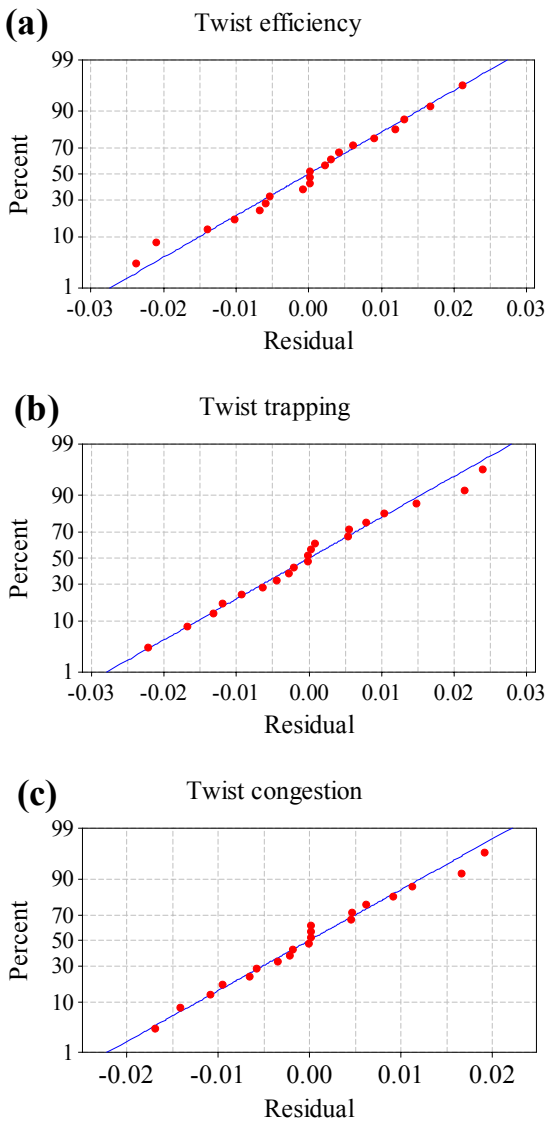

Figure 3-12 Normal probability plots of residuals for responses

Table 3-8 Model verifications for 9 cases

Order		1	2	3	4	5	6	7	8	9
Twist factor		2.5	2.8	3.3	3.7	4.2	2.7	3	4.3	4.1
Speed ratio		2.5	1.5	2.2	1.8	2.5	3	2	2.8	1.8
Wrap angle		30	40	50	65	50	60	45	75	85
Twist efficiency	A	0.0387	0.0982	0.1103	0.1427	0.0949	0.0849	0.1021	0.1087	0.1634
	P	0.0362	0.0909	0.1055	0.1422	0.0939	0.0861	0.0988	0.1167	0.1578
	E (%)	**6.46**	**7.43**	**4.35**	**0.35**	**1.05**	**1.41**	**3.23**	**7.36**	**3.43**
Trapping coefficient	A	0.9571	0.901	0.8878	0.8537	0.9035	0.9128	0.8966	0.8922	0.8295

	P	0.9629	0.9083	0.8924	0.8544	0.9042	0.912	0.8995	0.8789	0.8355
	E (%)	**0.61**	**0.81**	**0.52**	**0.08**	**0.08**	**0.09**	**0.32**	**1.49**	**0.72**
	A	0.9674	0.9172	0.9064	0.8789	0.9193	0.9277	0.9138	0.9096	0.8603
Congestion coefficient	P	0.9709	0.9239	0.9109	0.879	0.9204	0.9255	0.917	0.8994	0.8652
	E (%)	**0.36**	**0.73**	**0.5**	**0.01**	**0.12**	**0.24**	**0.35**	**1.67**	**0.57**

A: actual value P: predicted value E: error

3.4.2.4 Effect of control variables on the responses

Equation (3-41) is the empirical equations for the twist efficiency (Y_1), propagation coefficients of twist trapping (Y_2) and congestion (Y_3) as a function of the independent variables of speed ratio (X_2) and wrap angle (X_3) in coded units. It was found that the twist efficiency was increased with the decrease of X_2 and the increase of X_3. Besides, the trapping and congestion coefficients were increased with the increment of X_2 and the decrement of X_3. Moreover, the sign of the coefficients except constant for Y_1 was opposite to that of Y_2 and Y_3, while the coefficients of Y_2 and Y_3 had the same sign and similar value.

$$\begin{aligned} Y_1 &= 0.130823 - 0.013480X_2 + 0.030041X_3 - 0.007810X_2^2 - 0.009578X_3^2 \\ Y_2 &= 0.866177 + 0.013210X_2 - 0.032075X_3 + 0.008341X_2^2 + 0.009048X_3^2 \\ Y_3 &= 0.888895 + 0.011303X_2 - 0.026387X_3 + 0.006229X_2^2 + 0.008350X_3^2 \end{aligned} \quad (3\text{-}41)$$

The contour plot of control parameters on twist efficiency is shown in Figure 3-13a, where it could be seen intuitively that the twist efficiency was reduced as the wrap angle decreased and speed ratio increased. The wrap angle has a more significant effect than the speed ratio. Figure 3-13b shows that as the wrap angle went up, the trapping coefficient dropped sharply. Meanwhile, the trapping coefficient was reduced as the speed ratio decreased. A similar trend was noted in the congestion coefficient in the contour plot of Figure 3-13c.

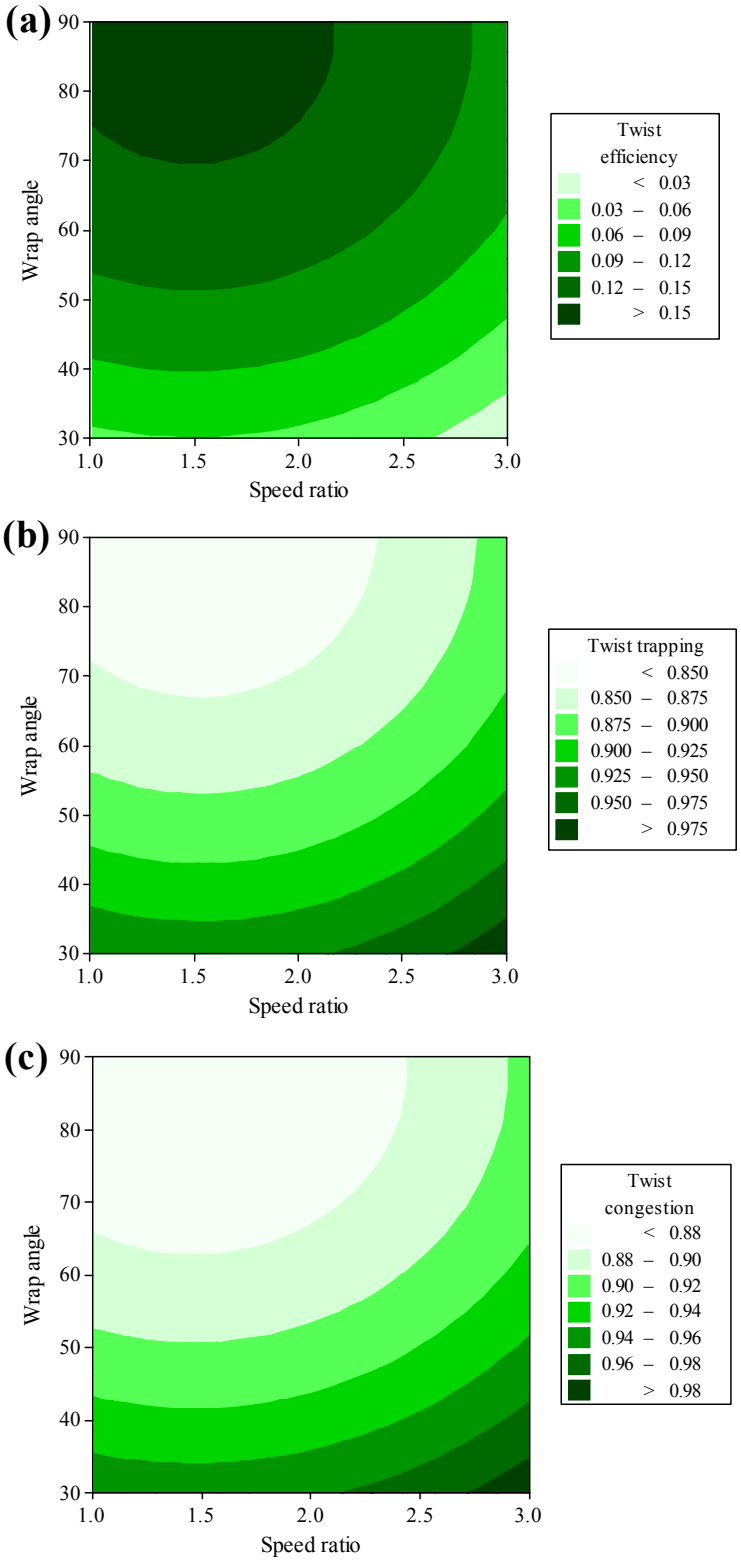

Figure 3-13 Response surface plots for (a) twist efficiency, (b) twist trapping, and (c) twist congestion

3.4.2.5 Relationships among three responses

Based on the analysis of the reduced regression equations, it was interesting to

unveil whether the three responses were related with each other. Thus, a fitting scheme was carried out in order to check their relationships. Figure 3-14a displays the experimental data of the twist efficiency and trapping coefficient. Results showed an approximately linear relationship between Y_1 and Y_2 with a high correlation coefficient of 0.998 and could be well explained by the following linear regression equation.

$$Y_2 = 1.002 - 1.04202Y_1 \tag{3-42}$$

Moreover, the relationship between Y_1 and Y_3 are shown in Figure 3-14b and a linear regression equation with a high correlation coefficient of 0.998 was indicated to explained the relationship as below,

$$Y_3 = 1.00118 - 0.86027Y_1 \tag{3-43}$$

In addition, Figure 3-14c depicts the experimental data of propagation coefficients of twist trapping and congestion, from which a linear relationship could be obtained with the same high correlation coefficient. The relationship was expressed by the following linear regression formula.

$$Y_3 = 0.17479 + 0.82463Y_2 \tag{3-44}$$

Finally, it was concluded that the three responses have linear relationships.

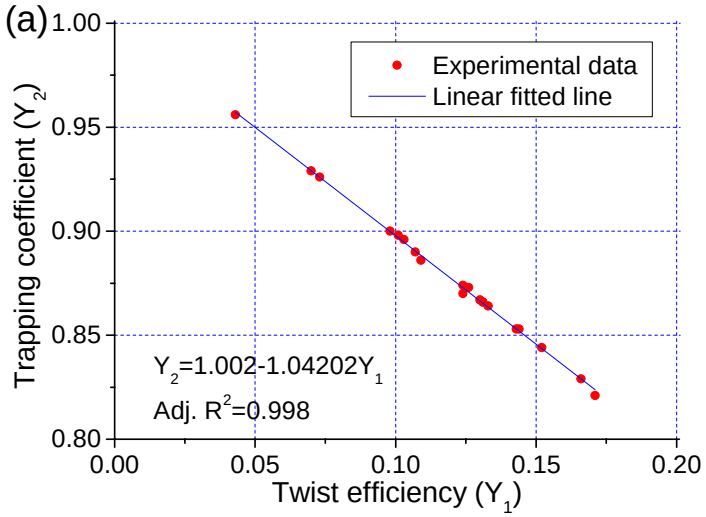

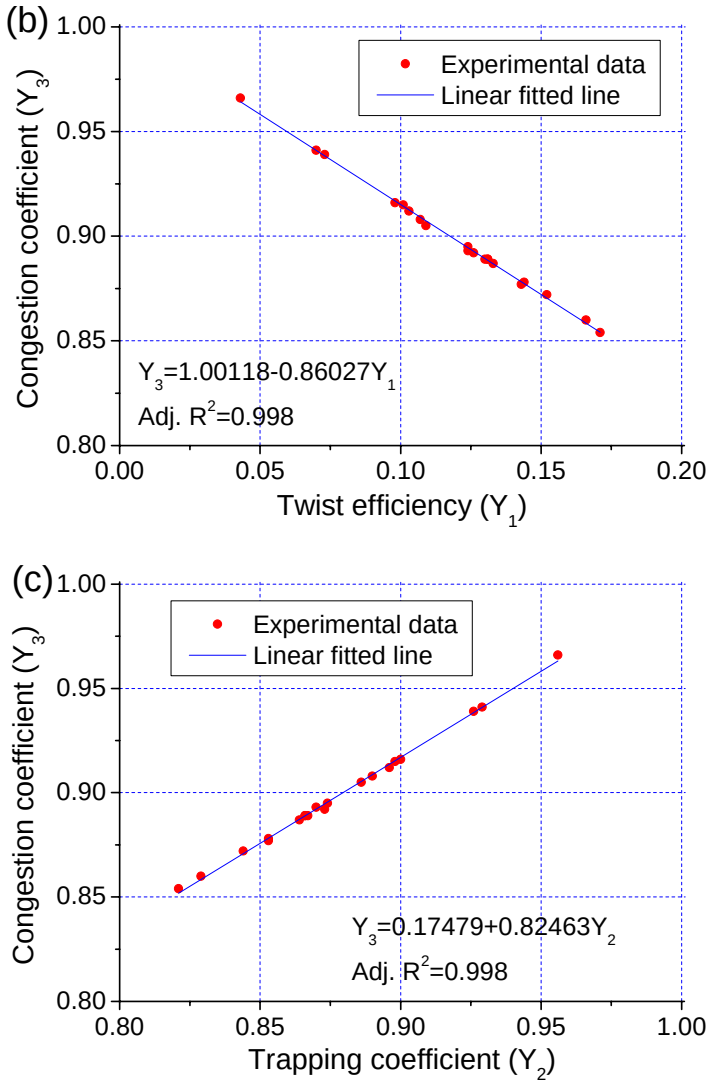

Figure 3-14 Linear relationships among three responses

3.5 Summary

In this chapter, we have developed a validated theoretical model of yarn dynamics on a moving belt. The simulation results were validated by experiments and a good agreement has been demonstrated for the ring spinning system with a single friction-belt as the twisting element. For the first time, influences of several parameters on the twisting process have been revealed in terms of twist efficiency of the moving friction-belt, propagation coefficients of twist trapping and congestion. Moreover, a systematic investigation has been carried out to study the twisting process of yarn on a moving belt using central composite response surface design. It was found that the speed ratio and wrap angle are statistically significant for the twist efficiency, propagation coefficients of twist trapping and congestion at 5% significant

level, while the twist factor has little effect on the responses. Then, the complete quadratic regression models were further simplified by eliminating insignificant terms, which were validated by normal probability analysis and another nine randomly selected experiments. Finally, it was important to discover that linear regression equations can be expressed the relationships among three responses with a high correlation coefficient of 0.998.

Chapter IV Yarn Kinematics in the Ring Spinning System with Single Friction-belt False-twister

This chapter reports on effects of variation of false twist on process stability and resultant yarn quality in a modified ring spinning frame. Based on twist kinematics, three idealized cases that cause twist variations in spinning process are investigated, namely step function, rectangular function and periodic function changes in false twist. The simulation results are validated by experiments and a good agreement has been demonstrated. The resultant properties of yarn within 30% periodic change in false twist demonstrated insignificance compared with yarn without variation. With the developed model, essential system parameters are numerically examined and their quantitative relationships are studied. The practical implications are discussed.

4.1 Theoretical Modeling

In this section, theoretical analysis of false twist variation on yarn twist redistributions is studied. Based on twist kinematics, three idealized cases that cause twist variations in twisting process are modeled, namely step change, rectangular change and sinusoidal variation in false twist. With the developed model, essential system parameters are numerically examined and their quantitative relationships are analyzed. The practical implications are discussed.

4.1.1 Assumptions

The following assumptions are made to simplify the theoretical modeling:

- ✧ Twist distribution in each zone is regarded as linear superposition of twists from the traveler and the false-twister;
- ✧ Yarn slippage rate on moving belt, coefficient of belt twist congestion and trapping are constant throughout;
- ✧ The effects of twist blockage caused by the yarn guide and the traveler are neglected;
- ✧ The effects of twist-contraction in each zone are neglected;
- ✧ The twist is evenly distributed in each zone.

✧ The yarn delivery speed is constant in each of the three zones.

4.1.2 Twist Distributions in the Steady-state

As shown in Figure 4-1, twist variations in a moving yarn maybe caused by the introduction of the columnar moving belt. Different from the tight crimp of rotor-pin type false-twister, the yarn slides on the moving belt. Therefore, only a certain percentage of the false-twists will be added into the yarn, which can be expressed by

$$T_b = \frac{\lambda v_b}{\pi d v} \tag{4- 1}$$

where T_b is the actual false-twist, λ is the belt twisting efficiency, v_b is the belt moving speed, v is the yarn delivery speed, d is the yarn nominal diameter.

Here, the belt twisting efficiency is a very important parameter determined by the belt material, yarn tension and wrap angle over the belt, the coefficient of the yarn and the belt, etc. As for the rotor-pin type, $\lambda = 1$. Simultaneously, twist blockage occurs when the yarn slides over the contacting surface of the belt, varying yarn twist along the threadline. In Figure 4-2a, the twist blocking action of the belt is called twist trapping, while that in Figure 5-2b is called twist congestion [184]. Let twister rotating at speed N, $T_{BC} = N / v$ is the nominal twist. $k = T_{AB} / T_{BC}$ is the coefficient of twist trapping in Figure 4-2a, and $\eta = T_{BC} / T_{AB}$ is the coefficient of twist congestion in Figure 4-2b. Therefore, the functions of the friction-belt are inserting false-twists above it, congesting the false twist downwards, and trapping the real twist upwards.

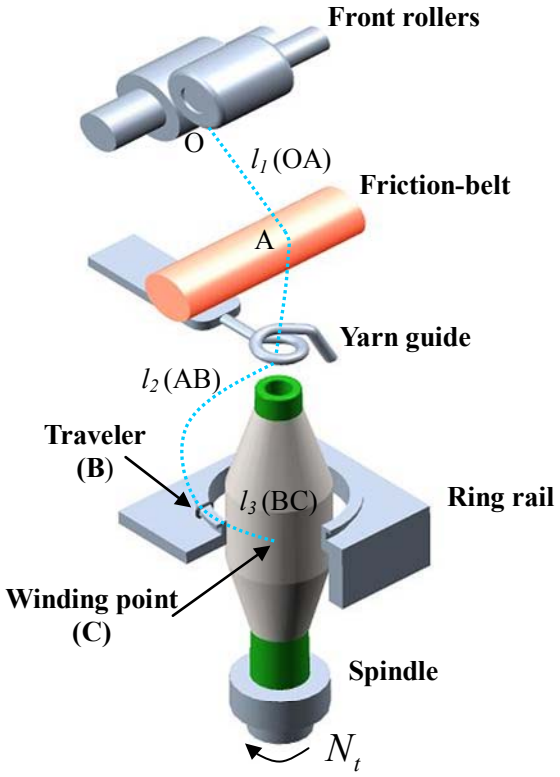

Figure 4-1 A schematic diagram of the novel twisting system

The yarn path in a novel twisting system is divided into three sections; the zone OA between the front roller and false-twister (l_1); the zone AB between the false-twister and the traveler (l_2); and the zone BC between the traveler and the winding point (l_3), as shown in Figure 4-1. In zone OA, turns are inserted into the yarn by the false-twister and the traveler. Due to the effect of twist blockage (congestion or trapping) and twist slippage of friction-belt, the twist in zone OA in the steady-state can be expressed by

$$\mathbf{T_1} = \frac{kN_t}{v} + \frac{\lambda N_b}{\eta v} \tag{4- 2}$$

where N_t is the traveler rotational speed, and N_b is the yarn theoretical rotational speed by belt.

In zone AB, the friction-belt inserts turns into the yarn at the same rate as in zone OA, but in the opposite sense, which cancels the positive twist passing from zone OA. Therefore, the twist in zone AB in the steady state is

$$\mathbf{T_2} = \frac{N_t}{v} \tag{4- 3}$$

In zone BC, no turns will be generated in this section and the twist in zone BC

remains the same as that in zone AB

$$\mathbf{T}_3 = \frac{N_t}{v} \tag{4- 4}$$

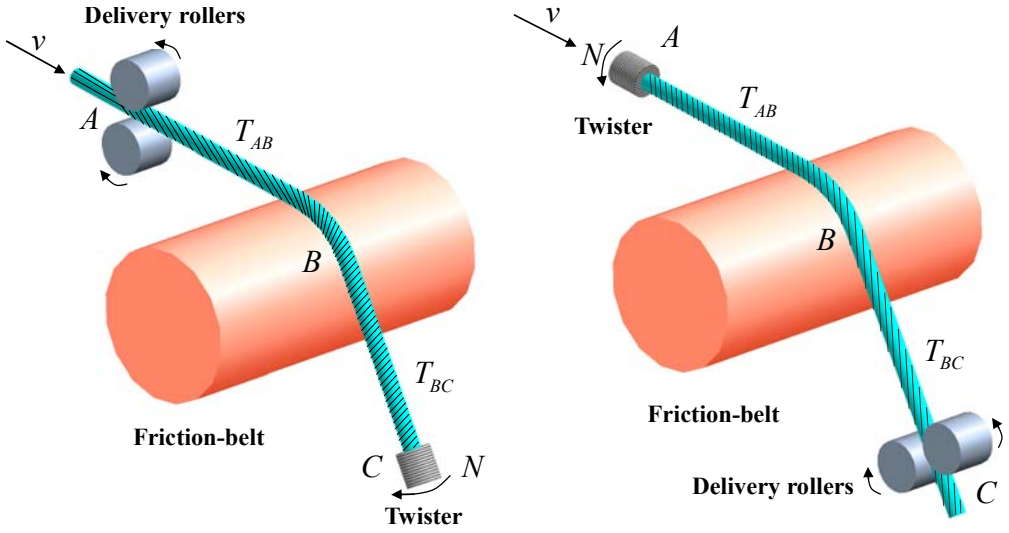

(a) (b)

Figure 4-2 Twist blockage in twisting zone: (a) twist trapping in region BC (b) twist congestion in region BC

4.1.3 Twist Redistributions in the Transient-state

In the transient-state, twist redistributions vary with time due to the altered false twist by changing the belt moving speed, while the real twist remains unchanged. As mentioned above, the twist redistribution in each zone is the linear superposition of real-twist and false-twist. Therefore, the total twist in each zone is the sum of the unchanged real twist and altered false twist.

4.1.3.1 Step function variation

The impact on the development of twist redistribution by false twist variations during nominally steady-state running is of much great practical interest. Hence, equations are developed that describes the way in which twists in the three zones of the twisting machine alter by a step change in twisting rate of moving belt. A step function change of false twist amount ΔN_b at time t_0 is assumed.

False Twist in Zone OA

When $t \le t_0$, yarn false twist in zone OA is

$$T_1 = \frac{\lambda N_b}{\eta v} \tag{4- 5}$$

When $t > t_0$, the turns gained by moving belt are $\lambda\left(N_b + \Delta N_b\right)dt$, turns lost through the belt are $\eta T_1 v dt$, therefore, the net twists gained are $dT_1 = \frac{\lambda\left(N_b + \Delta N_b\right) - \eta T_1 v}{l_1} dt$, integration of which together with the initial condition in Equation 5-5, gives

$$T_1 = \frac{1}{\eta v}\left(\lambda\left(N_b + \Delta N_b\right) - \left(\lambda\left(N_b + \Delta N_b\right) - \eta v T_1 |_{t=t_0}\right)\exp\left(-\frac{\eta v}{l_1}(t - t_0)\right)\right) \tag{4- 6}$$

False Twist in Zone AB

When $t \le t_0$, yarn false twist in zone AB is

$$T_2 = 0 \tag{4- 7}$$

When $t > t_0$, the turns passing through the false-twister from Zone OA are $\eta T_1 v dt$, the negative turns inserted by the moving belt are $-\lambda\left(N_b + \Delta N_b\right)dt$, the turns passing through the traveler are $T_2 v dt$, therefore, the net twists gained are $dT_2 = \frac{\eta T_1 v - \lambda\left(N_b + \Delta N_b\right) - T_2 v}{l_2} dt$, integration of which together with the initial condition in Equation 4-7, gives

$$\begin{aligned} T_2 = {} & T_2 |_{t=t_0} \exp\left(-\frac{v}{l_2}(t - t_0)\right) \\ & - \frac{\lambda\left(N_b + \Delta N_b\right) - \eta v T_1 |_{t=t_0}}{v} \frac{l_1}{l_1 - \eta l_2}\left(\exp\left(-\frac{\eta v}{l_1}(t - t_0)\right) - \exp\left(-\frac{v}{l_2}(t - t_0)\right)\right) \end{aligned} \tag{4- 8}$$

False Twist in Zone BC

When $t \le t_0$, yarn false twist in zone BC is

$$T_3 = 0 \tag{4- 9}$$

When $t > t_0$, the turns passing through the traveler from zone AB are $T_2 v dt$, the turns wound onto the bobbin are $T_3 v dt$, therefore, the net twists gained are $dT_3 = \frac{T_2 v - T_3 v}{l_3} dt$, integration of which together with the initial condition in Equation 4-9, gives

$$T_3 = T_3|_{t=t_0}\exp\left(-\frac{v}{l_3}(t-t_0)\right)+\frac{l_2}{l_2-l_3}T_2|_{t=t_0}\left(\exp\left(-\frac{v}{l_2}(t-t_0)\right)-\exp\left(-\frac{v}{l_3}(t-t_0)\right)\right)$$
$$-\frac{\lambda\left(N_b+\Delta N_b\right)-\eta v T_1|_{t=t_0}}{v}\frac{l_1}{\left(l_1-\eta l_2\right)\left(l_1-\eta l_3\right)\left(l_2-l_3\right)}$$
$$\left(l_1\left(l_2-l_3\right)\exp\left(-\frac{\eta v}{l_1}(t-t_0)\right)-l_2\left(l_1-\eta l_3\right)\exp\left(-\frac{v}{l_2}(t-t_0)\right)+l_3\left(l_1-\eta l_2\right)\exp\left(-\frac{v}{l_3}(t-t_0)\right)\right) \quad (4\text{-}10)$$

Therefore, yarn total twists in each zone can be expressed by the

$$\mathbf{T_1}=\begin{cases}\dfrac{kN_t}{v}+\dfrac{\lambda N_b}{\eta v} & ,t\le t_0\\ \dfrac{kN_t}{v}+\dfrac{1}{\eta v}\left(\lambda\left(N_b+\Delta N_b\right)-\left(\lambda\left(N_b+\Delta N_b\right)-\eta v T_1|_{t=t_0}\right)\exp\left(-\dfrac{\eta v}{l_1}(t-t_0)\right)\right) & ,t>t_0\end{cases} \quad (4\text{-}11)$$

$$\mathbf{T_2}=\begin{cases}\dfrac{N_t}{v} & ,t\le t_0\\ \dfrac{N_t}{v}+T_2|_{t=t_0}\exp\left(-\dfrac{v}{l_2}(t-t_0)\right)-\dfrac{\lambda\left(N_b+\Delta N_b\right)-\eta v T_1|_{t=t_0}}{v} & \\ \dfrac{l_1}{l_1-\eta l_2}\left(\exp\left(-\dfrac{\eta v}{l_1}(t-t_0)\right)-\exp\left(-\dfrac{v}{l_2}(t-t_0)\right)\right) & ,t>t_0\end{cases} \quad (4\text{-}12)$$

$$\mathbf{T_3}=\begin{cases}\dfrac{N_t}{v} & ,t\le t_0\\ \dfrac{N_t}{v}+T_3|_{t=t_0}\exp\left(-\dfrac{v}{l_3}(t-t_0)\right)+\dfrac{l_2}{l_2-l_3}T_2|_{t=t_0}\left(\exp\left(-\dfrac{v}{l_2}(t-t_0)\right)-\exp\left(-\dfrac{v}{l_3}(t-t_0)\right)\right) & \\ -\dfrac{\lambda\left(N_b+\Delta N_b\right)-\eta v T_1|_{t=t_0}}{v}\dfrac{l_1}{\left(l_1-\eta l_2\right)\left(l_1-\eta l_3\right)\left(l_2-l_3\right)} & ,t>t_0\\ \left(l_1\left(l_2-l_3\right)\exp\left(-\dfrac{\eta v}{l_1}(t-t_0)\right)-l_2\left(l_1-\eta l_3\right)\exp\left(-\dfrac{v}{l_2}(t-t_0)\right)+l_3\left(l_1-\eta l_2\right)\exp\left(-\dfrac{v}{l_3}(t-t_0)\right)\right) & \end{cases} \quad (4\text{-}13)$$

Transforming the above equations into the dimensionless form, one obtains

$$\overline{\mathbf{T_1}}=\begin{cases}k+\dfrac{\lambda\overline{N_b}}{\eta} & ,\bar{t}\le\overline{t_0}\\ k+\dfrac{1}{\eta}\left(\lambda\left(\overline{N_b}+\overline{\Delta N_b}\right)-\left(\lambda\left(\overline{N_b}+\overline{\Delta N_b}\right)-\eta\overline{T_1|_{t=t_0}}\right)\exp\left(-\dfrac{\eta}{\bar{l}_1}(\bar{t}-\overline{t_0})\right)\right) & ,\bar{t}>\overline{t_0}\end{cases} \quad (4\text{-}14)$$

$$\overline{\mathbf{T_2}}=\begin{cases}1 & ,\bar{t}\le\overline{t_0}\\ 1+\overline{T_2\,|_{t=t_0}}\exp\left(-\frac{1}{\overline{l_2}}(\bar{t}-\overline{t_0})\right)-\left(\lambda\left(\overline{N_b}+\overline{\Delta N_b}\right)-\eta\overline{T_1\,|_{t=t_0}}\right) & ,\bar{t}>\overline{t_0}\\ \frac{\overline{l_1}}{\overline{l_1}-\eta\overline{l_2}}\left(\exp\left(-\frac{\eta}{\overline{l_1}}(\bar{t}-\overline{t_0})\right)-\exp\left(-\frac{1}{\overline{l_2}}(\bar{t}-\overline{t_0})\right)\right)\end{cases} \tag{4- 15}$$

$$\overline{\mathbf{T_3}}=\begin{cases}1 & ,\bar{t}\le\overline{t_0}\\ 1+\overline{T_3\,|_{t=t_0}}\exp\left(-\frac{1}{\overline{l_3}}(\bar{t}-\overline{t_0})\right)+\frac{\overline{l_2}}{\overline{l_2}-1}\overline{T_2\,|_{t=t_0}}\left(\exp\left(-\frac{1}{\overline{l_2}}(\bar{t}-\overline{t_0})\right)-\exp\left(-\frac{1}{\overline{l_3}}(\bar{t}-\overline{t_0})\right)\right) & \\ -\left(\lambda\left(\overline{N_b}+\overline{\Delta N_b}\right)-\eta\overline{T_1\,|_{t=t_0}}\right)\frac{\overline{l_1}}{\left(\overline{l_1}-\eta\overline{l_2}\right)\left(\overline{l_1}-\eta\right)\left(\overline{l_2}-1\right)} & ,\bar{t}>\overline{t_0}\\ \left(\overline{l_1}\left(\overline{l_2}-1\right)\exp\left(-\frac{\eta}{\overline{l_1}}(\bar{t}-\overline{t_0})\right)-\overline{l_2}\left(\overline{l_1}-\eta\right)\exp\left(-\frac{1}{\overline{l_2}}(\bar{t}-\overline{t_0})\right)+\left(\overline{l_1}-\eta\overline{l_2}\right)\exp\left(-(\bar{t}-\overline{t_0})\right)\right)\end{cases} \tag{4- 16}$$

where $\bar{t}=\frac{vt}{l_3}$, $\overline{t_0}=\frac{vt_0}{l_3}$, $\overline{l_1}=\frac{l_1}{l_3}$, $\overline{l_2}=\frac{l_2}{l_3}$, $\overline{T_1}=\frac{vT_1}{N_t}$, $\overline{T_2}=\frac{vT_2}{N_t}$, $\overline{T_3}=\frac{vT_3}{N_t}$, $\overline{N_b}=\frac{N_b}{N_t}$, $\overline{\Delta N_b}=\frac{\Delta N_b}{N_t}$

4.1.3.2 Rectangular function variation

In some occurrences, a temporary or transient change of false twist may happen due to the variation of belt moving speed, yarn diameter variation, or increased/decreased yarn slippage on columnar belt, etc. In order to study this situation, a change of false twist amount ΔN_b at a short period Δt is assumed.

False Twist in Zone OA

When $t\le t_0$, yarn false twist in zone OA is

$$T_1=\frac{\lambda N_b}{\eta v} \tag{4- 17}$$

When $t_0<t\le t_0+\Delta t$, the turns gained by the false-twister are $\lambda\left(N_b+\Delta N_b\right)dt$, the turns lost through the false-twister are $\eta T_1 v dt$, therefore, the net twists gained are $dT_1=\frac{\lambda\left(N_b+\Delta N_b\right)-\eta T_1 v}{l_1}dt$, integration of which together with the initial condition in Equation 4-17, gives

$$T_1 = \frac{1}{\eta v}\left(\lambda\left(N_b+\Delta N_b\right)-\left(\lambda\left(N_b+\Delta N_b\right)-\eta v T_1\mid_{t=t_0}\right)\exp\left(-\frac{\eta v}{l_1}(t-t_0)\right)\right) \quad (4\text{-}18)$$

When $t > t_0 + \Delta t$, the turns gained by the moving belt are $\lambda N_b dt$, the turns lost through the false-twister are $\eta T_1 v dt$, the net twists gained are $dT_1 = \frac{\lambda N_b - \eta T_1 v}{l_1} dt$, integration of which together with the initial condition in Equation 4-18, gives

$$T_1 = \frac{1}{\eta v}\left(\lambda N_b - \left(\lambda N_b - \eta v T_1\mid_{t=t_0+\Delta t}\right)\exp\left(-\frac{\eta v}{l_1}(t-t_0-\Delta t)\right)\right) \quad (4\text{-}19)$$

False Twist in Zone AB

When $t \le t_0$, yarn false twist in zone AB is

$$T_2 = 0 \quad (4\text{-}20)$$

When $t_0 < t \le t_0 + \Delta t$, the turns passing through the false-twister from Zone OA are $\eta T_1 v dt$, the negative turns inserted by the moving belt are $-\lambda\left(N_b + \Delta N_b\right)dt$, the turns passing through the traveler are $T_2 v dt$, therefore, the net twists gained are $dT_2 = \frac{\eta T_1 v - \lambda\left(N_b + \Delta N_b\right) - T_2 v}{l_2} dt$, integration of which together with the initial condition in equation 4-20, gives

$$\begin{aligned} T_2 &= T_2\mid_{t=t_0}\exp\left(-\frac{v}{l_2}(t-t_0)\right) \\ &-\frac{\lambda\left(N_b+\Delta N_b\right)-\eta v T_1\mid_{t=t_0}}{v}\frac{l_1}{l_1-\eta l_2}\left(\exp\left(-\frac{\eta v}{l_1}(t-t_0)\right)-\exp\left(-\frac{v}{l_2}(t-t_0)\right)\right) \end{aligned} \quad (4\text{-}21)$$

When $t > t_0 + \Delta t$, the turns passing through the false-twister from Zone OA be $\eta T_1 v dt$, the negative turns inserted by the moving belt be $-\lambda N_b dt$, the turns passing through the traveler be $T_2 v dt$, therefore, the net twists gained be $dT_2 = \frac{\eta T_1 v - \lambda N_b - T_2 v}{l_2} dt$.,

integration of which together with the initial condition in Equation 4-21, gives

$$\begin{aligned} T_2 &= T_2\mid_{t=t_0+\Delta t}\exp\left(-\frac{v}{l_2}(t-t_0-\Delta t)\right) \\ &-\frac{\lambda N_b-\eta v T_1\mid_{t=t_0+\Delta t}}{v}\frac{l_1}{l_1-\eta l_2}\left(\exp\left(-\frac{\eta v}{l_1}(t-t_0-\Delta t)\right)-\exp\left(-\frac{v}{l_2}(t-t_0-\Delta t)\right)\right) \end{aligned} \quad (4\text{-}22)$$

False Twist in Zone BC

When $t \le t_0$, yarn false twist in zone BC is

$$T_3 = 0 \tag{4- 23}$$

When $t_0 < t \le t_0 + \Delta t$, the turns passing through the traveler from zone AB are $T_2 v dt$, the turns wound onto the bobbin are $T_3 v dt$, therefore, the net twists gained are $dT_3 = \frac{T_2 v - T_3 v}{l_3} dt$, integration of which together with the initial condition in Equation 4-23, gives

$$\begin{aligned} T_3 = {} & T_3|_{t=t_0} \exp\left(-\frac{v}{l_3}(t-t_0)\right) + \frac{l_2}{l_2 - l_3} T_2|_{t=t_0} \left(\exp\left(-\frac{v}{l_2}(t-t_0)\right) - \exp\left(-\frac{v}{l_3}(t-t_0)\right)\right) \\ & - \frac{\lambda(N_b + \Delta N_b) - \eta v T_1|_{t=t_0}}{v} \frac{l_1}{(l_1 - \eta l_2)(l_1 - \eta l_3)(l_2 - l_3)} \\ & \left(l_1(l_2 - l_3)\exp\left(-\frac{\eta v}{l_1}(t-t_0)\right) - l_2(l_1 - \eta l_3)\exp\left(-\frac{v}{l_2}(t-t_0)\right) + l_3(l_1 - \eta l_2)\exp\left(-\frac{v}{l_3}(t-t_0)\right)\right) \end{aligned} \tag{4- 24}$$

When $t > t_0 + \Delta t$, the turns passing through the traveler from Zone AB are $T_2 v dt$, the turns wound onto the bobbin are $T_3 v dt$, therefore, the net twists gained are $dT_3 = \frac{T_2 v - T_3 v}{l_3} dt$, integration of which together with the initial condition in Equation 4-24, gives

$$\begin{aligned} T_3 = {} & T_3|_{t=t_0+\Delta t} \exp\left(-\frac{v}{l_3}(t-t_0-\Delta t)\right) \\ & + \frac{l_2}{l_2 - l_3} T_2|_{t=t_0+\Delta t} \left(\exp\left(-\frac{v}{l_2}(t-t_0-\Delta t)\right) - \exp\left(-\frac{v}{l_3}(t-t_0-\Delta t)\right)\right) \\ & - \frac{\lambda N_b - \eta v T_1|_{t=t_0+\Delta t}}{v} \frac{l_1}{(l_1 - \eta l_2)(l_1 - \eta l_3)(l_2 - l_3)} \\ & \left(\begin{array}{l} l_1(l_2 - l_3)\exp\left(-\frac{\eta v}{l_1}(t-t_0-\Delta t)\right) - l_2(l_1 - \eta l_3)\exp\left(-\frac{v}{l_2}(t-t_0-\Delta t)\right) \\ + l_3(l_1 - \eta l_2)\exp\left(-\frac{v}{l_3}(t-t_0-\Delta t)\right) \end{array}\right) \end{aligned} \tag{4- 25}$$

Therefore, yarn total twists in each zone can be expressed by the

$$\mathbf{T_1}=\begin{cases}\dfrac{kN_t}{v}+\dfrac{\lambda N_b}{\eta v} & ,t\le t_0\\ \dfrac{kN_t}{v}+\dfrac{1}{\eta v}\left(\lambda\left(N_b+\Delta N_b\right)-\left(\lambda\left(N_b+\Delta N_b\right)-\eta v T_1\mid_{t=t_0}\right)\exp\left(-\dfrac{\eta v}{l_1}(t-t_0)\right)\right) & ,t_0<t\le t_0+\Delta t\\ \dfrac{kN_t}{v}+\dfrac{1}{\eta v}\left(\lambda N_b-\left(\lambda N_b-\eta v T_1\mid_{t=t_0+\Delta t}\right)\exp\left(-\dfrac{\eta v}{l_1}(t-t_0-\Delta t)\right)\right) & ,t>t_0+\Delta t\end{cases} \quad (4\text{-}26)$$

$$\mathbf{T_2}=\begin{cases}\dfrac{N_t}{v} & ,t\le t_0\\ \dfrac{N_t}{v}+T_2\mid_{t=t_0}\exp\left(-\dfrac{v}{l_2}(t-t_0)\right)-\dfrac{\lambda\left(N_b+\Delta N_b\right)-\eta v T_1\mid_{t=t_0}}{v} & \\ \dfrac{l_1}{l_1-\eta l_2}\left(\exp\left(-\dfrac{\eta v}{l_1}(t-t_0)\right)-\exp\left(-\dfrac{v}{l_2}(t-t_0)\right)\right) & ,t_0<t\le t_0+\Delta t\\ \dfrac{N_t}{v}+T_2\mid_{t=t_0+\Delta t}\exp\left(-\dfrac{v}{l_2}(t-t_0-\Delta t)\right)-\dfrac{\lambda N_b-\eta v T_1\mid_{t=t_0+\Delta t}}{v} & \\ \dfrac{l_1}{l_1-\eta l_2}\left(\exp\left(-\dfrac{\eta v}{l_1}(t-t_0-\Delta t)\right)-\exp\left(-\dfrac{v}{l_2}(t-t_0-\Delta t)\right)\right) & ,t>t_0+\Delta t\end{cases} \quad (4\text{-}27)$$

$$\mathbf{T_3}=\begin{cases}\dfrac{N_t}{v} & ,t\le t_0\\ \dfrac{N_t}{v}+T_3|_{t=t_0}\exp\left(-\dfrac{v}{l_3}(t-t_0)\right)+\dfrac{l_2}{l_2-l_3}T_2|_{t=t_0} & \\ \left(\exp\left(-\dfrac{v}{l_2}(t-t_0)\right)-\exp\left(-\dfrac{v}{l_3}(t-t_0)\right)\right) & \\ -\dfrac{\lambda\left(N_b+\Delta N_b\right)-\eta v T_1|_{t=t_0}}{v}\dfrac{l_1}{\left(l_1-\eta l_2\right)\left(l_1-\eta l_3\right)\left(l_2-l_3\right)} & ,t_0<t\le t_0+\Delta t\\ \left(\begin{array}{l} l_1\left(l_2-l_3\right)\exp\left(-\dfrac{\eta v}{l_1}(t-t_0)\right)-l_2\left(l_1-\eta l_3\right)\exp\left(-\dfrac{v}{l_2}(t-t_0)\right)\\ +l_3\left(l_1-\eta l_2\right)\exp\left(-\dfrac{v}{l_3}(t-t_0)\right)\end{array}\right) & \\ \dfrac{N_t}{v}+T_3|_{t=t_0+\Delta t}\exp\left(-\dfrac{v}{l_3}(t-t_0-\Delta t)\right) & \\ +\dfrac{l_2}{l_2-l_3}T_2|_{t=t_0+\Delta t}\left(\exp\left(-\dfrac{v}{l_2}(t-t_0-\Delta t)\right)-\exp\left(-\dfrac{v}{l_3}(t-t_0-\Delta t)\right)\right) & \\ -\dfrac{\lambda N_b-\eta v T_1|_{t=t_0+\Delta t}}{v}\dfrac{l_1}{\left(l_1-\eta l_2\right)\left(l_1-\eta l_3\right)\left(l_2-l_3\right)} & ,t>t_0+\Delta t\\ \left(\begin{array}{l} l_1\left(l_2-l_3\right)\exp\left(-\dfrac{\eta v}{l_1}(t-t_0-\Delta t)\right)-l_2\left(l_1-\eta l_3\right)\exp\left(-\dfrac{v}{l_2}(t-t_0-\Delta t)\right)\\ +l_3\left(l_1-\eta l_2\right)\exp\left(-\dfrac{v}{l_3}(t-t_0-\Delta t)\right)\end{array}\right) & \end{cases} \tag{4-28}$$

Transforming the above equations into the dimensionless form, one obtains

$$\overline{\mathbf{T_1}}=\begin{cases}k+\dfrac{\lambda\overline{N_b}}{\eta} & ,\bar{t}\le\overline{t_0}\\ k+\dfrac{1}{\eta}\left(\begin{array}{l}\lambda\left(\overline{N_b}+\overline{\Delta N_b}\right)\\ -\left(\lambda\left(\overline{N_b}+\overline{\Delta N_b}\right)-\eta\overline{T_1|_{t=t_0}}\right)\exp\left(-\dfrac{\eta}{\bar{l}_1}(\bar{t}-\overline{t_0})\right)\end{array}\right) & ,\overline{t_0}<\bar{t}\le\overline{t_0+\Delta t}\\ k+\dfrac{1}{\eta}\left(\lambda\overline{N_b}-\left(\lambda\overline{N_b}-\eta\overline{T_1|_{t=t_0+\Delta t}}\right)\exp\left(-\dfrac{\eta}{\bar{l}_1}(\bar{t}-\overline{t_0}-\overline{\Delta t})\right)\right) & ,\bar{t}>\overline{t_0+\Delta t}\end{cases} \tag{4-29}$$

$$\overline{\mathbf{T_2}}=\begin{cases}1 & ,\bar{t}\le\bar{t}_0\\ 1+\overline{T_2\,|_{t=t_0}}\exp\left(-\frac{1}{\bar{l}_2}(\bar{t}-\bar{t}_0)\right)-\left(\lambda\left(\overline{N_b}+\overline{\Delta N_b}\right)-\eta\overline{T_1\,|_{t=t_0}}\right) & \\ \frac{\bar{l}_1}{\bar{l}_1-\eta\bar{l}_2}\left(\exp\left(-\frac{\eta}{\bar{l}_1}(\bar{t}-\bar{t}_0)\right)-\exp\left(-\frac{1}{\bar{l}_2}(\bar{t}-\bar{t}_0)\right)\right) & ,\bar{t}_0<\bar{t}\le\bar{t}_0+\overline{\Delta t}\\ 1+\overline{T_2\,|_{t=t_0+\Delta t}}\exp\left(-\frac{1}{\bar{l}_2}(\bar{t}-\bar{t}_0-\overline{\Delta t})\right)-\left(\lambda\overline{N_b}-\eta\overline{T_1\,|_{t=t_0+\Delta t}}\right) & \\ \frac{\bar{l}_1}{\bar{l}_1-\eta\bar{l}_2}\left(\exp\left(-\frac{\eta}{\bar{l}_1}(\bar{t}-\bar{t}_0-\overline{\Delta t})\right)-\exp\left(-\frac{1}{\bar{l}_2}(\bar{t}-\bar{t}_0-\overline{\Delta t})\right)\right) & ,\bar{t}>\bar{t}_0+\overline{\Delta t}\end{cases} \quad (4\text{-}30)$$

$$\overline{\mathbf{T_3}}=\begin{cases}1 & ,\bar{t}\le\bar{t}_0\\ 1+\overline{T_3\,|_{t=t_0}}\exp\left(-(\bar{t}-\bar{t}_0)\right)+\frac{\bar{l}_2}{\bar{l}_2-1}\overline{T_2\,|_{t=t_0}}\left(\exp\left(-\frac{1}{\bar{l}_2}(\bar{t}-\bar{t}_0)\right)-\exp\left(-(\bar{t}-\bar{t}_0)\right)\right) & \\ -\left(\lambda\left(\overline{N_b}+\overline{\Delta N_b}\right)-\eta\overline{T_1\,|_{t=t_0}}\right)\frac{\bar{l}_1}{\left(\bar{l}_1-\eta\bar{l}_2\right)\left(\bar{l}_1-\eta\right)\left(\bar{l}_2-1\right)} & ,\bar{t}_0<\bar{t}\le\bar{t}_0+\overline{\Delta t}\\ \begin{pmatrix}\bar{l}_1\left(\bar{l}_2-1\right)\exp\left(-\frac{\eta}{\bar{l}_1}(\bar{t}-\bar{t}_0)\right)\\ -\bar{l}_2\left(\bar{l}_1-\eta\right)\exp\left(-\frac{1}{\bar{l}_2}(\bar{t}-\bar{t}_0)\right)+\left(\bar{l}_1-\eta\bar{l}_2\right)\exp\left(-(\bar{t}-\bar{t}_0)\right)\end{pmatrix} & \\ 1+\overline{T_3\,|_{t=t_0+\Delta t}}\exp\left(-(\bar{t}-\bar{t}_0-\overline{\Delta t})\right)+\frac{\bar{l}_2}{\bar{l}_2-1}\overline{T_2\,|_{t=t_0+\Delta t}}\begin{pmatrix}\exp\left(-\frac{1}{\bar{l}_2}(\bar{t}-\bar{t}_0-\overline{\Delta t})\right)\\ -\exp\left(-(\bar{t}-\bar{t}_0-\overline{\Delta t})\right)\end{pmatrix} & \\ -\left(\lambda\overline{N_b}-\eta\overline{T_1\,|_{t=t_0+\Delta t}}\right)\frac{\bar{l}_1}{\left(\bar{l}_1-\eta\bar{l}_2\right)\left(\bar{l}_1-\eta\right)\left(\bar{l}_2-1\right)} & ,\bar{t}>\bar{t}_0+\overline{\Delta t}\\ \begin{pmatrix}\bar{l}_1\left(\bar{l}_2-1\right)\exp\left(-\frac{\eta}{\bar{l}_1}(\bar{t}-\bar{t}_0-\overline{\Delta t})\right)-\bar{l}_2\left(\bar{l}_1-\eta\right)\exp\left(-\frac{1}{\bar{l}_2}(\bar{t}-\bar{t}_0-\overline{\Delta t})\right)\\ +\left(\bar{l}_1-\eta\bar{l}_2\right)\exp\left(-(\bar{t}-\bar{t}_0-\overline{\Delta t})\right)\end{pmatrix} & \end{cases} \quad (4\text{-}31)$$

where $\bar{t}=\frac{vt}{l_3}$, $\overline{\Delta t}=\frac{v\Delta t}{l_3}$, $\bar{t}_0=\frac{vt_0}{l_3}$, $\bar{l}_1=\frac{l_1}{l_3}$, $\bar{l}_2=\frac{l_2}{l_3}$, $\overline{T_1}=\frac{vT_1}{N_t}$, $\overline{T_2}=\frac{vT_2}{N_t}$, $\overline{T_3}=\frac{vT_3}{N_t}$, $\overline{N_b}=\frac{N_b}{N_t}$

4.1.3.3 Sinusoidal function variation

In this example, the twisting rate of the false-twister is given by the expression $N_b+\Delta N_b \sin \omega t$, where $\omega=2\pi f$ in the usual way.

False Twist in Zone OA

The turns gained by the moving belt in a time increment *dt* are $\lambda(N_b+\Delta N_b \sin \omega t)dt$, the turns lost through the false-twister are $\eta T_1 v dt$, and the net twists gained are $dT_1=\dfrac{\lambda(N_b+\Delta N_b \sin \omega t)-\eta T_1 v}{l_1}dt$, integration of which together with the initial condition $t=0$, $T_1=\dfrac{\lambda N_b}{\eta v}$, gives

$$T_1=\frac{\lambda N_b}{\eta v}+\frac{\lambda \Delta N_b}{l_1}\left(A\left(\exp\left(-\frac{\eta v}{l_1}t\right)-\cos(\omega t)\right)+B\sin(\omega t)\right) \tag{4- 32}$$

where $A=\dfrac{\omega}{\left(\dfrac{\eta v}{l_1}\right)^2+\omega^2}$, $B=\dfrac{\dfrac{\eta v}{l_1}}{\left(\dfrac{\eta v}{l_1}\right)^2+\omega^2}$

False Twist in Zone AB

The turns passing through the false-twister from Zone OA are $\eta T_1 v dt$, the negative turns inserted by the moving belt are $-\lambda(N_b+\Delta N_b \sin \omega t)dt$, and the turns passing through the traveler are $T_2 v dt$, so the net twists gained are $dT_2=\dfrac{\eta T_1 v-\lambda(N_b+\Delta N_b \sin \omega t)-T_2 v}{l_2}dt$, integration of which and rearranging, together with the initial condition $t_2=0$, $T_2=0$, gives

$$T_2=\frac{\lambda\eta A\Delta N_b}{l_1-\eta l_2}\left(\exp(-\frac{\eta v}{l_1}t)-\exp(-\frac{v}{l_2}t)\right)-\frac{\lambda\eta v A\Delta N_b}{l_1 l_2}\left(C\left(\cos(\omega t)-\exp\left(-\frac{v}{l_2}t\right)\right)+D\sin(\omega t)\right)$$
$$+\frac{(\eta v B-l_1)\lambda\Delta N_b}{l_1 l_2}\left(D\left(\exp\left(-\frac{v}{l_2}t\right)-\cos(\omega t)\right)+C\sin(\omega t)\right) \tag{4- 33}$$

where $C=\dfrac{\dfrac{v}{l_2}}{\left(\dfrac{v}{l_2}\right)^2+\omega^2}$, $D=\dfrac{\omega}{\left(\dfrac{v}{l_2}\right)^2+\omega^2}$

False Twist in Zone BC

The turns passing through the traveler from Zone AB be $T_2 v dt$, the turns wound onto the bobbin be $T_3 v dt$, so the net twists gained be $dT_3 = \frac{T_2 v - T_3 v}{l_3} dt$, integration of which and rearranging, together with the initial condition $t = 0$, $T_3 = 0$, gives

$$\begin{aligned} T_3 = & \frac{\lambda \eta A l_1 \Delta N_b}{(l_1 - \eta l_2)(l_1 - \eta l_3)} \left(\exp\left(-\frac{\eta v}{l_1} t \right) - \exp\left(-\frac{v}{l_3} t \right) \right) \\ & - \frac{\lambda \eta A l_2 \Delta N_b}{(l_1 - \eta l_2)(l_2 - l_3)} \left(\exp\left(-\frac{v}{l_2} t \right) - \exp\left(-\frac{v}{l_3} t \right) \right) \\ & - \frac{\lambda \eta v^2 A \Delta N_b}{l_1 l_2 l_3} \begin{pmatrix} (CE - DF)\left(\cos(\omega t) - \exp\left(-\frac{v}{l_3} t \right) \right) \\ + (CF + DE)\sin(\omega t) - \frac{C l_2 l_3}{v(l_2 - l_3)} \left(\exp\left(-\frac{v}{l_2} t \right) - \exp\left(-\frac{v}{l_3} t \right) \right) \end{pmatrix} \\ & + \frac{(\eta v B - l_1)\lambda v \Delta N_b}{l_1 l_2 l_3} \begin{pmatrix} -(CF + DE)\left(\cos(\omega t) - \exp\left(-\frac{v}{l_3} t \right) \right) \\ + (CE - DF)\sin(\omega t) + \frac{D l_2 l_3}{v(l_2 - l_3)} \left(\exp\left(-\frac{v}{l_2} t \right) - \exp\left(-\frac{v}{l_3} t \right) \right) \end{pmatrix} \end{aligned} \tag{4- 34}$$

where $E = \dfrac{\dfrac{v}{l_3}}{\left(\dfrac{v}{l_3}\right)^2 + \omega^2}$, $F = \dfrac{\omega}{\left(\dfrac{v}{l_3}\right)^2 + \omega^2}$

Therefore, yarn total twists in each zone can be expressed by the

$$\mathbf{T_1} = \frac{k N_t}{v} + \frac{\lambda N_b}{\eta v} + \frac{\lambda \Delta N_b}{l_1} \left(A\left(\exp\left(-\frac{\eta v}{l_1} t \right) - \cos(\omega t) \right) + B \sin(\omega t) \right) \tag{4- 35}$$

$$\begin{aligned} \mathbf{T_2} = & \frac{N_t}{v} + \frac{\lambda \eta A \Delta N_b}{l_1 - \eta l_2} \left(\exp(-\frac{\eta v}{l_1} t) - \exp(-\frac{v}{l_2} t) \right) \\ & - \frac{\lambda \eta v A \Delta N_b}{l_1 l_2} \left(C\left(\cos(\omega t) - \exp\left(-\frac{v}{l_2} t \right) \right) + D \sin(\omega t) \right) \\ & + \frac{(\eta v B - l_1)\lambda \Delta N_b}{l_1 l_2} \left(D\left(\exp\left(-\frac{v}{l_2} t \right) - \cos(\omega t) \right) + C \sin(\omega t) \right) \end{aligned} \tag{4- 36}$$

$$\begin{aligned}\mathbf{T_3} &= \frac{N_t}{v} + \frac{\lambda\eta A l_1 \Delta N_b}{(l_1-\eta l_2)(l_1-\eta l_3)}\left(\exp\left(-\frac{\eta v}{l_1}t\right)-\exp\left(-\frac{v}{l_3}t\right)\right)\\ &-\frac{\lambda\eta A l_2 \Delta N_b}{(l_1-\eta l_2)(l_2-l_3)}\left(\exp\left(-\frac{v}{l_2}t\right)-\exp\left(-\frac{v}{l_3}t\right)\right)\\ &-\frac{\lambda\eta v^2 A \Delta N_b}{l_1 l_2 l_3}\left(\begin{array}{l}(CE-DF)\left(\cos(\omega t)-\exp\left(-\frac{v}{l_3}t\right)\right)\\ +(CF+DE)\sin(\omega t)-\frac{C l_2 l_3}{v(l_2-l_3)}\left(\exp\left(-\frac{v}{l_2}t\right)-\exp\left(-\frac{v}{l_3}t\right)\right)\end{array}\right)\\ &+\frac{(\eta v B-l_1)\lambda v \Delta N_b}{l_1 l_2 l_3}\left(\begin{array}{l}-(CF+DE)\left(\cos(\omega t)-\exp\left(-\frac{v}{l_3}t\right)\right)\\ +(CE-DF)\sin(\omega t)+\frac{D l_2 l_3}{v(l_2-l_3)}\left(\exp\left(-\frac{v}{l_2}t\right)-\exp\left(-\frac{v}{l_3}t\right)\right)\end{array}\right)\end{aligned} \tag{4-37}$$

Transforming the above equations into the dimensionless form, one obtains

$$\overline{\mathbf{T_1}} = k + \frac{\lambda\overline{N_b}}{\eta} + \frac{\lambda\overline{\Delta N_b}}{\overline{l_1}}\left(\overline{A}\left(\exp\left(-\frac{\eta}{\overline{l_1}}\bar{t}\right)-\cos\left(\overline{\omega t}\right)\right)+\overline{B}\sin\left(\overline{\omega t}\right)\right) \tag{4-38}$$

$$\begin{aligned}\overline{\mathbf{T_2}} &= 1+\frac{\lambda\eta\overline{A\Delta N_b}}{\overline{l_1}-\eta\overline{l_2}}\left(\exp(-\frac{\eta}{\overline{l_1}}\bar{t})-\exp(-\frac{1}{\overline{l_2}}\bar{t})\right)\\ &-\frac{\lambda\eta\overline{A\Delta N_b}}{\overline{l_1}\overline{l_2}}\left(\overline{C}\left(\cos(\overline{\omega t})-\exp\left(-\frac{1}{\overline{l_2}}\bar{t}\right)\right)+\overline{D}\sin(\overline{\omega t})\right)\\ &+\frac{(\eta\overline{B}-\overline{l_1})\lambda\overline{\Delta N_b}}{\overline{l_1}\overline{l_2}}\left(\overline{D}\left(\exp\left(-\frac{1}{\overline{l_2}}\bar{t}\right)-\cos(\overline{\omega t})\right)+\overline{C}\sin(\overline{\omega t})\right)\end{aligned} \tag{5-39}$$

$$\begin{aligned}\overline{\mathbf{T_3}} &= 1+\frac{\lambda\eta\overline{A l_1\Delta N_b}}{(\overline{l_1}-\eta\overline{l_2})(\overline{l_1}-\eta)}\left(\exp\left(-\frac{\eta}{\overline{l_1}}\bar{t}\right)-\exp\left(-\bar{t}\right)\right)\\ &-\frac{\lambda\eta\overline{A l_2\Delta N_b}}{(\overline{l_1}-\eta\overline{l_2})(\overline{l_2}-1)}\left(\exp\left(-\frac{1}{\overline{l_2}}\bar{t}\right)-\exp\left(-\bar{t}\right)\right)\\ &-\frac{\lambda\eta\overline{A\Delta N_b}}{\overline{l_1}\overline{l_2}}\left(\begin{array}{l}(\overline{CE}-\overline{DF})\left(\cos(\overline{\omega t})-\exp\left(-\bar{t}\right)\right)\\ +(\overline{CF}+\overline{DE})\sin(\overline{\omega t})-\frac{\overline{Cl_2}}{\overline{l_2}-1}\left(\exp\left(-\frac{1}{\overline{l_2}}\bar{t}\right)-\exp\left(-\bar{t}\right)\right)\end{array}\right)\\ &+\frac{(\eta\overline{B}-\overline{l_1})\lambda\overline{\Delta N_b}}{\overline{l_1}\overline{l_2}}\left(\begin{array}{l}-(\overline{CF}+\overline{DE})\left(\cos(\overline{\omega t})-\exp\left(-\bar{t}\right)\right)\\ +(\overline{CE}-\overline{DF})\sin(\overline{\omega t})+\frac{\overline{Dl_2}}{\overline{l_2}-1}\left(\exp\left(-\frac{1}{\overline{l_2}}\bar{t}\right)-\exp\left(-\bar{t}\right)\right)\end{array}\right)\end{aligned} \tag{4-40}$$

where $\bar{t}=\frac{vt}{l_3}$, $\overline{l_1}=\frac{l_1}{l_3}$, $\overline{l_2}=\frac{l_2}{l_3}$, $\overline{T_1}=\frac{vT_1}{N_t}$, $\overline{T_2}=\frac{vT_2}{N_t}$, $\overline{T_3}=\frac{vT_3}{N_t}$, $\overline{\Delta N_b}=\frac{\Delta N_b}{N_t}$, $\overline{\omega}=\frac{\omega l_3}{v}$

$\overline{A}=\frac{vA}{l_3}$, $\overline{B}=\frac{vB}{l_3}$, $\overline{C}=\frac{vC}{l_3}$, $\overline{D}=\frac{vD}{l_3}$, $\overline{E}=\frac{vE}{l_3}$, $\overline{F}=\frac{vF}{l_3}$, $\overline{f}=\frac{fl_3}{v}$

4.2 Experimental Setup

The experiments were conducted on a ring spinning frame (Zinser 351) by installing a Polyurethane belt with diameter of 3 mm between the front rollers and the yarn guide. The belt was driven by a 0.75 kw AC motor (NERI MOTORI) and the belt speed was controlled by a 220V single-phase inverter (Shanghai JINQV Automation Ltd., Co.; Model:VFD-V-2S0007B). The online control of the instant belt moving speed was accomplished by the embedded PLC module. In order to monitor the instant belt speed, a Hall speed sensor (SHANG HAI CE ZHEN AUTOMATION INSTRUMENT Co., LTD; Model:Y62) was adopted to measure the gear with 50 teeth attached to a belt pulley. For this study, yarn twist in both high twist zone and final state were measured and compared with theoretical predictions. In order to measure the instant twist in high twist zone, a black and unstained combed roving (count 332 g/km, measured CV of 4.32%, and fiber specifications: fiber length 1.475 inch, fiber strength 32.5 g/tex, uniformity ratio 54.53%, elongation 6.53% and micronaire value 4.35) were fed without gap into the back rollers of the ring spinning machine to produce yarn with linear density of 18.45 g/km (Ne 32) and diameter of 0.164 mm for measurement. High-speed photography was applied for continual and automatic image acquisition, storage and analysis of yarn instant twist including a high-speed camera (Phantom MIRO 4, CMOS sensor, 800 x 600 pixels, over 1200 fps at full resolution, 22 μm pixel size, 12-bit depth), which was connected to a personal computer installed with camera control software and Nikon micro lens (AF Micro-Nikkor 60 mm f/2.8D). The belt speed and the yarn twist in OA zone were collected synchronously for model verification, The final yarn twist was measured by untwist-retwist method (ASTM D1422-99). In addition, the yarn properties such as tenacity, evenness, diameter and hairiness were tested and compared with control yarns.

4.2.1 Measurement of Belt Speed

Before online measurement of belt speed, the Hall speed sensor must be calibrated. The output signal corresponding to the rotating speed is analogy current ranging from 4-20 mA. After calculation, the relationship between output current and belt speed ratio was found. In the calibration process, six speed ratios were tested and the results are shown in Figure 4-3. The measuring value covers all the operational

range in the experiment and the results can be expressed by the linear regression formula as

$$Y=2.401X+4.089 \quad (4\text{-}41)$$

The correlation coefficient is 0.999.

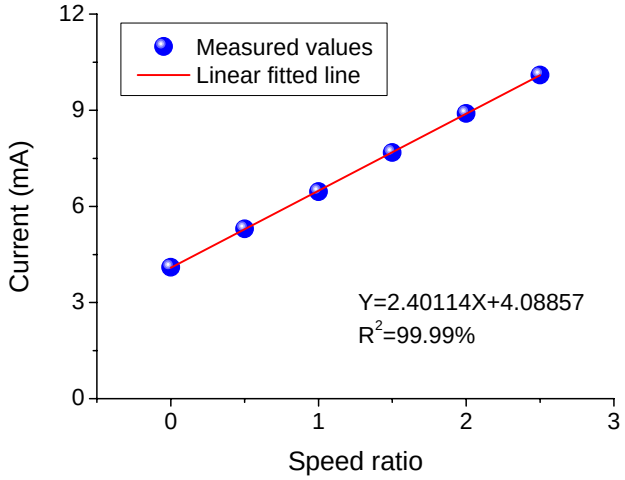

Figure 4-3 Calibration of the speed sensor

4.3 Results and Discussions

4.3.1Verification of Model

The kinetic model should be verified before further investigation. As shown in Table 4-1, the divided zone lengths for OA, AB and BC were set at 73, 327, and 20 mm, respectively. The wrap angle of the belt and yarn was fixed at 50°, and the twist factor for the yarn Ne 32 was 3.2, and the yarn delivery speed was 0.235 m/s. The traveler weight for the yarn was 35 mg and the frictional coefficient of the yarn and moving belt was 0.81 measured. The belt twisting efficiency, propagation coefficients of twist trapping and congestion were 0.11, 0.88 and 0.90, respectively.

Table 4-1 System parameters

l_1 (mm)	l_2 (mm)	l_3 (mm)	φ (°)	v (m/s)	α_e	m_w (mg)	μ	λ	k	η
73	327	20	50	0.235	3.5	35	0.81	0.11	0.88	0.90

According to our online twist measurement based on the high-speed photography, the twist variation for the conventional yarn in the spinning zone is 15-20% due to roving unevenness, error of the twist measurement, uneven distributions of yarn twist, etc. Therefore, in order to measure the yarn twist in OA zone, variation of the false twist should be chosen at a high level, which could suppress the noise caused by the aforementioned factors. In this study, we set speed ratio $v_b / v = 1.5$, amplitude of 1.5 with three frequency levels of 0.5 Hz, 0.2 Hz, and 0.1 Hz and then compare the experimental results with the theoretical model. For yarn properties evaluation, such large twist variation is not likely the case and of less practical interests, thus the following values were used for measuring the yarn properties and final yarn twists: speed ratio of 1.5, amplitude of 0.15, and frequency level of 0.5 Hz. The control yarn without belt speed variation was produced as a benchmark for comparison.

As shown in Figure 4-4, three cases of sinusoidal variation of the false twist with different frequencies were implemented, and the corresponding twist redistributions in OA zone were examined and compared with theoretical calculations. It can be found that the predicted curves generally follow a similar trend to the experimental data, despite some deviations are found with CV about 10% to 15%, implying that simulated yarn twist in OA zone matches well with actual data.

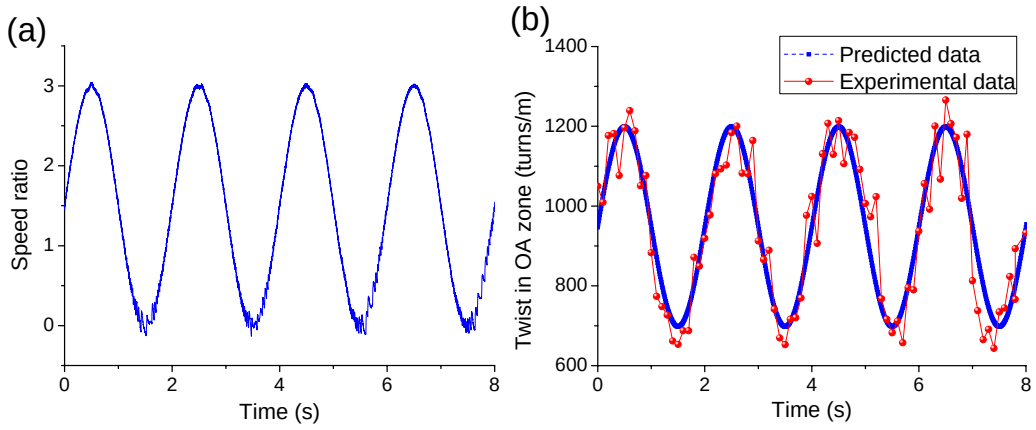

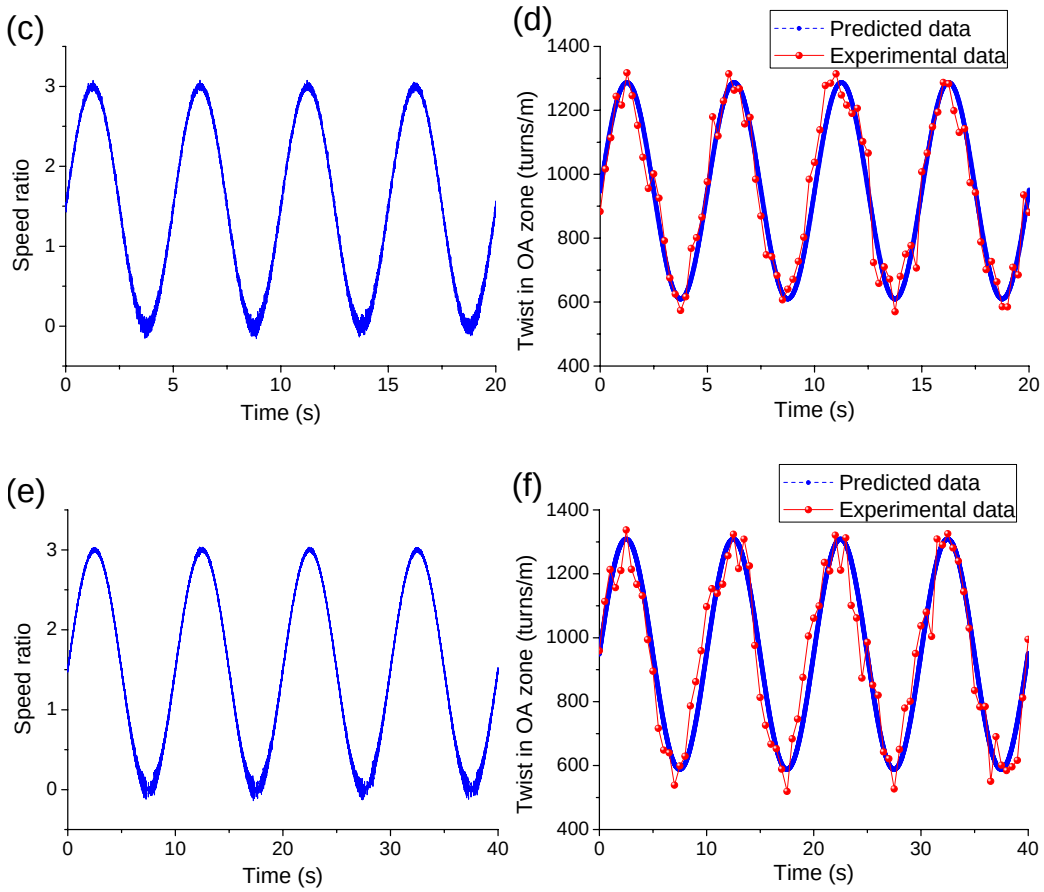

Figure 4-4 Sinusoidal variation of the false twist and comparison of experimental data against predicted data in OA zone

(a) Speed ratio changes periodically from 0 to 3 with period 2s; (b) The corresponding twist change in OA zone; (c) Speed ratio changes periodically from 0 to 3 with period 5s; (d) The corresponding twist change in OA zone; (e) Speed ratio changes periodically from 0 to 3 with period 10s; (f) The corresponding twist change in OA zone.

4.3.2 Yarn Properties and Final Twist

The properties of modified yarns with and without belt speed variations as well as conventional yarns are presented in Table 4-2. Four yarns with period 5 seconds and periodic variation of the belt speed of 10%, 20%, 30% and 40% were produced to study the effect of variation of false twist on yarn performances. Within 30% periodic variation of false twist, the yarn properties were not significantly affected. When the variation increased to 40%, the mean tenacity and minimum tenacity of the sample were decreased by 0.39, and 0.65 cN/Tex, respectively, and the neps of SB-40% were also increased by 10.08%. The final twist of the resultant yarns were also not significantly affected by the variation of false twist.

Table 4-2 Measured properties of conventional yarns and yarns with and without belt speed variations

Yarn code	Tenacity (cN/Tex) [cv%]	Mini. Tenacity	Evenness CVm% [cv%]	Neps (+140%) [cv%]	Twist (tpm)	Hairiness (S3) [cv%]
Conv TF3.6	17.59 [7.50]	14.23	12.71 [1.23]	224 [14.75]	892 [8.38]	1321 [27.76]
Conv TF3.2	16.16 [5.80]	13.10	12.93 [1.11]	215 [17.84]	793 [7.37]	1611 [26.76]
SB-TF3.2	16.90 [7.52]	14.28	12.82 [2.84]	248 [6.15]	789 [8.32]	846 [3.93]
SB-10%	16.89 [6.76]	14.45	12.82 [0.95]	245 [9.91]	782 [8.30]	758 [0.37]
SB-20%	16.90 [5.81]	14.71	12.85 [0.79]	248 [16.32]	790 [9.23]	794 [7.66]
SB-30%	16.75 [5.22]	14.13	12.86 [0.72]	250 [5.29]	786 [9.20]	845 [1.67]
SB-40%	16.51 [7.65]	13.63	12.74 [0.67]	273 [9.29]	792 [8.10]	793 [4.82]

4.4 Simulations

The dimensionless model shows that lengths of divided zone path, false twist, belt properties and so on influence on the twist redistribution. In order to fully evaluate the twist variation, a series of numerical simulations are carried out in this section. Among the twist distribution in three zones, yarn twists in zone OA and BC are of particular interests since they have large influence on yarn structure and properties. Maximum variation ($\overline{\Delta T_1} = \overline{\mathbf{T_1}}|_{\max} - \overline{\mathbf{T_1}}|_{\min}$, $\overline{\Delta T_3} = \overline{\mathbf{T_3}}|_{\max} - \overline{\mathbf{T_3}}|_{\min}$), and affected length $\overline{B_{T1}}$, $\overline{B_{T3}}$ (the corresponding length for $\overline{\mathbf{T_1}}$ and $\overline{\mathbf{T_3}}$ to reach 99% balancing value) are proposed to quantitatively investigate the twist variation in zone OA and BC.

4.4.1 Step Function Variation

Twist redistributions in three zones

The parameters used for simulation below are $\overline{N_b}=5$, λ=0.2, η=0.7, k=0.6, $\overline{l_1}=3.75$, $\overline{l_2}=20-\overline{l_1}$, unless otherwise stated. Figure 4-5 shows the results of twist redistribution in three zones under the condition of $\overline{\Delta N_b}=-0.2\overline{N_b}$. A sudden drop of false twist in the beginning makes twists in zone OA decrease dramatically in the first few seconds until reach a new balance value at 1.74. In the downstream of the false-twister, yarn twists in zone AB and BC go up because of the decreased negative false-twist, arriving at the maximum value of about 1.04, and then go down smoothly to the steady-state values.

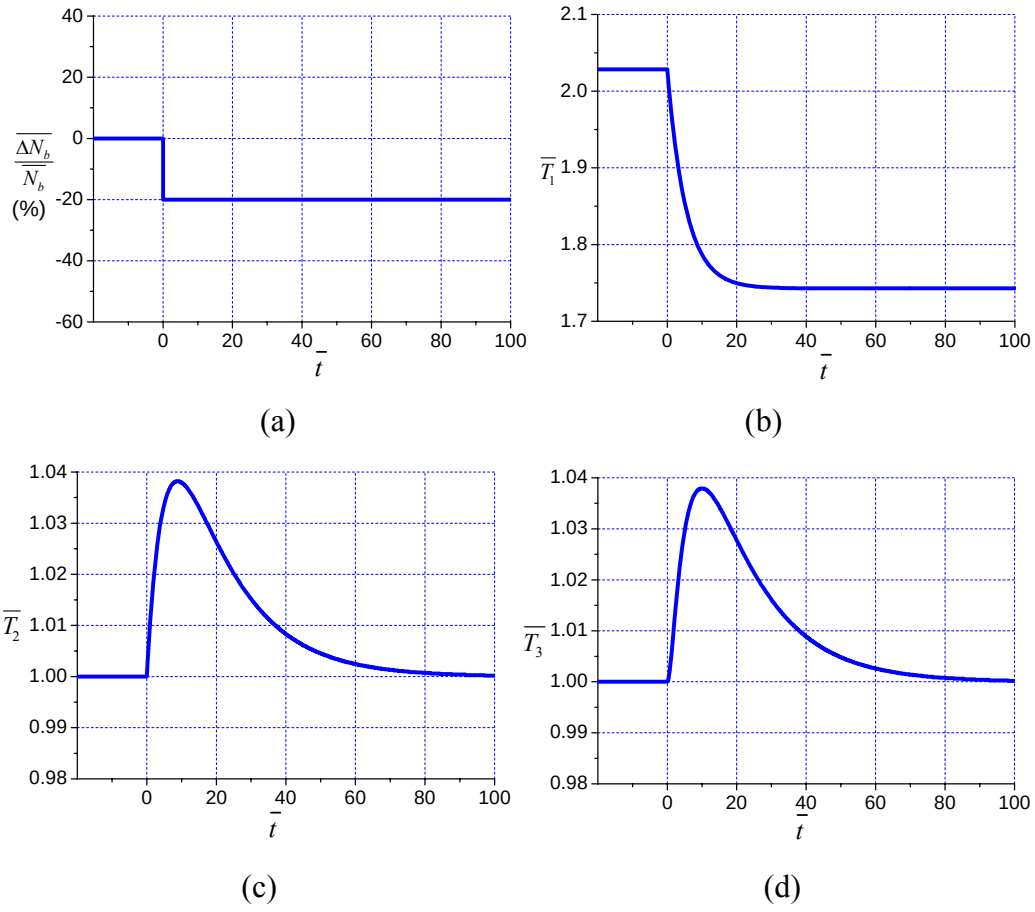

Figure 4-5 Twist variations in the three zones after a step change in false twist

Effects of system parameters on $\overline{\Delta T_1}$ *and* $\overline{B_{T1}}$

Figure 4-6 shows effects of system parameters on twist variation of $\overline{T_1}$ and affected length $\overline{B_{T1}}$. It is important to observe that, the variation size of false twist

plays a key role that affects the twist variation in zone OA. A larger variation of false twist results in a greater twist change in zone OA as expected and the relationship is linear. Besides, belt properties amplify or diminish the function of $\overline{\Delta N_b}$ at some extent. For instance, when the false-twisting efficiency increases from 0.1 to 0.3, together with coefficients of belt twist congestion and trapping decrease from 0.8 to 0.4 and 0.6, respectively, $\overline{\Delta T_1}$ enlarges from 0.13 to 0.50 at $\overline{\Delta N_b}$ / $\overline{N_b}$ of 0.2. It is also noted that twist variation in zone OA is independent on belt position, which is, however, the most important parameter determining $\overline{B_{T1}}$. With the increasing length of zone OA, $\overline{B_{T1}}$ is also proportionally increased. Moreover, $\overline{B_{T1}}$ is also affected by belt properties to some extent while the variation size of false twist has a much smaller influence on $\overline{B_{T1}}$.

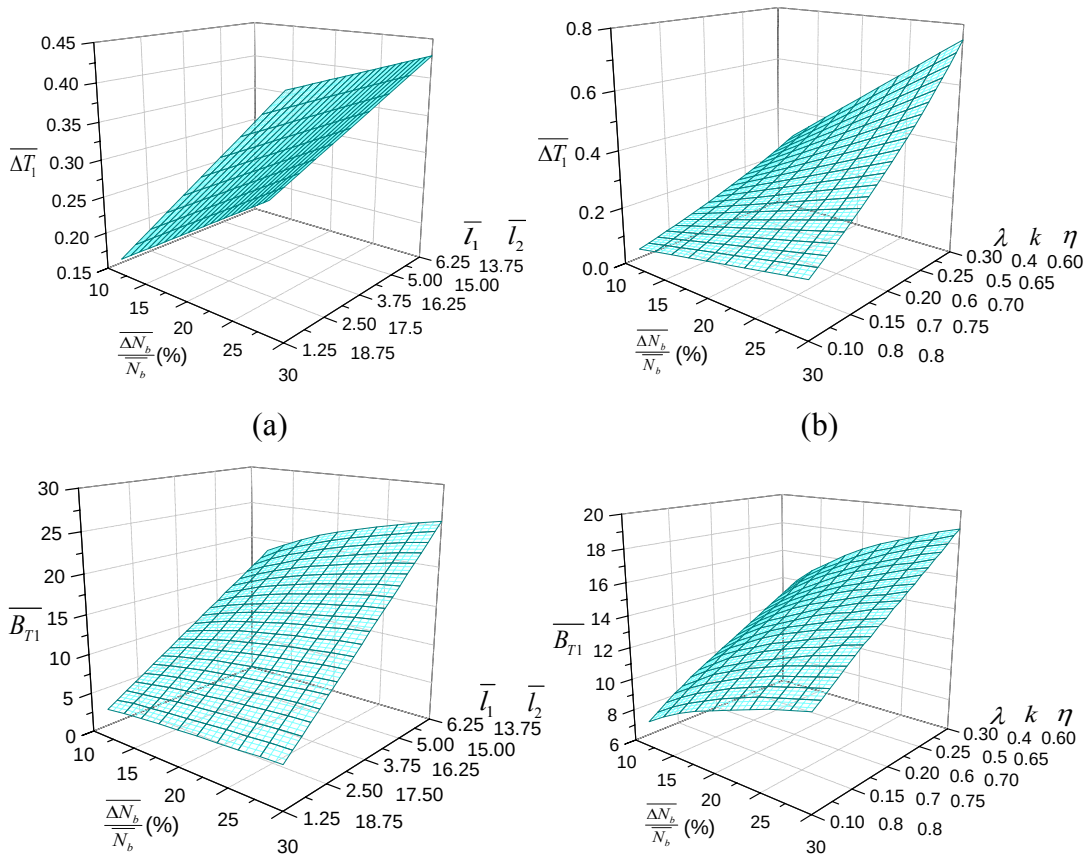

Figure 4-6 Effects of system parameters on $\overline{\Delta T_1}$ and $\overline{B_{T1}}$

Effects of system parameters on $\overline{\Delta T_3}$ *and* $\overline{B_{T3}}$

Figure 4-7 displays effects of system parameters on twist variation of $\overline{\mathbf{T}_3}$ and $\overline{B_{T3}}$. It is obvious that twist variation in zone BC is much smaller than twist variation in zone OA for a machine of the given dimensions; however it takes longer time for twist to reach steady-state. Generally, the value of $\overline{\Delta T_3}$ is greatly affected by belt installation position and belt properties, as shown in figure 4-7 a and b. Longer length of zone OA, higher value of belt twisting efficiency, lower values of coefficient of belt congestion and trapping lead to a larger twist variation and larger affected length in zone BC.

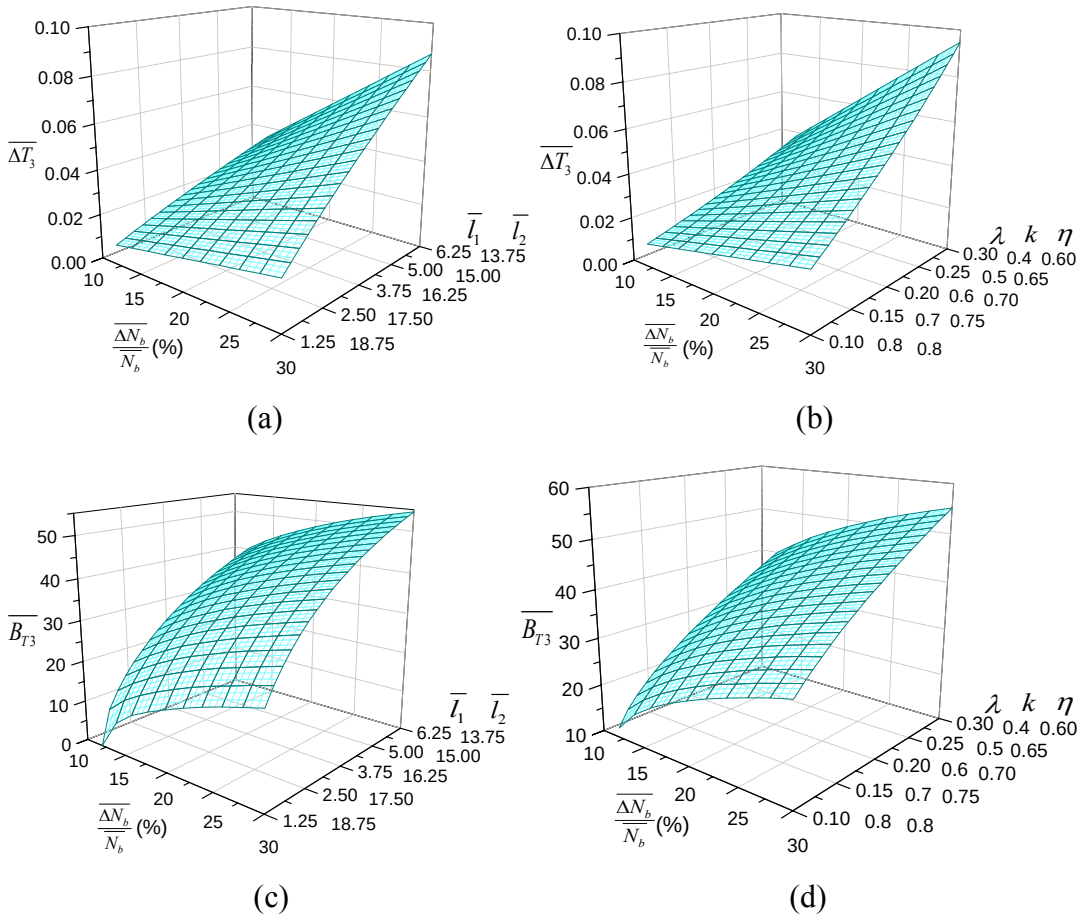

Figure 4-7 Effects of system parameters on $\overline{\Delta T_3}$ and $\overline{B_{T3}}$

4.4.2 Rectangular Function Variation

Twist redistributions in three zones

The rectangular transient change in false twist causes twist variation in three zones. Figure 4-8 shows the results of twist redistribution in three zones under the

condition of $\overline{\Delta N_b} = -0.2\overline{N_b}$, $\overline{\Delta t}$=15. A sudden drop of false twist in the beginning makes twists in zone OA decrease dramatically, and at the end of rectangular function, a sudden increase of false twist cause twists in zone OA returning back to its steady-state values. In the downstream of the false-twister, much more complicated twist changes are found in zone AB and BC. As can be seen in Figure 4-8 c and d, in the first few seconds of the sudden change of false twist, yarn twists in zone AB and BC go up because of the decreased negative false-twist, arriving at the maximum value of about 1.04, and then go down smoothly until a sudden change of false twist at the end of rectangular function. Accordingly, twist levels of $\overline{\mathbf{T}_2}$ and $\overline{\mathbf{T}_3}$ drop sharply, reaching the minimum value of about 0.98, and then go back to the steady-state gradually.

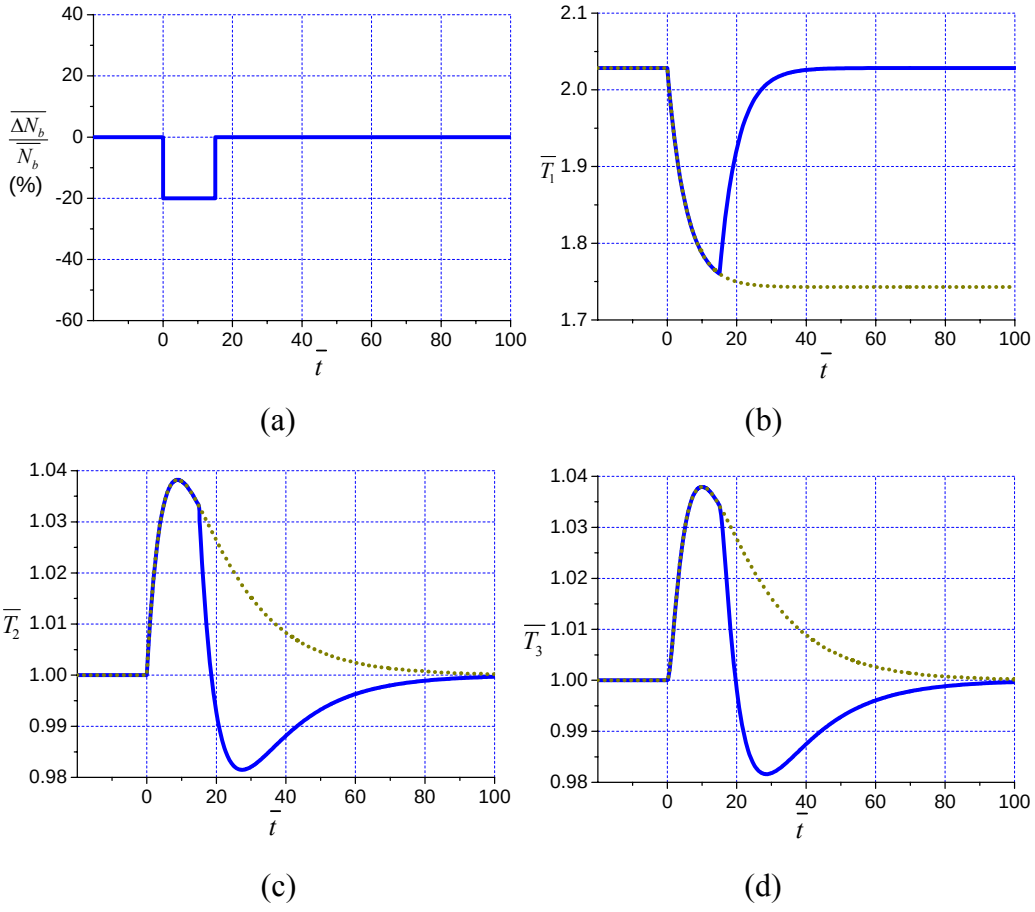

Figure 4-8 Twist changes in the three zones after a small rectangular change in false twist of duration $\overline{\Delta t}$

Effects of system parameters on $\overline{\Delta T_1}$ *and* $\overline{B_{T1}}$

Figure 4-9 describes effects of pulse time, false-twister position, and belt properties on the twist variation and affected length in zone OA. The value of $\overline{\Delta T_1}$ goes up with the increasing of the pulse time, the belt twisting efficiency and the decreasing of the length OA, coefficient of belt twist blockage. It can be clearly seen that belt properties have large influence on maximum variation of $\overline{\mathbf{T}_1}$. Under the belt twisting efficiency of 0.3, coefficient of belt twist trapping and congestion of 0.4 and 0.6, $\overline{\Delta T_1}$ reaches as high as 0.285. Besides, it can be concluded from Figure 4-26c and d that the length of zone OA has the largest impact on $\overline{B_{T1}}$, and the relationship is almost linear. For instance, as the $\overline{l_1}$ raises from 1.25 to 6.25, the value of $\overline{B_{T1}}$ is more than doubled.

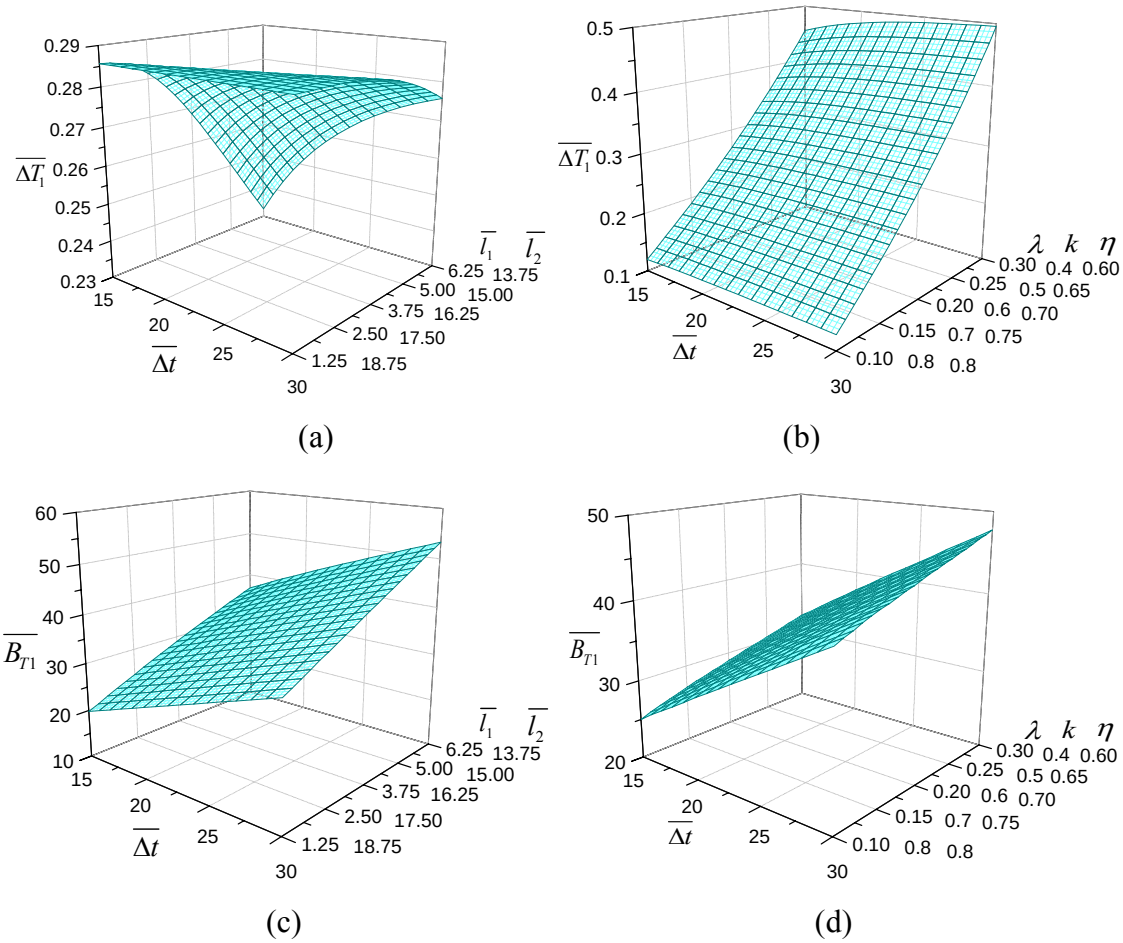

Figure 4-9 Effects of system parameters on $\overline{\Delta T_1}$ and $\overline{B_{T1}}$

Effects of system parameters on $\overline{\Delta T_3}$ *and* $\overline{B_{T3}}$

Figure 4-10 displays effects of pulse time, false-twister position, and belt

properties on the twist variation and affected length in zone BC. It is noted in Figure 4-10 a and b that the value of $\overline{\Delta T_3}$ is smaller than that of $\overline{\Delta T_1}$ at the same system parameters, which means the rectangular change in false twist has a less influence on the final yarn twist. However, the affected length is much longer compared with the length of $\overline{\mathbf{T}_1}$, as shown in Figure 4-10 c and d. Lower values of $\overline{\Delta t}$, λ and higher values of k, η result in smaller variation and shorter affected length, while lower value of $\overline{l_1}$ leads to smaller twist variation but longer affected length.

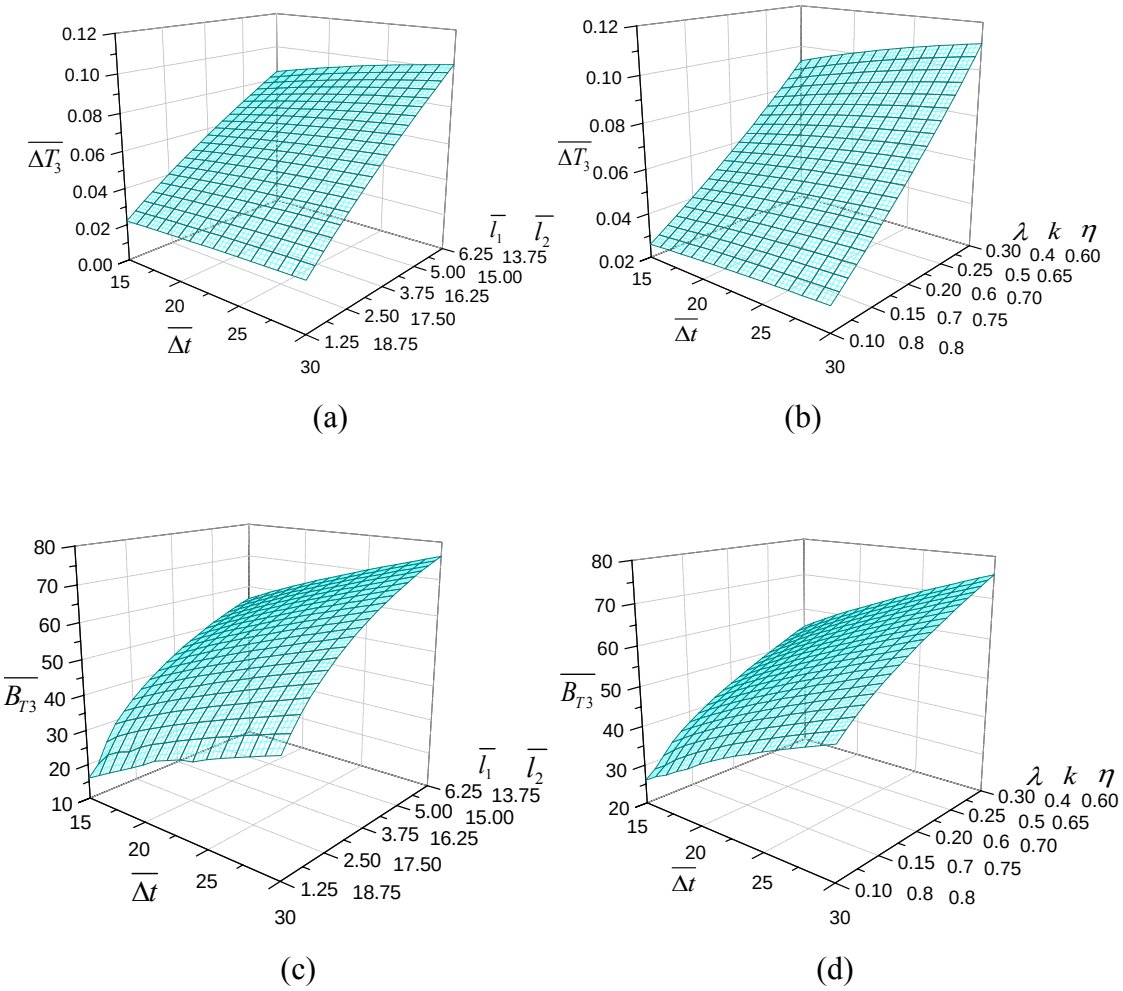

Figure 4-10 Effects of system parameters on $\overline{\Delta T_3}$ and $\overline{B_{T3}}$

For false-twister with a misalignment joint or a high bending rigidity joint, when the joint moves around the corner, it will cause a rectangular change in false twist. Moreover, the yarn imperfections, such as thick places and thin places, which changes

yarn diameter with a typical fiber length, also cause rectangular change in false twist in yarn formation process. In case of a misalignment joint running around the corner, the values of $\overline{\Delta T_1}$ and $\overline{\Delta T_3}$ are 0.403 and 0.055 at the condition $\overline{\Delta t}=10$, $\overline{\Delta N_b}=-0.3\overline{N_b}$, $\overline{l_1}$ of 2.5, and λ of 0.2. The values of $\overline{B_{T1}}$ and $\overline{B_{T3}}$ are 20.7 and 31.8, respectively. Therefore, the rectangular change in false twist caused by misalignment joint has large influence on twist variation and yarn affected length.

4.4.3 Sinusoidal Function Variation

Twist redistributions in three zones

Figure 4-11 illustrates the effect of the oscillation frequency of the false twist on the amplitude of the resulting twist oscillation in the three zones at $\overline{f}=0.15$. As might be predicted that, yarn twist in three zones varies periodically with the oscillation frequency of the false twist, but the phase angle and amplitude differ. The amplitude of $\overline{\mathbf{T_1}}$ can be nearly quarter that of the original twist oscillation, and the amplitude downstream the false-twister further attenuated as the yarn passes from one zone to the next. This is because the dwell time of the yarn in these zones is greater than the oscillation period.

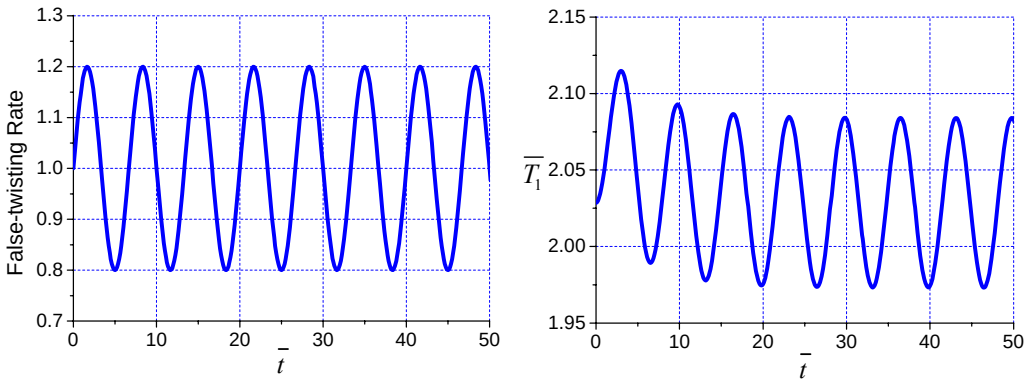

(a) (b)

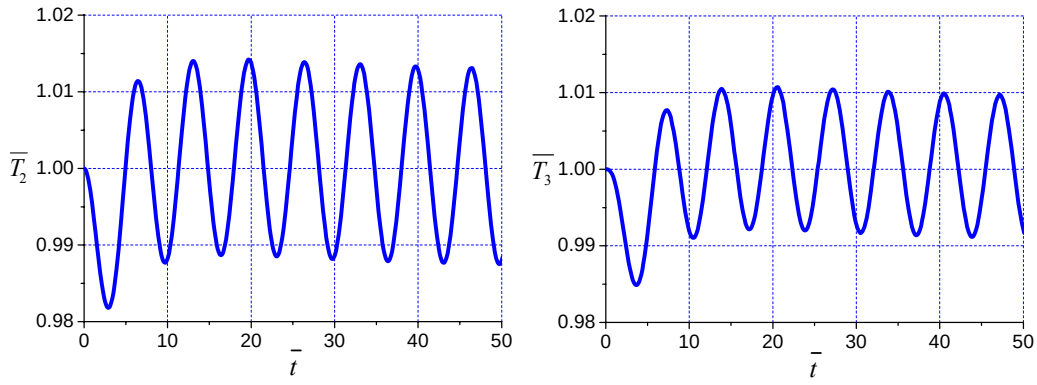

(c) (d)

Figure 4-11 Twist changes in three zones by sinusoidal variation in false twist

Effect of system parameters on amplitude of $\overline{\mathbf{T}}_1$ *and* $\overline{\mathbf{T}}_3$

Figure 4-12 shows effects of oscillation frequency, false-twister position, and belt properties on the amplitudes of the twist in zone OA and BC. As the frequency increases, the twist oscillation becomes more and more damped. It can be seen from Figure 4-12 a and c that at a higher $\overline{f}$ value of 0.25 and $\overline{l}_1$ of 3.75, the amplitudes of $\overline{\mathbf{T}}_1$ and $\overline{\mathbf{T}}_3$ are only 0.033 and 0.004, respectively. Besides, false-twister position has a certain influence on twist variation in zone OA. As the $\overline{l}_1$ increases, the amplitude of $\overline{\mathbf{T}}_1$ decreases, while the amplitude of $\overline{\mathbf{T}}_3$ raise sharply at low frequency rate and stably at high frequency rate. Nevertheless, the belt properties also affect twist changes in three zones; however the effect is small in high frequency rate.

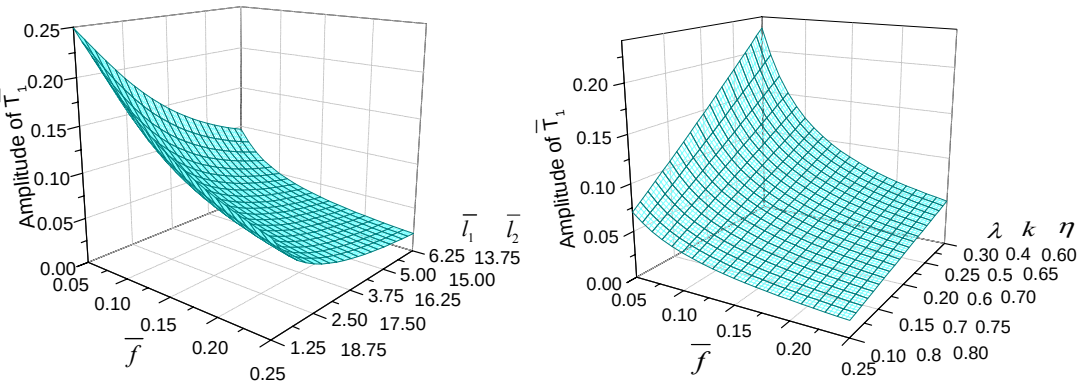

(a) (b)

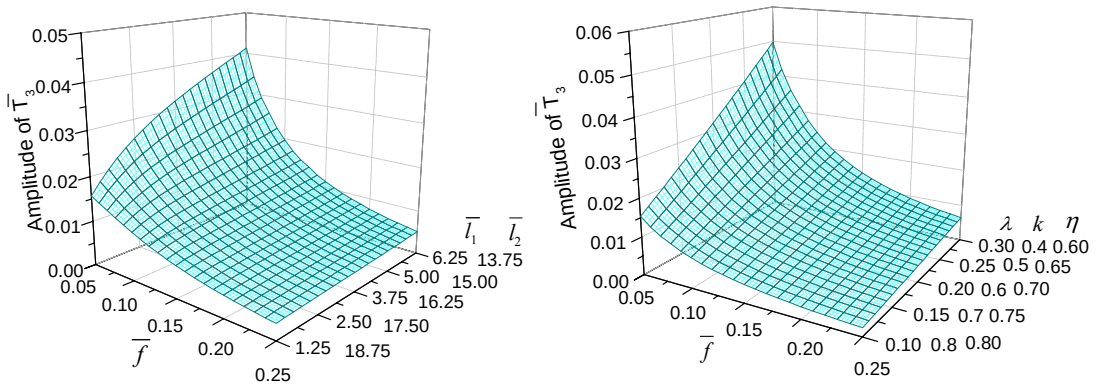

(c) (d)

Figure 4-12 Effects of $\overline{f}$, $\overline{l}_1$ and belt properties on the amplitude of $\overline{\mathbf{T}_1}$ and $\overline{\mathbf{T}_3}$

Practically, the vibration frequency of friction-belt transverse motion is the rate in single digits, and the vibration frequencies of belt torsional and longitudinal motion are at least one order of magnitude higher than that of transverse vibration, therefore the effect of friction-belt vibration on yarn twist variation in three zones is limited. On the other hand, the periodic variation of yarn diameter due to yarn unevenness is a promising factor that causes large twist variation. Take cotton spinning and wool spinning for example. The typical wavelengths of cotton-like fiber (33 mm) and wool-like fiber (66 mm) are 89 mm and 198 mm, respectively. The corresponding $\overline{f}$ values are 0.225 and 0.101, respectively. Thus, the variation amplitudes of $\overline{\mathbf{T}_1}$ and $\overline{\mathbf{T}_3}$ are 0.063 and 0.005, respectively, for cotton-like fiber at the diameter variation of 15%, $\overline{l}_1$ of 2.5, and λ of 0.3; while the variation amplitudes of $\overline{\mathbf{T}_1}$ and $\overline{\mathbf{T}_3}$ for wool-like fiber reach as high as 0.133 and 0.016 at the same condition. Hence, the twist variation is more serious in wool-like yarn than that of cotton-like yarn.

4.5 Summary

This chapter describes the effects of variations of false twist on process stability and resultant yarn quality in a modified ring spinning process. Even though several assumptions have been proposed to make the analysis manageable, the findings have provided a clear clue of the significant twist levels that can generate in the zones of the machine. It has been proved by the experiment that within 30% periodic variation in false twist, the yarn properties were not significantly affected. In another words, the

current configuration and system parameters are stable and robust as well as have a high tolerance for twist variations. From simulation, it has been demonstrated that belt oscillation has little effect on twist variation and wool-like fibre is easier to cause large twist variation in spinning process than that of cotton-like fiber at the same condition. In the end, the results give rise to a better comprehending of the mechanism of false-twister adopted in a ring spinning frame and provide method of calculating the actual levels of twist to reduce certain remarkable yarn faults.

Chapter V Study of Yarn Properties in the Ring Spinning System with Single Friction-belt False-twister

In order to solve the severe deterioration of yarn neps in the double-belt system, in this study systematic investigation of Ne 40 cotton yarns produced by the ring spinning system with the adoption of single friction-belt false-twister has been carried out. Firstly, belt positions in both single-belt and double-belt systems which determine the wrap angle of the yarn on the belt are analyzed and compared. Then, based on the preliminary analysis of belt friction suface and geometry, the belt with hardness 85 shore A, diameter 6mm and smooth surface, showing the highest false twist among other belts of different hardness, surface roughness and diameter has been chosen for systematic investigation and optimization. Next, fractional factorial methodology is employed to find out the statistically significant factors on yarn tenacity, evenness neps (+140%) and hairiness. After that, these factors are further explored using response surface methodology. Second order equations are obtained to examine and estimate the relationships between the factors and responses. Finally, the yarn with optimized parameters has been spun and compared with the conventional yarn. The results indicate that the neps (+140%) of the optimized yarn is still 50% worse than that of the ring spun yarn. In order to overcome the occurrence of neps in the single-belt system, promising solutions to alleviate or diminish such yarn imperfection have been put out and verified by the experiments.

5.1 Belt Position

As mentioned in Chapter 2, belt installation position is an important consideration of special interest for practical applications. It is not only restricted by the space of different spinning machines, but also affects the stability and quality of the yarn. More importantly, the belt position also determines the wrap angle of the yarn on the belt, which is a key factor affecting yarn properties. Therefore, it is necessary to analyze the belt positions in both single-belt and double-belt systems.

5.1.1 Single Belt

A schematic diagram of belt position in a ring spinning frame is plotted in Figure

5-1, in which O is the nip point of front rollers, O_1 is the center point of the belt, G_0 and G_1 are the two extreme points of the yarn guide, respectively, while A is the entrance point of the surface of the belt, and B_0, B_1 are exit points of the belt with regard to G_0 and G_1, respectively. The wrap angle $\angle AO_1B_0(B_1)$ is not a constant value and its variation is depended by the belt position and movement of yarn guide. The belt position can be determined by two parameters, L_{OA} and $\angle AOX$, denoted as L and γ, which can be easily measured and adjusted on site. The coordinate for point A and O_1 can be derived by $(L\cos\gamma, L\sin\gamma)$ and $(L\cos\gamma - r_0\sin\gamma, L\sin\gamma + r_0\cos\gamma)$, respectively, where r_0 be the radius of belt. G_0, G_1 have the coordinates (X_0, Y_0) and (X_0, Y_1), respectively, therefore $L_{O_1G_0}$, $L_{O_1G_1}$ can be obtained,

$$\begin{aligned} L_{O_1G_0} &= \sqrt{(L\cos\gamma - r_0\sin\gamma - X_0)^2 + (L\sin\gamma + r_0\cos\gamma - Y_0)^2} \\ L_{O_1G_1} &= \sqrt{(L\cos\gamma - r_0\sin\gamma - X_0)^2 + (L\sin\gamma + r_0\cos\gamma - Y_1)^2} \end{aligned} \tag{5-1}$$

Then the angles $\angle X_0G_0B_0$ and $\angle X_0G_1B_1$ can be correspondingly derived,

$$\begin{aligned} \angle X_0G_0B_0 &= \angle X_0G_0O_1 - \angle O_1G_0B_0 = \arctan\left(\frac{L\cos\gamma - r_0\sin\gamma - X_0}{L\sin\gamma + r_0\cos\gamma - Y_0}\right) - \arctan(r_0 / L_{O_1G_0}) \\ \angle X_0G_1B_1 &= \angle X_0G_1O_1 - \angle O_1G_1B_1 = \arctan\left(\frac{L\cos\gamma - r_0\sin\gamma - X_0}{L\sin\gamma + r_0\cos\gamma - Y_1}\right) - \arctan(r_0 / L_{O_1G_1}) \end{aligned} \tag{5-2}$$

And the wrap angle of the yarn on the belt can be derived,

$$\begin{aligned} \angle AO_1B_0 &= \frac{\pi}{2} - \angle X_0G_0B_0 - \gamma \\ \angle AO_1B_1 &= \frac{\pi}{2} - \angle X_0G_1B_1 - \gamma \end{aligned} \tag{5-3}$$

There are several considerations of belt position. Firstly, the belt position should not exceed the 45^o auxiliary line, which means $\angle AOY$ should be lower than 45^o. It is prohibited for the yarn to contact the front top roller because it deteriorates the spinning triangle and results in poor spinnability and yarn quality. Secondly, variations of the wrap angle should be smaller than $\angle G_0OG_1$, which means that variations of the wrap angle caused by movements of the yarn guide should not exceed the value in the conventional system. Thirdly, the frictional angle of the yarn guide in the proposed system should be smaller than that in the conventional system, which is $\angle BGX_0 < \angle OGX_0$.

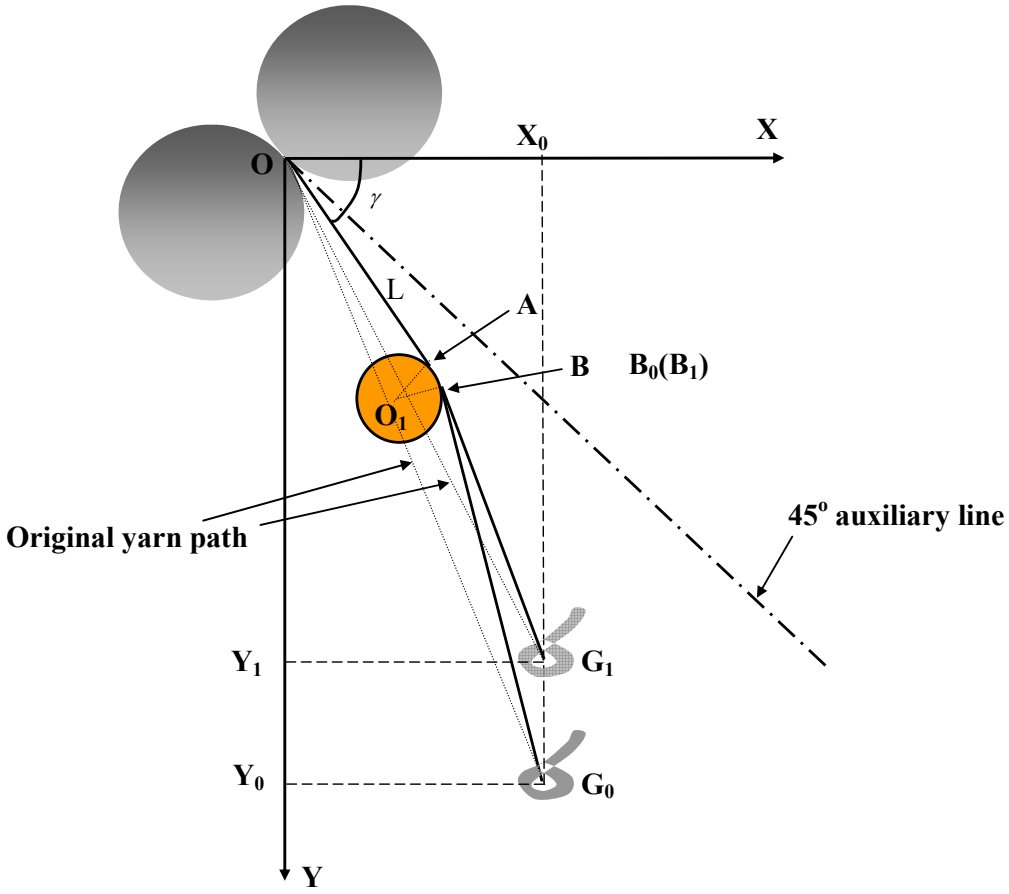

Figure 5- 1 Schematic view of belt position in a ring spinning frame

The ring spinning machine used for the experiments in our lab is Zinser 351, and the yarn guide extreme positions are $G_0(60, 165)$ and $G_1(60, 105)$, respectively. After calculation, the frictional angle of the yarn guide ranges from 20^o to 30^o, and the variation of the frictional angle is 10^o. Accordingly, the searching area for the belt position is L from 0 to 120mm and γ from 45 to 60^o, and the belt diameter is 6 mm in the following analysis unless otherwise stated.

Figure 5-2 displays the wrap angle at two extreme positions of the yarn guide, from which it can be seen that the yarn guide position has certain influence on the wrap angle. The maximum wrap angle for the single-belt in our machine is less than 80^o, and this value is greatly reduced when we further consider variations of the belt warp angle and friction angle of the yarn guide. In order to achieve a high wrap angle, the belt position should be close to the 45^o auxiliary line and keep far away from front rollers. Moreover, in some cases, $\angle AO_1B_0$ is smaller than $\angle AO_1B_1$, and this is because the belt is installed at the right side of the line X_0G_0 (see Figure 5-1).

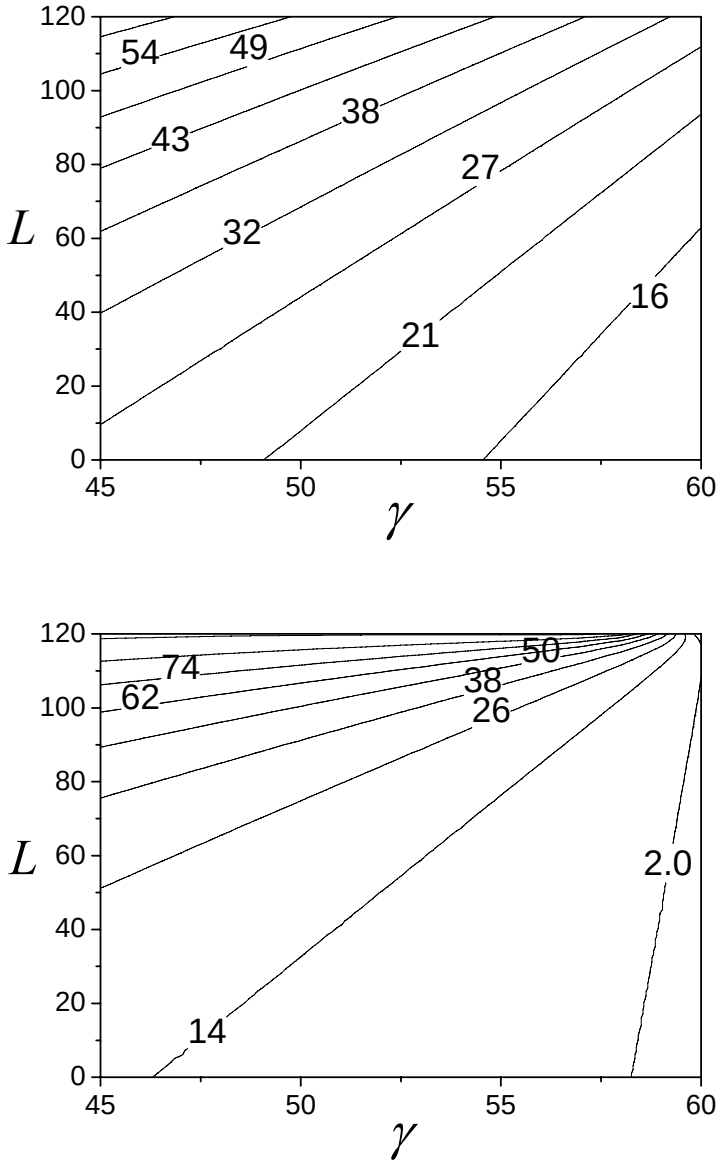

Figure 5- 2 Calculated wrap angles $\angle AO_1B_0$ (up) and $\angle AO_1B_1$ (down)

Figure 5-3 shows the maximum variation of the wrap angle at two extreme yarn guide positions and the value varies from -20 to +20^o in most cases. When the belt is installed right above the yarn guide, the variation of the wrap angle is zero. In another word, the wrap angle is a constant and not influenced by the movement of the yarn guide. Another advantage in this special case is that the friction angle between the yarn and yarn guide is zero all the time. For industrial applications, the accessible variation of the wrap angle is less than ±10^o according to the variation of the friction angle of the yarn guide.

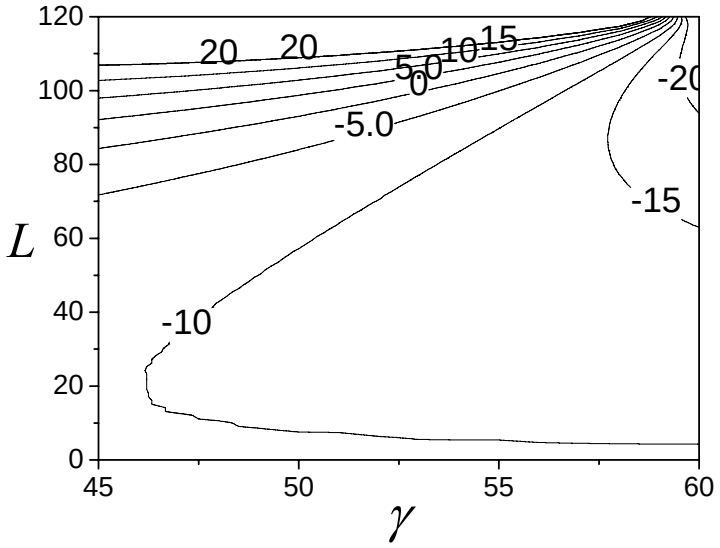

Figure 5- 3 Calculated maximum variations of the wrap angle

Figure 5-4 illustrates the friction angle between the yarn and yarn guide in terms of different belt installing positions. Generally speaking, the friction angle is relatively small in case the yarn guide locates at the bottom position and vise versa. For our spinning system, the maximum friction angle is 30^{o}, and this value is also used to be the boundary value for considering the belt position.

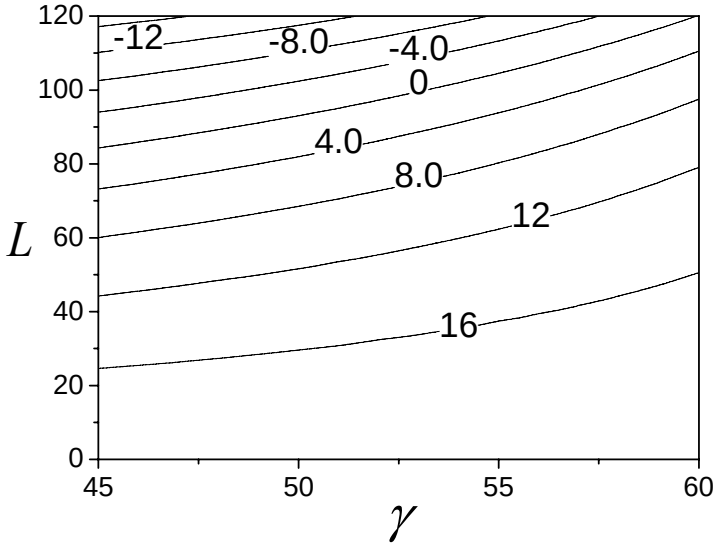

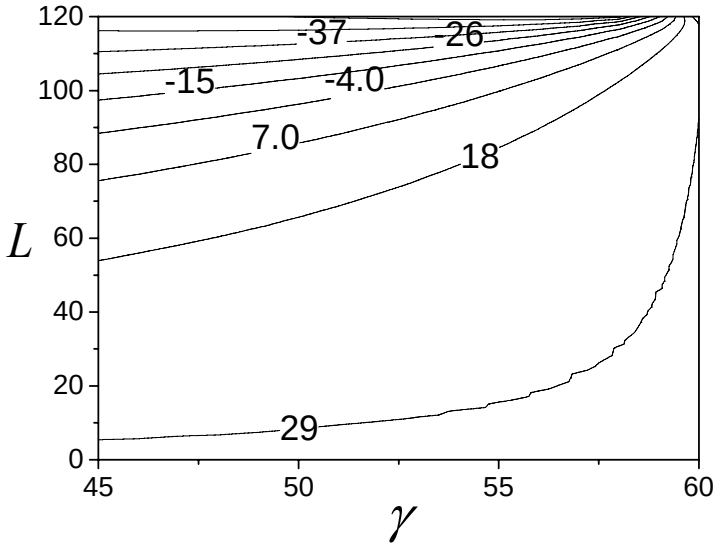

Figure 5- 4 Calculated yarn guide friction angles $\angle B_0G_0X_0$ (up) and $\angle B_1G_1X_0$ (down)

Figure 5-5 exhibits the feasible region of the belt position and its value of the wrap angle in Cartesian coordinate system. The feasible region is plotted under three conditions: γ is 45 to 60^o; the variation of belt wrap angle is less than 10^o; the friction angle of the yarn guide is less than 30^o. The maximum wrap angle in the feasible region reaches about 50^o, therefore the false-twisting efficiency is about 10% according to the theoretical model and experiments conducted in Chapter III. The belt diameter from 2mm to 10mm has no effect on the feasible region and wrap angle.

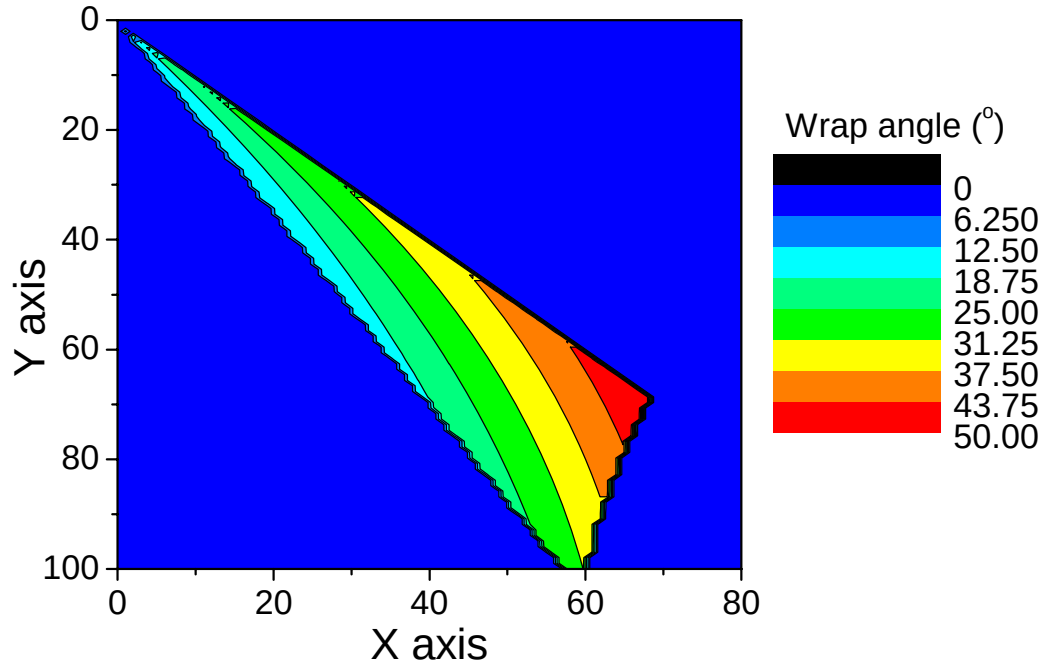

Figure 5- 5 The feasible region and wrap angle in Cartesian coordinate system

5.1.2 Double Belt

A schematic diagram of belts position in a ring spinning frame is plotted in Figure 5-6, in which O is the nip point of front rollers, O_1 and O_2 are center points of the upper and lower belts, G_0 and G_1 are the two extreme points of the yarn guide, respectively, while A and B are the entrance and exit points of yarn with the surface of the upper belt, and C and D are entrance and exit points of yarn with the surface of the lower belt, respectively. $\angle AO_1B$ and $\angle CO_2D$ are the wrap angles of the upper and lower belts, respectively. G_0 and G_1 are the two extreme points of the yarn guide, respectively, while D_0 and D_1 are exit points of the lower belt with regard to G_0 and G_1, respectively. The wrap angle $\angle CO_2D$ is not a constant value and its variation is depended by the belt position and movements of the yarn guide. In the double-belt system, it needs four independent parameters to ensure the coordinates of the upper and lower belts. The simplest way is to obtain the centre coordinates $O_1(X_{O1},Y_{O1})$, $O_2(X_{O2},Y_{O2})$ of the two belts, however these values can not be easily measured or controlled on site. A more suitable way to realize it is to control the four parameters as follows: L_{OA}, $\angle AOX$, L_{O1O2} and included angle of line O_2O_1 and OX, denoted as L , γ , l and ϕ . The coordinates for point A and O_1 can be derived by

$(L\cos\gamma, L\sin\gamma)$ and $(L\cos\gamma - r_0\sin\gamma, L\sin\gamma + r_0\cos\gamma)$, respectively, where r_0 be the radius of belt. Then the coordinate for point O_2 can be obtained by $(L\cos\gamma - r_0\sin\gamma + l\cos\phi, L\sin\gamma + r_0\cos\gamma + l\sin\phi)$. Line BC can be expressed by

$$Y = kX + b \tag{5-4}$$

where *k* and *b* can be solved by the following equations

$$\begin{cases} \left[L\sin\gamma + r_0\cos\gamma - k(L\cos\gamma - r_0\sin\gamma) - b\right]^2 = r_0^2(1+k^2) \\ \left[L\sin\gamma + r_0\cos\gamma + l\sin\phi - k(L\cos\gamma - r_0\sin\gamma + l\cos\phi) - b\right]^2 = r_0^2(1+k^2) \end{cases} \tag{5-5}$$

Then, the wrap angle of the upper belt can be obtained by

$$\angle \mathrm{AO_1B} = \begin{cases} \tan^{-1}(k) - \gamma & k \geq 0 \\ \pi + \tan^{-1}(k) - \gamma & k < 0 \end{cases} \tag{5-6}$$

Similarly, line DG_0 and DG_1 can be expressed by

$$\begin{cases} Y = pX + y_0 - px_0 \\ Y = qX + y_1 - qx_0 \end{cases} \tag{5-7}$$

Where *p* and *q* can be solved by the following equations

$$\begin{cases} \left[L\sin\gamma + r_0\cos\gamma + l\sin\phi - p(L\cos\gamma - r_0\sin\gamma + l\cos\phi) - y_0 + px_0\right]^2 = r_0^2(1+p^2) \\ \left[L\sin\gamma + r_0\cos\gamma + l\sin\phi - q(L\cos\gamma - r_0\sin\gamma + l\cos\phi) - y_1 + qx_0\right]^2 = r_0^2(1+q^2) \end{cases} \tag{5-8}$$

Then, the wrap angle of the lower belt can be obtained by

$$\begin{cases} \angle \mathrm{CO_2D_0} = \begin{cases} \tan^{-1}(k) - \tan^{-1}(p) & k \geq 0, p \geq 0 \ \ or \ \ k < 0, p < 0 \\ \pi + \tan^{-1}(k) - \tan^{-1}(p) & k < 0, p \geq 0 \end{cases} \\ \angle \mathrm{CO_2D_1} = \begin{cases} \tan^{-1}(k) - \tan^{-1}(q) & k \geq 0, q \geq 0 \ \ or \ \ k < 0, q < 0 \\ \pi + \tan^{-1}(k) - \tan^{-1}(q) & k < 0, q \geq 0 \end{cases} \end{cases} \tag{5-9}$$

Finally, the total wrap angle Φ of the two belts are

$$\Phi = \angle AO_1B + \angle CO_2D_0 \tag{5-10}$$

There are several considerations of belt position. Firstly, the upper belt position should not exceed the 45° auxiliary line, which means ∠AOY should be lower than 45°. It is prohibited for the yarn to contact the front top roller because it deteriorates the spinning triangle and results in poor spinnability and yarn quality. Secondly, variations of the wrap angle of the lower belt should be smaller than $\angle G_0OG_1$, which means that variations of the wrap angle caused by movements of the yarn guide should not exceed the value in the conventional system. Thirdly, the frictional angle of the yarn guide in the proposed system should be smaller than that in the conventional system, which is $\angle DGX_0 < \angle OGX_0$. Fourthly, the gap between the two

belts should be larger than 10mm for easy threading the yarn.

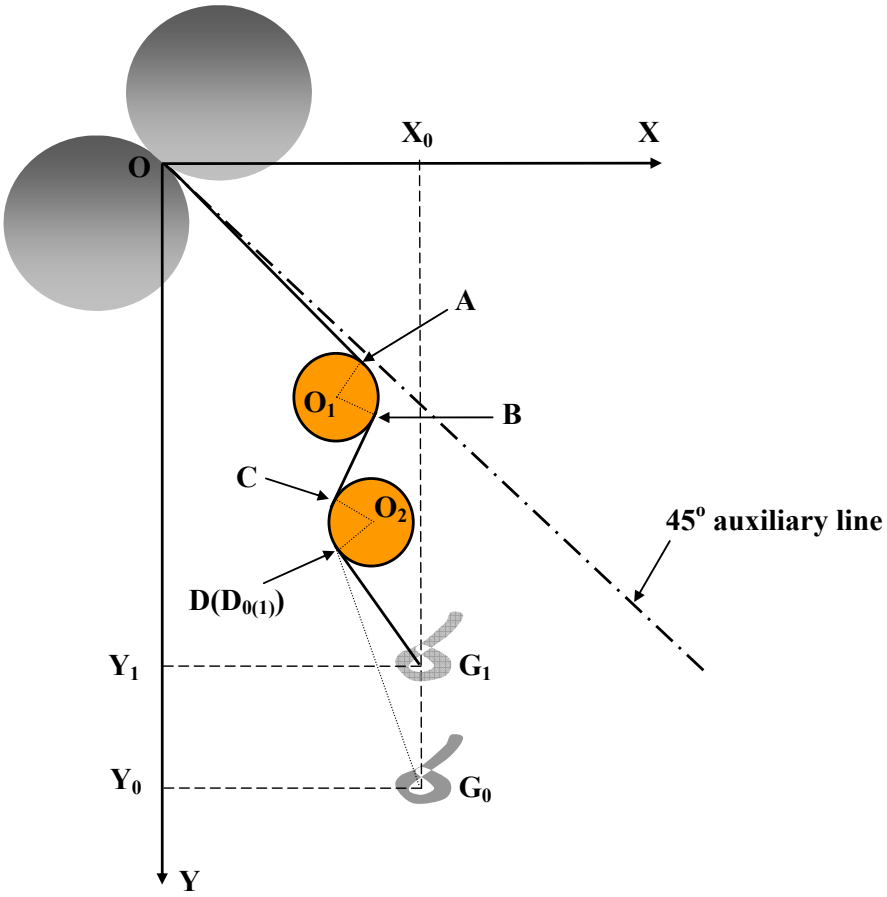

Figure 5-6 Schematic view of belts position in a ring spinning frame

After calculation, the frictional angle of the yarn guide ranges from 20° to 30°, and the variation of the frictional angle is 10°. For simplification, we can set L=70mm, l=16mm for studying the feasible region and wrap angles of the two belts. Accordingly, the searching area is γ from 45 to 65°, and ϕ from 30 to 105° and the belt radius is 3mm for the following analysis unless otherwise stated.

Figure 5-7 displays the wrap angles of the upper belt and lower belt, respectively. It can be seen that the two wrap angles are less sensitive to the angle γ than that of angle ϕ. For the upper belt, the conditions to reach high wrap angle are higher angle ϕ and lower angle γ, while for the lower belt, the conditions are both higher angle ϕ and angle γ. Moreover, the yarn guide position has a large influence on the change of the wrap angle of the lower belt. In some occasions, the variation reaches as far as 35°, as shown in Figure 5-7.

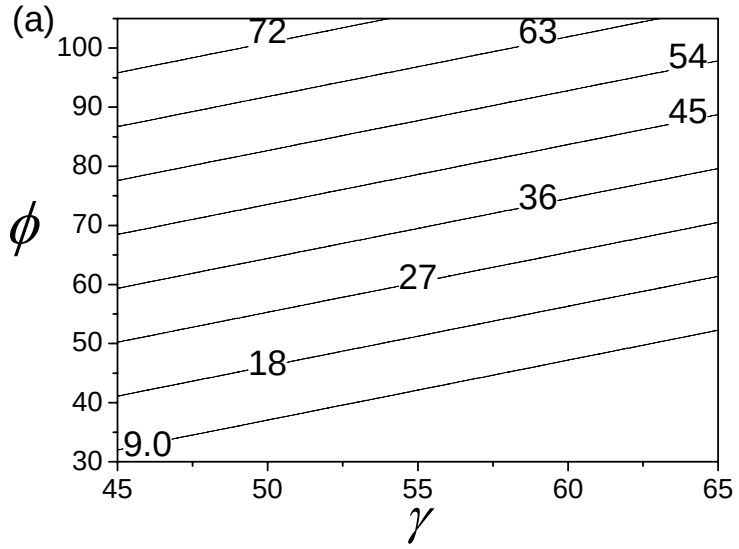
(a)
72
63
54
45
36
27
18
9.0
100
90
80
70
60
50
40
30
45
50
55
60
65
ϕ
γ

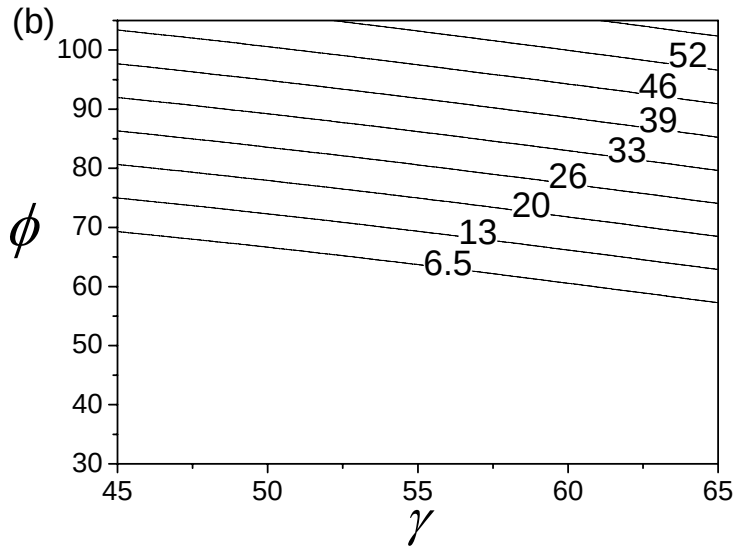
(b)
52
46
39
33
26
20
13
6.5
100
90
80
70
60
50
40
30
45
50
55
60
65
ϕ
γ

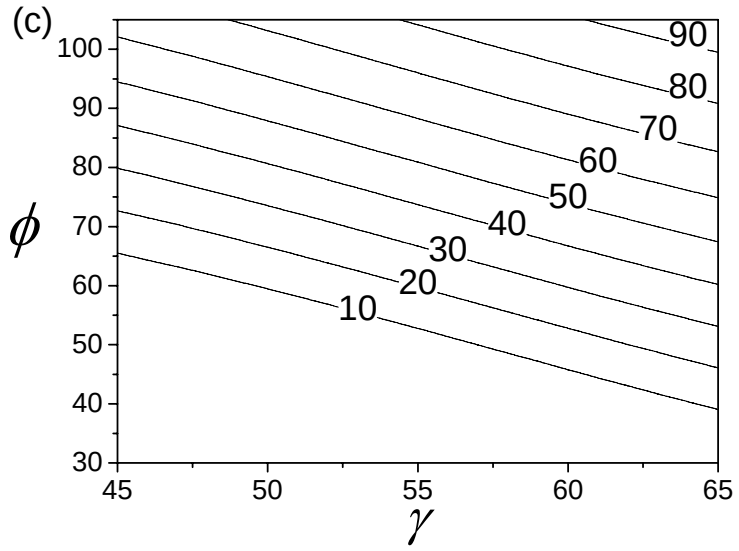

Figure 5-7 Calculated wrap angles of the upper belt $\angle AO_1B$ (a) and lower belt $\angle CO_2D_0$ (b) and $\angle CO_2D_1$ (c)

Figure 5-8 shows the maximum variation angle of the lower belt at two extreme yarn guide positions and the value varies from 0 to 35°. When the lower belt is installed close to the yarn guide in X direction and far away from it in Y direction, the influence of the yarn guide position has less effect on the variation of the wrap angle of the lower belt. Suppose the lower belt is located right above the yarn guide, then the wrap angle of the lower belt will be constant throughout. For industrial applications, the accessible variation of belt wrap angle should be less than ±10° according to the variation of the friction angle of the yarn guide.

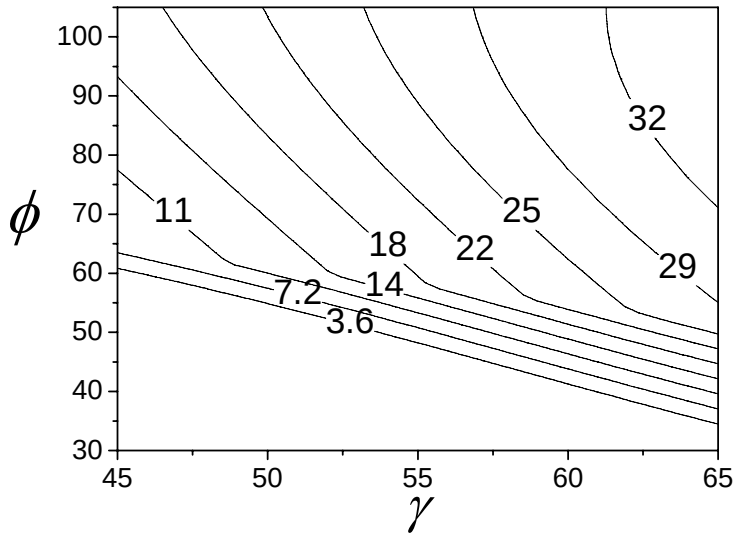

Figure 5-8 Calculated maximum variation angle of the lower belt

Figure 5-9 illustrates the friction angle between the yarn and yarn guide in terms of different belt installing positions. Generally, the two variables ϕ and γ have evident impact on the friction angle, and their effect is equal. Moreover, the friction angle is relatively small in case the yarn guide locates at the bottom position and vise versa. For our spinning system, the maximum friction angle is 30^{o}, and this value is also used to be the boundary value for considering the belt position.

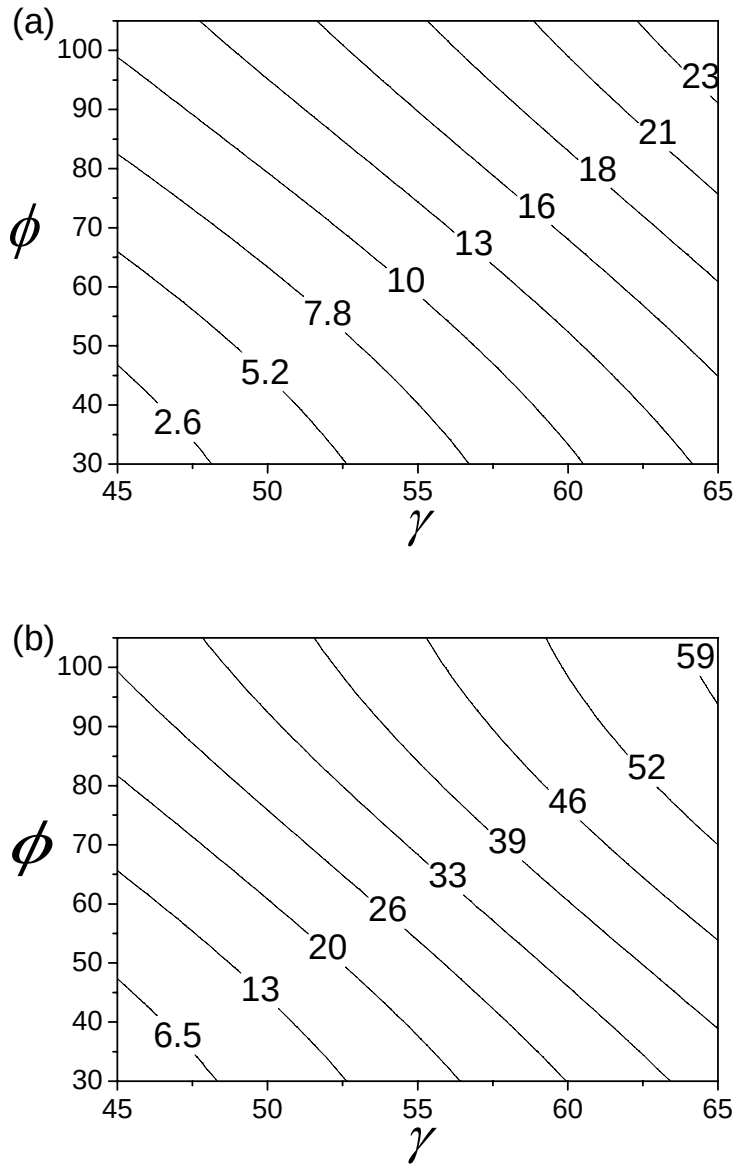

Figure 5-9 Calculated friction angle of the guide $\angle D_0G_0X_0$ (a) and $\angle D_1G_1X_0$ (b)

Figure 5-10 exhibits the feasible region of the belt position and the total value of belts wrap angle. The feasible region is plotted under the conditions of γ from 45

to 65°, ϕ from 30 to 105 °, L=70 mm, l=16 mm, r_0=3 mm; the variation of belt wrap angle is less than 10°; the friction angle of the yarn guide is less than 30°. Under these conditions, the maximum value of the total wrap angle in the feasible region is only about 61°, 11° larger than that of the single belt system. This is because in the beginning we preset two conditions, L and l, which may have evident impinge on the total wrap angle. The relationship between the total wrap angle and L is investigated and the results are plotted in Figure 5-11. With the increasing length L, the total wrap angle shows an evident increasing trend. When L equals 90 mm, the total wrap angle reaches about 120°, high enough to generate strong false twist into the yarn. And the feasible region and total value of wrap angle at L=90 mm is shown in Figure 5-12. The effect of the centre distance of the two belt is also investigated. In most cases, the total wrap angle is decreased as the centre distance is increased. When l changes from 10 to 25 mm, the total wrap angle is shortened almost by 50% in the case of L=90 mm.

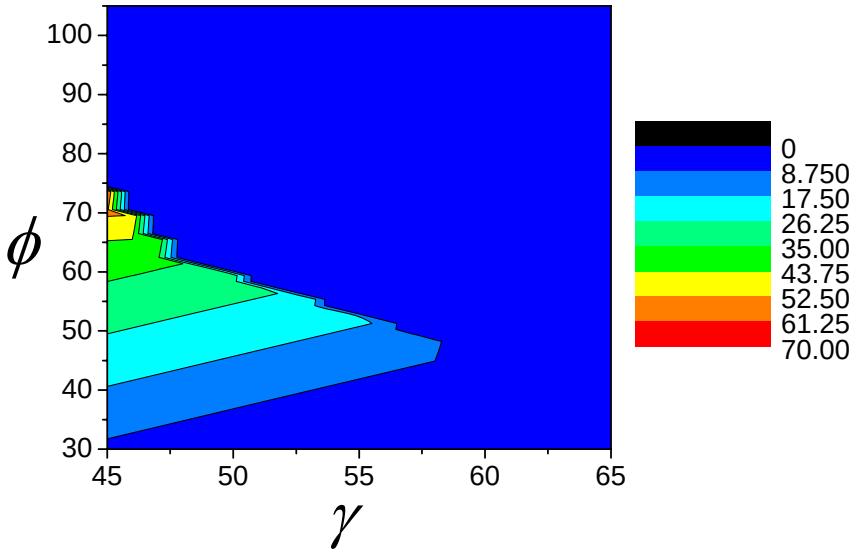

Figure 5-10 Calculated total wrap angle in the feasible region

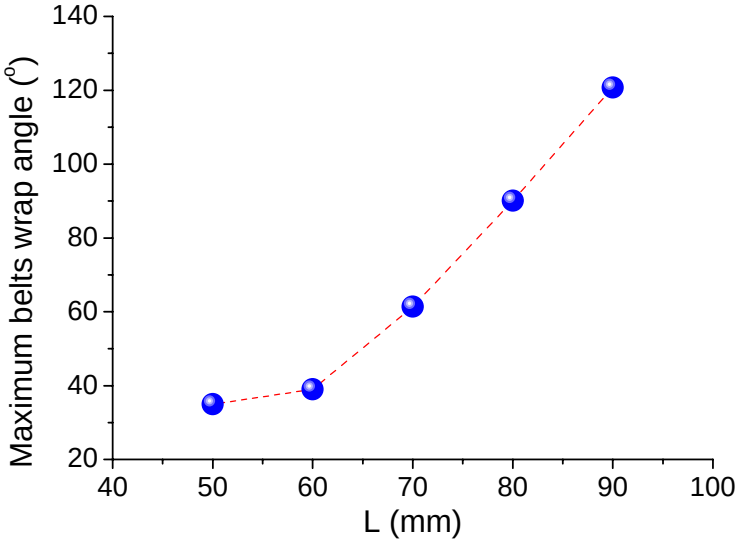

Figure 5-11 The effect of *L* on the maximum wrap angle of the two belts

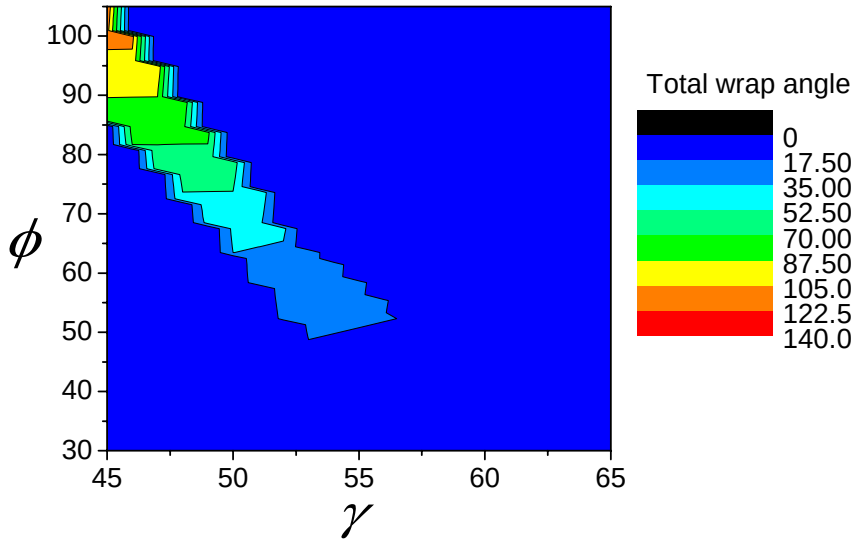

Figure 5-12 Calculated total wrap angle at *L*=90 mm

To sum up, the belt position in the ring spinning system determines the wrap angle of the yarn on the belt. For the single-belt system, the maximum wrap angle is around 50°, while the maximum wrap angle for the double-belt system reaches 140°.

5.2 Belt Friction Surface and Geometry

Currently, round belt has taken the place of glass fiber materials, steel cables and traditional rubber products and been widely used for transporting food, cans, wood products, ceramic tiles, etc. due to its high strength, low stretch characteristics as well as excellent abrasion resistance. By and large, round belt is made of

polyurethane, and various density, elasticity and stiffness can be easily obtained by modifying its formula. In the market, the diameter of the PU belt ranges from 2 to 30 mm, and hardness from 80 to 95 Shore A. In our study, the round belt has been employed as a false-twister and directly contacts the yarn. There are several concerns for choosing belt.

(1) Coefficient of friction

The coefficient of friction is a dimensionless scalar value describing the ratio of the force of friction between two bodies and the force pressing them together. In terms of false-twisting efficiency, the coefficient of friction between the belt and yarn is a very important consideration for choosing belt. According to the theoretical model shown in Chapter 3, coefficient of friction, speed ratio and wrap angle are the three most important factors deciding the false-twisting efficiency. However, its value is also affected by the surface roughness, hardness and geometric conditions. Therefore, it is necessary to measure the exact value for references.

(2) Hardness

Hardness is a measure of how resistant solid matter is to various kinds of permanent shape change when a compressive force is applied. The hardness of PU belt is 80-95A. The hardness also relates to the coefficient of friction. Normally, the higher the belt hardness, the lower the coefficient of friction. On the other hand, it is easier for belt with low hardness to make large local deformation, which decreases its service life.

(3) Surface roughness

Surface roughness is a component of surface texture, which plays an important role in determining how the belt interacts with yarn. There are two kinds of belt, one kind with smooth surface, and another with rough surface. For rough belt, the contacting surface with yarn is much smaller than that of smooth belt, thus has lower frictional coefficient.

(4) Load and extension

In the proposed system, the belt realizes two functions, one is to directly contact the belt as a false-twister, another function is to work as a power transmission component driven by a electric motor. The belt must be tensioned to a prescribe working load to running smoothly and stably. It is desirable to use the belt with high modulus and low extension.

(5) Diameter

Belt diameter determines the stiffness to resist deformation the yarn applied on the belt. For the same wrap angle, the contacting length with yarn is related to the belt diameter, but the coefficient of friction is independent of it. In the premise of quality assurance, it is suggested to use the belt with larger diameter.

Since the wrap angle in the single-belt is only 50^{o}, it is desirable to choose a belt with high false-twisting efficiency. Therefore, as an important index relating to false twist, the coefficient of friction has been used to investigate belts with different physical properties and geometry. More directly, yarn twists above the false-twisters using belts with different physical properties and geometry have been measured and compared.

5.1.1 Measurement of Coefficient of Friction

Assuming that the frictional coefficient of belt and belt is uniform in all direction, a device was designed for measuring the belt frictional coefficient, as shown in Figure 5-13. In this device, a 40Ne cotton yarn with a tension close to yarn spinning tension (10 cN) was driven by a set of rotating rollers at a constant speed close to yarn spinning speed (0.2 m/s) and the yarn contacted with the stationery belt with a wrapping angle of 90 degree. The coefficient of friction can be easily obtained according to the capstan equation.

$$T_2 = T_1 e^{\frac{\pi}{2}\mu} \tag{5-11}$$

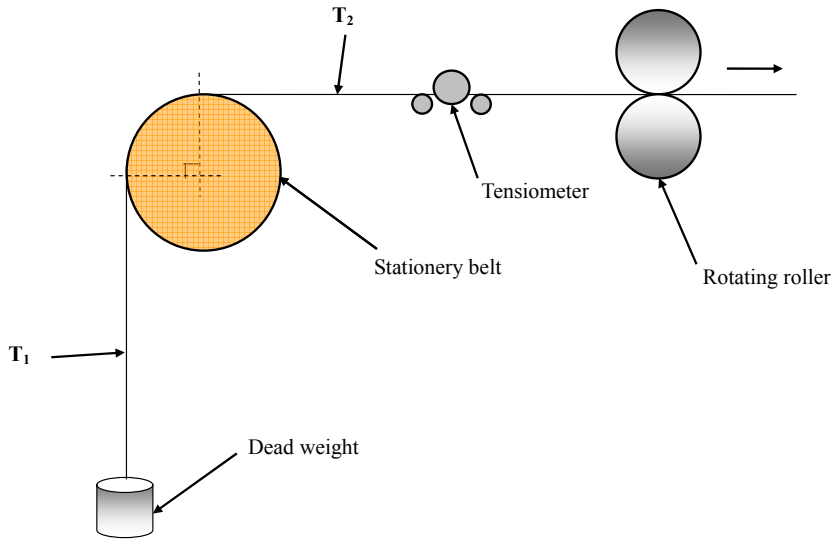

Figure 5- 13 Schematic view of the designed device for measuring the coefficient of friction

Five round belts with different diameter, surface morphology and material were employed for the experiments, as shown in Table 5-1. It can be seen that the belt with hardness of 85A has the highest frictional coefficient, which is independent of belt diameter, whereas 89T-4mm has the lowest frictional coefficient due to its roughness surface morphology. In particular, White 40D made of polyester shows the largest working load, 3 times larger than that of 85-4mm.

Table 5-1 Belt specifications

Code	Hardness	Coefficient of friction with Stainless Steel	Surface	Material	Diameter (mm)	Working load @ percent tension (N)	
						4%	10%
85-6mm	85A	0.70	Smooth	Polyurethane	6	7.7	19.4
85-4mm	85A	0.70	Smooth	Polyurethane	4	3.4	8.6
85-3mm	85A	0.70	Smooth	Polyurethane	3	1.9	4.9
89T-4mm	89A	0.50	Texture	Polyurethane	4	4.1	11.6
40D-4mm	40D	0.55	Smooth	Polyester	4	14.8	36

Table 5-2 lists the measured coefficients of friction of 5 belts with Ne 40 single cotton yarn. Generally, the coefficients of friction between various belts and yarns are higher than that with stainless steel, and they have the same ranking order, while the difference among 5 belts is smaller. Specifically, the round belts with hardness of 85A display the highest value of 0.81-0.82, followed by the belt of hardness 40D, whereas textured belt of hardness 89A has the lowest value of 0.73. Therefore, it can be concluded that the surface roughness has the largest effect on the frictional coefficient, whereas the diameter of the false-twister has almost no influence on the frictional coefficient. In terms of ring spinning system adopted single friction-belt false-twister, due to its relatively low wrap angle, it is advisable to use the belt with higher frictional coefficient to increase the false-twisting level.

Table 5-2 Measured coefficients of friction

Code	Coefficient of friction

	Mean	CV(%)
85-6mm	0.82	5.18
85-4mm	0.82	5.89
85-3mm	0.81	6.37
89T-4mm	0.73	4.20
40D-4mm	0.78	4.61

5.1.2 Measurement of Yarn Twist in High-twisted Zone

A black-white cotton yarn was adopted to evaluate the yarn twist above the false-twister in order to exam the false-twisting efficiency of these five belts. In the experiment, the wrap angle of each belt was 50^{o}, the speed ratio was set at 2.0, and the twist factor was 3.2. The Ne 40 black-white cotton yarn was produced and the yarn twist was captured by using the high-speed photography mentioned in Chapter III. The results are displayed in Figure 5-14, from which it can be seen that all the belts generate almost same amount of twists in high-twisted zone ranging from 1087-1145 turns/m, except for 85-3mm belt of 896 turns/m. The reason for low false twist of 85-3mm belt may result from its relatively low contacting area of the yarn and belt, which has a linear relationship to yarn diameter under the same wrap angle. Among these five belts, 85-6mm belt has the highest twist with 1145 turns/m, followed by 85-4mm belt with twist of 1126 turns/m, whereas the values of 89T-4mm and 40D-4mm are 1104 and 1087 turns/m, respectively. Therefore, combing the results of the belt frictional coefficients and yarn twist in high-twisted zone, we can conclude that 85-6mm belt has the highest false-twisting efficiency, thus was chosen for further optimization and investigation.

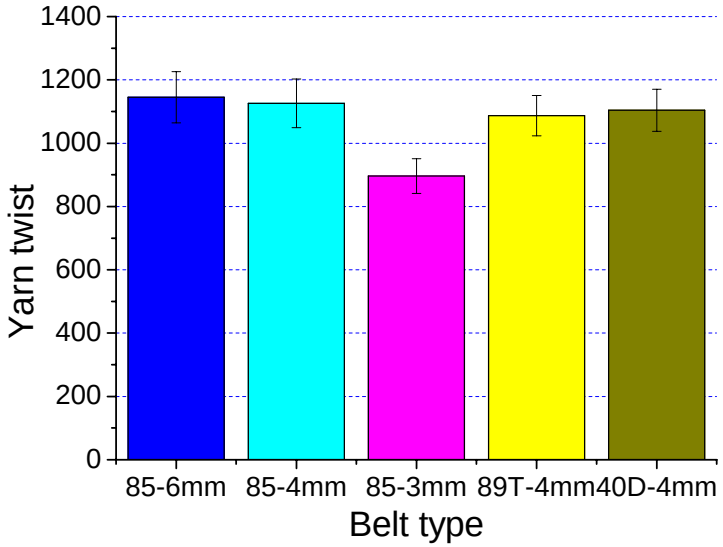

Figure 5- 14 Yarn twists in high-twisted zone for different belts

5.2 Most Influencing Factors on the Yarn Properties

5.2.1 Material Preparation

In this experiment, all Ne 40 single cotton yarns were spun on spinning frame Zinser 351. The combed roving of 535 tex and mass variation of 4.26% provided by the Central Textiles (Hong Kong) Ltd was used. In the spinning process, the spindle speed and total draft ratio are 13000 rpm and 36.25, respectively. The 85-6mm belt was chosen for the experiment due to its relatively high false-twisting efficiency and high bending rigidity. Main physical properties of fiber material were tested by the Spinlab 900 and roving evenness was tested by Uster evenness tester 3. Before testing, all samples were kept under standard laboratory conditions ($20^{o}C \pm 2^{o}C$ and 65% ± 2% relative humidity) for at least 24 hours, and the results are listed in the Table 5-3.

Table 5-3 Fiber and roving specifications

Items	Mean Value	[CV%]
Fiber length (mm)	31.75	[1.7]
Uniformity ratio (%)	60.2	[2.3]
Fiber strength (gf/tex)	24.5	[2.6]
Elongation (%)	5.6	[3.6]

Micronaire Value	4.2	[3.6]
Roving count (tex)	535	[1.5]
Evenness (CVm%)	4.26	[6.7]

5.2.2 Yarn Measurement

Three cop yarns spun on three different spindles were produced for measurement. Before each testing, all yarns were balanced under standard laboratory conditions ($20^oC \pm 2^oC$ and 65% ± 2% relative humidity) for at least 24 hours, and all yarn properties measurement followed the methods as shown in Table 5-4. Yarn tenacity, evenness, hairiness and wet snarlings were important properties for the yarn. Yarn breaking strength was tested by the Uster Tensorapid tester, from which fifty subtests were measured for each sample, with a testing length of 500 mm and testing speed of 5,000 mm/min. Yarn evenness was evaluated by the Uster evenness tester, from which 400 meter yarn sample was tested at a testing speed of 400 m/min. Zweigle hairiness tester was introduced for the measurement of hairiness, from which 100 meter yarn sample was adopted for each sample, at a testing speed of 100 m/min. In particular, yarn wet snarlings was measured per 25 cm to evaluate residual torque of single yarns. The smaller the wet snarlings, the lower the yarn residual torque.

Table 5-4 Yarn tests and standards

Properties	**Test Method**	**Test Apparatus**	**Procedure**
Tenacity	ASTM 2256-02	Uster Tensorapid 3	-Test speed:5m/min - Pretension: 0.5cN/tex - Test length: 500mm - Tests within: 50
Evenness	Uster Standard	Uster Tester 3 Evenness Convertor	-Test speed: 400m/min - Testing time: 1min - Tests within: 1
Hairiness	ASTM D1423	Zweigle G566	- Test speed: 100m/min - Evaluation time: 1min - Tests within: 1

5.2.3 Experimental Design

Different spinning parameters have different effects on the yarn structures and properties, and their importance levels are varied. In order to obtain a desirable yarn properties, the first step is to identify the significant spinning parameters and their interplay with the yarn properties. Among all the factors aforementioned, twist factor, speed ratio, traveler weight, wrap angle were selected for the study. Aiming to identify the statistically significant factors, the factorial method was adopted as discussed in Chapter 2. Table 5-5 lists the levels of five independent variables for the experiment, covering a practical range of system parameters based on feasibility and spinnability.

The number of runs for the factorial design depends on the number of independent variables to be investigated. In case of four independent variables, a complete factorial design requires 16 runs. In practice, the fractional factorial design is commonly employed to identify the really important parameters by considerably reducing experimental size without loss of important information about the response. In this study, aiming to acquire a more accurate data on the interactive relationships among the parameters, a half fraction of four factors at two levels factorial experiments with 8 runs was carried out and the according experimental arrangements expressed in natural variables are shown in Table 5-6.

Table 5-5 Fractional factorial design

	A	B	C	D
Level	Twist Factor (turns/inch sqrt(tex))	Speed ratio	Traveler (mg)	Wrap angle (^{o})
-1	3.0	1.0	20	30
+1	3.6	2.5	45	50

Table 5-6 Experimental design expressed in natural variables

Run order	Natural variables

	A	B	C	D
1	3.6	2.5	45	50
2	2.8	1.0	20	30
3	3.6	1.0	20	50
4	2.8	1.0	45	50
5	3.6	2.5	20	30
6	3.6	1.0	45	30
7	2.8	2.5	45	30
8	2.8	2.5	20	50

5.2.4 Results and Discussion

The yarn properties of the experiment in terms of mean value and cv percentage are listed in Table 5-7.

Table 5-7 Yarn properties of fractional factorial experiments

Run order	Tenacity (cN/Tex) [cv%]	Evenness [cv%]	Neps(+140%) [cv%]	Hairiness(S3) [cv%]
1	17.78 [8.84]	13.27 [0.96]	469 [14.54]	214 [7.56]
2	11.52 [12.28]	13.95 [13.52]	350 [10.30]	2349 [18.79]
3	17.85 [7.91]	13.06 [1.52]	402 [15.25]	601 [31.21]
4	14.7 [8.65]	13.7 [1.59]	497 [10.72]	368 [22.66]
5	17.49 [6.92]	12.49 [1.53]	244 [5.13]	1053 [18.20]
6	17.41 [7.10]	13.06 [1.04]	293 [8.20]	632 [49.05]
7	14.71 [8.70]	12.68 [0.62]	238 [29.71]	726 [1.59]
8	15.8	13.13	476	797

	[6.90]	[0.57]	[10.27]	[9.45]

The first 6 terms of the most significant factors in terms of twist factor, speed ratio, traveler weight, wrap angle as well as their combinations on the yarn performances of tenacity, evenness, neps and hairiness are displayed in Figure 5-15. With regards to tenacity, twist factor is the only statistically significant factor with a significant level of 0.1, followed by wrap angle and speed ratio, whereas traveler weight has less effect on yarn tenacity. It can be found that the speed ratio, twist factor, combinations of speed ratio and wrap angle as well as twist factor and speed ratio are statistically significant for evenness at a significant level of 0.05. In terms of Neps, the wrap angle has the highest significance at a significant level of 0.05, while other factors are less important. It can be seen that there is no significance of selected four parameters on yarn hairiness at a significant level of 0.1, although traveler weight has the highest impact on hairiness. It is obvious that twist factor is statistically significant for tenacity and evenness, speed ratio is statistically significant for evenness, wrap angle is statistically significant for neps, while traveller weight has no significant influence.

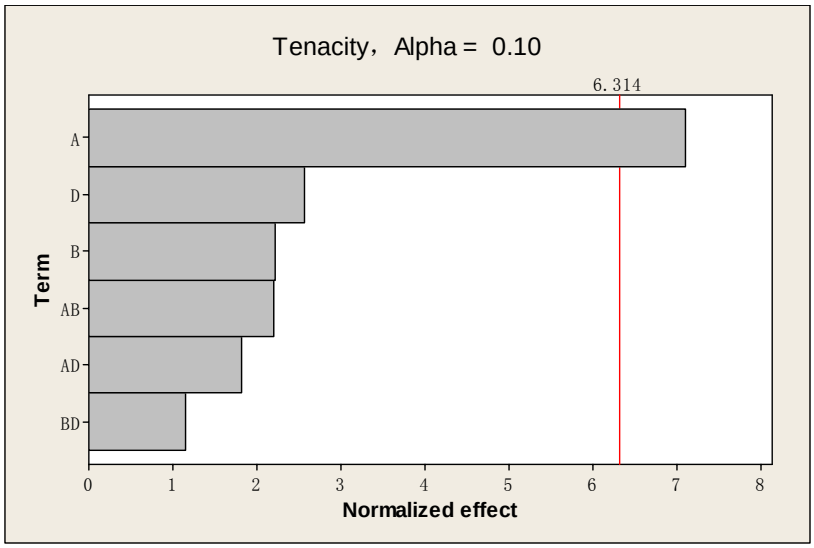

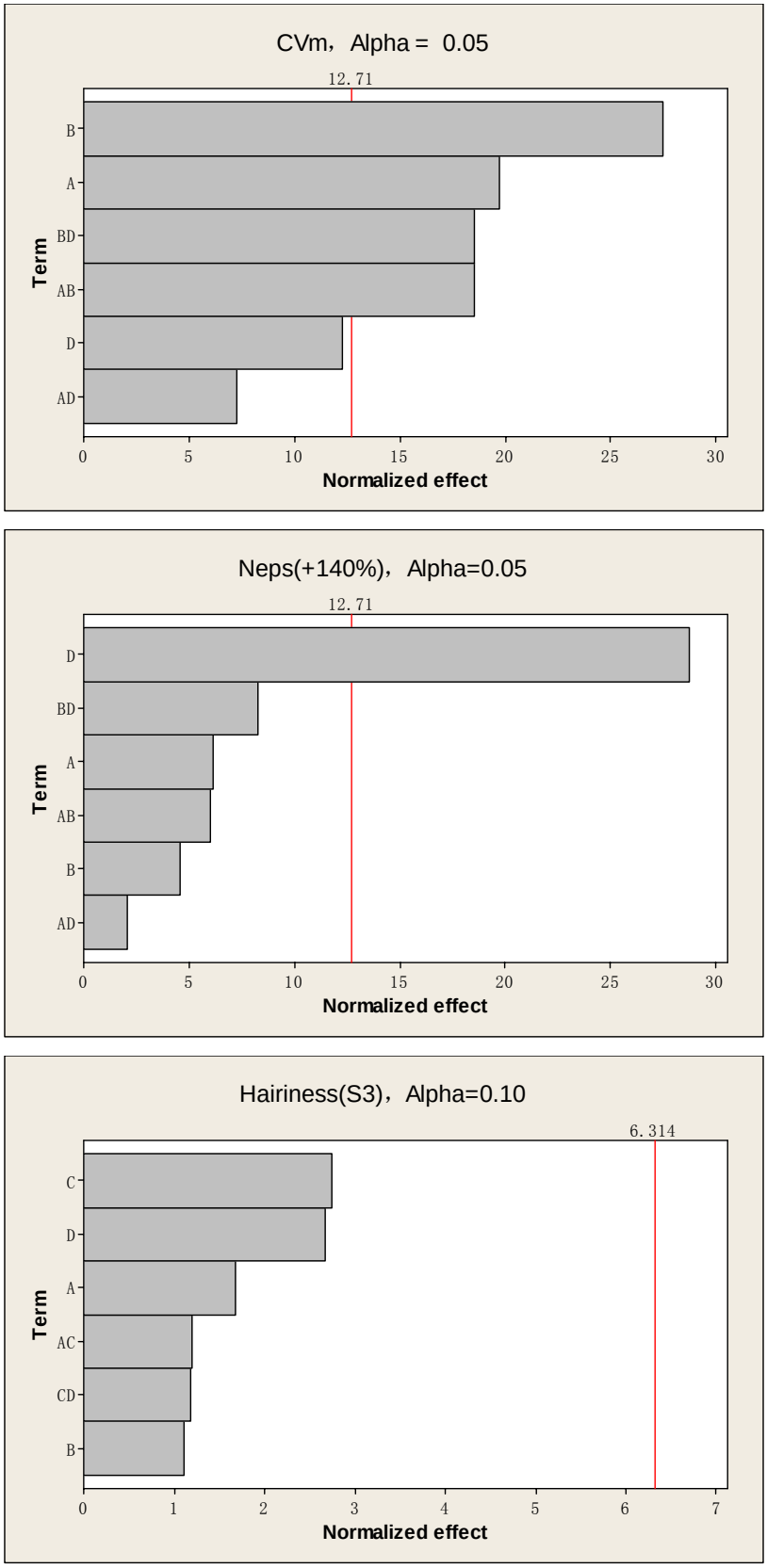

Figure 5-15 Significance of four selected parameters on yarn performance

(A=Twist factor, B=Speed ratio, C=traveler weight, D=wrap angle)

The ANOVA data in Table 5-8 lists F and p values for tenacity, evenness, neps

and hairiness. Table 5-8 also shows multiple correlation coefficient (R^2) and adjusted R^2. The values of R^2 were calculated to be 98.62%, 99.95%, 99.99% and 95.57% for tenacity, evenness, neps, and hairiness respectively, implying that the experimental data was well-fitted. In this study, the values of adjusted R^2 for tenacity, evenness and neps were 90.37%, 99.66% and 99.30%, respectively, which means the regression models were statistically significant.

Table 5-8 Analysis of variance for responses

Term	DF	Seq. SS	Adj. MS	*F*	*p*
Tenacity					
A	1	23.8050	23.8050	50.60	0.089
B	1	2.3113	2.3113	4.91	0.270
D	1	3.1250	3.1250	6.64	0.236
A B*	1	2.2898	2.2898	4.87	0.271
A D*	1	1.5664	1.5664	3.33	0.319
*B*D*	1	0.6272	0.6272	1.33	0.454
Residual error	1	0.4705	0.4705		
Total	7	34.1951			
R^2=98.62%	R^2(adj.)=90.37%				
CVm					
A	1	0.31205	0.31205	390.06	0.035
B	1	0.60500	0.60500	756.25	0.023
D	1	0.12005	0.12005	150.06	0.052
A B*	1	0.27380	0.27380	342.25	0.034
A D*	1	0.04205	0.04205	52.56	0.087
*B*D*	1	0.27380	0.27380	342.25	0.034
Residual error	1	0.00080	0.00080		
Total	7	1.62755			
R^2=99.95%	R^2(adj.)=99.66%				
Neps(+140%)					
A	1	2926.1	2926.1	37.45	0.103
B	1	1653.1	1653.1	21.16	0.136
D	1	64620.1	64620.1	827.14	0.022
A B*	1	2850.1	2850.1	36.40	0.121
A D*	1	325.1	325.1	4.16	0.290
*B*D*	1	5356.1	5356.1	68.56	0.077
Residual error	1	78.1	78.1		
Total	7	77809.9			
R^2=99.90%	R^2(adj.)=99.30%				
Hairiness(S3)					
A	1	378450	378450	4.69	0.332
B	1	168200	168200	1.24	0.465
C	1	1022450	1022450	7.56	0.222
D	1	966050	966050	7.15	0.228
A C*	1	193442	193442	1.43	0.443
C D*	1	188498	188498	1.39	0.447
Residual error	1	135200	135200		

Total	7	3052290
R^2=95.57%	R^2(adj.)=68.99%	

Figure 5-16 shows the main effect of yarn performance with the changes of four parameters. It was found that twist factor and speed ratio were positively related to tenacity, evenness, neps and hairiness. Traveler weight had an evidently positive relationship with yarn hairiness, however it had little effect on yarn tenacity, evenness and neps; while wrap angle had a sharply negative correlation with neps, but strong positive effect on yarn hairiness.

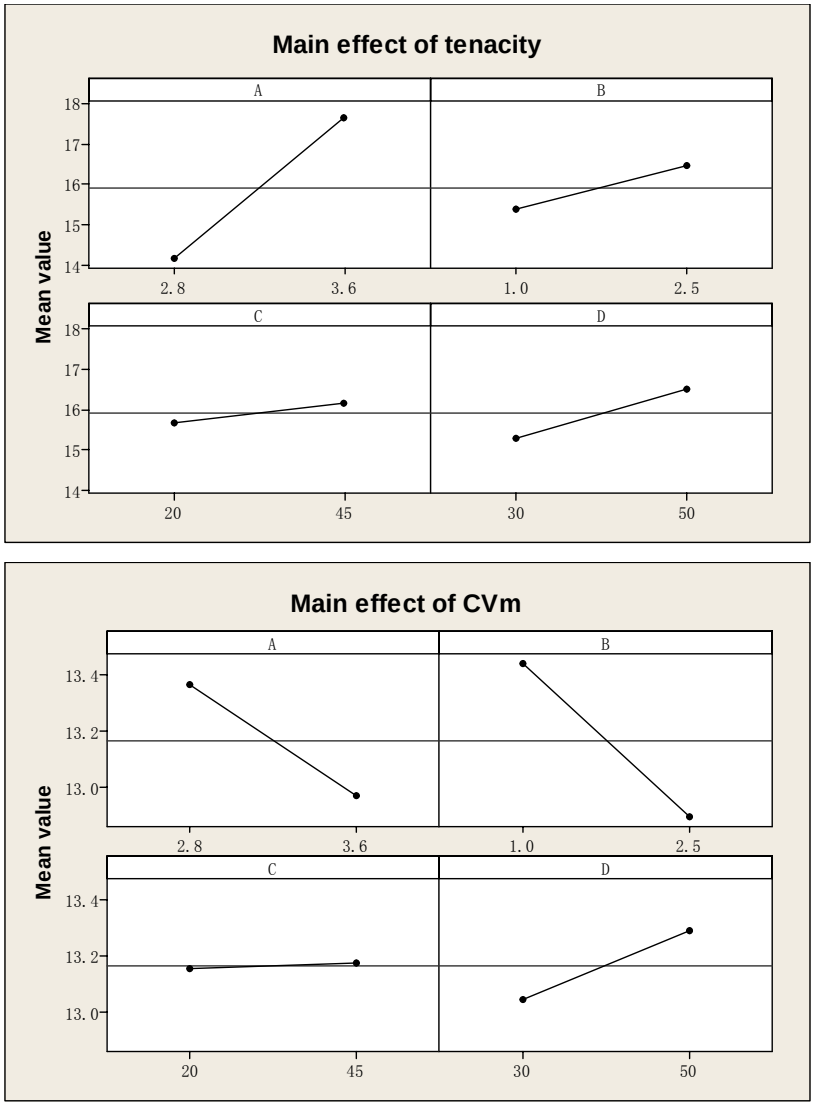

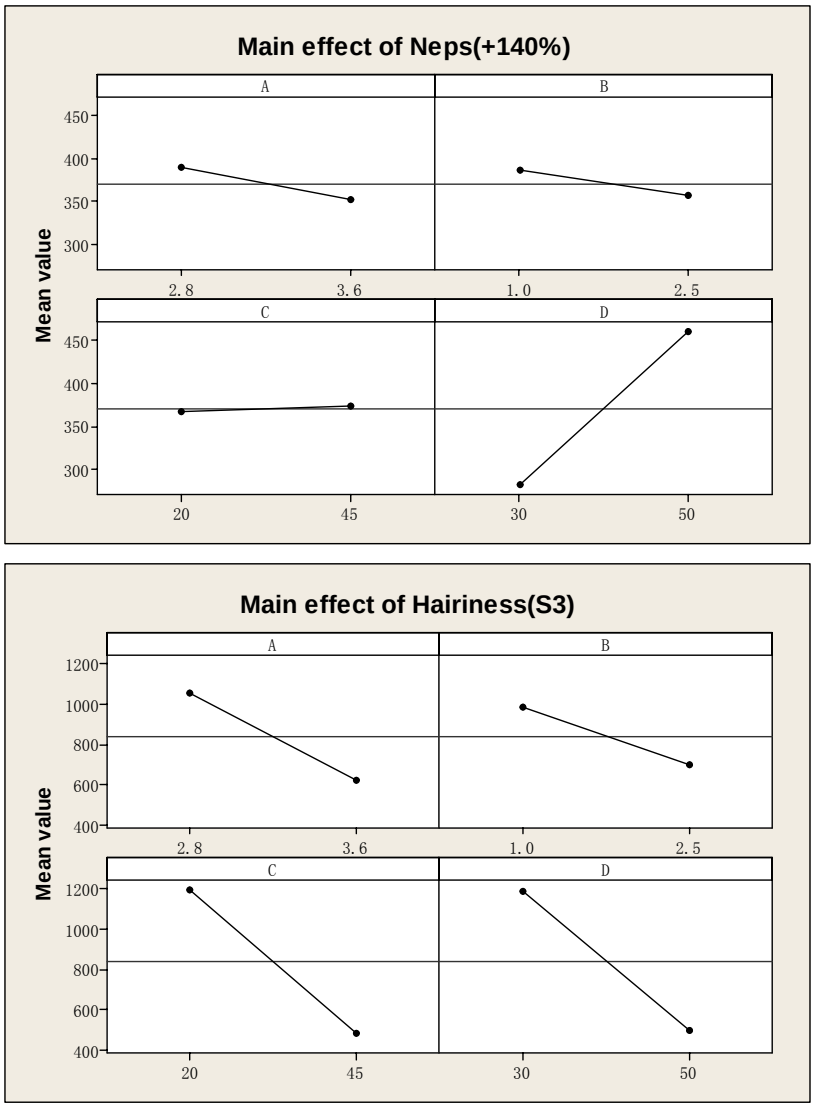

Figure 5-16 Main effect of yarn performance

(A=Twist factor, B=Speed ratio, C=traveler weight, D=wrap angle)

According to the above analysis, twist factor, speed ratio and wrap angle were confirmed as the significant parameters on yarn properties, therefore, these three parameters were selected for further study using response surface methodology to find the optimal value for yarn production.

5.3 Parameter Optimization

5.3.1 Experimental Design

As introduced in Chapter 3, Response Surface Methodology is employed for the parameter optimization with the statically significant parameters: twist factor (X),

speed ratio (*Y*), and wrap angle (*Z*). The range and levels of the independent variables investigated are listed in Table 5-9. The independent variables were tested in an orthogonal 2^3 CCD with six center points and six star points. Each of the independent variables was conducted at five different levels as per CCD in three variables with a total of 20 experiments. The plan of CCD in coded levels of three independent variables is shown in Table 5-10. The statistical significance level (*p* value) was set at 0.05. The coded and actual values of the design were generated in a randomized run order using Minitab 16 software.

Table 5-9 Coded and actual level for each variables of the CCD

Variables	Code	Variation levels				
		-1.682	-1	0	+1	+1.682
Twist factor	*X*	2.8	2.96	3.2	3.44	3.6
Speed ratio	*Y*	0.99	1.3	1.75	2.2	2.51
Wrap angle (^{o})	*Z*	19.82	28	45	52	60.18

Table 5-10 Actual levels in experimental design by CCD method

Run order	*X*	*Y*	*Z*
1	2.96	2.20	52.00
2	3.20	1.75	40.00
3	3.20	0.99	40.00
4	2.80	1.75	40.00
5	3.20	1.75	40.00
6	3.44	1.30	52.00
7	3.20	1.75	40.00
8	3.44	2.20	28.00
9	3.20	1.75	40.00
10	3.44	2.20	52.00
11	2.96	1.30	28.00
12	2.96	2.20	28.00
13	3.20	2.51	40.00
14	3.20	1.75	40.00
15	2.96	1.30	52.00
16	3.20	1.75	19.82
17	3.44	1.30	28.00

18	3.60	1.75	40.00
19	3.20	1.75	40.00
20	3.20	1.75	60.18

5.3.2 Results and Discussion

5.3.2.1 Measured yarn performance

The results of the RSM experiments in terms of mean value and cv percentage are listed in Table 5-11.

Table 5-11 Measured yarn performance of RSM experiments

Run order	Tenacity (cN/Tex) [cv%]	Minimum Tenacity (cN/Tex)	Evenness CVm% [cv%]	Thin places (-40%) [cv%]	Thick places (+50%) [cv%]	Neps (+140%) [cv%]	Hairiness (S3) [cv%]
1	16.43 [7.39]	13.65	13.2 [2.58]	177 [27.86]	31 [31.11]	396 [35.97]	584 [22.10]
2	17.3 [7.40]	13.69	13.14 [0.89]	143 [11.65]	35 [24.74]	325 [15.89]	509 [26.89]
3	15.59 [8.73]	13.02	13.29 [1.23]	170 [10.26]	35 [33.69]	374 [25.97]	703 [50.44]
4	14.74 [7.23]	12.62	13.12 [1.18]	145 [20.89]	36 [4.81]	528 [20.61]	777 [21.88]
5	17.21 [6.95]	14.40	12.99 [0.08]	123 [19.04]	22 [39.25]	281 [12.95]	469 [21.66]
6	17.73 [7.57]	14.82	13.21 [2.78]	151 [30.44]	33 [29.60]	313 [30.04]	439 [31.84]
7	17.11 [7.76]	14.56	12.79 [1.25]	113 [18.96]	23 [44.61]	325 [17.43]	445 [22.12]
8	17.55 [7.10]	14.55	12.88 [0.47]	107 [5.99]	30 [6.67]	382 [12.64]	693 [21.83]
9	16.89 [6.42]	13.54	12.98 [1.15]	121 [12.59]	28 [12.39]	276 [14.71]	486 [32.25]

10	17.63 [8.39]	14.43	13.47 [1.21]	208 [14.16]	36 [38.49]	386 [23.90]	335 [27.28]
11	13.53 [10.84]	10.09	13.24 [1.63]	128 [20.22]	39 [16.81]	462 [8.96]	1743 [13.03]
12	14.41 [9.16]	11.42	13.09 [1.30]	116 [11.15]	31 [7.53]	624 [11.49]	1240 [16.73]
13	17.26 [7.71]	13.48	12.9 [1.17]	114 [8.13]	28 [9.1]	298 [26.10]	562 [24.29]
14	16.33 [8.47]	12.23	13.08 [0.91]	131 [15.32]	21 [5.41]	288 [17.24]	524 [27.31]
15	15.6 [8.02]	12.01	13.4 [2.68]	164 [18.52]	45 [11.11]	496 [35.74]	756 [31.22]
16	14.77 [5.53]	12.46	12.67 [0.46]	110 [9.84]	22 [52.28]	279 [9.77]	1444 [8.62]
17	17.11 [7.80]	14.31	12.95 [0.73]	109 [32.53]	30 [43.78]	438 [6.73]	995 [29.47]
18	17.58 [8.45]	12.59	13.14 [3.99]	161 [33.23]	35 [37.80]	234 [25.53]	377 [21.14]
19	16.8 [6.33]	13.68	13.18 [0.55]	133 [10.29]	31 [26.36]	360 [30.84]	579 [36.31]
20	16.98 [9.40]	12.79	13.45 [1.85]	198 [10.24]	35 [48.57]	374 [17.35]	312 [7.22]

5.3.2.2 Fitted equations

Based on the experimental data, second-order equations were employed to fit the relationships between the three chosen variables and responses, as shown in Table 5-12. Except for neps (+140%), the R^2 values of all expressions exceed 0.7, which indicates that all the equations fitted well with the results and the obtained equations can well explain the effect of each variable on the responses. However, the equation for neps can not match well with the model, thus the analysis on neps from the fitted model is not convincing.

Table 5-12 Fitted equations of Ne 40 yarns in coded values

Yarn properties	Response surface equations	R^2
Tenacity	$16.9354+1.0856X+0.3558Y+0.6229Z-0.2456X^2-0.1519Y^2$ $-0.3463Z^2-0.1713XY-0.4237XZ-0.0738YZ$	0.949
Evenness	$13.0241-0.0283X-0.0597Y+0.1781Z+0.0536X^2+0.0412Y^2$ $+0.0288Z^2+0.0675XY+0.0725XZ+0.035YZ$	0.757
Thin places (-40%)	$127.528+1.238X-2.796Y+28.41Z+7.804X^2+3.915Y^2$ $8.157Z^2+6.75XY+5.75XZ+10.5YZ$	0.836
Thick places (+50%)	$26.5947-1.3679X-2.2533Y+2.6993Z+3.5933X^2+2.1791Y^2$ $1.1184Z^2+3.125XY+0.375XZ-0.375YZ$	0.712
Neps (+140%)	$306.359-69.815X-3.574Y-11.366Z+43.745X^2+27.835Y^2$ $+24.476Z^2-5.625XY+9.125XZ-16.625YZ$	0.614
Hairiness (S3)	$497.46-185.53X-96.52Y-326.63Z+56.17X^2+75.79Y^2$ $+162.59Z^2+33.62XY+91.12XZ+66.13YZ$	0.946

5.3.2.3 Model validation

The regression models were also investigated by nine sets of randomly selected data. As shown in Table 5-13, the estimated results generally agreed well with the experimental data, particularly for tenacity and evenness. Errors between the estimated and experimental values were mainly less than 15%, expect for neps (+140%). All the above results implied that the reduced regression equations provided sufficient accuracy for predicting the responses. Based on the analysis above, the reduced regression models were capable of estimating and explaining the actual relationships between yarn properties and the various system parameters of twist factor, speed ratio and wrap angle.

Table 5-13 Model verifications for 9 cases

Order	1	2	3	4	5	6	7	8	9
Twist factor	3.0	3.0	3.2	3.2	3.2	3.4	3.4	3.6	2.8
Speed ratio	1.2	1.7	2.2	1	2	1.5	2.5	1	2.5
Wrap angle	30	40	50	35	45	25	55	50	50

Tenacity	A	13.62	15.49	17.04	15.02	17.42	16.78	17.32	17.85	15.80
	P	13.90	15.80	17.36	15.55	17.27	16.57	17.25	17.32	15.86
	E (%)	**2.06**	**2.00**	**1.87**	**3.41**	**0.86**	**1.25**	**0.42**	**2.97**	**0.38**
Evenness	A	13.34	13.32	13.18	13.23	13.02	12.89	13.24	13.06	13.13
	P	13.25	13.10	13.2	13.19	13.09	12.82	13.56	13.37	13.16
	E (%)	**0.67**	**1.65**	**0.15**	**0.30**	**0.54**	**0.54**	**2.42**	**2.37**	**0.23**
Thin places(-40%)	A	135	122	152	159	139	123	242	157	156
	P	145	133	167	140	143	112	226	171	171
	E (%)	**7.40**	**9.02**	**9.87**	**11.95**	**2.88**	**8.94**	**6.61**	**8.92**	**9.62**
Thick places(+50%)	A	35	32	26	41	27	24	34	34	31
	P	38	31	29	35	27	26	39	39	34
	E (%)	**8.57**	**3.13**	**11.54**	**14.63**	**0.00**	**8.33**	**14.71**	**14.71**	**9.68**
Neps(+140%)	A	421	442	402	443	359	301	382	442	756
	P	451	395	324	387	309	323	341	454	602
	E (%)	**7.13**	**10.63**	**19.40**	**12.64**	**13.93**	**7.31**	**10.73**	**2.71**	**20.37**
Hairiness(S3)	A	1542	729	399	1182	402	982	532	551	797
	P	1472	706	373	1079	375	1056	557	498	725
	E (%)	**4.54**	**3.16**	**6.52**	**8.71**	**6.72**	**7.53**	**4.70**	**9.62**	**9.03**

5.3.2.4 Effects of control variables on the responses

Figure 5-17 shows the effects of twist factor, speed ratio and wrap angle on yarn mean tenacity. As a whole, yarn mean tenacity increases with the increments of three factors in the entire optimization region, in which twist factor has the highest impact on yarn mean tenacity, followed by wrap angle and speed ratio. In the low twist region, the adoption of a larger wrap angle can significantly enhance the yarn tenacity, however this effect is greatly reduced in case of a high twist factor.

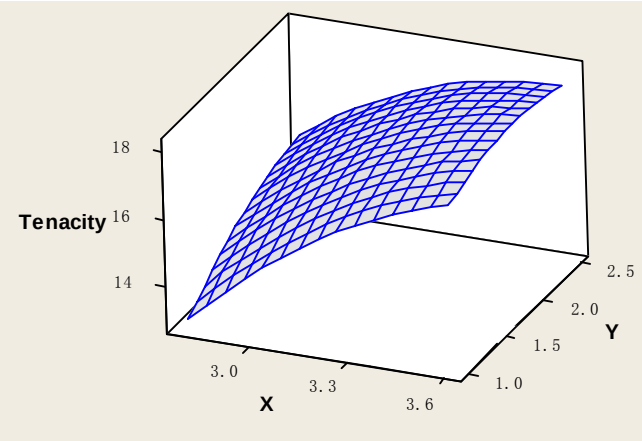

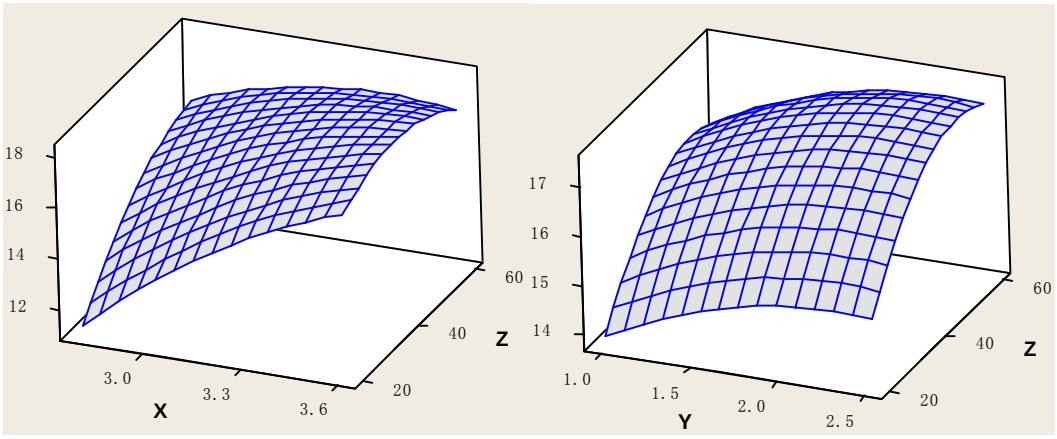

Figure 5-17 Effects of three factors on yarn mean tenacity

Figure 5-18 displays the effects of three factors on yarn evenness. In the traditional ring spinning system, the evenness of yarn becomes better with the increase in twist, but this is not likely the case in Nu-torque system. It can be found in Figure 5-18 that for a fixed wrap angle, 40^{o} for instance, the optimal value of yarn evenness appears at a twist factor of about 3.2 and speed ratio of about 2.0. Generally, wrap angle has a negative impact on yarn evenness, the greater the wrap angle, the worse the evenness. Speed ratio has the weakest effect on yarn evenness, and its role and value are depended by the other two factors.

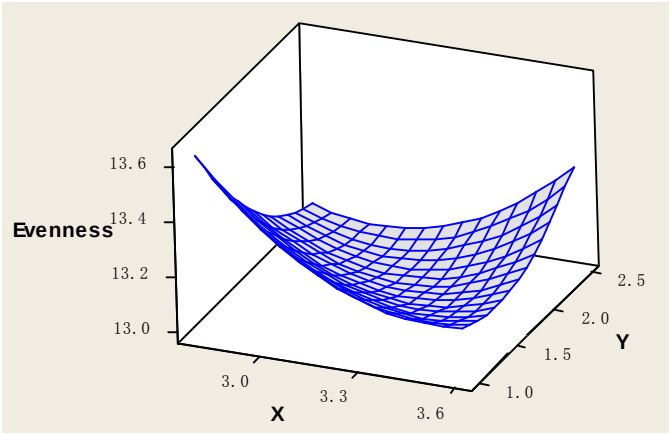

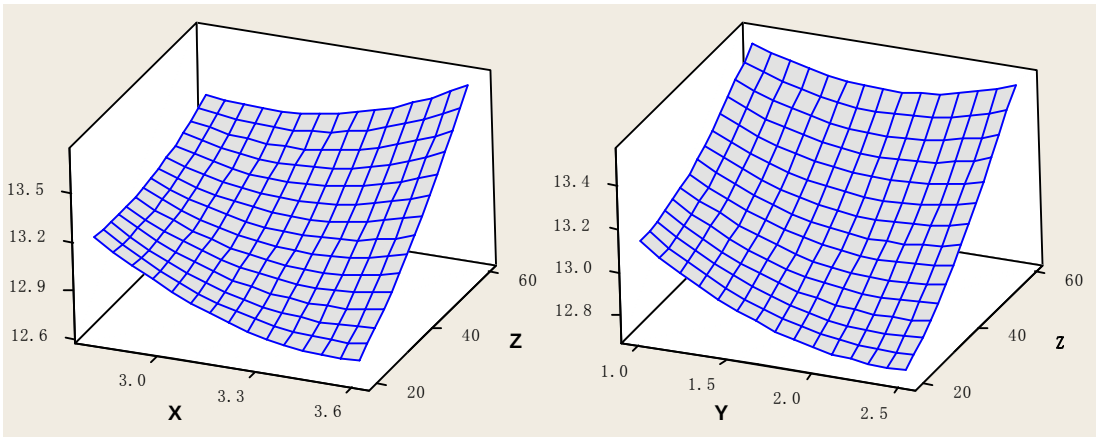

Figure 5-18 Effects of three factors on yarn evenness

Figure 5-19 shows the effects of three factors on thin places (-40%), which have the similar trends as those effects on yarn evenness shown in Figure 5-10. The thin places (-40%) more than twice as the wrap angle increases from 20° to 60°. Wrap angle and twist factor have much weaker effects on yarn thin places (-40%) than wrap angle.

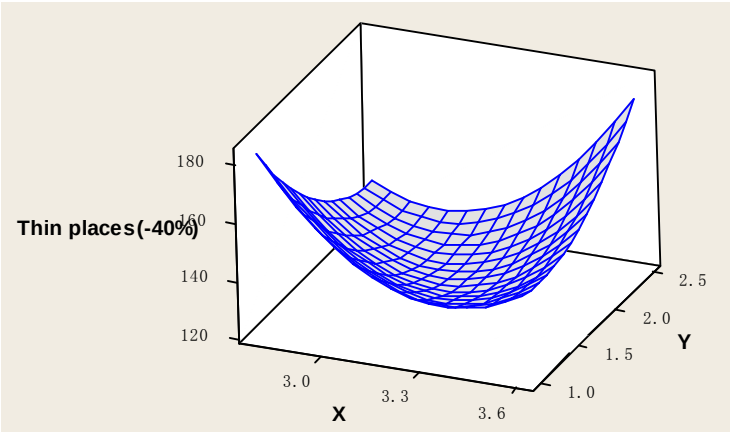

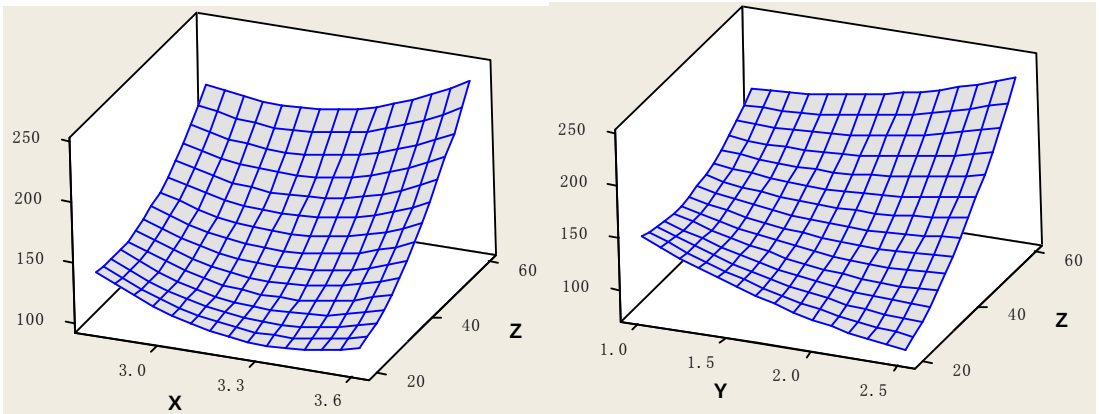

Figure 5-19 Effects of three factors on thin places (-40%)

Figure 5-20 shows the effects of three factors on yarn thick places (+50%). As the twist factor increases from 2.8 to 3.6, the yarn thick places (+50%) decreases initially and reaches a minimum value at around 3.3, then goes up. Similar trend can be found in speed ratio. It is implied from Figure 5-20 that wrap angle has a negative effect on thick places (+50%). Therefore, it is not suggest to use high wrap angle due to the deterioration of yarn thick places (+50%).

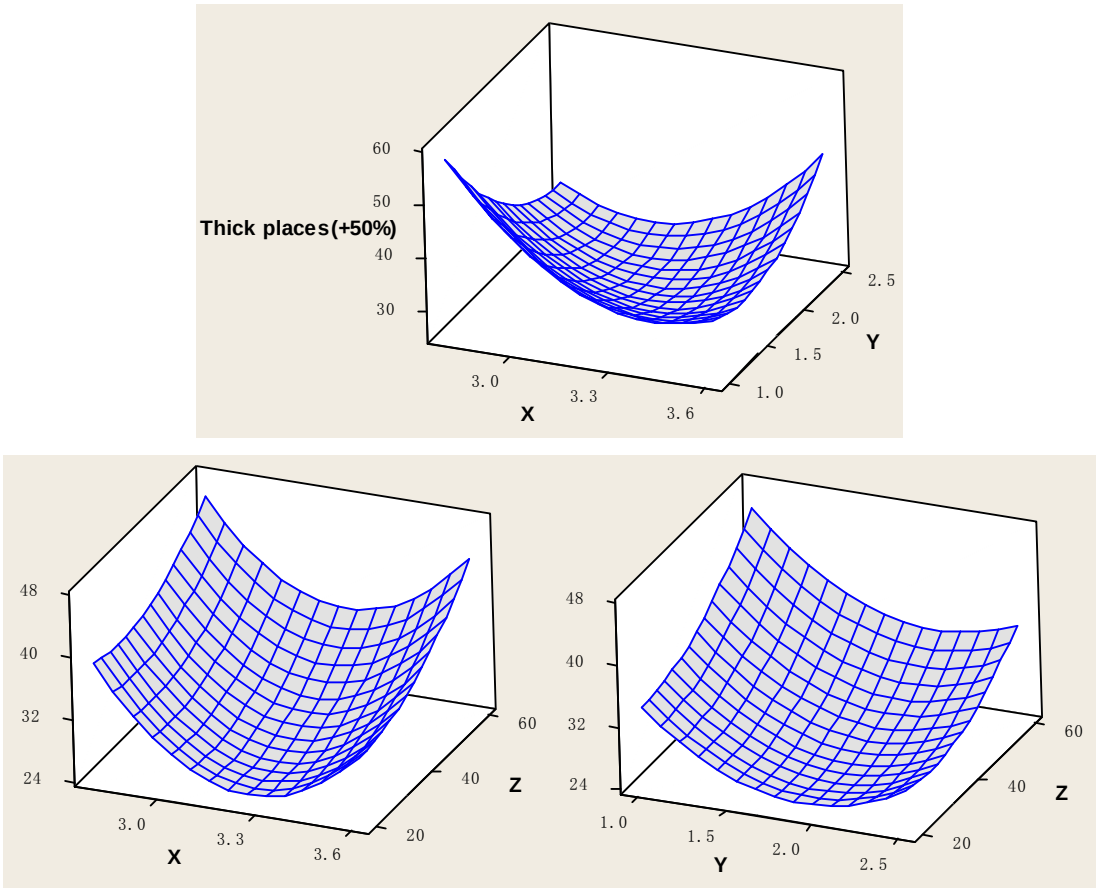

Figure 5-20 Effects of three factors on thick places (+50%)

Figure 5-21 illustrates the trends of three factors on neps, but the experimental data were not fitted well with the model listed in Table 5-12, which means that the trends of three factors may not account for the fact. In terms of the fitted model, it can be found that twist factor has a lead effect to control yarn neps (+140%); the higher the twist factor, the lower the yarn neps. However the objective of this study is to use lower yarn twist to obtain a soft handle feeling and low twist yarn. Therefore, it needs to find a balance point to meet both demands. Wrap angle and speed ratio also have some effects on neps (+140%), reaching the best result at speed

ratio of 2.0 and wrap angle of 43°.

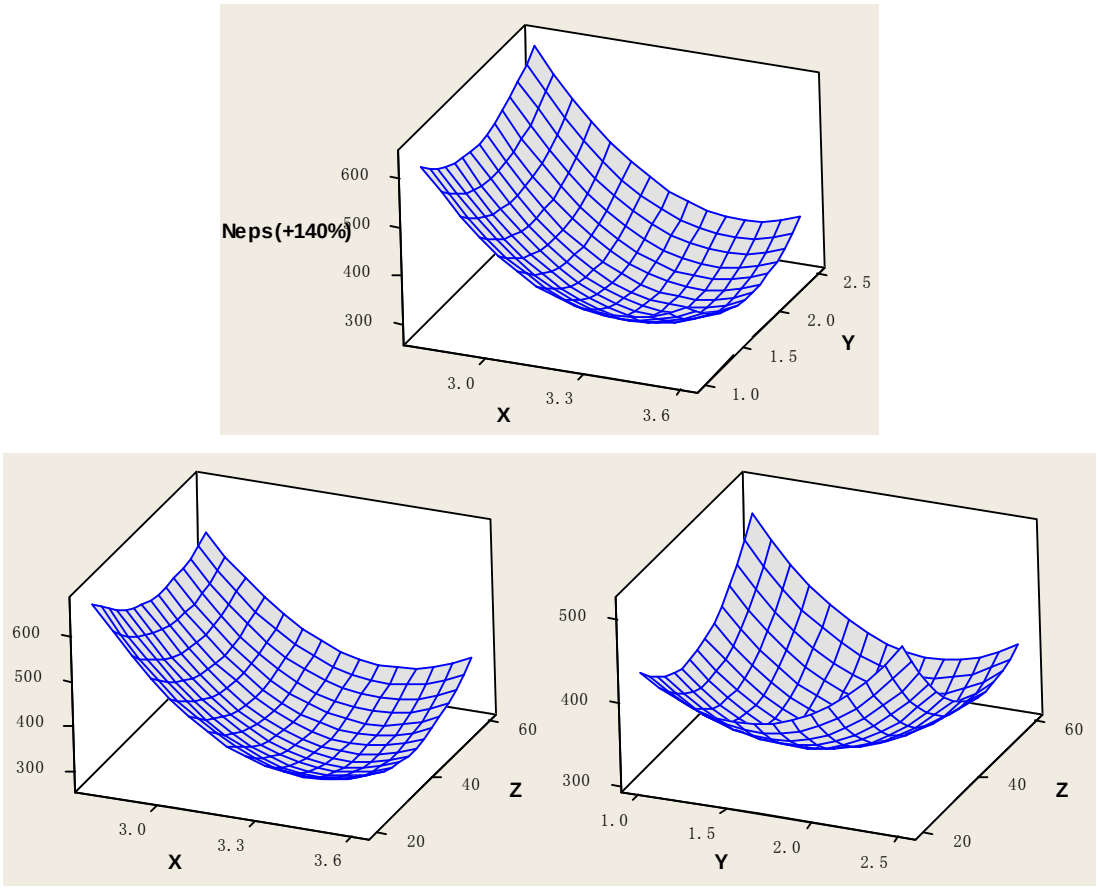

Figure 5-21 Effects of three factors on neps (+140%)

Figure 5-22 demonstrates the effects of three factors on yarn hairiness. Wrap angle plays a key role in hairiness reduction; with wrap angle increasing from 20° to 60°, yarn hairiness is cut more than 70%. Twist factor also plays a positive role in hairiness reduction, especially in the case of lower wrap angle. Speed ratio contributes less to yarn hairiness, and its optimized value is around 2.0 in the whole region. Therefore, in order to produce yarn with least hairiness, it is suggested to choose a high twist factor and wrap angle together with a middle level of speed ratio.

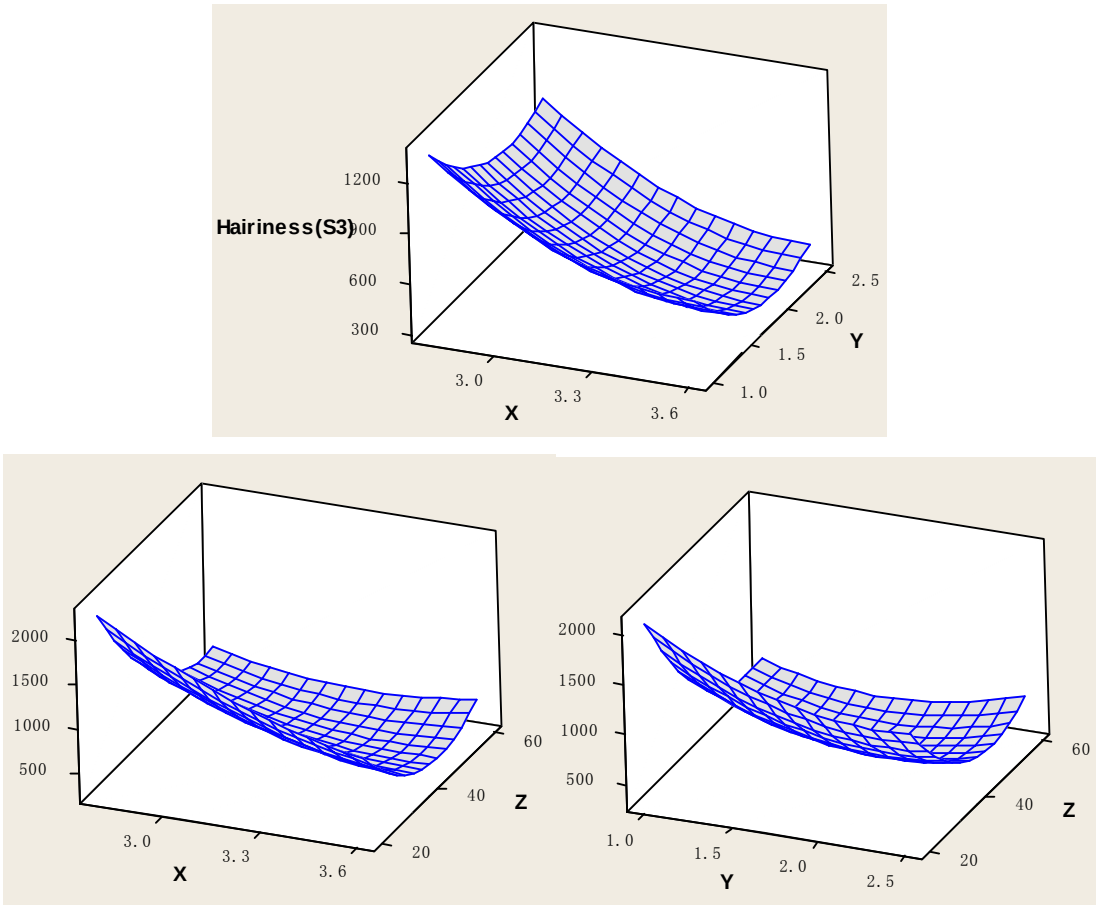

Figure 5-22 Effects of three factors on hairiness (S3)

5.3.2.4 Optimization of yarn properties

The overlaid contour plot was employed to analyze the RSM experiments. In this step, the upper and lower boundaries of each objective need to be specified. As shown in Figure 5-23, the mean tenacity of Ne 40 cotton yarn was set in the range of 17 to 20 cN/tex. For yarn evenness, the objective CVm% was higher than 11 and lower than 13.1; thin places (-40%) from 50 to 140; thick places (+50%) from 10 to 30 and the neps (+140%) from 200 to 320. The boundary of yarn hairiness was 200 to 500. The blank area in Figure 5-23 was the desired optimization regions, in which any arrangement of three factors is capable of obtaining the yarn with the defined objective properties. From the above optimized regions, a set of spinning parameters was chosen to obtain the favourable yarn properties and the optimized spinning parameters are listed in Table 5-14.

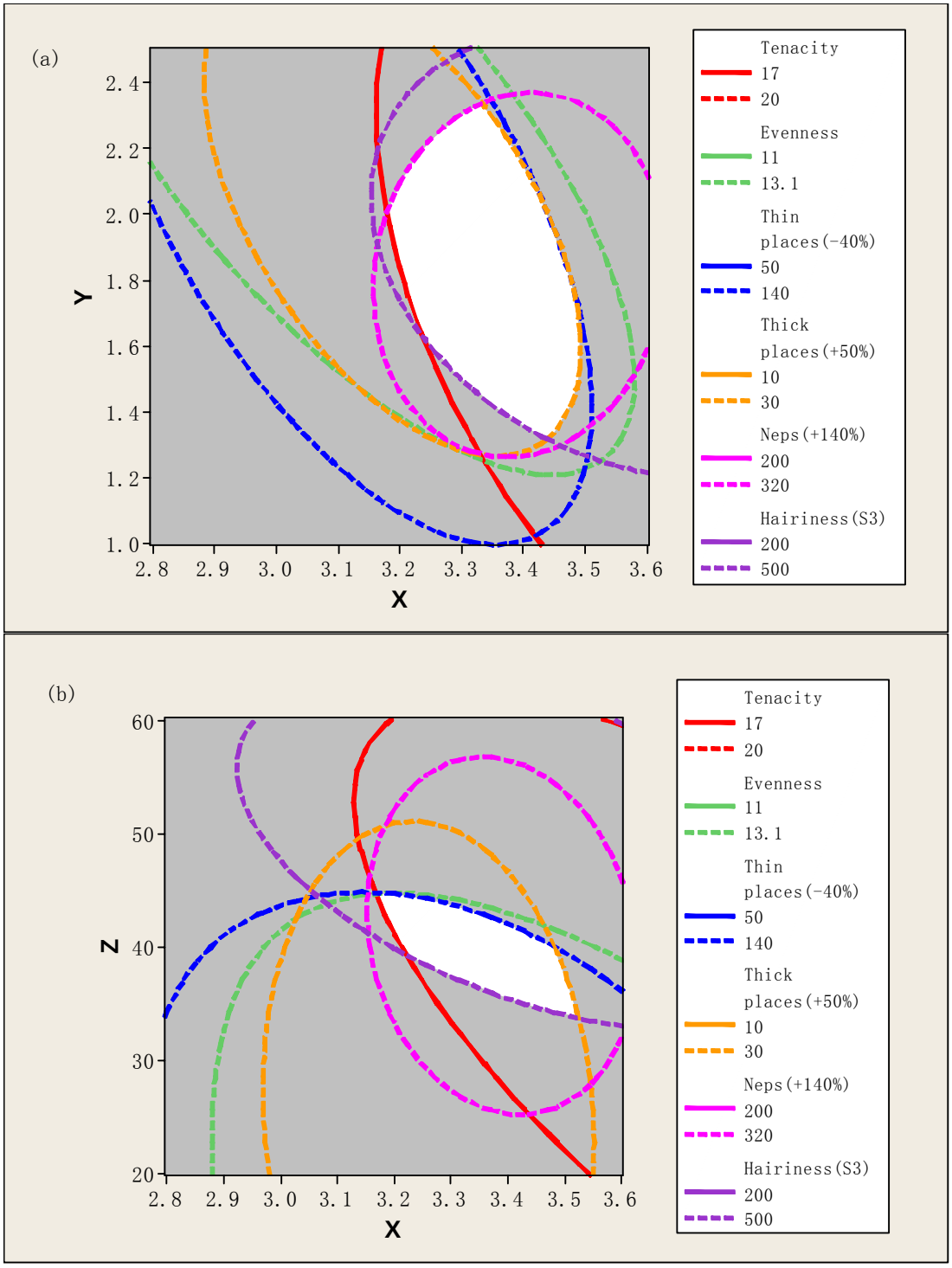

Figure 5-23 Overlaid contour plot of yarn performances

Table 5-14 The optimized parameters for Ne 40 cotton yarn

Purpose	Twist factor	Speed ratio	Wrap angle
Knitting	3.2	2.0	43

The properties of optimized and conventional yarns are presented in Table 5-15.

From Table 5-15, it can be found that the predicted properties of the optimized yarn match well with the experimental data with error percentage less than 13%. The estimated CVm% and thin places (-40%) were larger than the measured results; while the estimated values of yarn tenacity, thick places (+50%), neps (+140%) and hairiness were lower than the actual values.

Additionally, by comparing the properties of the optimized yarns with that of conventional ring yarns with normal twist factor of 3.6, as shown in Table 5-15, the optimized yarn with 11.1% twist reduction apparently outweighed the conventional yarns in hairiness and has slight improvements in yarn evenness and thick places (+50%); whereas the neps (+140%) of the optimized yarns was 50% worse than that of the corresponding ring yarns. Compared with the conventional ring yarns with the same twist factor, the optimized yarns has 1.26 cN/Tex higher in tenacity and much less hairiness.

In order to make a contrastive analysis of the yarns produced in single-belt and double-belt systems, a systematic optimization for the double-belt system was carried out based on the same belt and raw material, and the optimization details are shown in Appendix C. The optimized yarns in double-belt system with 22.2% twist reduction shows 0.83 cN/Tex weaker in tenacity, mild improvements in evenness, thin places (-40%) and thick places (+50%), significantly hair control ability whereas 37.35% more neps (+140%) compared to that of single-belt system.

Table 5-15 Properties of the optimized and conventional yarns

Ne 40 yarn	Tenacity (cN/Tex) [cv%]	Mini. Tenacity	Evenness CVm% [cv%]	Thin places (-40%) [cv%]	Thick places (+50%) [cv%]	Neps (+140%) [cv%]	Hairiness (S3) [cv%]
Conv TF3.6	17.59 [7.50]	14.23	12.71 [1.23]	110 [7.27]	34 [29.85]	224 [14.75]	1321 [27.76]
Conv TF3.2	16.16 [5.80]	13.10	12.93 [1.11]	114 [23.25]	30 [7.53]	215 [17.84]	1611 [26.76]
Double-belt	16.59 [8.30]	12.56	12.60 [0.67]	106 [6.76]	23 [49.73]	467 [19.38]	217 [18.53]
Optimized	17.42	14.70	12.88	134	31	340	439

	[7.50]		[2.94]	[31.73]	[41.18]	[24.44]	[24.73]
Predicted	17.21	/	13.05	136	27	309	405
Error (%)	1.21	/	1.32	1.49	12.90	9.12	7.74

The blackboard evenness of the optimized and conventional yarns were tested and evaluated according to ASTM D2255 standard. The grade is based on fuzziness, neppiness, unevenness, and visible foreign matter. Table 5-16 and Figure 5-24 apparently depict that the optimized yarns produced in single-belt system is half grade lower than that of the conventional ring yarns, but half grade higher than that of the optimized yarns spun in double-belt system.

Table 5-16 Blackboard evenness of the optimized and conventional yarns

Yarn code	Conv TF3.6	Double-belt	Single-belt
Grade	A [4.32]	B [5.04]	B+ [5.21]

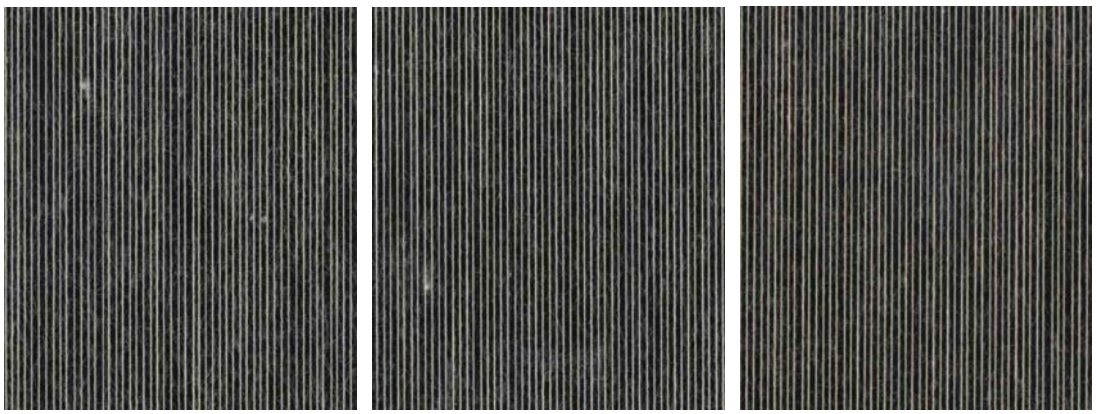

(a) Conv TF3.6 (b) Double-belt (c) Single-belt

Figure 5-24 Scanned images of blackboard evenness

5.4 Further Investigation on Yarn Neps

5.4.1 The occurrence of neps during spinning

In order to overcome the occurrence of neps, which so far becomes the bottleneck for further developing this technique, we have studied the mechanism for neps generation and promising solutions to alleviate or diminish such yarn

imperfections have also been put out. By our limited understanding, several reasons may account for it.

Neps generated in this system are mainly caused by rearrangement of the surface fibers along yarn axis. Firstly, it was found by the experiments that neps occurred in the condition of a low twist factor. Actually, the yarn undergoes an untwisting process on the belt, from high twist in the entrance of the belt to low twist in the exit. For the yarn in high-twist state, the surface fibers are densely packed and many long protruding fibers are held tightly together with the relatively low yarn tension at the entrance of the belt, thus the friction with the belt will not cause severe surface fiber migration, whereas for the yarn in low-twist state, the surface fibers may be in a loose state and the yarn tension is in a high level depending on the wrap angle, especially in cause of many long hairs protruding outside the yarn body, and the friction with the belt will easily cause yarn surface fiber movement, which in the end evolutes into a nep on the yarn surface.

Secondly, the moving directions between the yarn and belt at their contacting area are different, resulting in frictional force along the yarn delivery direction. As shown in Figure 5-25, in the spinning process, the belt moves right at a constant speed which turns the yarn, and at the same time the yarn slides across the belt which generates sliding friction. The frictional force between the yarn and belt can easily rearrange the loose surface fiber and generate the neps on the yarn surface.

Thirdly, the yarn transverse movement on the belt further deteriorate yarn surface morphology and force migration of the surface fiber along the yarn axis. High-speed photography was employed to capture the yarn movement on the belt, and then these images were processed by image processing techniques including filtering the original image to reduce the white noise, converting grayscale image into binary image by threshold, edge detection and coordinate extraction, and the results are shown in Figure 5-26. The sampling frequency was 100 Hz and total 4000 frames were recorded. The time domain data were also converted into frequency domain by Fast Fourier Transform, but the basic frequency was not found. The random movement of the yarn is a result of balancing yarn force and moment at any point-in-time. Yarn transverse movement deteriorates even twist distribution along yarn path, leading to weak points in the yarn, thus increases the chance of neps occurrence.

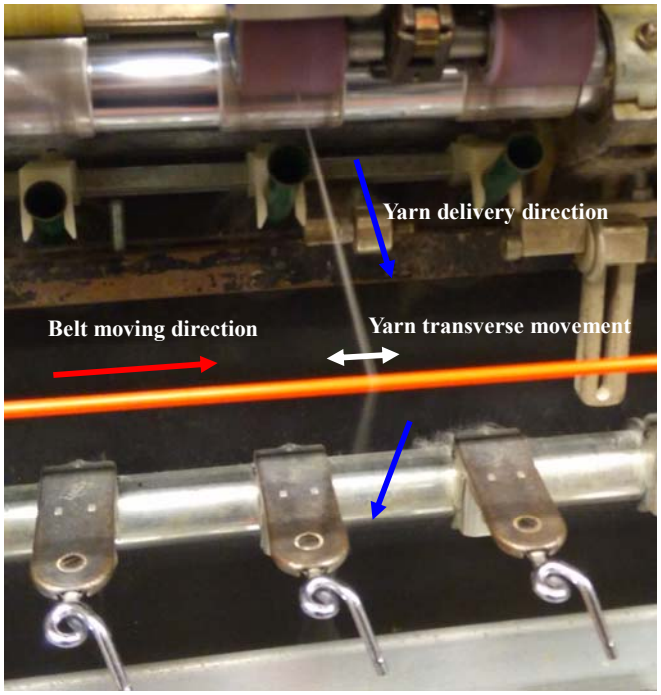

Figure 5-25 Movements of the yarn and belt in the system

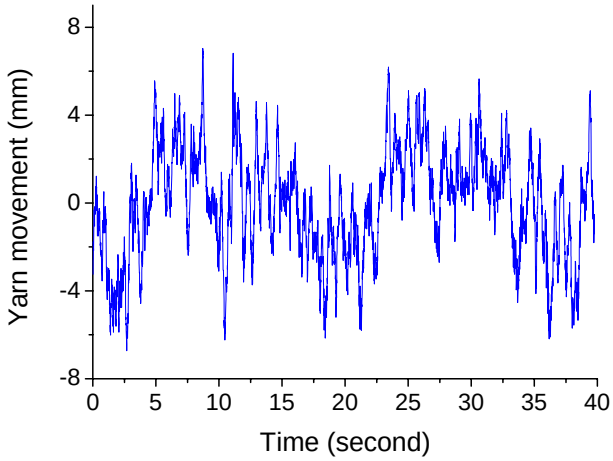

Figure 5-26 Transverse movement of the yarn on the belt

Accordingly, promising solutions to alleviate or diminish certain yarn neps during spinning are given. Firstly, the yarn neps may be suppressed by shortening yarn path on the belt. This can be achieved by either decreasing the yarn wrap angle or decreasing the belt diameter. Secondly, the yarn neps may be improved by introducing belts with hard surface and rough morphology. The textured belt can reduce the contacting area with the yarn and the belt with hard surface can change the contact deformation of the yarn, leading to a less neppiness yarn. Thirdly, the yarn neps can be effectively controlled by arranging the fibers in a completely

parallel and close position before untwisting is imparted. This can be accomplished by using Compact spinning technology. Since the fibers are well arranged and have less long fibers protruding outside the yarn body, this decreases the chance to form neps during untwisting process.

5.4.2 Improving yarn neps by shortening yarn path on the belt

As mentioned above, yarn neps may be controlled by shortening yarn path on the belt. Under the same wrap angle, yarn path can be reduced by applying smaller belt diameter. In order to verify the hypothesis, an experiment was conducted using belts with the same material and hardness but different yarn diameter. The belt with diameter below 3mm has low bending rigidity to hold itself from deformation when the forces act on the belt. The spinning parameters used for the experiment was the optimized values, and the results are shown in Table 5-17. It can be seen that as the belt diameter decreases from 6mm to 4mm and 3mm, the yarn paths on the belt under the same wrap angle are reduced by 33.33% and 50%, respectively, and the corresponding yarn neps are reduced by 10.88% and 27.06%, respectively. Therefore, the experiment well verifies the hypothesis, and a good agreement has been demonstrated. Moreover, the evenness, thick places and thin places are also improved as the belt diameter decreases, whilst yarn tenacity and hairiness are deteriorated.

Table 5-17 Yarn properties affected by belt diameter

Ne 40 yarn	Tenacity (cN/Tex) [cv%]	Mini. Tenacity (cN/Tex)	Evenness CVm% [cv%]	Thin places (-40%) [cv%]	Thick places (+50%) [cv%]	Neps (+140%) [cv%]	Hairiness (S3) [cv%]
85-6mm	17.42 [7.50]	14.70	12.88 [2.94]	134 [31.73]	31 [41.18]	340 [24.44]	439 [24.73]
85-4mm	16.84 [6.98]	14.42	12.88 [2.70]	119 [15.02]	19 [61.86]	303 [21.41]	624 [30.96]
85-3mm	16.90 [7.52]	14.28	12.82 [2.84]	104 [13.87]	21 [31.23]	248 [6.15]	846 [3.93]

5.4.3 Improving yarn neps by increasing belt hardness and surface roughness

As mentioned above, yarn neps may also be affected by belt hardness and surface roughness. An experiment was therefore designed to exam such effect and three belts with same diameter but different hardness and surface roughness were employed as shown in Table 5-18, in which 85-4mm belt was made of PU with a hardness of 85 shore A and smooth surface, 89T-4mm belt was made of PU with a hardness of 89 shore A and textured surface, whereas 40D-4mm belt was made of Polyester with a hardness of 40 shore D and smooth surface. The spinning parameters used for the experiment was the optimized values, and the results are shown in Table 5-18. It can be seen that the yarns produced by 85-4mm and 40D-4mm have the same amount of neps (+140%), which means the belt hardness is independent of the occurrence of neps (+140%). Moreover, the neps (+140%) for 89T-4mm is 384, 26.7% higher than the corresponding one produced by smooth belt, which indicates that the rough belt further deteriorates local deformation of surface fibers and causes more neps. Moreover, the yarn manufactured by the rough belt shows slightly higher tenacity and lower hairiness compared to smooth belts.

Table 5-18 Yarn properties affected by belt surface hardness and roughness

Ne 40 yarn	Tenacity (cN/Tex) [cv%]	Mini. Tenacity (cN/Tex)	Evenness CVm% [cv%]	Thin places (-40%) [cv%]	Thick places (+50%) [cv%]	Neps (+140%) [cv%]	Hairiness (S3) [cv%]
85-4mm	16.84 [6.98]	14.42	12.88 [2.70]	119 [15.02]	19 [61.86]	303 [21.41]	624 [30.96]
89T-4mm	17.35 [7.14]	14.59	12.94 [1.93]	112 [2.24]	17 [50.26]	384 [6.83]	515 [7.41]
40D-4mm	16.96 [7.15]	14.11	12.92 [1.16]	125 [20.21]	22 [30.03]	303 [18.69]	605 [8.88]

5.4.4 Improving yarn neps by controlling fibers in the spinning triangle

As mentioned above, yarn neps can also be improved by controlling fibers in the spinning triangle. Here, Rotorcraft RoCoS compacting device was attached in the

spinning frame and combined with the single-belt for the experimental verification. The 85-3mm belt was used for the experiment, and the optimized spinning parameters with twist factor of 3.2, wrap angle of 43^o and speed ratio of 2.0 was set . Table 5-19 illustrates the resultant yarn which was coded as SCM-43-3.2, from which it can be seen that the neps (+140%) is only 164 per km and this value is even better than the corresponding conventional ring yarn. The compact yarn with a twist factor of 3.2 was also spun for comparison. Although SCM-43-3.2 shows a slightly weaker yarn tenacity, it has slightly better evenness, much superior thin places (-40%), thick places (+50%), neps (+140%) and fantastic hairiness value than the compact yarn with the same twist factor.

In order to improve yarn tenacity in the combined system, the wrap angle was enlarged to 90^o by introducing a rotatable guide installed between the front rollers and the belt, as shown in Figure 5-27. The guide is made of Al_2O_3 ceramic with the properties of anti-static, low frictional resistance and high wear resistance. Low frictional resistance is important to diminish the yarn tension variation and twist blockage level when the yarn passes over the guide. The ceramic material is chosen because it has a low frictional coefficient with the yarn. The rotatable guide with rolling bearing is used to further reduce the friction, as shown in Figure 5-28. The surface smoothness of the ceramic reaches Ra 0.2, circular run-out is smaller than 0.15, and the material of the ceramic is 99% Al_2O_3 with hardness HRA 88 and density 3.85 g/cm^3. The spun yarn was coded as SCM-90-3.2, and the result is shown in Table 5-19. It indicates that as the wrap angle increases, the yarn tenacity and minimum tenacity can be greatly improved to 19.10 and 16.65 cN/Tex, respectively. Although yarn neps (+140%) is slightly deteriorated, its value is still better than the corresponding compact yarn. Moreover, the hairiness of SCM-90-3.2 is further improved by 12.33% against SCM-43-3.2 yarn..

The twist factor was further decreased from 3.2 to 2.8 in the combined spinning system to achieve a low residual torque and soft handle feeling yarn, and the data coded as SCM-90-2.8 are shown in Table 4-19. With 22.22% twist reduction, the SCM-90-2.8 yarn shows an acceptable but slightly weaker yarn tenacity, a little bit worse yarn evenness, thin places (-40%) and thick places (+50%), similar yarn neps (+140%), and one-order of magnitude lower hairiness than the corresponding conventional ring yarn with a twist factor of 3.6.

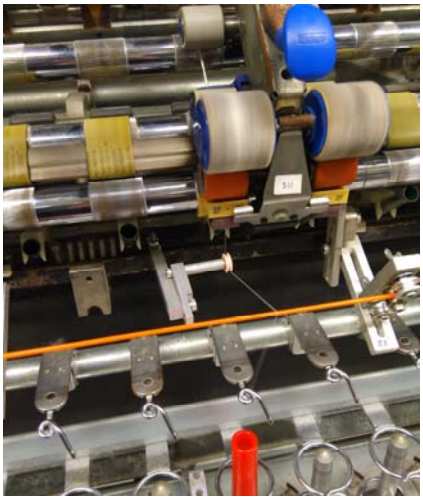

Figure 5-27 Enlarging wrap angle by introducing a rotatable guide

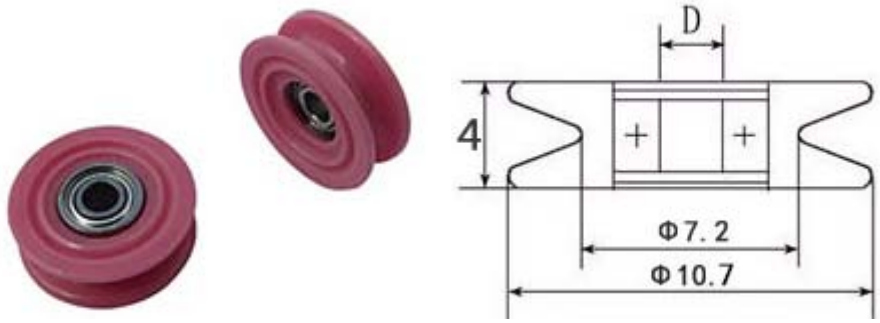

Figure 5-28 The rotatable guide (left) and its dimension (right)

Table 5-19 Yarn properties produced by the combination of Nu-Toruqe and Compact

Ne 40 yarn	Tenacity (cN/Tex) [cv%]	Mini. Tenacity (cN/Tex)	Evenness CVm% [cv%]	Thin places (-40%) [cv%]	Thick places (+50%) [cv%]	Neps (+140%) [cv%]	Hairiness (S3) [cv%]
SCM-43-3.2	17.59 [8.89]	13.63	12.23 [2.74]	64 [22.53]	17 [53.29]	164 [19.21]	73 [13.07]
SCM-90-3.2	19.10 [6.28]	16.65	12.93 [1.42]	134 [23.50]	35 [25.39]	201 [8.90]	64 [17.51]
SCM-90-2.8	17.08 [6.73]	14.12	13.19 [1.66]	133 [15.95]	44 [4.88]	225 [18.86]	125 [1.13]
CM-TF3.2	18.16 [5.96]	15.92	13.18 [1.48]	172 [10.46]	38 [51.50]	202 [18.37]	270 [38.07]

5.5 Summary

In this chapter, systematic investigation and evaluation of Ne 40 cotton yarns produced by the ring spinning system with single friction-belt false-twister have been carried out.

Firstly, the belt position in the spinning frame which determines wrap angle of the yarn and false-twister has been studied. Under the constraints that the yarn is prohibited to contact the front top roller, the variation of the wrap angle should be smaller than the corresponding frictional angle of the yarn guide, and the frictional angle of the yarn guide in the belt system should be smaller than that in the conventional system, it has been found that the maximum wrap angle in the single-belt system reaches only 50^{o}, and belt diameter has almost no effect on maximum wrap angle.

Based on the preliminary analysis of belt friction surface and geometry, it has been demonstrated that the belt with diameter 6mm and soft hardness of 85 shore A shows the highest twist above the false-twister, which means the false-twisting effect is related to not only the belt hardness but also the contacting yarn path depended by the belt diameter.

The belt with hardness 85 shore A, diameter 6mm and smooth surface which has demonstrated the highest false-twisting value among other belts was chosen for systematic investigation and optimization. Fractional factorial method has been employed to identify the significance of each spinning factor. According to the experimental results, twist factor, speed ratio and wrap angle were confirmed as the significant parameters on yarn properties in terms of tenacity, evenness, neps (+140%), and hairiness, therefore, these three parameters were selected for further study using response surface methodology to find the optimal value for yarn production. The second order equations were obtained to examine and estimate the relationships between the factors and responses, and the overlaid contour plot was employed to find the optimal results. The optimized yarn with 11.1% twist reduction apparently outweighed the conventional yarn in hairiness and has slight improvements in yarn evenness and thick places (+50%); whereas the neps (+140%) of the optimized yarn was 50% worse than that of the corresponding ring yarn.

In order to overcome the occurrence of neps, we have studied the mechanism for neps generation and promising solutions to alleviate or diminish such yarn

imperfection have also been put out. Neps generated in this system are mainly caused by rearrangement of the surface fibers along yarn axis. The yarn neps have been successfully suppressed by either shortening yarn path on the belt or arranging the fibers in a completely parallel and close position before untwisting is imparted, which have been verified by the experiments. It was also revealed from the experiments that the belt hardness is independent of the occurrence of neps (+140%) and the belt with rough surface morphology even deteriorates the situation. With the combination of compact device and belt-type false-twister, the wrap angle can be further enlarged by introducing a rotatable guide installed between the front roller and the belt to enhance the yarn tenacity and the twist factor can be further decreased from 3.2 to 2.8 to achieve a low residual torque and soft handle feeling yarns.

Chapter VI Performances of Knitted Fabrics Made from the Modified and Conventional Yarns

As introduced in Chapter 5, the Ne 40 modified yarns under 85-3mm belt demonstrated higher tenacity, comparable evenness and less hairiness than the conventional yarns with the same twist factor, as well as comparable tenacity, evenness and improved hairiness than the conventional yarns with a 12.5% higher twist factor. All of these characteristics in yarns may give rise to unique properties and performances of the resultant fabrics. For preparing fabric samples, quantities of the Ne 40 modified yarns as well as conventional yarns are spun, respectively. Then, the prepared cop yarns are wound on the cone before knitting. After that, three single yarns are fed into the gauge of flat knitting machine and the interlock structure is adopted to avoid the fabric spirality. Properties and performances of the knitted fabrics are evaluated and compared, including fabric weight, thickness, loop length, bursting strength, air permeability, thermal property, pilling resistance, etc.

6.1 Experimental

6.1.1 Yarn Preparation

The raw material used for the experiments was the same as those mentioned in Chapter 5. In this trial, all Ne 40 yarns were produced on the spinning fame Zinser 351. Three spindles were used for yarn production. Two types of yarns were spun, namely the conventional ring yarn with a twist factor of 3.6 and modified yarn using 85-3mm belt with a twist factor of 3.2. The details of yarn specifications are shown in Table 6-1.

Table 6-1 Yarn spinning parameters

Yarn code	Yarn count (Ne)	Twist factor	Speed ratio	Wrap angle	Traveller weight (mg)	Spindle speed (rpm)
Y-3.6C	40	3.6	/	/	30	13000
Y-3.2S	40	3.2	2.0	43	30	13000

After spinning, all yarns in cop form were wound on cones using SAVIO

automatic winding machine E1136047. The winding cleaner LOEPFE TK840 is closed so that all the yarn characteristics were kept and reflected on the fabrics. There is no waxing during the winding process.

6.1.2 Fabric Preparation

The cone yarns were knitted to produce plain fabrics. Since the gauge of the flat knitting machine is 14, three cone yarns were fed together into the knitting machine in order to produce the fabrics with normal tightness. The interlock structure was adopted to balance the residual torque of the cone yarns, avoiding spirality of the resultant fabrics. The interlock knitted fabrics were produced on STOLL CMS822, and the detailed knitting parameters are displayed in Table 6-2. Two types of fabrics were prepared made from the conventional yarns and the modified yarns, respectively.

Table 6-2 Knitting parameters

Code	Yarn	Structure	Speed(rpm)	Gauge	Tension (gf)
F-3.6C	3.6C	Interlock	200	14	2
F-3.2S	3.2S	Interlock	200	14	2

6.1.3 Testing Method

All yarn samples were conditioned under the standard conditions of 20±2℃ and 65±2% RH before testing. Yarn count, tenacity, evenness and hairiness were measured according to the standards and apparatus mentioned in Chapter 4. In addition, the surface characteristics of cone yarns were evaluated by blackboard evenness according to the standards ASTM D2255. Cone yarns were wrapped onto a blackboard at a density of 32 turns per inch by Zweigle yarn board winder, and were graded by three experts.

Before testing, all fabrics were conditioned at 20±2℃and 65±2% RH for 24 hours. The properties of the interlock fabrics were examined including fabric weight, thickness, loop length, bursting strength, pilling resistance, air permeability as well as thermal properties. The fabric weight, thickness and loop length were measured according to their specific standards, and the apparatus used for each testing are

listed in Table 6-3. Then the bursting strength of the fabrics were measured by the Instron according to the standard ASTM D6797. Three tests were measured and averaged. Fabric pilling resistance was tested by ICI pilling tester according to the standard ISO 12945-1. Four samples of each fabric with 125 x 125 mm were evaluated and averaged. The air permeability and thermal properties of the fabrics were tested by Kawabata Evaluation System (KES-F). Each properties were measured 5 times and averaged.

Table 6-3 Fabric testing standards and apparatus

Fabric properties	Standards	Apparatus
Weight	ASTM D3776: 2013	Textile testing and quality control equipment
Loop length	BS EN 14970: 2006	TAUTEX digital crimp tester
Thickness	ISO 5084: 1997	Feather touch thickness tester
Bursting strength	ASTM D6797: 2002	Instron 4411
Pilling	ISO 12945-1: 2000	ICI pilling tester
Air permeability	KES	KES-FB-AP1 tester
Thermal properties	KES	KES-F7 Thermo lab II

6.2 Results and Discussions

6.2.1 Yarn Properties

Table 6-4 exhibits the physical properties of Ne 40 cone yarns made by the conventional ring spinning and modified spinning methods, coded as C-3.6C and C-3.2S, respectively. The C-3.2S yarns show a higher minimum tenacity and better yarn hairiness, comparable mean tenacity, evenness and imperfection than the corresponding C-3.6C yarns. Moreover, the snarling of the modified yarns was 25% lower than the conventional ring yarns, which could bring about softer handle feeling of the resultant fabrics.

Table 6-4 Properties of the cone yarns

Yarn code	Tenacity (cN/Tex) [cv%]	Mini. Tenacity	Evenness CVm% [cv%]	Thin places (-40%) [cv%]	Thick places (+50%) [cv%]	Neps (+140%) [cv%]	Hairiness (S3) [cv%]	Snarling (turns/m)
C-3.6C	17.40 [7.16]	14.76	12.97 [0.39]	122 [10.29]	33 [19.64]	243 [3.39]	1562 [9.98]	96 [10.23]
C-3.2S	17.45 [7.20]	15.01	13.07 [0.27]	121 [19.67]	25 [16.97]	269 [1.42]	1186 [9.23]	72 [8.23]

The blackboard evenness of cone yarns made by the conventional spinning and modified spinning methods are displayed in Table 6-5 and Figure 6-1, from which it could be found that the blackboard evenness of C-3.2S yarns presents the same grade with that of C-3.6C yarns, which obtains the similar results as tested by USTERIII.

Table 6-5 Blackboard evenness of the Ne 40 cone yarns

Yarn code	C-3.6C	C-3.2S
Grade	B+ [5.32]	B+ [5.93]

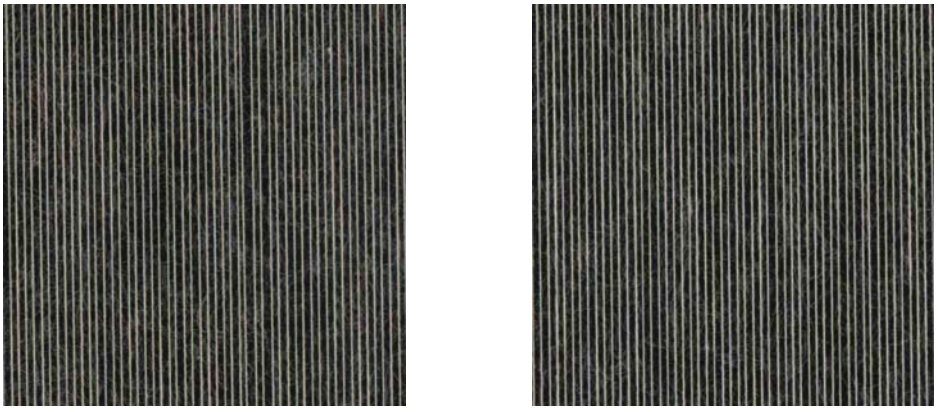

C-3.6C C-3.2S

Figure 6-1 Blackboard evenness of C-3.6C and C-3.2S cone yarns

6.2.2 Fabric Properties

The specifications of the fabrics made from C-3.6C and C-3.2S yarns are shown in Table 6-6, coded as F-3.6C and F-3.2s, respectively. It can be seen that F-3.6C

fabrics have heavier weight but less thick and shorter loop length than the F-3.2S fabrics, and the differences are statistically significant because the *p*-value is below 0.05. The difference in fabric weight is caused by the variation of the yarn count, the difference in thickness may be ascribed to the distinct difference in diameter of the two yarns, and the difference in loop length may be resulted from the systematic errors by knitting machine and measurement. The bulkiness of the fabrics was calculated by fabric weight and thickness, and the results indicates that the F-3.2S fabrics shows a 6.28% higher in bulkiness than that of the F-3.6S fabrics.

Table 6-6 Fabric specifications

Code	Weight (g/m^2)	Thickness (mm)	Loop length (mm)	Bulkiness (cm^3/g)
F-3.6C	339.93 [0.40]	1.702 [2.09]	5.80 [0.12]	1.974
F-3.2S	335.57 [0.65]	1.844 [1.56]	6.17 [0.94]	2.098
t-test (*p*-value)	0.06	0.00	0.01	-

In order to evaluate the mechanical strength of the knitted fabrics, tests of fabric bursting strength were conducted and the results are displayed in Figure 6-2. The bursting strength for the F-3.6C and F-3.2S fabrics are 715.53 and 707.92 N, respectively. Although the fabrics made by the modified yarns show a slightly weaker in bursting strength than that of the fabrics made by conventional ring yarn, the two fabrics are statistically no difference since the *p*-value of the t-test is very close to unity.

Fabric air permeability is related to fabric bulkiness when the raw material and fabric structure are the same. It is measured by the air resistance when the air flow permeates the fabric sample in thickness direction with a flow velocity of 1m/s. The lower the permeating resistance, the better the air permeability of the fabric. Figure 6-3 displays that the air permeability of the fabrics made from the modified yarns was 3.96% lower than that of the conventional yarns, therefore the F-3.2S fabrics had a relatively better air permeability, but the results were not statistically significant.

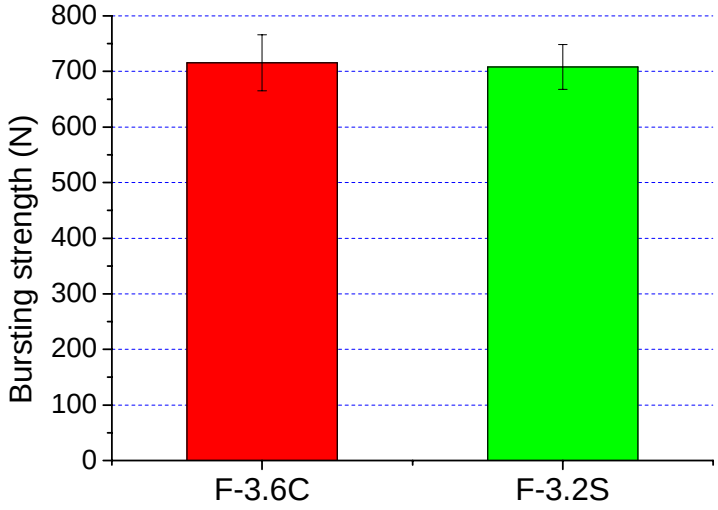

Figure 6-2 Bursting strength of knitted fabrics (t-test *p*-value: 0.85)

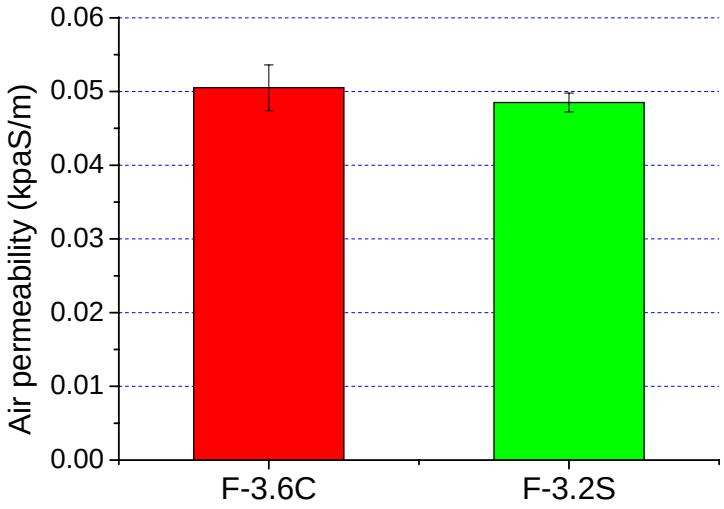

Figure 6-3 Air permeability of knitted fabrics (t-test *p*-value: 0.30)

The thermal properties of the fabrics were tested in terms of thermal conductivity (W/m^oC) and Q-max (W/cm^2). By comparing the measured data displayed in Figure 6-4 and 6-5, statistical significances were found between the two fabrics. According to Figure 6-4, F-3.2S fabrics show a 9.16% lower value in thermal conductivity than the F-3.6C fabrics, which indicates that the fabrics made from the modified yarns own a better capability of thermal insulation due to its relatively higher bulkiness. In addition, q-max measures the maximum value of heat current transferring onto the measured fabric when the heated plate touches the fabric surface. Actually, Q-max indicates the cool feeling of a person's experience when touches the tested fabric.

The higher the Q-max, the cooler the feeling. As shown in Figure 6-5, the Q-max of fabric samples for F-3.6C and F-3.2S are 0.0728 and 0.0644 W/cm^2, respectively, which implies that the fabrics made from the modified yarns have a warmer feeling than that of the fabrics made from the modified yarns.

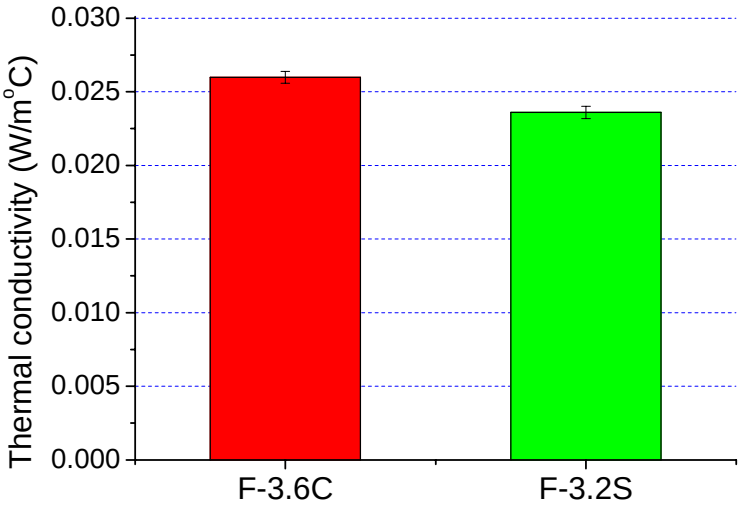

Figure 6-4 Thermal conductivity of knitted fabrics (t-test *p*-value: 0.00)

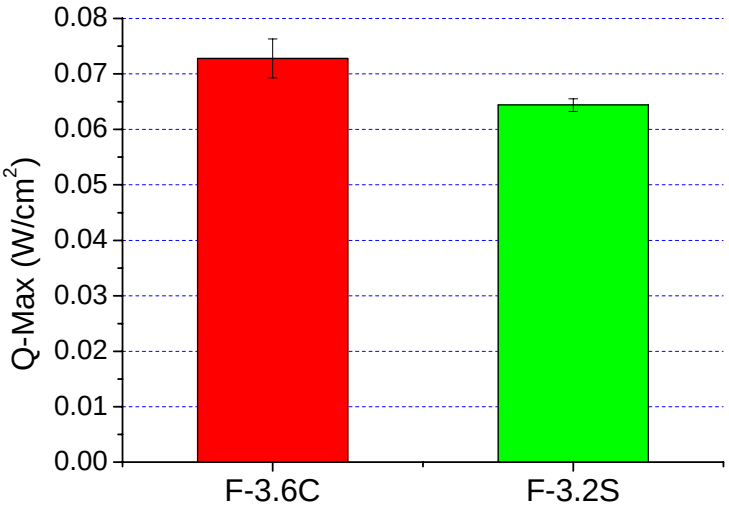

Figure 6-5 Q-Max of knitted fabrics (t-test *p*-value: 0.01)

Pilling tests unsightly appearance of fabric surface caused by the entanglement of loose fibers protruding from the fabric surface during wear and washing. Under the rubbing action these loose fibers form into small spherical bundles anchored to the fabric by a few unbroken fibers. In terms of pilling grade, the higher the value, the

better the fabric performance. As displayed in Figure 6-6, the pilling grades for both fabrics have the same value of 3.75, even though the twist factor of the modified yarns have a 11.11% twist lower than that of the conventional ring yarns.

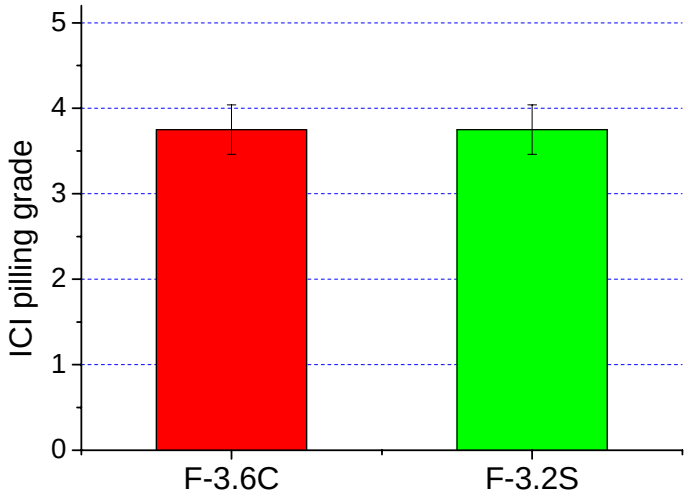

Figure 6-6 ICI pilling grade of knitted fabrics (t-test *p*-value: 1.00)

6.3 Summary

In this chapter, systematic evaluation of the surface appearance, physical properties of the fabrics made from the conventional ring yarns and modified yarns have been carried out. For preparation of fabric samples, quantities of Ne 40 modified yarns and conventional yarns were spun, and then these cop yarns wound on the cone and the winding cleaner was closed so that all the yarn characteristics were kept and reflected on the fabrics. Due to the large gauge of the flat knitting machine, three single yarns were fed into the gauge for producing fabrics with normal tightness. And the interlock structure was used to avoid the fabric spirality caused by the yarn residual torque since plying process was not adopted.

The modified cone yarns demonstrated a higher minimum tenacity, better yarn hairiness, 25% lower snarling, same blackboard evenness, as well as comparable mean tenacity, evenness and imperfection than the corresponding conventional yarns. The knitted fabrics made from modified yarns show a 6.28% higher in bulkiness than that of the conventional yarns, resulting to a better capacity of thermal insulation and warmer feeling. Moreover, these two fabrics show similar bursting strength and same pilling grade.

Chapter VII Conclusions and Future Work

This research work has provided a systematic and intensive study on yarn dynamics and properties in the ring spinning system with single friction-belt false-twister. Major findings and contributions of the work are concluded. Due to time and resource limitations, the research is far from being mature and complete, which needs further exploration in the future.

7.1 Conclusions

7.1.1 Yarn Dynamic Model

Twist generation and propagation are of particular interest in this study because they address several key questions including the amount of false-twist generated by the false-twister, false-twisting efficiency and blockage rate, as well as the relationships between false-twisting efficiency and system parameters.

To answer them, a theoretical model of yarn dynamics in a modified ring spinning system has been proposed in order to quantitatively characterize the twisting process, which deals with two important phenomena simultaneously, that is, twist generation and twist propagation. The model was validated by experiments and a good agreement has been demonstrated. For the first time, influences of several parameters on the twisting process have been revealed in terms of false-twisting efficiency, propagation coefficients of twist trapping and congestion.

Based on the proposed model, a systematic investigation has been carried out to evaluate the effects of system parameters on the false-twisting efficiency as well as propagation coefficients. Response surface methodology involving a central composite design in three factors of twist multiplier, speed ratio and wrap angle was successfully employed for the study and analysis. The reduced regression models were validated by normal probability analysis and another nine randomly selected experiments. The significant terms of the models were studied and it reveals that the speed ratio and wrap angle are statistically significant for the responses of twist efficiency, propagation coefficients of twist trapping and congestion. And more importantly, linear relationships were found among the three responses.

7.1.2 Yarn Kinematic Model

In this study, special attentions have been focused on twisting process because it is of great importance to determine the structure and properties of resultant yarn. Uniform twists inserted into the yarn ensure even features and good yarn quality. Twist variation in the spinning process may results in poor spinnability as well as uneven features or imperfections of the resultant yarns, such as strength deterioration, diameter irregularity and wrapping fibers along yarn length. On the other hand, for a stable process or product, it should permit a certain tolerance for the system variation or error.

Therefore, it is crucial to investigate the impinge of twisting robustness in the spinning process as well as evaluation of the yarn quality subject to external perturbations. Based on twist kinematics, equations were derived to evaluate the twist variations subject to external perturbations. The model was then verified by the experimental observations and a good agreement has been made. It has been proved by the experiment that with ±30% periodic variation in false twist, the yarn properties are not significantly affected. In another words, the current configuration and system parameters are stable and robust as well as have a high tolerance for twist variations.

The main purpose of this study was to assess the stability and robustness of the modified technique as well as comprehending the effect of system parameters on dynamical twist redistributions. At least, the results should give rise to a better comprehending of the mechanism of false-twister adopted in a ring spinning frame and provide method of calculating the practical levels of twist to reduce certain remarkable yarn faults.

7.1.3 Investigation of Yarn Properties

In order to solve the severe deterioration of yarn neps in the double-belt system, in this study systematic investigation of Ne 40 cotton yarns produced by the ring spinning system with the adoption of single friction-belt false-twister has been carried out. The study includes three aspects, namely belt geometric positions, system parameters, and physical properties of the belt.

Firstly, the belt position in the spinning frame which determines wrap angle of the yarn and false-twister has been studied. Under the constraints that the yarn is

prohibited contact the front top roller, the variation of the wrap angle should be smaller than the corresponding frictional angle of the yarn guide, and the frictional angle of the yarn guide in the modified system should be smaller than that in the conventional system, it has been found that the maximum wrap angle in the single-belt system reaches only 50^{o}, and belt diameter has almost no effect on maximum wrap angle.

Based on the preliminary analysis of belt physical properties and geometry, it has been demonstrated that the belt with diameter 6mm and soft hardness of 85 shore A shows the highest twist above the false-twister, which means the false-twisting effect is related to not only the belt hardness but also the contacting yarn path depended by the belt diameter.

The belt with hardness 85 shore A, diameter 6mm and smooth surface which has demonstrated the highest false-twisting value among other belts was chosen for systematic investigation and optimization. Fractional factorial method has been employed to identify the significance of each spinning factor. According to the experimental results, twist factor, speed ratio and wrap angle were confirmed as the significant parameters on yarn properties in terms of tenacity, evenness, neps (+140%), and hairiness, therefore, these three parameters were selected for further study using response surface methodology to find the optimal value for yarn production. The second order equations were obtained to examine and estimate the relationships between the factors and responses, and the overlaid contour plot was employed to find the optimal results. The optimized yarn with 11.1% twist reduction apparently outweighed the conventional yarn in hairiness and has slight improvements in yarn evenness and thick places (+50%); whereas the neps (+140%) of the optimized yarn was 50% worse than that of the corresponding ring yarn.

In order to overcome the occurrence of neps, the mechanism of neps generation has been studied and promising solutions to alleviate or diminish such yarn imperfection have also been put out. Neps generated in this system are mainly caused by rearrangement of the yarn surface fiber along its axis. The yarn neps can be successfully suppressed by either shortening yarn path on the belt or arranging the fibers in a completely parallel and close position before untwisting is imparted, which have been verified by the experiment. It was also found from the experiments that the belt hardness is independent of the occurrence of neps (+140%) and the belt with rough surface morphology even deteriorates the situation. With the combination

of compact device and belt-type false-twister, the wrap angle can be further enlarged by introducing a rotatable guide installed between the front roller and the belt to enhance the yarn tenacity and the twist factor can be further decreased from 3.2 to 2.8 to achieve a low residual torque and soft handle feeling yarns.

7.1.4 Evaluation of knitted Fabrics

The fabrics made from the modified yarns using 85-3mm belt were produced and then compared with the fabrics made from conventional yarns. For preparation of fabric samples, quantities of Ne 40 modified yarns and conventional yarns were spun, and then these cop yarns wound on the cone and the winding cleaner was closed so that all the yarn characteristics were kept and reflected on the fabrics. Due to the large gauge of the flat knitting machine, three single yarns were fed into the gauge for producing fabrics with normal tightness. And the interlock structure was used to avoid the fabric spirality caused by the yarn residual torque since plying process was not adopted.

The modified cone yarns demonstrate a higher minimum tenacity, better yarn hairiness, 25% lower snarling, same blackboard evenness, as well as comparable mean tenacity, evenness and imperfection than the corresponding conventional cone yarns. The knitted fabrics made from modified yarns show a 6.28% higher in bulkiness than that of the conventional yarns, resulting to a better capacity of thermal insulation and warmer feeling. Moreover, these two fabrics show similar bursting strength and same pilling grade.

7.2 Limitations and Future Work

Although the proposed work has been completed, there are still some limitations need to be improved in the future, which are summarised as follows.

Even though the theoretical model of yarn dynamics on single friction-belt false-twister has been established and is validated by experiments with a good agreement, this model can not predict the yarn motion without the boundary conditions obtained by the experiments, which constraints its wide application. In the current model, yarn twist at both ends are measured as inputs to solve the equations, because of the reason that the torsional rigidity of the yarn is not a constant value and

is varied with the spinning parameters.

For systematic investigation on single friction-belt false-twister system, the potential significant parameter yarn tension is not employed for the study and analysis. This is not only because its value can not be arbitrarily changed at such a wide range in industry production, but also the fact that it is not a continuously adjustable parameter for the experiment. Moreover, due to the time constraint, the investigation only covers single-belt system, therefore in the future, the systematic investigation on the double-belt system should be explored.

In the study of spinning process subject to external perturbations, a theoretical model is proposed based on yarn twist kinematics. In this model, several strong assumptions are used. Firstly, only twist variation is considered, while the influences of tension variation and their coupling term are neglected. Secondly, false-twisting efficiency, coefficients of belt twist congestion and trapping are constant throughout. This assumption is not strictly correct when the spinning parameters are varied from time to time, and only workable when the variation is small. Thirdly, the effects of twist blockage caused by the yarn guide and traveler are neglected. In fact, the twist blockage rates in these areas should be considered since they have the same magnitude. Moreover, the investigation mainly focuses on single belt, therefore in the future, the stability of the double-belt system should be explored.

Study of yarn properties of Ne 40 cotton yarns has revealed that the friction surface, specifically the interactive yarn path, has evident influence on yarn neps occurrence. In the future, experimental results can be further explained and verified by using the proposed dynamic model in Chapter 3, and the relationships between yarn path and yarn neps can be further digged out.

Last but not least, the current study primarily focuses on the cotton fiber and Ne 40 yarn count due to the time limitation. For further study, it is worthwhile exploiting a variety of other fiber types like wool, flax, polyester, viscose and their blends. In addition, it is recommended to study the possibility of using this technology to produce high count yarns for better performance and high add values.

Appendices

Appendix A: Jacobian matrix *A(x)*

$$\begin{bmatrix} \overline{|\mathbf{P}|}_1 \\ \vdots \\ \overline{|\mathbf{P}|}_n \\ \theta_1 \\ \vdots \\ \theta_n \\ \overline{T}_1 \\ \vdots \\ \overline{T}_n \\ \overline{K} \end{bmatrix}_{i+1} = \begin{bmatrix} \overline{|\mathbf{P}|}_1 \\ \vdots \\ \overline{|\mathbf{P}|}_n \\ \theta_1 \\ \vdots \\ \theta_n \\ \overline{T}_1 \\ \vdots \\ \overline{T}_n \\ \overline{K} \end{bmatrix}_i - \begin{bmatrix} \frac{\partial F_{1,1}(x_i)}{\partial \overline{|\mathbf{P}|}_1} & \cdots & \frac{\partial F_{1,1}(x_i)}{\partial \overline{|\mathbf{P}|}_n} & \frac{\partial F_{1,1}(x_i)}{\partial \theta_1} & \cdots & \frac{\partial F_{1,1}(x_i)}{\partial \theta_n} & \frac{\partial F_{1,1}(x_i)}{\partial \overline{T}_1} & \cdots & \frac{\partial F_{1,1}(x_i)}{\partial \overline{T}_n} & \frac{\partial F_{1,1}(x_i)}{\partial \overline{K}} \\ \vdots & \ddots & \vdots & \vdots & \ddots & \vdots & \vdots & \ddots & \vdots & \vdots \\ \frac{\partial F_{1,n-1}(x_i)}{\partial \overline{|\mathbf{P}|}_1} & \cdots & \frac{\partial F_{1,n-1}(x_i)}{\partial \overline{|\mathbf{P}|}_n} & \frac{\partial F_{1,n-1}(x_i)}{\partial \theta_1} & \cdots & \frac{\partial F_{1,n-1}(x_i)}{\partial \theta_n} & \frac{\partial F_{1,n-1}(x_i)}{\partial \overline{T}_1} & \cdots & \frac{\partial F_{1,n-1}(x_i)}{\partial \overline{T}_n} & \frac{\partial F_{1,n-1}(x_i)}{\partial \overline{K}} \\ \frac{\partial F_{2,1}(x_i)}{\partial \overline{|\mathbf{P}|}_1} & \cdots & \frac{\partial F_{2,1}(x_i)}{\partial \overline{|\mathbf{P}|}_n} & \frac{\partial F_{2,1}(x_i)}{\partial \theta_1} & \cdots & \frac{\partial F_{2,1}(x_i)}{\partial \theta_n} & \frac{\partial F_{2,1}(x_i)}{\partial \overline{T}_1} & \cdots & \frac{\partial F_{2,1}(x_i)}{\partial \overline{T}_n} & \frac{\partial F_{2,1}(x_i)}{\partial \overline{K}} \\ \vdots & \ddots & \vdots & \vdots & \ddots & \vdots & \vdots & \ddots & \vdots & \vdots \\ \frac{\partial F_{2,n-1}(x_i)}{\partial \overline{|\mathbf{P}|}_1} & \cdots & \frac{\partial F_{2,n-1}(x_i)}{\partial \overline{|\mathbf{P}|}_n} & \frac{\partial F_{2,n-1}(x_i)}{\partial \theta_1} & \cdots & \frac{\partial F_{2,n-1}(x_i)}{\partial \theta_n} & \frac{\partial F_{2,n-1}(x_i)}{\partial \overline{T}_1} & \cdots & \frac{\partial F_{2,n-1}(x_i)}{\partial \overline{T}_n} & \frac{\partial F_{2,n-1}(x_i)}{\partial \overline{K}} \\ \frac{\partial F_{3,1}(x_i)}{\partial \overline{|\mathbf{P}|}_1} & \cdots & \frac{\partial F_{3,1}(x_i)}{\partial \overline{|\mathbf{P}|}_n} & \frac{\partial F_{3,1}(x_i)}{\partial \theta_1} & \cdots & \frac{\partial F_{3,1}(x_i)}{\partial \theta_n} & \frac{\partial F_{3,1}(x_i)}{\partial \overline{T}_1} & \cdots & \frac{\partial F_{3,1}(x_i)}{\partial \overline{T}_n} & \frac{\partial F_{3,1}(x_i)}{\partial \overline{K}} \\ \vdots & \ddots & \vdots & \vdots & \ddots & \vdots & \vdots & \ddots & \vdots & \vdots \\ \frac{\partial F_{3,n-1}(x_i)}{\partial \overline{|\mathbf{P}|}_1} & \cdots & \frac{\partial F_{3,n-1}(x_i)}{\partial \overline{|\mathbf{P}|}_n} & \frac{\partial F_{3,n-1}(x_i)}{\partial \theta_1} & \cdots & \frac{\partial F_{3,n-1}(x_i)}{\partial \theta_n} & \frac{\partial F_{3,n-1}(x_i)}{\partial \overline{T}_1} & \cdots & \frac{\partial F_{3,n-1}(x_i)}{\partial \overline{T}_n} & \frac{\partial F_{3,n-1}(x_i)}{\partial \overline{K}} \\ \frac{\partial f_1(x_i)}{\partial \overline{|\mathbf{P}|}_1} & \cdots & \frac{\partial f_1(x_i)}{\partial \overline{|\mathbf{P}|}_n} & \frac{\partial f_1(x_i)}{\partial \theta_1} & \cdots & \frac{\partial f_1(x_i)}{\partial \theta_n} & \frac{\partial f_1(x_i)}{\partial \overline{T}_1} & \cdots & \frac{\partial f_1(x_i)}{\partial \overline{T}_n} & \frac{\partial f_1(x_i)}{\partial \overline{K}} \\ \vdots & \ddots & \vdots & \ddots & \vdots & \ddots & \vdots & \ddots & \vdots & \vdots \\ \frac{\partial f_5(x_i)}{\partial \overline{|\mathbf{P}|}_1} & \cdots & \frac{\partial f_5(x_i)}{\partial \overline{|\mathbf{P}|}_n} & \frac{\partial f_5(x_i)}{\partial \theta_1} & \cdots & \frac{\partial f_5(x_i)}{\partial \theta_n} & \frac{\partial f_5(x_i)}{\partial \overline{T}_1} & \cdots & \frac{\partial f_5(x_i)}{\partial \overline{T}_n} & \frac{\partial f_5(x_i)}{\partial \overline{K}} \end{bmatrix}^{-1} \begin{bmatrix} F_1(x_i) \\ \vdots \\ F_3(x_i) \\ f_1(x_i) \\ \vdots \\ f_5(x_i) \end{bmatrix}$$

Appendix B: Flow diagram of calculating the three coefficients

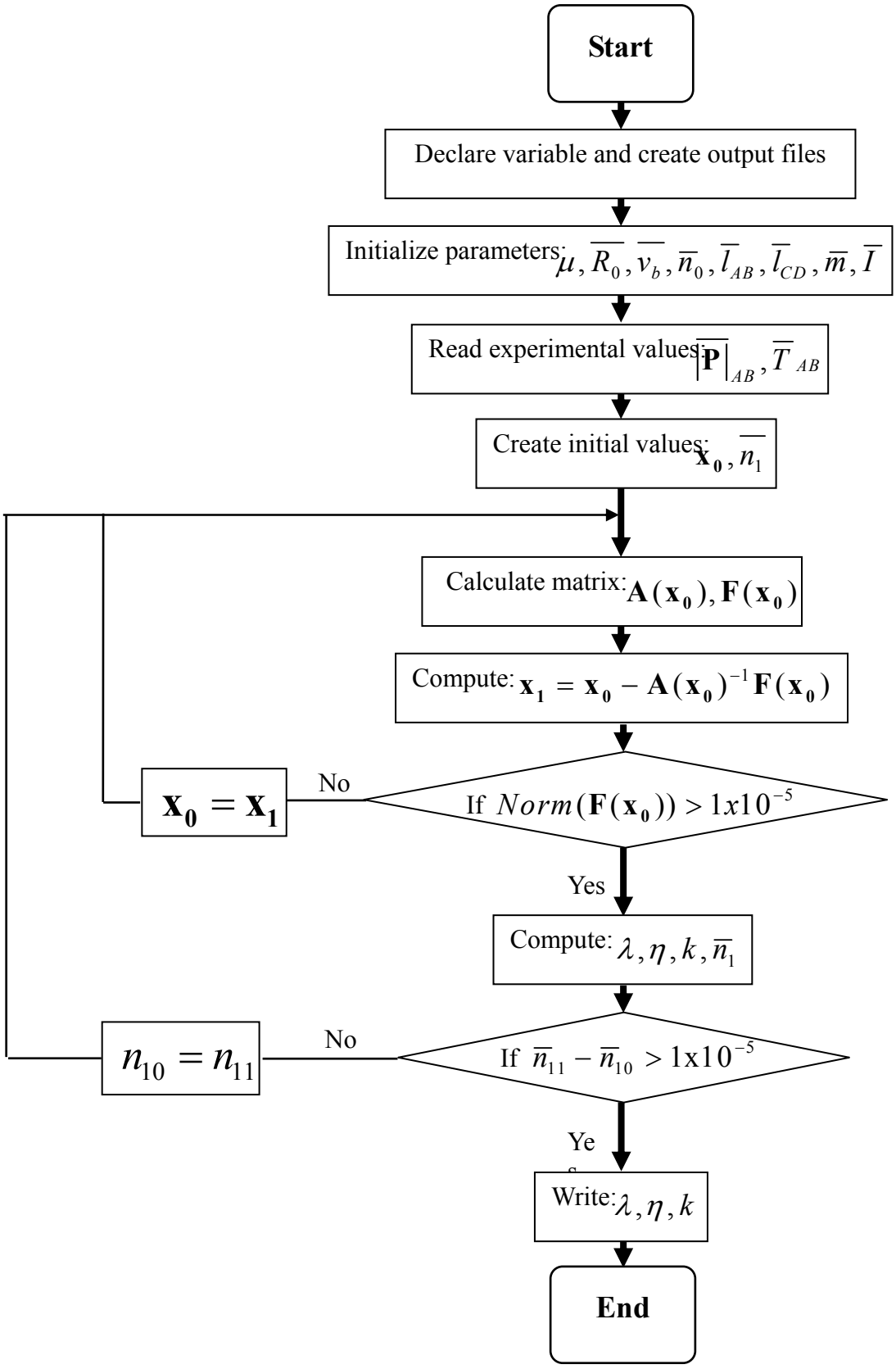

Appendix C: Parameter optimization in double-belt system

Based on the previous research [185], the most important spinning parameters that affect the modified spinning system with double-belt were twist factor, upper and lower speed ratios. For the modified system, the levels of speed ratios and twist factor that can produce a yarn with a low level of snarling but a high level of tenacity and good evenness and hairiness need to be found. To explore this region more closely, a Central Composite design to support a second-order response surface model was designed with 20 experimental runs. The raw material and testing method are the same as introduced in Chapter 4. The two belts used for this experiment were 85-6mm. With the help of response surface design, second-order polynomial response surface models are set-up to predict and explain the relationship between yarn properties and the three variables. Table C-1 and Table C-2 show the experimental variables and arrangements randomly generated by using the Minitab software. Table C-3 lists the measured physical properties of modified yarns.

Table C-1 Experimental variables and levels for optimization

Levels	Twist factor	Upper ratio	Lower ratio
+1.682	4.3	2.2	2.2
+1	3.87	1.92	1.92
0	3.25	1.5	1.5
-1	2.63	1.08	1.08
-1.682	2.2	0.8	0.8

Table C-2 Design matrix for optimization

Run Order	Twist Factor	Upper Ratio	Lower Ratio
1	3.25	1.50	1.50
2	2.63	1.08	1.92
3	3.87	1.92	1.08
4	2.63	1.08	1.08
5	3.87	1.08	1.92
6	4.29	1.50	1.50
7	3.25	1.50	1.50
8	3.25	1.50	0.79

9	3.25	2.21	1.50
10	2.21	1.50	1.50
11	3.25	1.50	1.50
12	3.87	1.08	1.08
13	3.25	0.79	1.50
14	3.25	1.50	1.50
15	3.25	1.50	1.50
16	2.63	1.92	1.08
17	3.87	1.92	1.92
18	3.25	1.50	2.21
19	2.63	1.92	1.92
20	3.25	1.50	1.50

Table C-3 Yarn properties of response surface analysis

Run Order	Tenacity (cN/Tex) [CV%]	Min Ten (cN/Tex)	Elongation (%)	CVm (%) [CV%]	/1000m						Hairiness (S3) (/100m) [CV%]	Snarling (/25cm) [CV%]
					Thin (-40%) [CV%]	Thin (-50%) [CV%]	Thick (+35%) [CV%]	Thick (+50%) [CV%]	NEP (+140%) [CV%]	NEP (+200%) [CV%]		
1	16.79 [11.81]	10.9	4.39	12.64 [1.24]	96 [34]	1 [223.61]	275 [5.24]	25 [32.66]	613 [25.86]	100 [24.45]	250 [38.79]	65 [7.29]
2	15.6 [8]	11.69	4.34	12.98 [1.1]	131 [5.64]	3 [115.47]	322 [11.67]	28 [41.34]	632 [21.3]	94 [30.81]	248 [33.76]	47 [7.84]
3	16.48 [13.69]	10.26	4.4	13.09 [1.47]	145 [21.84]	5 [60]	340 [16.82]	28 [58.68]	809 [26.22]	135 [40.23]	187 [49.45]	79 [5.75]
4	16.63 [7.83]	12.64	4.31	13.14 [1.62]	132 [14.27]	7 [47.43]	342 [8.91]	40 [36.32]	940 [31.55]	153 [31.93]	227 [44.14]	54 [4.01]
5	16.66 [12.55]	11.06	4.56	12.77 [1.05]	135 [6.26]	3 [124.09]	279 [10.36]	25 [13.19]	709 [34.15]	122 [29.73]	142 [45.36]	71 [7.37]
6	15.74 [13.75]	9.33	4.39	12.45 [1.98]	95 [18.09]	2 [136.93]	248 [13.28]	22 [36.54]	684 [40.59]	117 [33.27]	138 [59.18]	82 [3.89]
7	16.96 [11.21]	8.88	4.45	12.79 [0.39]	116 [15.59]	2 [113.86]	261 [19.57]	22 [62.57]	708 [31.61]	105 [36.35]	182 [46.62]	60 [4.3]
8	17.23 [10.81]	12.11	4.47	13.4 [0.84]	192 [14.25]	4 [77.06]	370 [10.58]	38 [18.98]	912 [17.42]	144 [20.24]	177 [46]	73 [5.31]
9	16.71 [12.57]	10.03	4.5	13.26 [1.04]	177 [8.38]	5 [100]	371 [12.67]	42 [32.5]	989 [21.85]	173 [26.24]	200 [45.37]	59 [7.95]

10	14.4 [9.06]	9.12	4.03	12.91 [1.33]	127 [10.7]	2 [136.93]	318 [8.44]	28 [27.55]	788 [29.3]	119 [38.93]	268 [35.18]	37 [9.46]
11	16.72 [12.15]	10.39	4.34	12.69 [1.51]	109 [19.45]	2 [81.31]	268 [16.08]	23 [26.45]	472 [24.28]	69 [18.16]	221 [56.76]	62 [4.99]
12	16.92 [12.39]	10.76	4.48	12.56 [1.46]	82 [11.91]	1 [136.93]	250 [18.15]	22 [18.98]	504 [26.82]	82 [18.66]	118 [57.15]	85 [2.93]
13	17.09 [9.63]	9.96	4.65	12.88 [0.49]	126 [15.47]	5 [42.43]	276 [6.1]	27 [18.46]	544 [17.32]	82 [26.06]	150 [22.71]	65 [5.63]
14	16.77 [12.49]	9.49	4.46	12.67 [1.01]	105 [16.78]	2 [0]	253 [16.92]	25 [19.92]	607 [14.6]	94 [31.01]	158 [33.58]	62 [6.33]
15	16.78 [11.97]	9.01	4.48	12.66 [1.58]	98 [42.5]	3 [148.12]	265 [9.37]	24 [36.15]	526 [19.9]	80 [37.16]	162 [20.05]	60 [8.19]
16	16.01 [9.55]	7.47	4.38	13.43 [1.05]	188 [15.66]	7 [94.76]	396 [9.59]	40 [16.66]	780 [16.63]	129 [11.87]	289 [26.2]	54 [6.74]
17	15.83 [14.27]	8.51	4.44	12.65 [1.68]	96 [23.6]	2 [113.86]	261 [8.46]	28 [36.72]	685 [19.49]	102 [24.91]	139 [42.61]	67 [8.94]
18	15.84 [13.01]	8.7	4.31	12.7 [1.48]	105 [15.27]	2 [173.21]	282 [7.3]	28 [34.6]	550 [18.44]	91 [26.73]	125 [17.03]	57 [7.79]
19	16.09 [9.23]	9.71	4.33	12.97 [0.77]	131 [14.86]	2 [113.86]	324 [11.59]	27 [43.31]	680 [10.67]	112 [26.04]	188 [16.07]	40 [14.84]
20	16.73 [12.08]	10.06	4.34	12.53 [1.29]	86 [33.09]	1 [136.93]	233 [7.64]	16 [53.53]	483 [11.16]	77 [7.9]	155 [28.01]	61 [7.42]

According to the analytical results generated by Minitab, the second-order models were established to examine the relationship between yarn properties and system parameters of twist factor (X1), upper ratio (X2), and lower ratio (X3) for Ne 40 modified yarns, as shown in Table C-4. The R^2 values in these equations are above 0.8 except for Neps (+140%), which indicates that these second-order models well fit the experimental results and a sufficient accuracy is provided to estimate yarn properties. Figure C-1 to C-7 display the relationship between three independent variables and seven responses.

Table C-4 The second-order response surface equations in coded units

Yarn properties	Response surface equations	R^2
Tenacity	$Y_2 = 16.7869 + 0.2792X_1 - 0.1493X_2 - 0.3074X_3 - 0.5777X_1^2 + 0.0693X_2^2 - 0.0597X_3^2 - 0.1425X_1X_2 + 0.005X_1X_3 + 0.09X_2X_3$	0.925
Evenness	$Y_5 = 12.6634 - 0.1628X_1 + 0.0973X_2 - 0.1484X_3 + 0.0057X_1^2 + 0.1436X_2^2 + 0.1365X_3^2 + 0.0163X_1X_2 + 0.0487X_1X_3 - 0.1187X_2X_3$	0.939
Thin places (-40%)	$Y_6 = 101.96 - 13.02X_1 + 12.14X_2 - 14.67X_3 + 1.37X_1^2 + 15.69X_2^2 + 14.63X_3^2 - 4X_1X_2 + 7.75X_1X_3 - 19.75X_2X_3$	0.872
Thick places (+50%)	$Y_7 = 22.551 - 3.082X_1 + 2.433X_2 - 2.842X_3 + 0.549X_1^2 + 3.907X_2^2 + 3.377X_3^2 + 1.25X_1X_2 + 3.5X_1X_3 - 0.5X_2X_3$	0.865
Neps (+140%)	$Y_8 = 569.39 - 36.6X_1 + 67.17X_2 - 68.52X_3 + 51.36X_1^2 + 62.14X_2^2 + 49.59X_3^2 + 49.12X_1X_2 + 61.13X_1X_3 - 15.13X_2X_3$	0.687
Hairiness (S3)	$Y_9 = 187.46 - 42.81X_1 + 11.14X_2 - 14.02X_3 + 8.81X_1^2 - 1.09X_2^2 - 9.57X_3^2 + 8X_1X_2 + 7X_1X_3 - 24.25X_2X_3$	0.805
Wet snarling	$Y_{10} = 61.669 + 13.376X_1 - 1.984X_2 - 5.412X_3 - 0.781X_1^2 + 0.103X_2^2 + 1.163X_3^2 - 0.375X_1X_2 - 0.625X_1X_3 - 0.625X_2X_3$	0.989

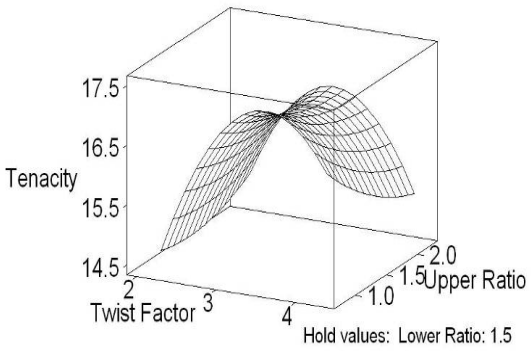

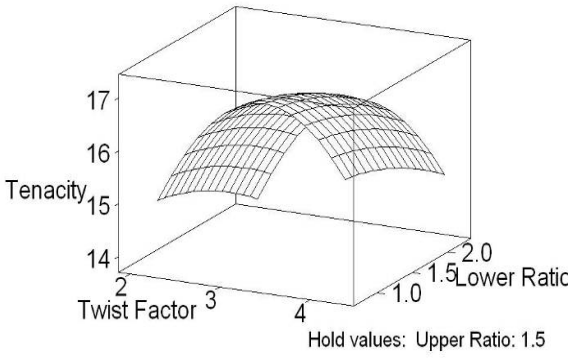

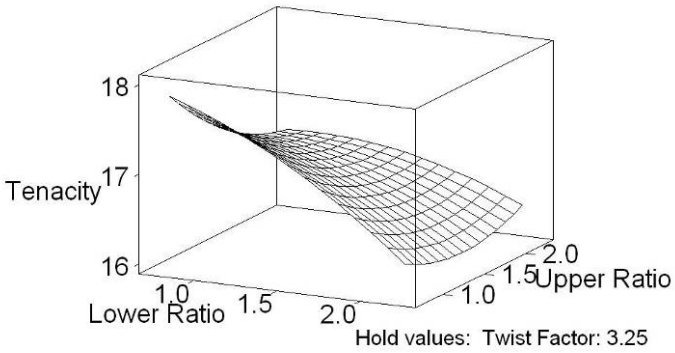

Figure C-1 Effect on yarn tenacity

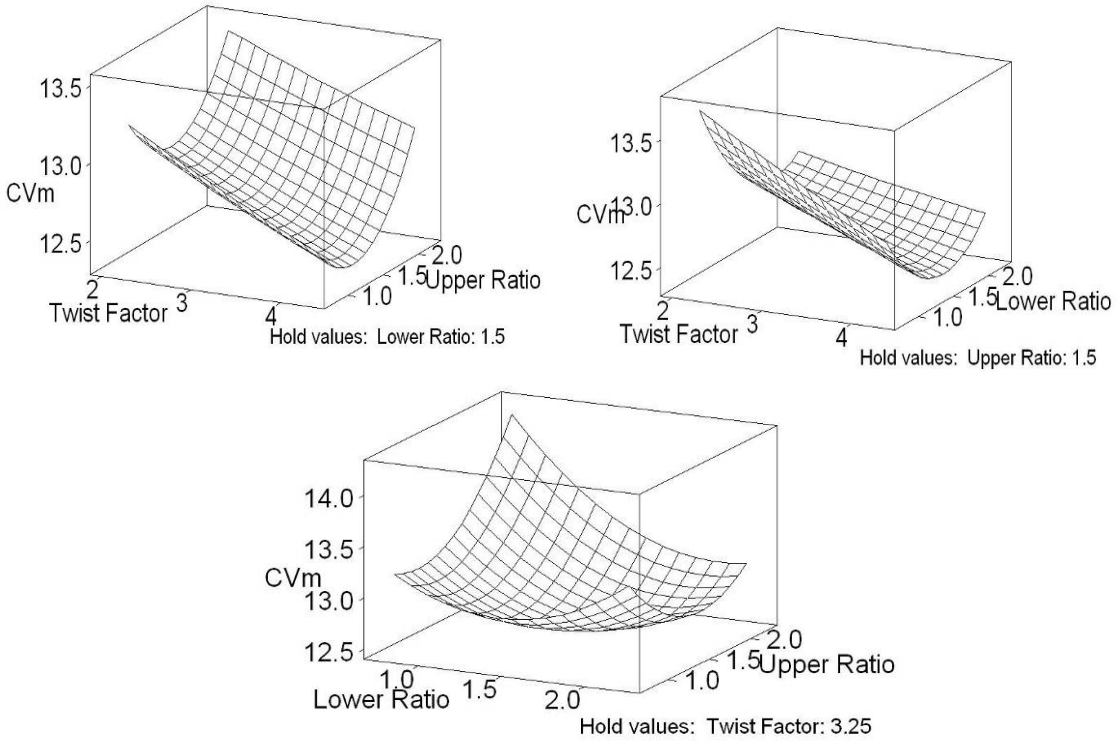

Figure C-2 Effect on yarn evenness

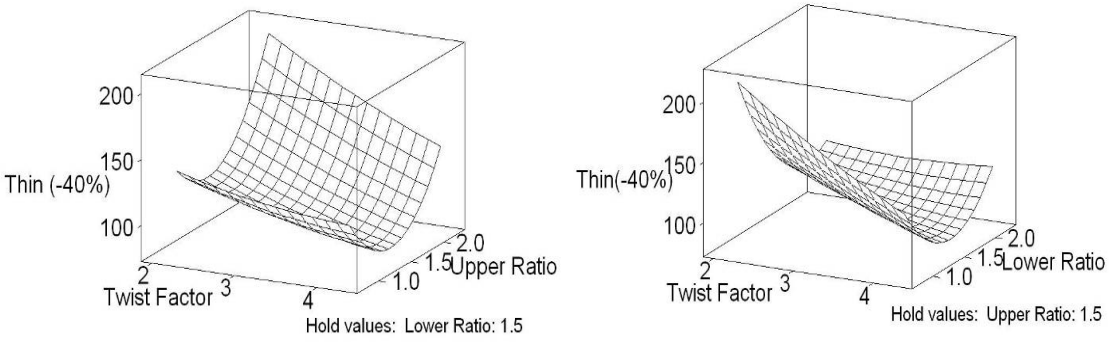

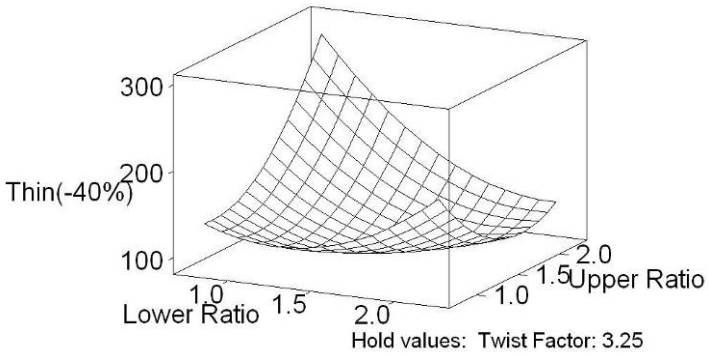

Figure C-3 Effect on yarn thin places (-40%)

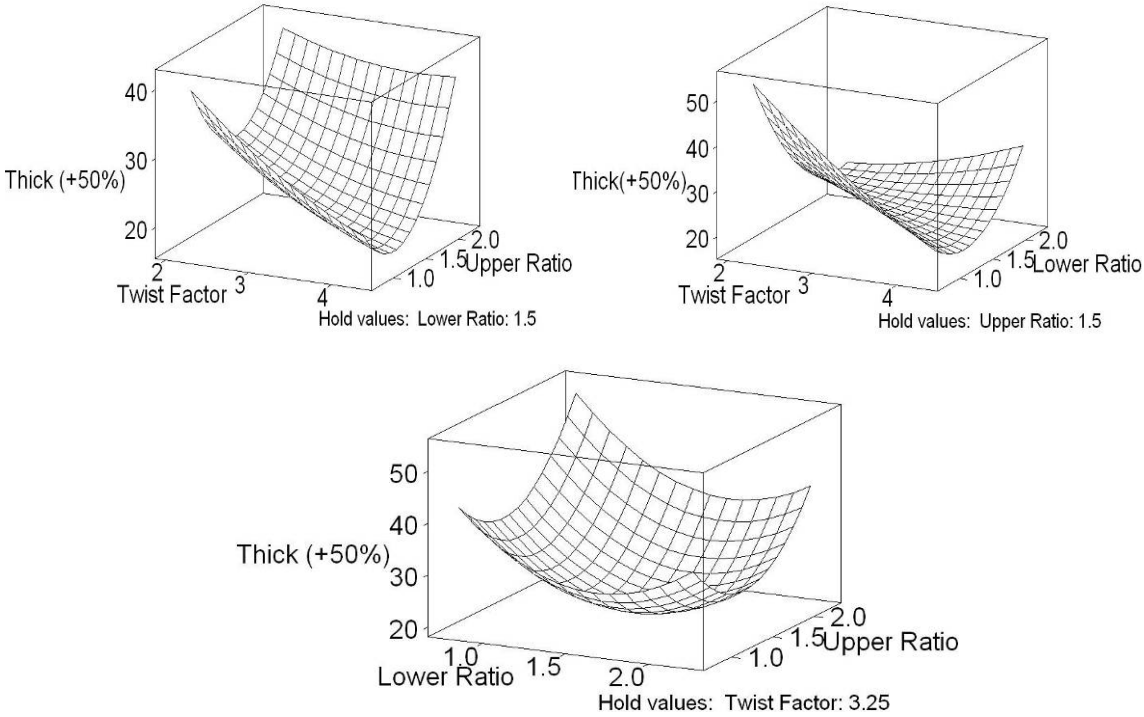

Figure C-4 Effect on yarn thick places (+50%)

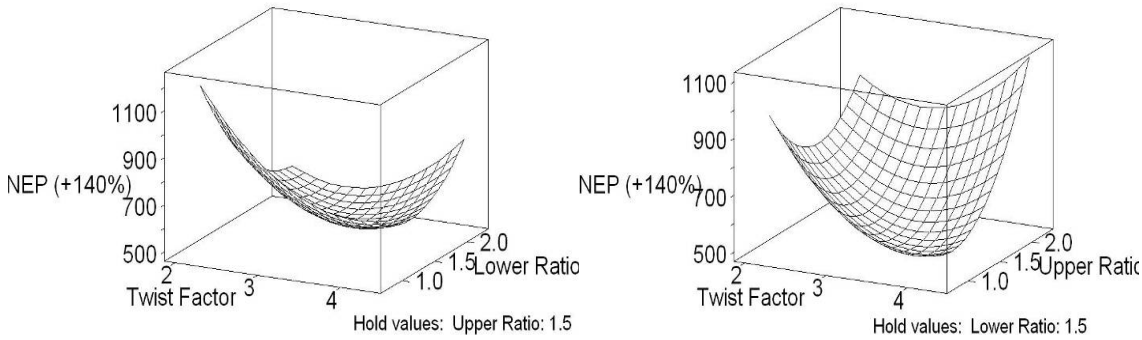

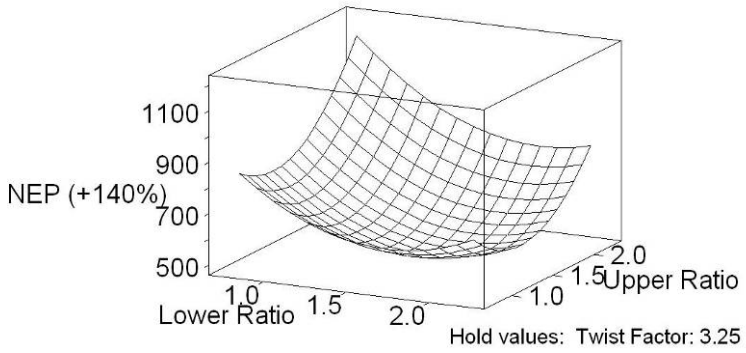

Figure C-5 Effect on yarn neps (+140%)

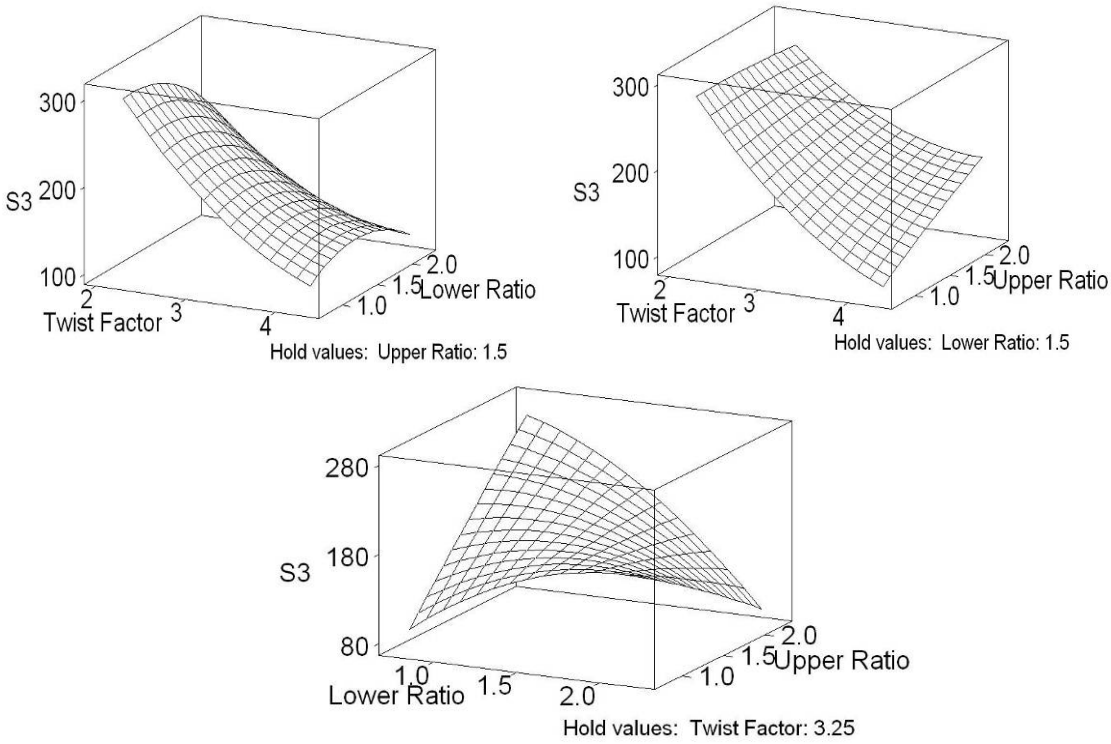

Figure C-6 Effect on yarn hairiness (S3)

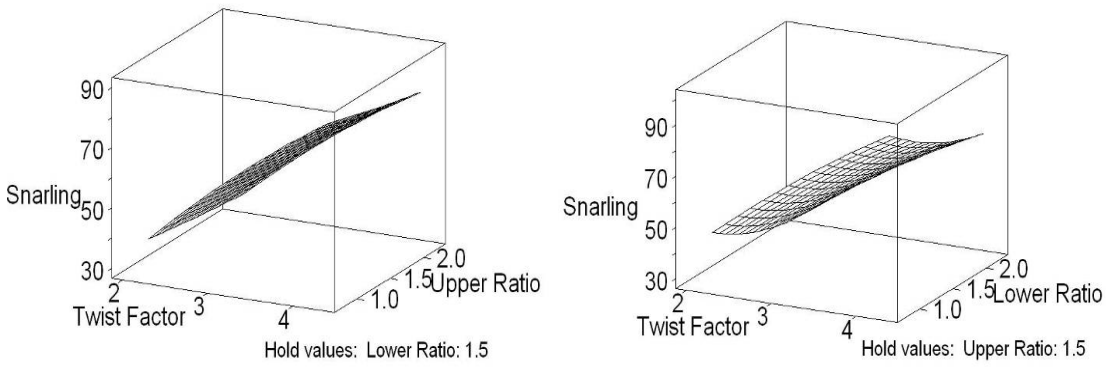

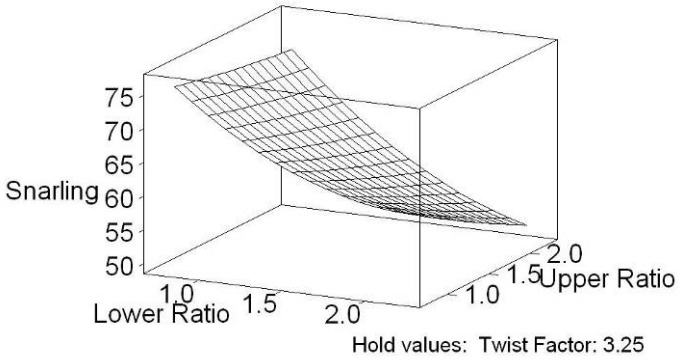

Figure C-7 Effect on yarn wet snarling

Figure C-8 and C-9 show the two optimization methods for parameter optimization, respectively. The final results are shown in Table C-5, and the optimized yarn properties were compared with the conventional ring yarn and are listed in Table C-6. The results show that the optimized yarn has slightly weaker yarn tenacity than the conventional one. The evenness values are similar, however the yarn neps (+140%) are doubled to the conventional one. The hairiness values of the optimized yarn are such better and the wet snarlings are also cut by 42.22%.

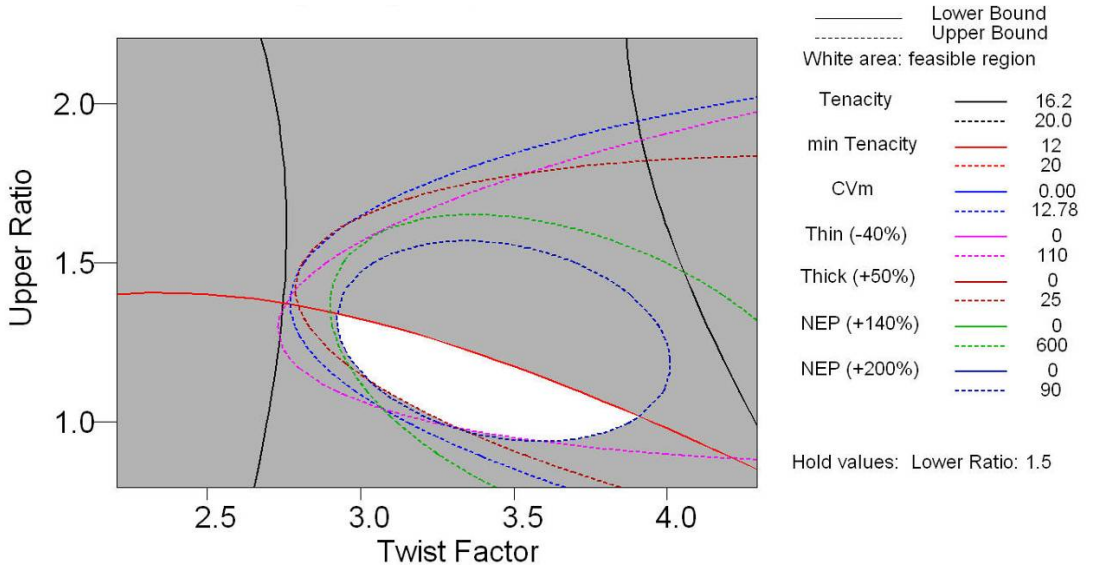

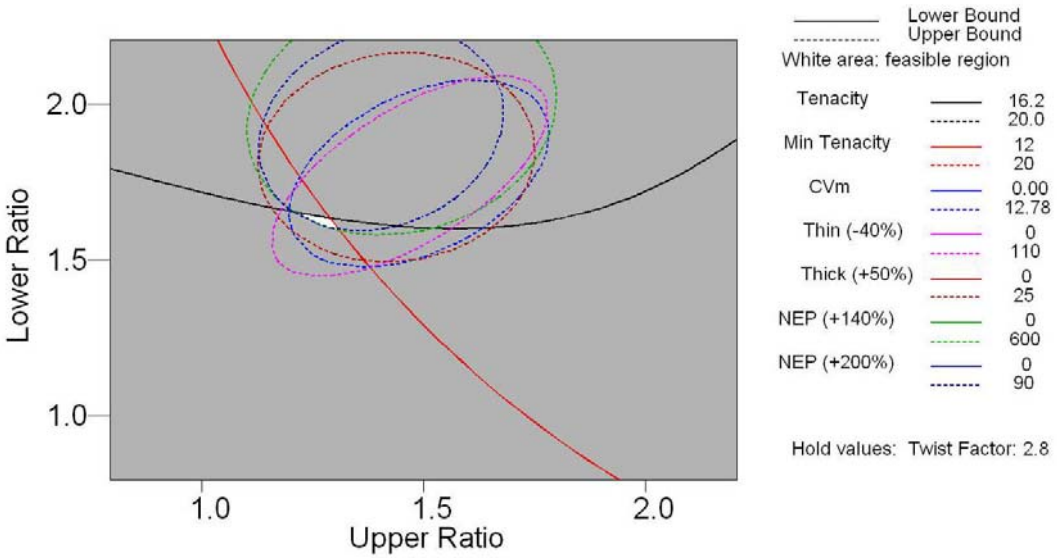

Figure C-8 Optimization using contour plot

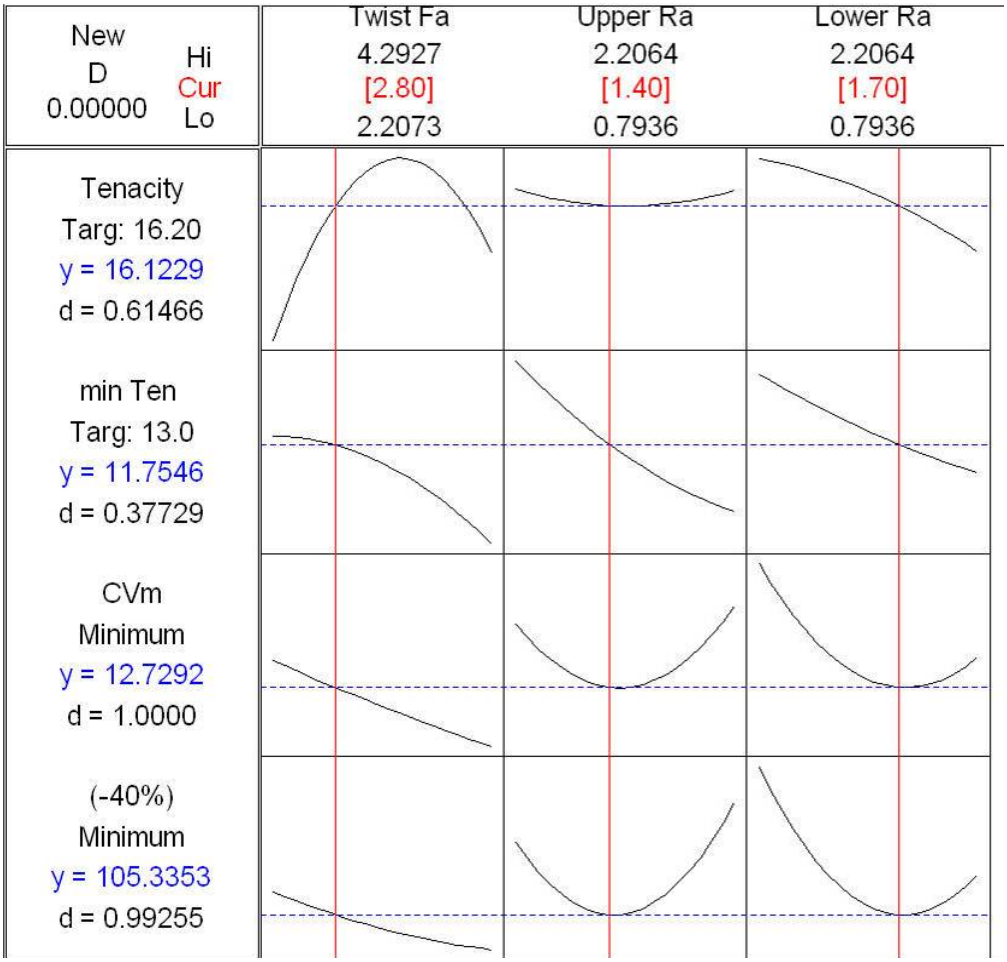

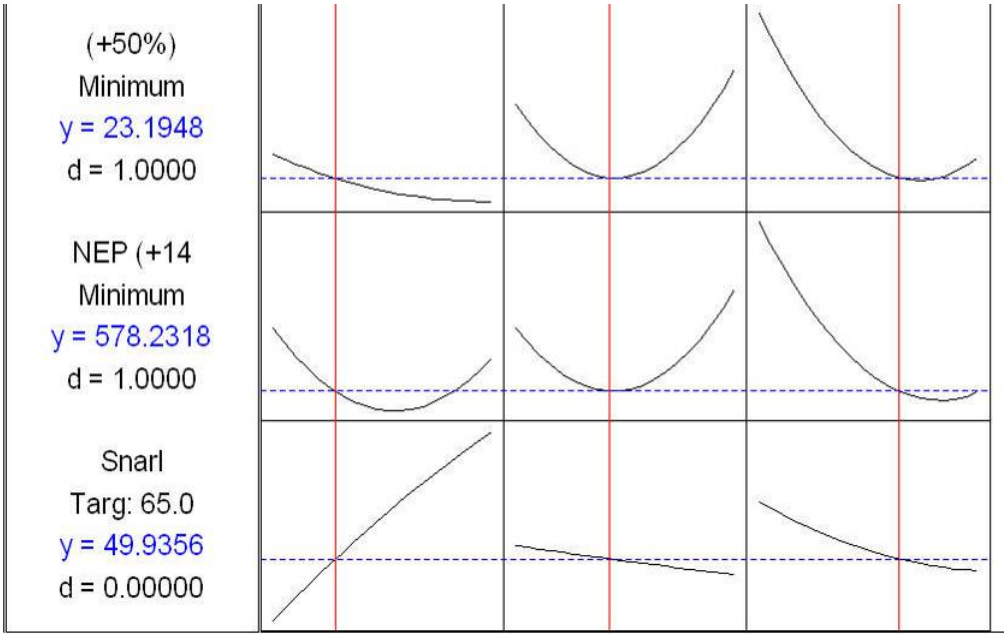

Figure C-9 Optimization using desirability functions

Table C-5 The optimized parameters for 40Ne modified yarn

Purpose	Twist factor	Upper ratio	Lower ratio
Knitting	2.8	1.4	1.7

Table C-6 Comparison of the optimized yarn properties

Yarn	Tenacity (cN/Tex) [CV%]	Min Ten (cN/Tex)	CVm (%) [CV%]	/1000m			Hairiness (S3) (/100m) [CV%]	Snarling (/25cm) [CV%]
				Thin (-40%) [CV%]	Thick (+50%) [CV%]	NEP (+140%) [CV%]		
NT	16.59 [8.30]	12.56	12.60 [0.67]	106 [6.76]	23 [49.73]	467 [19.38]	217 [18.53]	52 [8.03]
CONV	17.59 [7.50]	14.23	12.71 [1.23]	110 [7.27]	34 [29.85]	224 [14.75]	1321 [27.76]	90 [3.31]

References

[1] Hearle, J. W. S.,Grosberg, P.,Backer, S., *Structural Mechanics of Fibers, Yarns, and Fabrics*. Wiley-Interscience: New York, 1969; p 61.

[2] Lawrence, C. A., *Advances in yarn spinning technology*. Woodhead Publishing Ltd: Cambridge, 2010; p 262.

[3] Batra, S. K.,Fraser, W. B., *Engineering fundamentals of ring spinning/twisting, over-end unwinding and two-for-one twisting in textile processes*. 2015.

[4] Fraser, W. B., On the Theory Of Ring Spinning. *Philos T Roy Soc A* 1993, 342, 439-468.

[5] Guo, B. P.,Tao, X. M.,Lo, T. Y., A mechanical model of yarn twist blockage in rotor spinning. *Text Res J* 2000, 70, 11-17.

[6] Xu, B. G.,Tao, X. M., Integrated approach to dynamic analysis of yarn twist distribution in rotor spinning. *Text Res J* 2003, 73, 79-89.

[7] Long, J. L.,Xu, B. G.,Tao, X. M., A Nonlinear Dynamic Model for Periodic Motion of Slender Thread line Structures. *Cmes-Comp Model Eng* 2011, 72, 273-297.

[8] Lunenschloss, J.,Brockmanns, K. J., Review Of Open-End Friction Spinning. *Melliand Textil Int* 1982, 63, 261-263.

[9] Modelski, T. W., Repco Self-Twist Spinning. *Text I Ind* 1975, 13, 285-289.

[10] Grosberg, P.,Oxenham, W.,Miao, M., The Insertion Of Twist into Yarns by Means Of Air-Jets .2. Twist Distribution And Twist-Insertion Rates In Air-Jet Twisting. *J Text I* 1987, 78, 204-219.

[11] De Barr, A. E.,Catling, H., Twist Insertion in Ring Spinning and Doubling. *J Text Inst.* 1959, 50, T239-T240.

[12] Weinsdoerfer, H.,Bocht, B., Twist Slippage or Accumulation on False-twist Spindles. *Textil-Prax Int.* 1976, 31, 34.

[13] Kohlhaas, O., Weft Storage/feed Systems - Operation and Application. *Int Textile Bull Weaving* 1980, 3, 199-218.

[14] Chi, P. C.,Ki, L. C.,Tao, X. M. Method of Industrially Producing Yarn at a Lower Twist Multiplier for Textile Products. U. S. Patent No: 7,841,161 B2, 2010.

[15] Xu, B. G.,Tao, X. M.,Leung, C. S., A comparative study of cotton knitted fabrics and garments produced by the modified low twist and conventional ring yarns. *Fiber Polym* 2010, 11, 899-904.

[16] Hua, T.,Tao, X. M.,Cheng, K. P.,Wong, K. K.,Xu, B. G., Application of New Method Spinning Nu-torque Yarn for Weaving. *J Text Res* 2004, 25, 38-40.

[17] Xu, B. G.,Tao, X. M., Techniques for Torque Modification of Singles Ring Spun Yarns. *Text Res J* 2008, 78, 869-879.

[18] Feng, J.,Xu, B. G.,Tao, X. M., A Comparative Study of Finer Conventional and Modified Cotton Yarns and Their Resultant Woven Fabrics. *Fiber Polym* 2013, 14, 1899-1905.

[19] Hua, T.,Tao, X. M.,Cheng, K. P. S.,Xu, B. G., Effects of geometry of ring spinning triangle on yarn torque part I: Analysis of fiber tension distribution. *Text Res J* 2007, 77, 853-863.

[20] Hua, T.,Tao, X. M.,Cheng, K. P. S.,Xu, B. G., Effects of Geometry of Ring Spinning Triangle on Yarn Torque: Part II: Distribution of Fiber Tension within a Yarn and Its Effects on Yarn Residual Torque. *Text Res J* 2010, 80, 116-123.

[21] Feng, J.,Xu, B. G.,Tao, X. M.,Hua, T., Theoretical Study of a Spinning Triangle with Its Application in a Modified Ring Spinning System. *Text Res J* 2010, 80, 1456-1464.

[22] Feng, J.,Xu, B. G.,Tao, X. M., Dynamic measurement and modelling of flexible yarn dynamic behaviour on a moving cylindrical solid structure. *Meas Sci Technol* 2012, 23.

[23] Feng, J.,Xu, B. G.,Tao, X. M., Systematic investigation and optimization of fine cotton yarns produced in a modified ring spinning system using statistical methods. *Text Res J* 2013, 83, 238-248.

[24] Lawrence, C. A., *Fundamentals of spun yarn technology*. CRC Press: Boca Raton, Fla., 2003.

[25] Lord, P. R. Handbook of yarn production technology, science and economics. http://www.crcnetbase.com/isbn/9780849317811.

[26] Gupta, B. S., Fiber Migration In Staple Yarns .2. Geometric Mechanism Of Fiber Migration And Influence Of Roving And Drafting Variables. *Text Res J* 1970, 40, 15-&.

[27] Gupta, B. S., Fiber Migration In Staple Yarns .3. Analysis Of Migration Force And Influence Of Variables In Yarn Structure. *Text Res J* 1972, 42, 181-&.

[28] Hearle, J. W. S.,Bose, O. N., Migration of fibers in yarns: Part II: A geometrical explanation of migration. *Text Res J* 1965, 35, 972-978.

[29] Hearle, J. W. S.,Gupta, B. S.,Merchant, V. B., Migration of fibers in yarns: Part I: Characterization and idealization of migration behavior. *Text Res J* 1965, 35, 329-334.

[30] Xia, Z. G.,Xu, W. L., A Review of Ring Staple Yarn Spinning Method Development and Its Trend Prediction. *J Nat Fibers* 2013, 10, 62-81.

[31] Bunger, C. M., Limits To Ring Spinning. *Melliand Textil Int* 1985, 66, 31-31.

[32] Deussen, H., *Rotor spinning technology*. Schlafhorst Inc.: Charlotte, N.C., 1993.

[33] Grosberg, P.,Mansour, S. A., High-Speed Open-End Rotor-Spinning. *J Text I* 1975, 66, 389-396.

[34] Sengupta, A. K.,Murthy, H. V. S., Structure Of Fiber Assembly during Yarn Formation In Rotor Spinning. *Text Res J* 1984, 54, 692-694.

[35] Lawrence, C. A.,Chen, K. Z., A Study Of the Fiber-Transfer-Channel Design In Rotor-Spinning .1. The Fiber Trajectory. *J Text I* 1988, 79, 367-392.

[36] Neckar, B.,Ishtiaque, S. M.,Svehlova, L., Rotor Yarn Structure by Cross-Sectional Microtomy. *Text Res J* 1988, 58, 625-632.

[37] Ishtiaque, S. M., Longitudinal Fiber Distribution In Relation To Rotor Spun Yarn Properties. *Text Res J* 1989, 59, 696-699.

[38] Koc, E.,Lawrence, C. A., Mechanisms of wrapper fibre formation in rotor spinning: An experimental approach. *J Text I* 2006, 97, 483-492.

[39] Lawrence, C. A.,Chen, K. Z., Factors Affecting the Spinning Of Fine Rotor-Spun Yarns. *J Text I* 1986, 77, 139-145.

[40] Steadman, R. G.,Gipson, J. R.,Mehta, R. D.,Soliman, A. S., Factors Affecting Rotor Spinning Of Fine Cotton Yarns. *Text Res J* 1989, 59, 371-382.

[41] Kato, H. The development of ultra high speed spinning machine. Gifu University, Gifu, Japan, 2004.

[42] Ashkenazi, B., Friction Spinning as the Technology Of the Future. *Colourage* 1988, 35, 24-26.

[43] Fuchs, H., Mechanical-Aerodynamic Friction Spinning Processes. *Melliand Textil Int* 1979, 60, 289-291.

[44] Ishtiaque, S. M.,Agrawal, D., The internal structure of sheath fibre in DREF-3 yarn. *J Text I* 2000, 91, 546-562.

[45] Lord, P. R.,Rust, J. P., Fiber Assembly In Friction Spinning. *J Text I* 1991, 82, 465-478.

[46] Tyagi, G. K.,Kaushik, R. C. D.,Salhotra, K. R., Radial packing density and related properties of polyester DREF-3 yams. *Indian J Fibre Text* 2000, 25, 20-24.

[47] Johnson, N. A. G.,Lord, P. R., Fluid-Flow Phenomena In Friction Spinning. *J Text I* 1988, 79, 526-542.

[48] Lord, P. R.,Rust, J. P., The Surface Of the Tail In Open-End Friction Spinning. *J Text I* 1990, 81, 100-103.

[49] Lord, P. R.,Rust, J. P., Fiber Assembly In Friction Spinning. *J Text I* 1991, 82, 109-113.

[50] Zhu, R. Y.,Leaf, G. A. V.,Oxenham, W., Fiber Behavior In the Twisting Zone Of a Friction-Spinning Process. *J Text I* 1993, 84, 57-67.

[51] Lord, P. R.,Radhakrishnaiah, P., Tenacities Of Plied Friction-Spun, Rotor-Spun, And Ring-Spun Yarns. *J Text I* 1987, 78, 140-142.

[52] Louis, G. L.,Salaun, H. L.,Kimmel, L. B., Comparison Of Properties Of Cotton Yarns Produced by the Dref-3, Ring, And Open-End Spinning Methods. *Text Res J* 1985, 55, 344-351.

[53] Barella, A.,Manich, A. M., Friction Spun Yarns Versus Ring And Rotor Spun Yarns - Resistance To Abrasion And Repeated Extensions. *Text Res J* 1989, 59, 767-769.

[54] Barella, A.,Vega, P. A. A.,Castro, L., Yarn Attrition by Abrasion - a Comparison Of Polyester-Fiber Cotton Blended-Fiber Yarns Spun by Different Spinning Processes. *J Text I* 1989, 80, 599-603.

[55] Yu, C. W., Open-end spinning using air-jet twisting. *Text Res J* 1999, 69, 535-538.

[56] Pei, Z. G.,Yu, C. W., Study on the Principle of Yarn Formation of Murata Vortex Spinning Using Numerical Simulation. *Text Res J* 2009, 79, 1274-1280.

[57] Zhong, Y. H.,Ma, J. H.,Xing, M. J., Fiber configuration of air jet vortex spinning yarns. *Research In Materials And Manufacturing Technologies, Pts 1-3* 2014, 835-836, 1784-1788.

[58] Li, M. L.,Yu, C. W.,Shang, S. S., Effect of Vortex Tube Structure on Yarn Quality in Vortex Spinning Machine. *Fiber Polym* 2014, 15, 1786-1791.

[59] Basal, G.,Oxenham, W., Vortex Spun Yarn vs. Air-Jet Spun Yarn. *AUTEX Res. J.* 2003, 3, 96-101.

[60] Deno, K. Spinning apparatus with twisting guide surface. US Patent No. 5528895, 1996.

[61] Emmanuel, A.,Plate, D. E. A., An Alternative Approach To 2-Fold Weaving Yarn .2. The Theoretical-Model. *J Text I* 1982, 73, 107-116.

[62] Emmanuel, A.,Plate, D. E. A., An Alternative Approach To 2-Fold Weaving Yarn .3. Testing Of the Theoretical-Model. *J Text I* 1982, 73, 117-123.

[63] Plate, D. E. A.,Lappage, J., An Alternative Approach To 2-Fold Weaving Yarn .1. Control Of Surface Fibers. *J Text I* 1982, 73, 99-106.

[64] Plate, D. E. A., An Alternative Approach To 2-Fold Weaving Yarn .5. The Properties Of 2-Strand Yarns. *J Text I* 1983, 74, 320-328.

[65] Plate, D. E. A.,Feehan, J., An Alternative Approach To 2-Fold Weaving Yarn .4. Factors Affecting Strand-Twist. *J Text I* 1983, 74, 204-212.

[66] Cheng, K. P. S.,Sun, M. N., Effect of strand spacing and twist multiplier on cotton sirospun yarn. *Text Res J* 1998, 68, 520-527.

[67] Sun, M. N.,Cheng, K. P. S., Structure and properties of cotton Sirospun (R) yarn. *Text Res J* 2000, 70, 261-268.

[68] Schwarz, I.,Brnada, S.,Kovacevic, S., Comparison of the processing of Siro-spun yarns and conventional ply yarns into the fabric. *Annals of DAAAM for 2006 & Proceedings of the 17th International DAAAM Symposium* 2006, 371-372.

[69] Subramaniam, V.,Natarajan, K. S., Frictional-Properties Of Siro Spun Yarns. *Text Res J* 1990, 60, 234-239.

[70] Plate, D. E., Personal communication. 2009.

[71] Prins, M. W.,Lamb, P. R.,Naylor, G. R. S.,Tao, X., Yarn spinning from fibre sub-assemblies with variation of their paths of travel, relative positions or twist levels. Google Patents: 2000.

[72] Zhao, B., New technology of Solospun and Prospect of its Application and Development. *Frontier In Functional Manufacturing Technologies* 2010, 136, 312-315.

[73] Prins, M. W., Personal communication. 2010.

[74] Chang, L. L.,Wang, X. G., Comparing the hairiness of Solospun and ring spun worsted yarns. *Text Res J* 2003, 73, 640-644.

[75] Cheng, L. D.,Fu, H.,Yu, X. Y., Relationship between hairiness and the twisting principles of solospun and ring spun yarns. *Text Res J* 2004, 74, 763-766.

[76] Huang, L. X.,Zhu, C. X., Research on the technology and product characteristics of Solospun spinning. *Proceedings of 2006 China International Wool Textile Conference & IWTO Wool Forum* 2006, 234-238.

[77] Ono, Y., Future developments of the in-rotating-liquid spinning process - Giving an example of the spinning in gas followed by winding in rotating liquid. *Tetsu To Hagane* 2005, 91, 511-520.

[78] Nikolic, M.,Stjepanovic, Z.,Lesjak, F.,Stritof, A., Compact spinning for improved quality of ring-spun yarns. *Fibres Text East Eur* 2003, 11, 30-35.

[79] Altas, S.,Kadoglu, H., Comparison of the evenness, faults and hairiness of compact and conventional spun ring yarns. *Ind Textila* 2013, 64, 65-69.

[80] Gokarneshan, N.,Anbumani, N.,Subramaniam, V., An investigation on the minimum twist of cohesion of ring and compact spun yarns. *Indian J Fibre Text* 2005, 30, 340-343.

[81] Becerir, B.,Omeroglu, S., Comparison of color values of plain cotton fabrics knitted from ring- and compact-spun yarns. *Aatcc Rev* 2007, 7, 41-46.

[82] Taskin, C.,Ozguney, A. T.,Gurkan, P.,Ozcelik, G.,Ozerdem, A., Comparison of woven fabrics' properties from traditional and compact ring-spun yarns after dyeing processes. *Fibres Text East Eur* 2007, 15, 86-90.

[83] Can, Y., Researching the Effects Of Some Finishing Process on Strength And Elongation Characteristics Of Compact And Ring Spun Yarns. *Tekst Konfeksiyon* 2009, 19, 56-60.

[84] Almetwally, A. A.,Salem, M. M., Comparison Between Mechanical Properties Of Fabrics Woven From Compact And Ring Spun Yarns. *Autex Res J* 2010, 10, 35-40.

[85] Chen, J.,Xu, Q. L.,Xia, Z. G.,Xu, W. L., An Experimental Study of Influence of Filament and Roving Location on Yarn Properties during Embeddable and Locatable Spinning. *Fiber Polym* 2012, 13, 1196-1200.

[86] Wang, H. S.,Xia, Z. G.,Xu, W. L., A study of an embeddable and locatable spinning system via quasi-static mechanical analysis. *Text Res J* 2012, 82, 2071-2077.

[87] Xia, Z. G.,Wang, X.,Ye, W. X.,Eltahir, H. A.,Xu, W. L., Fiber trapping comparison of embeddable and locatable spinning with sirofil and siro core-spinning with flute pipe air suction. *Text Res J* 2012, 82, 1255-1262.

[88] Xu, W. L.,Xia, Z. G.,Wang, X.,Chen, J.,Cui, W. G.,Ye, W. X.,Ding, C. L.,Wang, X. G., Embeddable and locatable spinning. *Text Res J* 2011, 81, 223-229.

[89] Cheng, K. P. S.,Li, C. H. L., JetRing spinning and its influence on yarn hairiness. *Text Res J* 2002, 72, 1079-1087.

[90] Panchal, D., Jetring Spinning: A New Concept In Spinning Technology. *Itc&Dc: 4th International Textile Clothing & Design Conference, Book Of Proceedings* 2008, 248-252.

[91] Wang, X. G.,Miao, M. G.,How, Y. L., Studies of JetRing spinning .1. Reducing yarn hairiness with the JetRing. *Text Res J* 1997, 67, 253-258.

[92] Hasani, H.,Hasani, M., Simulation Approach to Investigate the Effect of the Jet Structure and Air Pressure on the Performance of Siro-jet Spinning. *Fibres Text East Eur* 2012, 20, 46-50.

[93] Nejad, A. S.,Najar, S. S.,Hasani, H., Application of air-jet nozzle in short staple Siro spinning system. *J Text I* 2011, 102, 14-18.

[94] Yilmaz, D.,Usal, M. R., A Study on Siro-jet Spinning System. *Fiber Polym* 2012, 13, 1359-1367.

[95] Yilmaz, D.,Usal, M. R., Improvement in yarn hairiness by the siro-jet spinning method. *Text Res J* 2013, 83, 1081-1100.

[96] Thilagavathi, G.,Udayakumar, D.,Sasikala, L.,Kannaian, T., Yarn hairiness controlled by various left diagonal yarn path offsets by modified bottom roller flute blocks in ring spinning. *Indian J Fibre Text* 2009, 34, 328-332.

[97] Wu, T. T.,Xie, C. P.,Su, X. Z.,Liu, X. J.,Huang, B., A Modified Ring Spinning System with Various Diagonal Yarn Path Offsets. *Second Sree Conference on Chemical Engineering (Cce 2011)* 2011, 18.

[98] Xia, Z. G.,Xu, W. L.,Zhang, M.,Qiu, W. B.,Feng, S. L., Reducing Ring Spun Yarn Hairiness via Spinning with a Contact Surface. *Fiber Polym* 2012, 13, 670-674.

[99] Ghasemi, R.,Mozafari-Dana, R.,Etrati, S. M.,Najar, S. S., Comparing the physical properties of produced Sirospun and new hybrid Solo-Siro spun blend wool/polyester worsted yarns. *Fibres Text East Eur* 2008, 16, 24-27.

[100] Najar, S. S.,Khan, Z. A.,Wang, X. G., The new Solo-Siro spun process for worsted yarns. *J Text I* 2006, 97, 205-210.

[101] Miao, M. H., Yarn spun from carbon nanotube forests: Production, structure, properties and applications. *Particuology* 2013, 11, 378-393.

[102] Gu, H. B.,Miao, M. H., Optimising fibre alignment in twisted yarns for natural fibre composites. *J Compos Mater* 2014, 48, 2993-3002.

[103] Hearle, J. W. S.,Hollick, L.,Wilson, D. K.,Textile, I., *Yarn Texturing Technology*. Woodhead Publishing: Boca Raton, 2001.

[104] Hua, T. Production, Properties and Sturctures of Short Staple Low Torque Singles Ring Yarn for Weaving. the Hong Kong Polytechnic University, 2006.

[105] Yang, K.,Tao, X. M.,Xu, B. G.,Lam, J., Structure and properties of low twist short-staple singles ring spun yarns. *Text Res J* 2007, 77, 675-685.

[106] Guo, Y.,Tao, X. M.,Xu, B. G.,Choi, K. F.,Hua, T.,Wang, S. Y., A continuous measurement system for yarn structures by an optical method. *Meas Sci Technol* 2010, 21.

[107] Guo, Y.,Tao, X. M.,Xu, B. G.,Feng, J.,Wang, S. Y., Structural characteristics of low torque and ring spun yarns. *Text Res J* 2011, 81, 778-790.

[108] Guo, Y. Analyses on the Internal Structures and Properties of Low Torque Singles Ring Yarn. Donghua University, Shanghai, 2011.

[109] Xu, B. G.,Tao, X. M., Techniques for Torque Modification of Singles Ring Spun Yarns. *Text Res J* 2008, 78, 869-879.

[110] Yang, K. Torsional Behavior of Short-staple Torque-balanced Singles Ring Spun Yarns and Spirality of Resultant Knitted Fabrics. the Hong Kong Polytechnic University, 2006.

[111] Xu, B. G.,Tao, X. M.,Leung, C. S., A comparative study of cotton knitted fabrics and garments produced by the modified low twist and conventional ring yarns. *Fiber Polym* 2010, 11, 899-904.

[112] Feng, J. Study of Structure, Properties and Manufacturing Conditions of Staple Yarns in a Modified Ring Spinning System. the Hong Kong Polytechnic University, Hong Kong, 2013.

[113] Ravichandran, M.,Hettiarachchy, N., Optimization of preparation of soy protein hydrolysates using response surface methodology with Alzheimer's beta-amyloid (A beta 1-42) peptide aggregation inhibition property. *Abstr Pap Am Chem S* 2013, 245.

[114] Miao, M. H.,Chen, R. Z., Yarn Twisting Dynamics. *Text Res J* 1993, 63, 150-158.

[115] Denton, M. J., The Development of False Twist in Bulking. *J Text Inst* 1968, 59, 344-350.

[116] Denton, M. J., Twisting-Rate Variations In False-Twist Threadline .1. Background And Effect Of a Step Change In Twisting Rate. *J Text Inst* 1975, 66, 282-288.

[117] Denton, M. J., Twisting-Rate Variations In False-Twist Threadline .2. Effects Of a Rectangular-Pulse Transient Change And a Sinusoidal Variation In Twisting Rate. *J Text Inst* 1975, 66, 289-296.

[118] Fraser, W. B.,Stump, D. M., Yarn twist in the ring-spinning balloon. *P Roy Soc a-Math Phy* 1998, 454, 707-723.

[119] Yao, M., *Fang zhi cai liao xue*. Zhongguo fang zhi chu ban she: Beijing, 2009.

[120] Czaplicki, Z., A new method of measuring twist of yarn. *Fibres Text East Eur* 2006, 14, 27-29.

[121] du Bois, W. F.,ten Cate, G. J. H., Measuring Twist in Short Lengths of Spun Yarns. *The Journal of The Textile Institute* 1967, 58, 518-520.

[122] Morton, W. E.,Yen, K. C., The arrangement of fibres in fibro yarns. *J. Text. Inst.* 1952, 43, T60-66.

[123] Vas, L. M.,Halasz, G.,Takacs, M.,Eordogh, I.,Szasz, K., Measurement of yarn diameter and twist angle with image processing system. *Periodica Polytechnica, Mechanical Engineering* 1994, 38, 277-296.

[124] Cybulska, M., Assessing yarn structure with image analysis methods. *Textile Research Journal* 1999, 69, 369-373.

[125] Huang, C. C.,Liu, S. C., Woven fabric analysis by image processing - Part II: Computing the twist angle. *Textile Research Journal* 2001, 71, 362-366.

[126] Basu, A.,Doraiswamy, I.,Gotipamul, R. L., Measurement of Yarn Diameter and Twist by Image Analysis. *J Text I* 2003, 94, 37-48.

[127] Jia, L. F., Determining the twist of yarns based on image analysis. *J. Text. R.* 2005, 26, 39-40.

[128] Ozkaya, Y. A.,Acar, M.,Jackson, M. R., Yarn twist measurement using digital imaging. *J Text I* 2010, 101, 91-100.

[129] Pei, Z. G.,Tao, X. M., Measurement of yarn twist based on backward light scattering and small-angle far-field diffraction. *Measurement Science And Technology* 2015, 26.

[130] Jasper, W. J.,Gunay, M.,Suh, M. W., Measurement of eccentricity and twist in spun and plied yarns. *J Text I* 2005, 96, 93-97.

[131] Mei, S. Q.,Xiang, X. Z.,Du, X. X.,Zhao, Y. W.,Wu, S. L.,Yu, L. Q.,Zhang, Z. M.,You, H. S. Non-contact measuring device and method for dynamic tension and twist of yarn. CN1140770C, 2004.

[132] Vuyst, D., Quality monitoring for twisting machines. *Textile Month* 1995, 8, 54-57.

[133] Tang, H. B.,Xu, B. G.,Tao, X. M.,Feng, J., Mathematical modeling and numerical simulation of yarn behavior in a modified ring spinning system. *Appl Math Model* 2011, 35, 139-151.

[134] Diwaniyan, S.,Sharma, K. K.,Kuhad, R. C., Laccase from an alkalitolerant basidiomycetes Crinipellis sp RCK-1: Production optimization by response surface methodology. *J Basic Microb* 2012, 52, 397-407.

[135] Ludicke, A., Ein Studie uber die Ringspindel. *Dinglers Polytech. J.* 1881, 334-340.

[136] de Barr, A. E.,Catling, H., *The principles and theory of ring spinning*. Butterworths Press: Manchester and London, 1965.

[137] Batra, S. K.,Ghosh, T. K.,Zeidman, M. I., An Integrated Approach To Dynamic Analysis Of the Ring Spinning Process .2. With Air Drag. *Text Res J* 1989, 59, 416-424.

[138] Batra, S. K.,Ghosh, T. K.,Zeidman, M. I., An Integrated Approach To Dynamic Analysis Of the Ring Spinning Process .1. Without Air Drag And Coriolis Acceleration. *Text Res J* 1989, 59, 309-317.

[139] Fraser, W. B., The Effect Of Yarn Elasticity on an Unwinding Balloon. *J Text I* 1992, 83, 603-613.

[140] Yin, R.,Gu, H. B., Numerical simulation of quasi-stationary ring spinning process linear elastic yarn. *Text Res J* 2011, 81, 22-27.

[141] Fraser, W. B.,Famell, L.,Stump, D. M., The effect of a slub on the stability of the ring-spinning balloon. *J Text I* 1995, 86, 610-634.

[142] Fraser, W. B.,Farnell, L.,Stump, D. M., Effect Of Yarn Nonuniformity on the Stability Of the Ring-Spinning Balloon. *P R Soc-Math Phys Sc* 1995, 449, 597-621.

[143] Stump, D. M.,Fraser, W. B., Transient solutions of the ring-spinning balloon equations. *J Appl Mech-T Asme* 1996, 63, 523-528.

[144] Love, A. E. H., *A Treatise on The Mathematical Theory of Elasticity*. Cambridge University Press: New York, 1927.

[145] Fraser, W. B.,Clark, J. D.,Ghosh, T. K.,Zeng, Q., The effect of a control ring on the stability of the ring-spinning balloon. *P Roy Soc a-Math Phy* 1996, 452, 47-62.

[146] Yang, R. H.,Gao, W. D.,Wang, J.,Wang, H. B.,Xie, C. P.,Wang, S. Y., Dynamic model and numerical approach for rotor-spun composite yarn spinning process. *Ind Textila* 2012, 63, 171-175.

[147] Yang, R. H.,Wang, S. Y., A Mathematical Model for Rotor-Spun Composite Yarn Spinning Process. *Text Res J* 2010, 80, 487-490.

[148] Yang, R. H.,Xue, Y.,Wang, S. Y., A nonlinear dynamic model for a rotor-spun composite yarn spinning process. *Nonlinear Anal-Theor* 2009, 71, E98-E102.

[149] Lim, J. H.,Kim, J. S.,Huh, Y., Model identification of the bundle thickness dynamics in drum friction spinning. *Fiber Polym* 2012, 13, 96-103.

[150] Kireenkov, A. A., Generalized two-dimensional model of sliding and spinning friction. *Dokl Phys* 2010, 55, 186-190.

[151] Pei, Z. G.,Yu, C. W., Investigation on the Dynamic Behavior of the Fiber in the Vortex Spinning Nozzle and Effects of Some Nozzle Structure Parameters. *J Eng Fiber Fabr* 2011, 6, 16-29.

[152] Shankam, V. P. Novel method for dynamic yarn tension measurement and control in direct cabling process. North Carolina State University, 2005.

[153] Hossain, M.,Abdkader, A.,Nocke, A.,Unger, R.,Krzywinski, F.,Hasan, M. M. B.,Cherif, C., Measurement Methods of Dynamic Yarn Tension in a Ring Spinning Process. *Fibres Text East Eur* 2016, 24, 36-43.

[154] Xu, Q.,Mei, S. Q.,Zhang, Z. M., Measurement Method of Yarn Tension Based on CCD Technology. *Frontiers Of Manufacturing Science And Measuring Technology, Pts 1-3* 2011, 230-232, 89-93.

[155] Wang, L., *Intelligent optimization algorithme with applications*. Tsiinghua University Publication: Beijing, 2001.

[156] Loucks, D. P.,Beek, E. V.,Stedinger, J. R.,Dijkman, J. P.,Villars, M. T., *Water resources systems planning and management: An introduction to methods, models and applications*. UNESCO Publishing: 2005.

[157] Koch, K. R., *Parameter estimation and hypothesis testing in linear models*. Springer Berlin; New York, 1999.

[158] Akhbari, M.,Zahiri, A.,Bassam, S. J. E., Optimization of Parameters Influencing Mercerization Using the RSM Method in Order to Increase the Tensile Strength of Mercerized Yarn. *Fibres Text East Eur* 2012, 20, 30-35.

[159] Guo, Y.,Feng, J.,Yin, R.,Wang, X. G.,van der Sluijs, M.,Tao, X. M., Investigation and evaluation on fine Upland cotton blend yarns made by the modified ring spinning system. *Text Res J* 2015, 85, 1355-1366.

[160] van der Heijden, G. H. M.,Thompson, J. M. T., Helical and localised buckling in twisted rods: A unified analysis of the symmetric case. *Nonlinear Dynam* 2000, 21, 71-99.

[161] van der Heijden, G. H. M.,Champneys, A. R.,Thompson, J. M. T., Spatially complex localisation in twisted elastic rods constrained to a cylinder. *Int J Solids Struct* 2002, 39, 1863-1883.

[162] Audoly, B.,Pomeau, Y., *Elasticity and Geometry*. Oxford University Press,: New York, 2010.

[163] Dhingra, R. C.,Postle, R., Measurement Of Torque In Continuous-Filament Yarns .2. Effect Of Yarn Tension. *J Text I* 1974, 65, 171-181.

[164] Bennett, J. M.,Postle, R., Study Of Yarn Torque And Its Dependence on the Distribution Of Fiber Tensile-Stress In the Yarn .2. Experimental. *J Text I* 1979, 70, 133-141.

[165] Fraser, W. B., On the Theory Of Ring Spinning. *Philosophical Transactions Of the Royal Society Of London Series a-Mathematical Physical And Engineering Sciences* 1993, 342, 439-468.

[166] Montgomery, D. C., *Design and analysis of experiments*. Wiley: New York, 1991.

[167] Box, G. E. P.,Wilson, K. B., On the Experimental Attainment of Optimum Conditions (with discussion). *J R Stat Soc Ser B-Stat Methodol* 1951, 13, 1-45.

[168] Hong, B.,Chen, L. Z.,Xue, G. X.,Xie, Q.,Chen, F., Optimization of oxalic acid pretreatment of moso bamboo for textile fiber using response surface methodology. *Cellulose* 2014, 21, 2157-2166.

[169] Siddh, M. M.,Gadekar, G.,Soni, G.,Jain, R., Integrating Lean Six Sigma and Supply Chain Approach for Quality and Business Performance. *2014 2nd International Conference on Business And Information Management (Icbim)* 2014.

[170] Swamy, G. J.,Sangamithra, A.,Chandrasekar, V., Response surface modeling and process optimization of aqueous extraction of natural pigments from Beta vulgaris using Box-Behnken design of experiments. *Dyes Pigments* 2014, 111, 64-74.

[171] Anawa, E. M.,Olabi, A. G., Using Taguchi method to optimize welding pool of dissimilar laser-welded components. *Opt Laser Technol* 2008, 40, 379-388.

[172] Siyal, A. N.,Memon, S. Q.,Khaskheli, M. I., Optimization and equilibrium studies of Pb(II) removal by Grewia Asiatica seed: a factorial design approach. *Pol J Chem Technol* 2012, 14, 71-77.

[173] Oliveira, R.,Oliveira, V.,Aracava, K. K.,Rodrigues, C. E. D., Effects of the extraction conditions on the yield and composition of rice bran oil extracted with ethanol-A response surface approach. *Food Bioprod Process* 2012, 90, 22-31.

[174] Braga, A. R. C.,Gomes, P. A.,Kalil, S. J., Formulation of Culture Medium with Agroindustrial Waste for beta-Galactosidase Production from Kluyveromyces marxianus ATCC 16045. *Food Bioprocess Tech* 2012, 5, 1653-1663.

[175] Altemimi, A.,Lightfoot, D. A.,Kinsel, M.,Watson, D. G., Employing Response Surface Methodology for the Optimization of Ultrasound Assisted Extraction of Lutein and beta-Carotene from Spinach. *Molecules* 2015, 20, 6611-6625.

[176] Wang, A. X.,Li, Y. F.,Yang, B.,Xu, B. Q.,Kong, L. X.,Liu, D. C., Process optimization for vacuum distillation of Sn-Sb alloy by response surface methodology. *Vacuum* 2014, 109, 127-134.

[177] Ghaedi, M.,Jaberi, S. Y. S.,Hajati, S.,Montazerozohori, M.,Asfaram, A.,Zareh, M., Modified Carbon Paste Electrode for Pb2+ Ion Determination: Response Surface Methodology. *Ieee Sens J* 2015, 15, 2974-2983.

[178] Samuel, M. S.,Abigail, E. A. M.,Chidambaram, R., Isotherm Modelling, Kinetic Study and Optimization of Batch Parameters Using Response Surface Methodology for Effective Removal of Cr(VI) Using Fungal Biomass. *Plos One* 2015, 10.

[179] Valencia, P.,Espinoza, K.,Ceballos, A.,Pinto, M.,Almonacid, S., Novel modeling methodology for the characterization of enzymatic hydrolysis of proteins. *Process Biochem* 2015, 50, 589-597.

[180] Madani, S.,Gheshlaghi, R.,Mahdavi, M. A.,Sobhani, M.,Elkamel, A., Optimization of the performance of a double-chamber microbial fuel cell through factorial design of experiments and response surface methodology. *Fuel* 2015, 150, 434-440.

[181] Savasari, M.,Emadi, M.,Bahmanyar, M. A.,Biparva, P., Optimization of Cd(II) removal from aqueous solution by ascorbic acid-stabilized zero valent iron nanoparticles using response surface methodology. *J Ind Eng Chem* 2015, 21, 1403-1409.

[182] Chang, B. P.,Akil, H. M.,Nasir, R. B.,Khan, A., Optimization on wear performance of UHMWPE composites using response surface methodology. *Tribol Int* 2015, 88, 252-262.

[183] Nagar, S.,Gupta, V. K.,Kumar, D.,Kumar, L.,Kuhad, R. C., Production and optimization of cellulase-free, alkali-stable xylanase by Bacillus pumilus SV-85S in submerged fermentation. *J Ind Microbiol Biot* 2010, 37, 71-83.

[184] Zhang, W. G., *Jia nian guo cheng ji ben li lun*. Fang zhi gong ye chu ban she: Beijing, 1983.

[185] Huang, X. X. Surface characteristics of low-twist worsted yarns and knitted fabrics. the Hong Kong Polytechnic University, Hong Kong, 2016.